INTERNATIONAL SCIENTIFIC JOURNAL

GEOGRAPHICA PANNONICA

Volume 26, Issue 3 (September 2022)

SPECIAL ISSUE

UNIVERSITY OF NOVI SAD, FACULTY OF SCIENCES

DEPARTMENT OF GEOGRAPHY, TOURISM AND HOTEL MANAGEMENT

UNIVERSITY OF NOVI SAD | FACULTY OF SCIENCES
DEPARTMENT OF GEOGRAPHY, TOURISM & HOTEL MANAGEMENT

INTERNATIONAL SCIENTIFIC JOURNAL

GEOGRAPHICA PANNONICA

Volume 26, Issue 3, September 2022

SPECIAL ISSUE

"Natural Hazards and the Mitigation of their Impact"

ISSN 0354-8724 (hard copy) | ISSN 1820-7138 (online) | UDC 05:91(497.1)=20

ISSN 0354-8724 (hard copy) | ISSN 1820-7138 (online) | UDC 05:91(497.1)=20

INTERNATIONAL SCIENTIFIC JOURNAL

GEOGRAPHICA PANNONICA

UNIVERSITY OF NOVI SAD | FACULTY OF SCIENCES | DEPARTMENT OF GEOGRAPHY, TOURISM & HOTEL MANAGEMENT

EDITORIAL OFFICE

Faculty of Sciences
Department of Geography, Tourism and Hotel Management
Trg Dositeja Obradovića 3, 21000 Novi Sad, Serbia
tel. +381 21 450-105
fax +381 21 459-696
Official site: www.dgt.uns.ac.rs

CONTACTS

Lazar Lazić, PhD, full professor
Department of Geography, Tourism and Hotel Management, Serbia, lazar.lazic@dgt.uns.ac.rs

Dragan Milošević, teaching assistant
Department of Geography, Tourism and Hotel Management, Serbia, dragan.milosevic@dgt.uns.ac.rs

Official mail of the Journal
gpscijournal@dgt.uns.ac.rs

Internet portal
www.dgt.uns.ac.rs/pannonica.html

Instructions to authors
www.dgt.uns.ac.rs/pannonica/instructions.htm

Contents

Editorial Note and Book Review

Natural Hazards and the Mitigation of their Impact

György Sipos[A], Lazar Lazić[B]

Under a changing climate and an intensifying human impact on the environment, managing and mitigating natural hazards are increasingly important for our society to tackle the serious challenges of the future concerning population and economic growth, food safety, preservation of ecosystem services and biodiversity; moreover, this task should be accomplished in a sustainable and eco-friendly way. Therefore, it is not enough to realise natural hazards and study their geographical aspects, but we need to learn and share the multitude of practices applied worldwide among specific conditions.

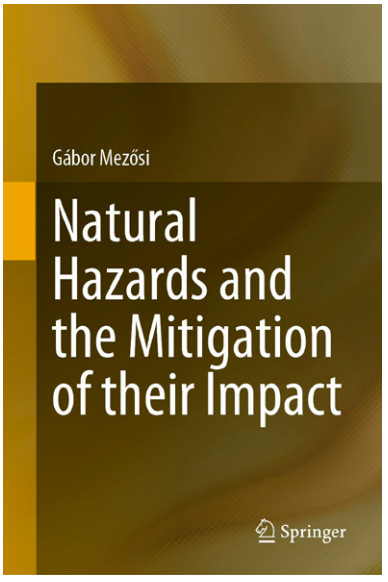

There have been numerous books dealing with the issue of natural hazards and risks from a wide variety of perspectives; thus, the reader might ask what novelty this compilation can add to the discourse. One answer is partly hidden in the first paragraph of this review; namely, the book contains not only the description of different types of natural hazards and information on their spatial occurrence, but just as indicated in the title, it attempts to outline the set of potential actions by which hazards can be managed, and their impact can be reduced. Another major strength of the book is that it describes hazards and mitigation strategies by bringing examples not only from developed countries with high prevention and recovery potential but also from less developed regions, such as Eastern Europe or Eastern and Central Asia. This way, the reader gets information on problems and solutions undercited in the international literature.

The book is comprised of 7 Chapters. The first is a general introduction to the definition, typification, and human and economic aspects of natural hazards but also touching some practical management issues using a rather global perspective. In the following chapters, different classes of hazards are discussed in the following order: geophysical hazards, meteorological hazards, hydrological hazards, biosphere-related natural hazards, extraterrestrial hazards and finally, climate change and its impacts. Within the main chapters, several subchapters detail individual hazards; thus, for example, the chapter on geophysical hazards includes volcanic, earthquake, tsunami and landslide hazards. The chapters' and subchapters' structure is similar, providing a coherent image for the book. Necessarily, each chapter starts by explaining the formation and physical background of the hazard, followed by an assessment of associated damages and risks and their geographical occurrence. Subsequently, where relevant, the reader gets an overview of existing forecast systems; finally, potential actions for management and mitigation are introduced. The two strongest chapters, covering more than 40% of the 260-page book, are geophysical and hydrological hazards. The dominance of the later is understandable due to the high

[A] University of Szeged, Department of Geoinformatics, Physical and Environmental Geography, 6722 Szeged, Egyetem u. 2-6, Hungary, gysipos@geo.u-szeged.hu,
[B] University of Novi Sad, Department of Geography, Tourism and Hotel Management, Trg Dositeja Obradovića 3, 21000 Novi Sad, Serbia, lazar.lazic@dgt.uns.ac.rs

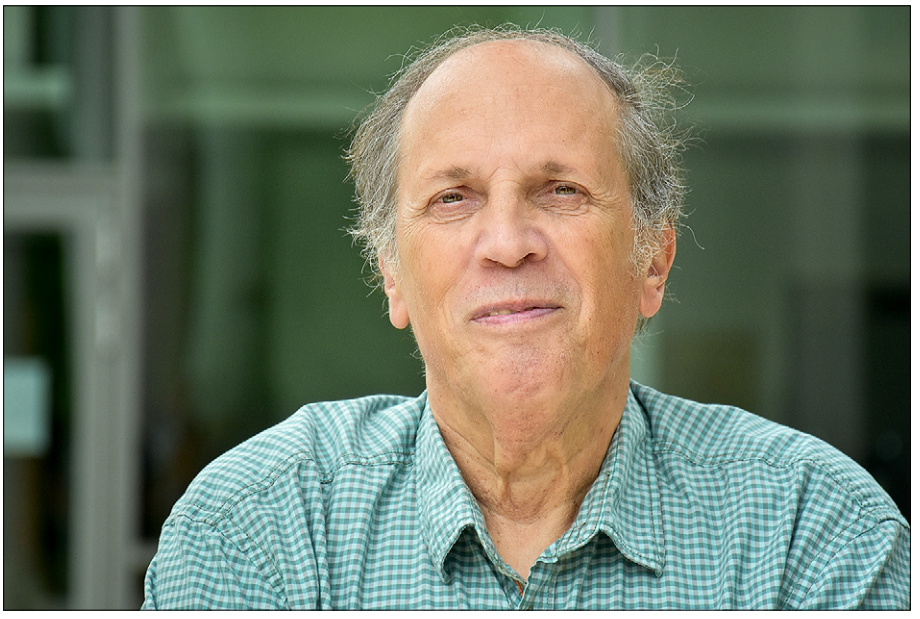

Professor Gábor Mezősi,
former head of the Department of Geoinformatics, Physical and Environmental Geography, and former dean of the Faculty of Sciences and Informatics, University of Szeged

relevance of hydrological hazards in the geographical regions covered by the book and due to the diverse background of the author in this field.

In summary, the book provides a systematic synthesis of natural hazards from both physical and human geographical aspects and, therefore, can serve as a reference textbook for students in geography, environmental sciences and related disciplines. By including a wide collection of hazard-related digitally accessible information, the book can also be a useful resource for professionals and decision-makers.

Finally, a few words on the author himself: Professor Gábor Mezősi, 70, former head of the Department of Geoinformatics, Physical and Environmental Geography, and former dean of the Faculty of Sciences and Informatics, University of Szeged, devoted his life and career to finding and initiating new and relevant directions within Hungarian geographical research. Starting with geomorphology and landscape ecology, he was among the first to apply computer-aided quantitative methods in physical geography in the mid-1980s. As he recognised the growing potential in spatial data analysis, he became one of the pioneers in introducing GIS techniques in Hungary as early as the beginning of the 1990s. Later, he turned to the development and application of complex environmental models to reveal processes in landscape evolution and already emphasised the significance of climate change. From the mid-2000s, he has focused on environmental hazards, conflicts and risks, with special respect to landscape sensitivity and hydrological hazards, such as inland excess water inundations and droughts. More recently, he has dealt with forecasting changes in different elements of the environment at different climate scenarios. The present book, therefore, fits very well to the oeuvre of Professor Mezősi, since it synthetises his broad knowledge and experience in many of his previous research topics. Moreover, this compilation, just as numerous of his previous works, can also be a trend-setting publication for geographical research in the region. Nothing proves this better than the present special issue of Geographica Pannonica, which is, on the one hand, dedicated to him and, on the other hand, attempts to provide a cross-section of the versatile work his colleagues do concerning the assessment of natural hazards.

ISSN 0354-8724 (hard copy) | ISSN 1820-7138 (online)

Pixel and Object-based Land Cover Mapping and Change Detection from 1986 to 2020 for Hungary Using Histogram-based Gradient Boosting Classification Tree Classifier

András Gudmann[A*], László Mucsi[A]

Received: May 06, 2022 | Revised: July 31, 2022 | Accepted: August 10, 2022
doi: 10.5937/gp26-37720

Abstract

The large-scale pixel-based land use/land cover classification is a challenging task, which depends on many circumstances. This study aims to create LULC maps with the nomenclature of Coordination of Information on the Environment (CORINE) Land Cover (CLC) for years when the CLC databases are not available. Furthermore, testing the predicted maps for land use changes in the last 30 years in Hungary. Histogram-based gradient boosting classification tree (HGBCT) classifier was tested at classification. According to the results, the classifier, with the use of texture variance and landscape metrics is capable to generate accurate predicted maps, and the comparison of the predicted maps provides a detailed image of the land use changes.

Keywords: land use; land cover; image classification; change detection; gradient boosting

Introduction

Land use and land cover (LULC) changes can alter the ecosystem and its services, and they can indicate socio-economic changes that have occurred in a particular area (Wulder et al., 2018). By analyzing the LULC changes in detail, we can estimate their complex effects on the environment (impact on landscape structure, biodiversity) and agricultural complexes. With the acceleration of LULC changes that occurred with urban expansion, economic growth, and explicitly/implicitly increasing human needs, the monitoring of LULC changes became a key tool that could be used in work associated with environmental protection and sustainable development. LULC maps are often used as base data in environmental studies conducted in fields such as agriculture (Bezdan et al., 2019), hydrology (Tobak et al., 2019), ecology (Csikós & Szilassi, 2021), urbanization (Steurer & Bayr, 2020), and change detection (Szilassi, 2017). LULC mapping is a widely discussed topic in the field of remote sensing because remote sensing can provide tools, and reliable and extensive data with a high temporal and spatial resolution for LULC mapping (Townshend et al., 1991). It is a challenging classification task, because land use and its categories (nomenclature) depend on the socio-economic environment, thus each country or region will have its own set of land use classes (Choudhury & Jansen, 1999). Thus, the number of land use classes has become large and interclass separability small, which makes training data unbalanced and difficult to classify. Moreover, in most cases, the efficiencies of the spectral values obtained from satellite images are small. Thus, new variables have to

[A] Department of Geoinformatics, Physical and Environmental Geography, University of Szeged, Egyetem utca 2, 6722 Szeged, Hungary; mucsi@geo.u-szeged.hu, gudmandras@geo.u-szeged.hu
[*] Corresponding author: András Gudmann, e-mail: gudmandras@geo.u-szeged.hu

be incorporated into land use classification, which is computationally challenging.

The dataset dimensions (size and number of variables) greatly depend on the scale of mapping and the amount of data used. In large-scale land use mapping, we need to consider the spectral differences among the satellite images and the exponential growth of the dataset as new variables are added, which causes the modeling and prediction times to increase. Therefore, the selection of new data required for land use classification through the application of different sensors in combination (Zhou et al., 2018), use of multitemporal images (Bui & Mucsi, 2021), or extraction of new features (indices, textures, and metrics) from the original image is important (Gudmann et al., 2020; Zhou et al., 2018). In land use change mapping, the use of different sensor data or multitemporal images is not possible in most cases because of the limitations of old datasets. Thus, the only option available is to extract new features, such as spectral indices, texture data, and segmentation from the original satellite images.

In this study, large-scale LULC maps were created on four dates between 1986 and 2020 based on Landsat images, their derivates, and CLC databases. Using these maps, pixel-based change analyses were performed to estimate a detailed picture of the environmental changes that had occurred. Two research questions were tested: first, can we generate LULC maps with CLC nomenclature, accurate enough to use them as a base for a pixel-scale change analysis? Second, if the pixel-scale change analysis is performed based on the generated maps, would the results provide more details than the CLC change layers?

To answer these questions, first, with the use of a histogram-based gradient boosting classification tree, LULC maps were generated. Second, the improvement in land use classification was estimated using pixel-based comparison. Furthermore, pixel-based change detection was performed using the classified maps and the results were compared with the CLC datasets.

Data and methods

Study area

The study area selected was the entire territory of Hungary, located in the Carpathian Basin (Figure 1), with an area of 93 023 km^2. Most of the land area of this east-central European country is occupied by lowlands (more than 80% of the land area is at an elevation between 75 and 200 m above sea level) and only 0.6% of its land area is at an elevation more than 500 m above sea level. The soil in most areas of the country has high organic content, which favors agriculture (Mezősi, 2017). Most of the land area of the country (78.7%) is productive because of its specific soil type and favorable climate, and more than half of the land area (57.1%) is used for agriculture (Hungarian Central Statistical Office, 2020). The agricultural land has a one-sided structure dominated by small holdings (<5 ha in size), which account for more than 80% of the agricultural holdings in the area (European Commission - DG Agriculture and Rural Development, 2020). Most of the landscape of the country

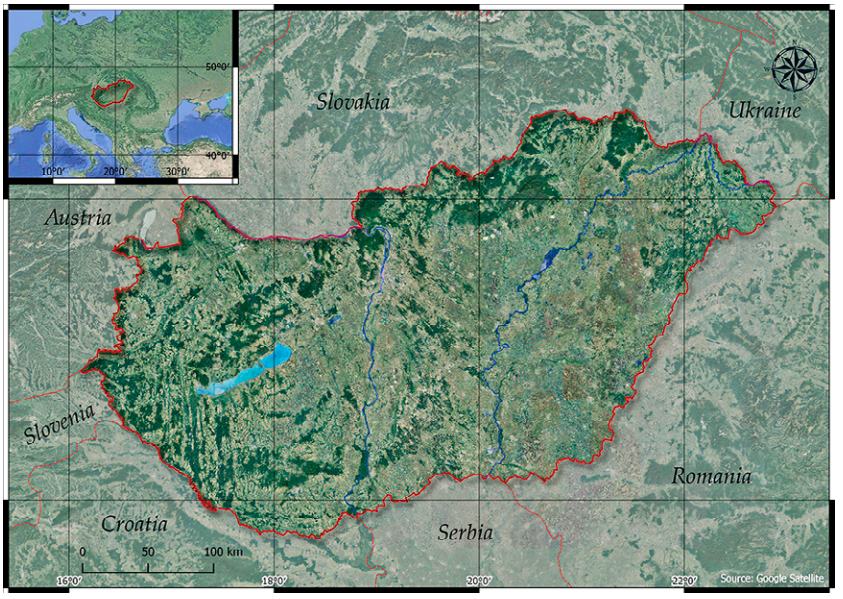

Figure 1. Study area: Hungary in East-Central Europe

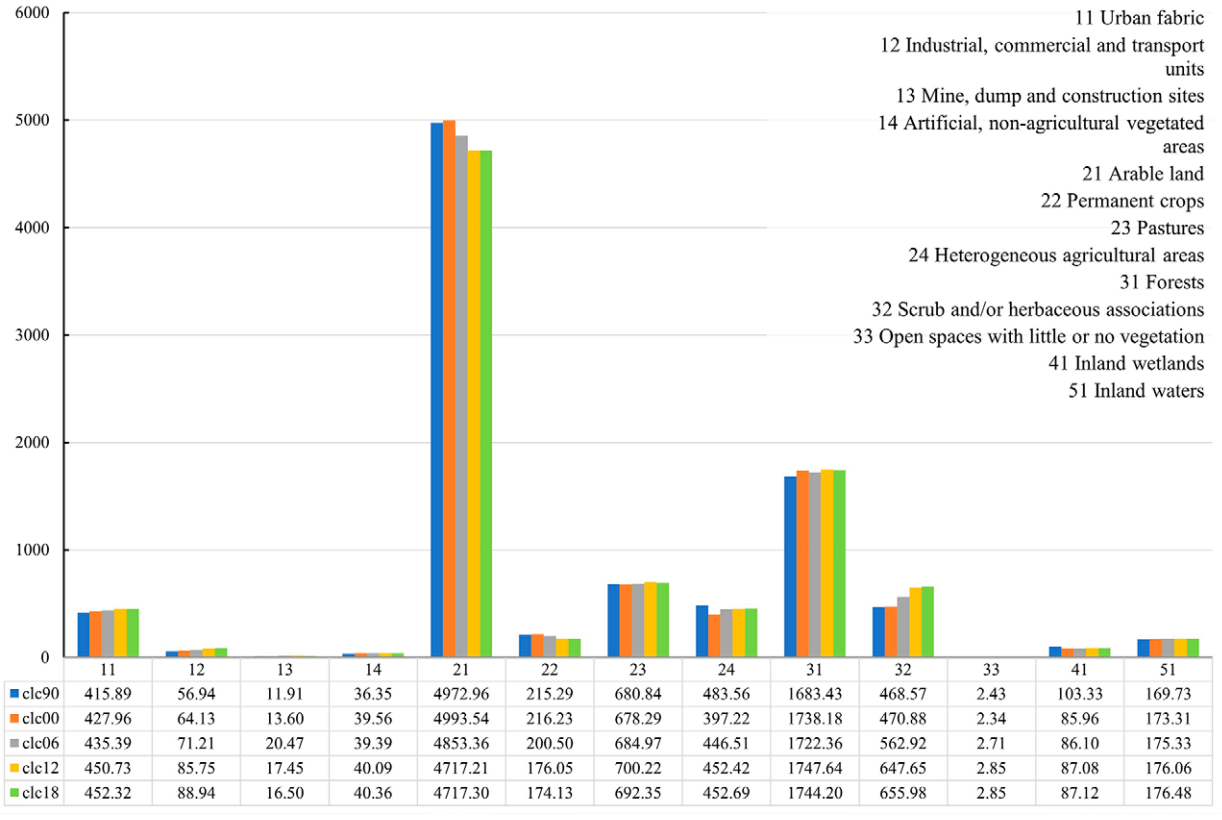

	11	12	13	14	21	22	23	24	31	32	33	41	51
clc90	415.89	56.94	11.91	36.35	4972.96	215.29	680.84	483.56	1683.43	468.57	2.43	103.33	169.73
clc00	427.96	64.13	13.60	39.56	4993.54	216.23	678.29	397.22	1738.18	470.88	2.34	85.96	173.31
clc06	435.39	71.21	20.47	39.39	4853.36	200.50	684.97	446.51	1722.36	562.92	2.71	86.10	175.33
clc12	450.73	85.75	17.45	40.09	4717.21	176.05	700.22	452.42	1747.64	647.65	2.85	87.08	176.06
clc18	452.32	88.94	16.50	40.36	4717.30	174.13	692.35	452.69	1744.20	655.98	2.85	87.12	176.48

Figure 2. Distribution of CLC categories in Hungary in thousand hectares

is fragmented, with low patch sizes, because of its agricultural land structure. According to the CLC databases (Buttner & Kosztra, 2017), more than half of the area of Hungary was covered by arable lands (Figure 2). Besides, the main land cover categories are the forests (~18%), pastures (7%), scrub and/or herbaceous associations (~5-7%), heterogeneous agricultural area (~5%), and urban fabric (~4%).

Data

The reference data of our study was the CORINE Land Cover datasets. These databases were created using a 1:100 000 scale, a minimum mapping unit (MMU) of 25 ha, and a minimum width of 100 m for the linear elements (Mari & Mattányi, 2002). The nomenclature of CLC data is hierarchically structured, with three levels: 5 classes at level 1, 15 classes at level 2, and 44 classes at level 3. Thanks to the detailed nomenclature, spatial (CLC90: 27 countries; CLC18: 39 countries) and temporal coverage (from 1990, five times), and thematic accuracy (>85%), the CLC database is the basis of various research activities. To provide further support to these studies, change layers were created and the changes exceeding 5 ha were mapped. Even with a small MMU, the change layers could not display most of the changes that had occurred at the parcel level because the average size of those changes was below 5 ha (Volker et al., 1998) (Figure 3). In this study, the CLC datasets CLC90, CLC00, CLC06, CLC12, and CLC18 were used as reference datasets in land use classification. The CLC change layer was used as the reference in the change analysis. The CLC databases were downloaded from the website of the Copernicus Land Monitoring Service at https://land.copernicus.eu/pan-european/corine-land-cover.

For the study, Landsat satellite images were selected, because of the similarity of their spatial and spectral resolutions. The data acquisition devices provided in the satellites are designed to take images, comparable to one another, to facilitate data continuity and time-series analyses (Wulder et al., 2016). The Landsat images have a medium spatial resolution (30, 60, and 80 m), multispectral resolution (4–11 bands), and a 16-day temporal resolution (U.S.Geological Survey, 2012). The image archive has global coverage and is freely available to any user (Wulder et al., 2019). Ten Landsat images were required to cover the study area, with low cloud cover and low temporal differences, which reduced the spectral image differences. According to these conditions, 4 dates were selected, with a large time interval: 1986, 2003, 2015, and 2020. The atmospherically corrected Landsat images with surface reflectance were ordered and downloaded from the USGS Earth Resources Observation and Science Center Science Processing Architecture system on-demand interface, available at https://espa.cr.usgs.gov/.

Figure 3. Parcel-level changes in an agricultural area, near Nagyszénás village. Based on the CLC polygons (yellow lines), no change occurred

Derivatives describing the pixel neighborhood were calculated using the satellite images to provide the information required by the classification model. Two types of derivatives were generated: variance texture information with different kernel sizes (7x7, 17x17) and landscape metrics (the mean patch size, the total edge, mean shape index, and mean fractal dimension).

Methods

Data processing was conducted using ERDAS Imagine 2020, QGIS 3.4.4, and ArcMap 10.3 software, and the classifications were performed in a Python 3.7 programming environment (Figure 5). To reduce the loss of accuracy due to spectral differences, the Landsat images (10 images per date) were mosaicked along the same path (according to the WRS-2 catalogue, 4 paths: 189, 188, 187, 186). The images along the paths (i.e., zones) were put together using manually drawn seamline polygons (Figure 4). These zones were the base areas of the classification. The created mosaics were used for texture and landscape metric calculations. For each band, texture images were generated using variance metric and two different kernel sizes: 7 × 7 (210 × 210 m) and 17 × 17 (510 × 510 m) with ERDAS built-in texture calculator. For the landscape metrics, each satellite mosaics were segmented at a minimal size of 25 ha, and

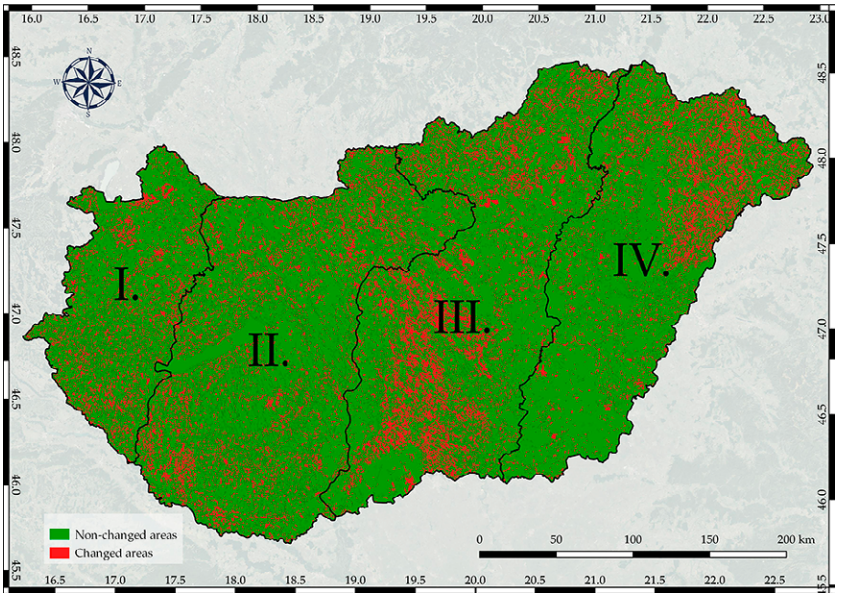

Figure 4. The four zone and the changed/non-changed areas

the metrics were calculated using the V-Late 2 ArcGIS tool (Comber et al., 2000). The six spectral bands (B, G, R, NIR, SWIR 1, and SWIR 2), texture bands, and landscape metrics of the satellite images were stacked together to generate images with 22 layers.

The CLC datasets were processed to identify the areas that have not changed over the last 30 years, in order to reduce the uncertainty (<=15%) of the points from the CLC reference data. To this end, all CLC datasets were intersected with one another, and the polygons with the same CLC code were selected. These unchanged areas are 81.1% of the whole area, thus they are capable to represent the whole study area (Figure 4). The selected polygons were exported and were split into four parts like the stacked images (Figure 4). For each part, training and validation point sets were generated inside the selected polygons. The validation points were generated around the polygons' centroids, while the training points are randomly inside the polygons. The number of training points is less than 2% of the whole area.

From the training and validation points, 20 points per class per set were randomly selected and visually checked based on medium- and high-resolution satellite images and high-resolution aerial images at all dates. The result of the points verification showed all CLC categories reached the CLC base thematic accuracy, thanks to the use of the non-changed areas. The mean accuracy of the training points, on one date is greater than 93% (lowest, 2020: 93.7%, highest, 1986: 95.18%), while the validation points' mean accuracy is greater than 97% (lowest, 2020: 97.59%, highest, 1986: 98.89%).

Using the point sets created the values of each band of the stacked images and the codes of the CLC databases were extracted and exported to the csv files. For each date and each part of the study area, one training and one validation file was created. These csv files were used in the HGBCT classification python script. The HGBCT is a type of gradient boosting machine (GBM) (Friedman, 2001). It is an ensemble machine learning method, which can use different base learners (decision trees and neural networks) for classification or regression tasks. The GBM builds the model in a forward stage-wise mode, which allows for the optimization of an arbitrary differentiable loss function (Friedman, 2002). The HGBCT displays high accuracy when used with big datasets, is robust in handling missing values and unbalanced datasets, and has a low model building and prediction times. The classification method was implemented using the grid-search parameter estimation (or hypertuning) method to estimate the best parameters that can be used in model building. For each zone, different models were built.

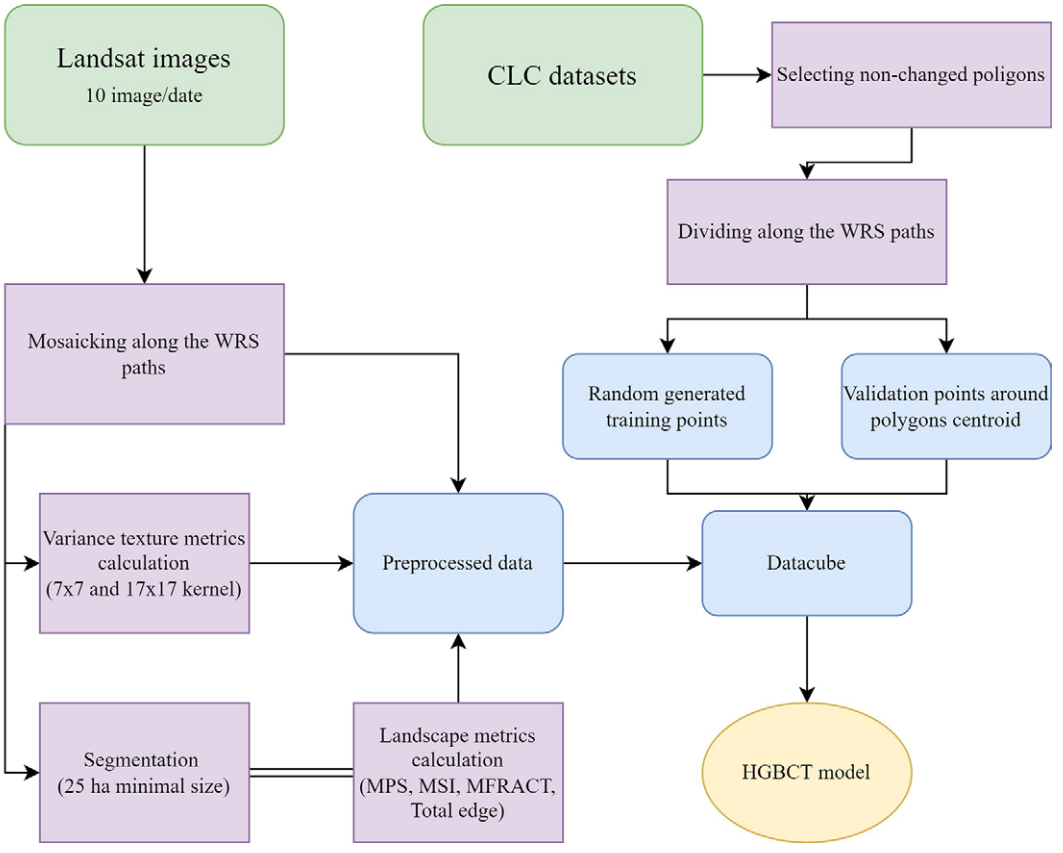

Figure 5. Data processing workflow

Results

Modeling and mapping

During the modeling and mapping stage, the HGBCT classification method was applied and tested. The test model building, and predictions were made using the training and validation sets of the datasets collected on different date's datasets. As a result of hypertuning, the following hyperparameters of HGBCT enabled its highest accuracy: maximum number of iterations: 1200 with early stopping applied, learning rate: 0.01, maximum depth of each tree: 20; minimum number of samples per leaf: 75, and maximum number of leaves allowed for each tree: 256. During model building, different values were observed, like overall accuracy (OVRA), kappa, and logarithmic loss. The overall accuracies of the gradient boosting models were between 83.35% (2015: Zone II.) – 92.63% (1986: Zone I.). The User's accuracies (UAs) of the classifier were varied between 61.79% and 100%, 60.30% and 100%, 60.61% and 100%, and 62.30% and 100% in 1986, 2003, 2015, and 2020, respectively. More than half the classes (15 of 27) had UAs exceeding 90% and none of the classes had UAs below 60%. Only one class, the originally mixed, 242–Complex cultivation patterns, had a UA near 60%. The PAs were in the 56.49%–99.69%, 56.34%–99.85%, 53.86%–100%, and 51.19%–100% ranges in 1986, 2003, 2015, and 2020, respectively. Most of the Producer's accuracies (PAs) had high accuracies as the UAs, with 17 of the 27 classes recording accuracies higher than 90%. Only the "Non-irrigated arable land" class has a low accuracy (51.19%–56.49%), it deserves to be highlighted because it has the largest extent in the study area thus, it has a huge impact on change mapping. The average overall accuracy of the models per date was between a small range of 85.99% – 87.33%. The kappa values of the models varied between 0.83 and 0.92, while the log loss values were be-

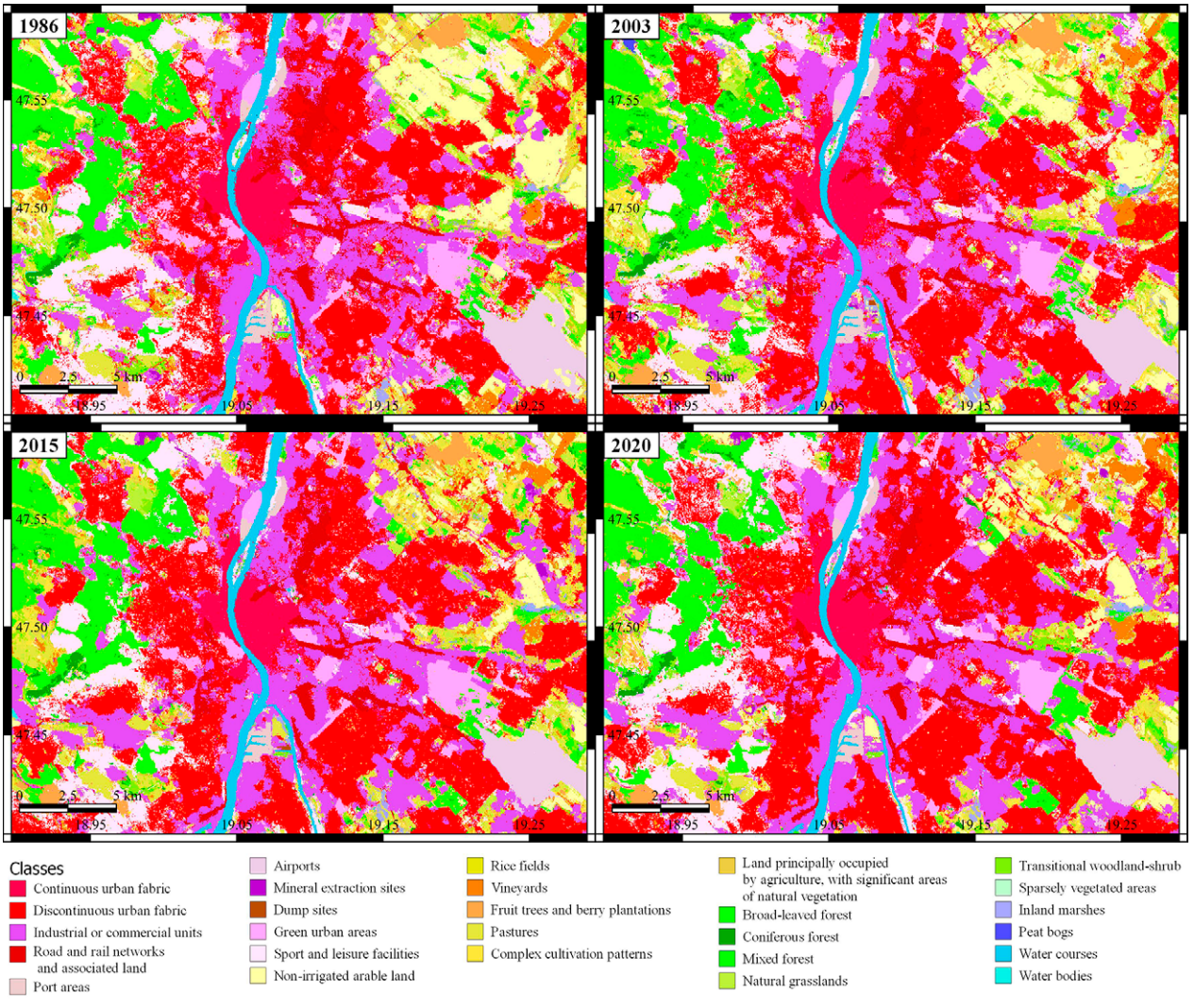

Figure 6. Classified maps of Budapest, the capital of Hungary, at different date

tween 0.26 and 0.56. The appearances of the classified maps are compact and smooth (Figure 6). The different values of the model building indicate that all models were suitable for accurate land use classification.

Land use change analysis

Land use change mapping was performed using a pixel-based comparison of the predicted maps of the HG-BCT models. The maps were compared, and three land use change maps were generated (1986–2003, 2003–2015, and 2015–2020). Using these maps, land use change matrixes were created and the changes were categorized into six groups based on the work of Feranec (Feranec et al., 2010). The six groups are urbanization, agricultural intensification, agricultural extensification, afforestation, deforestation, and water body construction. This categorization includes permanent and temporary land use changes, thereby enabling short- and long-time series analyses. However, the magnitude of the detected changes could be large. The first period of the changes is between 1986-2003. During this period, the socialist system has replaced, and the economy drastically changed. The most spectacular sign of these changes was the fragmentation of agricultural land, due to compensations and privatization. According to the CLC change layer, the magnitude of the mean yearly area transformation was 0.497% (1990–2000) (Table 1).

The biggest mean yearly changes were afforestation and deforestation, where the afforestation had a bigger magnitude, thus the proportion of the forest increased. Besides, the intensification and extensification of agriculture had a similar value, with notable magnitude. According to the comparison of the predicted maps, the magnitude of changes was apparently larger than what the CLC change layer displayed (Table 2).

Unlike, the CLC change layers, the biggest change was in agriculture (intensification and extensification), where intensification had a clearly bigger role. Like at CLC change layers, the afforestation and deforestation had a big magnitude, but the difference between the two opposite processes was much bigger. Furthermore, the urbanization process was clearly more serious, than the values of the CLC. The second period was between 2003-2015. During this period, the driving force of the changes was Hungary's accession to the EU, the responsibilities associated with it, and the significant subsidies for different projects. Due to this, the image of the production of Hungary had changed, which brought with it a change in land use/land cover. In the middle of the period, because of the economic crisis, the changes slowed down. However, after the recovery, large-scale industrial and public investment began. In this period, financially supported afforestation began. Despite this, the CLC change layers show only a slight change in the magnitude of the afforestation and a strong decrease in deforestation, while the agricultural changes remained significant, and accelerated. Besides, the rate of urbanization was slightly increased, and the water body construction was decreased. According to the predicted maps, the magnitude of the agriculture (intensification and exten-

Table 1. Mean yearly categorized land use changes, based on CLC change maps

Date	1990–2000	2006–2012	2012–2018
Urbanization	0.0112%	0.0176%	0.0151%
Intensification of agriculture	0.0804%	0.1305%	0.042%
Extensification of agriculture	0.0728%	0.0865%	0.0215%
Afforestation	0.1815%	0.1831%	0.0938%
Deforestation	0.1465%	0.0948%	0.0848%
Water body construction	0.0052%	0.0035%	0.0023%
Total change	0.497%	0.516%	0.259%

Table 2. Mean yearly categorized land use changes, based on the predicted change maps

Date	1986–2003	2003–2015	2015–2020
Urbanization	0.184%	0.323%	0.71%
Intensification of agriculture	0.632%	0.866%	2.162%
Extensification of agriculture	0.428%	0.609%	1.424%
Afforestation	0.345%	0.538%	1.264%
Deforestation	0.178%	0.247%	0.726%
Water body construction	0.035%	0.061%	0.128 %
Total change	1.802%	2.643%	6.414%

sification) changes was increased, compared to the previous period. Furthermore, the rate of afforestation had increased, and thus twice as much as deforestation. In addition, the rate of urbanization increased by 0.134%/year. These results are in line with the economic measures introduced. The last period was only 5 years, between 2015-2020. During these 5 years, the large public investments continued and began the growth of the housing sector. Furthermore, the financially supported afforestation continued with greater magnitude. These events are well discernible from the predicted map values. In this short time range, the urbanization, the afforestation, the deforestation, and the water body construction processes were accelerated, and thus their values were doubled. While, agricultural changes remained the causes of the biggest impact, with a significant increase. On contrary to that, the CLC change layers show slowing changes. The rate of afforestation was halved, while the rate of the intensification of agriculture showed a bigger decrease. Besides, the extensification of agriculture decreased substantially. In the other categories, the magnitude of the slowing was small. In conclusion, at the CORINE Land Cover change layers, the magnitude of the area transformation can be between 0.497%/year (1990–2000), 0.516%/year (2006-2012), and 0.259%/year (2012–2018) of the total area, with a decreasing rate. The main change flows are afforestation and deforestation and the transition of agricultural lands. Considering deforestation, afforestation would have the largest impact on an area. The transitions of the agricultural lands had a big impact in the first and second periods, while in the third period it had a small impact. Urbanization had a moderate impact on the changes in every period. The water body construction had the smallest volume, with a continuous decrease. While, according to the results of pixel-based analysis of the predicted maps, the magnitude of changes was apparently larger than what the CLC change layer displayed (1.802%/year – 6.414%/year). The urbanization was between 0.184%/year and 0.71%/year, which is significantly bigger, than the CLC values. The transformation of the agricultural lands dominates agricultural intensification, which is approximately one and half times the magnitude of extensification. These values are more than hundred times bigger than the values of the CLC change layers. The afforestation is almost twice deforestation, and thus, the size of the forests is on the increase, in the same way as the CLC layers, but the magnitude of these changes is bigger. The rate of water body construction is low and is the smallest of all, but with continuous increase. Apart from these change categories, some uncategorized changes also exist, but their magnitudes are low. Thus, they were not included in this study. The magnitude of the changes detected is large, because of the pixel level scale used. Using pixel-based categorization, permanent and temporary changes can be predicted. Most of these changes are temporary, and they appear in turns in a particular area, such as agricultural intensification and extensification or afforestation and deforestation. Further information can be obtained by visually analyzing the maps. The visual analysis of the maps helps determine the localization and the level of permanency of the changes. According to the analysis results, most changes were not permanent and were due to the behavior of the economy (cutting and replanting artificial forests, setting aside arable land, and crop rotation). Urbanization and afforestation are two permanent changes. Urbanization is a one-way change (as mentioned earlier) and thus, it is permanent. It appears mainly in and around the main cities of Hungary. Afforestation is not a permanent transformation, but if afforestation is higher than deforestation in magnitude, a permanent change has occurred. According to the results of the visual analysis, permanent afforestation is concentrated mainly in agricultural areas in the Great Hungarian and Little Hungarian Plains. These permanent changes reduce the size of agricultural land, and explains the rate of agricultural intensification. Overall, the land use change maps created provide detailed information about land use transformations in Hungary that have occurred over the last 30 years, which were dominated by agricultural intensification, afforestation, and gradual and slow urbanization.

Discussion

This study aimed to test a possible classification method, to create large-scale LULC maps on 4 dates. Furthermore, we tested these predicted maps in a large-scale, pixel-based change analysis. In the presented method, we used the HGBCT classifier to create maps, based on Landsat imagery with landscape metrics and texture data. By considering the predicted map, land use change analysis was performed, which matched the CLC change layers. The land use change mapping method presented meets the preliminary expectations.

Many studies have focused on land use/land cover classification in different scenarios. McCarty et al. compared three different algorithms (random forest, SVM, and light GBM) for large-scale land use mapping (McCarty et al., 2020). In their classification sce-

nario, seven classes were targeted, and the light GBM had the highest overall accuracy (65.3%) and random forest had the lowest overall efficiency (59.4%). Malinowski et al. created an automated CLC mapping method using the random forest classifier and a modified nomenclature, which had only 13 classes (Malinowski et al., 2020). Using this method, they could successfully create land use maps for the whole area of Europe, with an overall accuracy of 86.1% at the continental level. A very similar study to our research wasmade by Marco Calder 'on-Loor et al. (Calderón-Loor et al., 2021). They made a land cover/use mapping and change analysis for Australia from 1985 to 2015, with 5-year steps. They used Google Earth Engine to process a high amount of Landsat images (>200 000) to create composite images. They classified the preprocessed images into six land cover classes with a random forest model. With this high number of images and a low number of classes they reach a very high accuracy (<93%) and made a satisfactory change analysis. A global land cover map made by Karra et al. (Karra et al., 2021). They created land use maps with the use of Sentinel-2 images and hand-labeled reference datasets, which contains 10 classes. For classification purposes, they utilized a UNet neural network for image segmentation and to classify the segments. The results showed, the usefulness of the UNet network at land cover classification, where every class reached >85% accuracy. These surveys are showing very good results at large-scale classification, but the applied nomenclatures were mainly limited to land cover classes.

The results of our presented method show a significant progress. In our classification scenarios, we used more than 20 classes with low separability values and big monotemporal datasets. Despite the use of this difficult scenario, the HGBCT classifier achieved satisfactory results (83.35%–92.63%). The other model-performance metrics, such as log loss and kappa, show corresponding results. Furthermore, the UAs and PAs of the models were high, only the class 211–Non-irrigated arable land, which has the largest extent, obtains a low PA. This low PA can occur for reasons such as training point randomness, class mixture caused by the CLC's MMU, and combination of the pixel-based mapping unit and an accurate model. As most of these reasons cannot be eliminated, the problem could occur in every setting of the method. According to these results, our predicted map was suitable for change mapping. Land use change mapping is difficult to evaluate because the relevant databases would have been created using different methodologies (nomenclatures, MMUs, and reference data). In this study, land use change maps were created at the pixel level (900 m^2) using the CLC nomenclature. The CLC change layers and the predicted change maps were comparable. However, the two datasets have different time-range, which slightly distorts the comparison. Besides, the MMUs of the two datasets were different (CLC change layers had 5-ha changes). Thus, the predicted maps had more details and larger values in certain categories than the CLC change layers, and their range of statistics was much larger. This difference could be attributed to the magnitudes of the changes, which were much bigger in the predicted maps (1.802%/year – 6.414%/year) than in the CLC change layers (0.259%/year – 0.516%/year). The MMU had a large impact on the analysis because the majority of the changes occurred in small and separate areas; thus, they are not shown in CLC change layers and may not be permanent, which is true especially in agriculture in which are many small parcels. These temporary, likely parcel-level, agricultural changes are responsible for approximately half of the changes. Overall, the predicted maps contain both permanent and temporary changes and thus provide a detailed picture of the land use changes in the country. Thus, the maps can be used in detailed surveys.

Conclusion

The large-scale land use mapping contains several difficulties: available data sources, size of the data, nomenclature, etc. Our study demonstrated a possible solution, where we created LULC maps with the combined use of spectral bands, and variance texture data landscape metrics. According to the study findings, with the aforementioned information, when used as input layers in classification, we predicted maps with high accuracy (83.35%–92.63%). Land use change maps were created by comparing the land use maps at pixel-level, that were created. The created maps contain details of permanent and temporary changes, and are, therefore, adequate for the various types of analyses. The results revealed that more studies using carefully chosen training points are required to examine the impact of training point selection, and the importance of the MMU of the reference data. Moreover, using different change categorizations, detailed change flows would become observable.

Acknowledgments

This research was supported by National Scientific Research Funds (Hungary) in support of the ongoing research: 'Time series analysis of land cover dynamics using medium- and high-resolution satellite images' (NKFIH 124648K) at the Department of Geoinformatics, Physical and Environmental Geography of the University of Szeged. This research was supported by the Ministry of Innovation and Technology of Hungary from the National Research, Development and Innovation Fund, financed under the TKP2021-NVA-09 project number.

References

Bezdan, A., Vranešević, M., Blagojević, B., Pejić, B., Bezdan, J., Milić, D., Tica, N., & Zekić, V. (2019). Agricultural Drought Risk Assessment in Vojvodina. In Z. Ladányi & V. Blanka (Eds.), *Monitoring, risks and management of drought and inland excess water in South Hungary and Vojvodina* (pp. 226–239). University of Szeged Department of Physical Geography and Geoinformatics Projekt.

Bui, D. H., & Mucsi, L. (2021). From Land Cover Map to Land Use Map: A Combined Pixel-Based and Object-Based Approach Using Multi-Temporal Landsat Data, a Random Forest Classifier, and Decision Rules. *Remote Sensing*, 13(9), 1700. https://doi.org/10.3390/rs13091700

Buttner, G., & Kosztra, B. (2017). CLC2018 *Technical Guidelines*.

Calderón-Loor, M., Hadjikakou, M., & Bryan, B. A. (2021). High-resolution wall-to-wall land-cover mapping and land change assessment for Australia from 1985 to 2015. *Remote Sensing of Environment*, 252, 112148. https://doi.org/10.1016/j.rse.2020.112148

Choudhury, K., & Jansen, L. (1999). T*erminology for Integrated Resources Planning and Management*.

Comber, A. J., Birnie, R. V., & Hodgson, M. (2000). Using landscape metrics to model land cover change. In T. Clare & D. Howard (Eds.), *9th annual conference of the international-association-for-landscape ecology* (pp. 143–161). Proceedings of the International Association of Landscape Ecology (UK) Conference: Quantitative approaches to Landscape Ecology.

Csikós, N., & Szilassi, P. (2021). Modelling the Impacts of Habitat Changes on the Population Density of Eurasian Skylark (Alauda arvensis) Based on Its Landscape Preferences. *Land*, 10(3), 306. https://doi.org/10.3390/land10030306

European Commission - DG Agriculture and Rural Development, F. E. U. (2020). *Statistical Factsheet - Hungary*.

Feranec, J., Jaffrain, G., Soukup, T., & Hazeu, G. (2010). Determining changes and flows in European landscapes 1990–2000 using CORINE land cover data. *Applied Geography*, 30(1), 19–35. https://doi.org/10.1016/j.apgeog.2009.07.003

Friedman, J. (2001). Greedy Function Approximation: A Gradient Boosting Machine. *Annals of Statistics*, 29, 1189–1232. https://doi.org/10.2307/2699986

Friedman, J. (2002). Stochastic Gradient Boosting. *Computational Statistics & Data Analysis*, 38, 367–378. https://doi.org/10.1016/S0167-9473(01)00065-2

Gudmann, A., Csikós, N., Szilassi, P., & Mucsi, L. (2020). Improvement in Satellite Image-Based Land Cover Classification with Landscape Metrics. *Remote Sensing*, 12(21), 3580. https://doi.org/10.3390/rs12213580

Hungarian Central Statistical Office. (2020). *Statistical Pocketbook of Hungary, 2019* (V. G. Dr. Bódiné (ed.)). Hungarian Central Statistical Office.

Karra, K., Kontgis, C., Statman-Weil, Z., Mazzariello, J. C., Mathis, M., & Brumby, S. P. (2021). GLOBAL LAND USE/LAND COVER WITH SENTINEL 2 AND DEEP LEARNING. *International Geoscience and Remote Sensing Symposium (IGARSS), 2021-July*, 4704–4707. https://doi.org/10.1109/IGARSS47720.2021.9553499

Malinowski, R., Lewiński, S., Rybicki, M., Gromny, E., Jenerowicz, M., Krupiński, M., Nowakowski, A., Wojtkowski, C., Krupiński, M., Krätzschmar, E., & Schauer, P. (2020). Automated Production of a Land Cover/Use Map of Europe Based on Sentinel-2 Imagery. *Remote Sensing*, 12(21), 3523. https://doi.org/10.3390/rs12213523

Mari, L., & Mattányi, Z. (2002). Egységes európai felszínborítási adatbázis a CORINE Land Cover program (A uniform european land cover database the CORINE Land Cover program). *Földrajzi Közlemények*, 76 (50), 31–38.

McCarty, D. A., Kim, H. W., & Lee, H. K. (2020). Evaluation of Light Gradient Boosted Machine Learning Technique in Large Scale Land Use and Land Cover Classification. *Environments*, 7(10), 84. https://doi.org/10.3390/environments7100084

Mezősi, G. (2017). *The Physical Geography of Hungary*. Springer International Publishing.

Steurer, M., & Bayr, C. (2020). Measuring urban sprawl using land use data. *Land Use Policy*, 97, 104799. https://doi.org/10.1016/j.landusepol.2020.104799

Szilassi, P. (2017). Land cover variability and the changes of land cover pattern in landscape units of Hungary. *Journal of Landscape Ecology*, 15, 131–138.

Tobak, Z., Leeuwen van, B., Kovács, F., & Szatmári, J. (2019). High precision mapping and monitoring of inland excess water inundations. In Z. Ladányi & V. Blanka (Eds.), *Monitoring, risks and management of drought and inland excess water in South Hungary and Vojvodina* (pp. 13–23). University of Szeged Department of Physical Geography and Geoinformatics.

Townshend, J., Justice, C., Li, W., Gurney, C., & McManus, J. (1991). Global land cover classification by remote sensing: present capabilities and future possibilities. *Remote Sensing of Environment*, 35(2), 243–255. https://doi.org/10.1016/0034-4257(91)90016-Y

U.S.Geological Survey. (2012). Landsat: A global land-imaging mission. In *Fact Sheet*. https://doi.org/10.3133/fs20123072

Volker, A., Mezősi, G., & Mucsi, L. (1998). Die Pußta. Historisch-geographische und geoökologische Aspekte eines schulgeographischen und touristischen Leitbildes von Ungarn in Ungarn. In *Natur - Raum - Geselschaft* (pp. 175-217.). Johann Wolfgang Goethe-Universität Frankfurt.

Wulder, M. A., Coops, N. C., Roy, D. P., White, J. C., & Hermosilla, T. (2018). Land cover 2.0. *International Journal of Remote Sensing*, 39(12), 4254–4284. https://doi.org/10.1080/01431161.2018.1452075

Wulder, M. A., Loveland, T. R., Roy, D. P., Crawford, C. J., Masek, J. G., Woodcock, C. E., Allen, R. G., Anderson, M. C., Belward, A. S., Cohen, W. B., Dwyer, J., Erb, A., Gao, F., Griffiths, P., Helder, D., Hermosilla, T., Hipple, J. D., Hostert, P., Hughes, M. J., … Zhu, Z. (2019). Current status of Landsat program, science, and applications. *Remote Sensing of Environment*, 225, 127–147. https://doi.org/10.1016/j.rse.2019.02.015

Wulder, M. A., White, J. C., Loveland, T. R., Woodcock, C. E., Belward, A. S., Cohen, W. B., Fosnight, E. A., Shaw, J., Masek, J. G., & Roy, D. P. (2016). The global Landsat archive: Status, consolidation, and direction. *Remote Sensing of Environment*, 185, 271–283. https://doi.org/10.1016/j.rse.2015.11.032

Zhou, T., Li, Z., & Pan, J. (2018). Multi-Feature Classification of Multi-Sensor Satellite Imagery Based on Dual-Polarimetric Sentinel-1A, Landsat-8 OLI, and Hyperion Images for Urban Land-Cover Classification. *Sensors*, 18(2), 373. https://doi.org/10.3390/s18020373

ISSN 0354-8724 (hard copy) | ISSN 1820-7138 (online)

Towards an Understanding of the Geographical Background of Plants Invasion as a Natural Hazard: a Case Study in Hungary

Péter Szilassi[A*], Georgina Veronika Visztra[A], Anna Soóky[B], Zoltán Bátori[B], Alida Anna Hábenczyus[B], Kata Frei[B], Csaba Tölgyesi[B], Márton Bence Balogh[A]

Received: May 06, 2022 | Revised: July 31, 2022 | Accepted: August 10, 2022
doi: 10.5937/gp26-37866

Abstract

Biological invasion is a worldwide phenomenon that can be considered a natural hazard. Protection against invasive plant species can only be successful if we know the anthropogenic factors that influence their occurrence, such as changes in land cover. In our study, we investigated the LUCAS based spatial distribution of five common invasive plant species (2015) and its connections with the recent (2012-2018) land CORINE based cover changes. The LUCAS points infected with this species are much closer to the CORINE land cover change polygons than the non-infected points. Our results suggest that the occurrence of *Asclepias syriaca*, *Solidago* spp, *Ailanthus altissima* and *Robinia pseudoacacia* is significantly dependent on whether land use has changed in the vicinity of LUCAS points infected with these species. Only the occurrence of *Elaeagnus angustifolia* does not show any correlation with changes in land cover.

Keywords: land use change; biological invasion; natural risk; vegetation naturalness; anthropogenic processes

Introduction

Biological invasion is one of the greatest environmental challenges of our days and a geographical hazard with significant health and economic impacts (Kleinbauer et al., 2010; Genovesi & Monaco, 2014; Kézdy et al., 2018). Biological invasion is an environmental risk that has been accelerating in recent decades. Globalisation processes (e.g. international trade and transport of goods) allow plant and animal species to move easily from one continent to another. These moving species can be more successful than the native vegetation in the new geographical context. In addition to global market processes, climate change may also accelerate the spread of certain invasive plant species and the decline of biodiversity (Hulme, 2021; Manzoor et al., 2021). Biological invasion is therefore a spatial process that poses a significant environmental risk, and only a holistic approach, which is offered by geography can be successful to understand its consequences (Kitka & Szilassi, 2016; Szilassi et al., 2019; Szilassi et al., 2021). Exploring the causes of biological invasion using spatial methods (e.g. GIS-based spatial statistical analyses) can bring us closer to understanding the natural and anthropo-

[A] Department of Geoinformatics, Physical and Environmental Geography, University of Szeged, Egyetem utca 2, H-6722 Szeged, Hungary; myosotis.sylvatica12@gmail.com; balogh.marton.bence@gmail.com
[B] Department of Ecology, University of Szeged, Közép fasor 52, H-6726 Szeged, Hungary; sookyanna001@gmail.com; zbatory@gmail.com; alidaanna@gmail.com; freikata98@gmail.com; festuca7@yahoo.com
[*] Corresponding author: Péter Szilassi; e-mail: toto@geo.u-szeged.hu

genic processes that drive the spread of invasive species worldwide (Mezősi et al., 2014; Mezősi, 2022).

The five invasive plant species- tree of heaven (*Ailanthus altissima*), common milkweed (*Asclepias syriaca*), Russian olive (*Elaeagnus angustifolia*), black locust (*Robinia pseudoacacia*), Goldenrods (*Solidago* spp.)- we have studied are spread extensively across the Eurasian continent (Pyšek et al., 2009).

Ailanthus altissima has been popularly planted in cities, but in addition to completely infesting cities and other degraded areas, it also infests natural communities. Many parts of *Ailanthus altissima* contain allelopathic substances that inhibit the growth of other plants (Mihály & Botta-Dukát, 2004).

Asclepias syriaca is a plant of disturbed habitats and can prevent the regeneration of semi-natural communities in the areas it occupies. The spread of *Asclepias syriaca* in sandy grasslands has resulted in a significant reduction in the cover of native species, especially those with low competitive ability (Kelemen et al., 2016).

Elaeagnus angustifolia prefers saline soils, so it was planted in Hungary to bind sandy areas and to cover saline soils. In addition, it was also planted along motorways and at the edge of forests (Bartha & Csiszár 2012; Lundgren et al., 2004). In the case of infestation of open habitats, it crowds out light-demanding species, thereby reducing species richness (Csiszár, 2012).

Robinia pseudoacacia has been planted for a long time in Hungary for a wide range of purposes almost everywhere. Where it has been planted or spontaneously established, it is quite difficult to remove, as it spreads well from rootstocks and its seeds germinate for a very long time. *Robinia pseudoacacia* induces nitrogen enrichment in the soil (as does Elaeagnus angustifolia), thus facilitating the establishment of nitrogen-favouring weeds, in addition, similar to *Ailanthus angustifolia*, it releases allelopathic substances (Kleinbauer et al., 2010).

Solidago spp. also spreads rapidly and aggressively and they produce pollen which is harmful to human health (Csiszár et al., 2020; Mihály & Botta-Dukát, 2004).

About 3% of the Hungarian flora (approximately 70 species) are invasive weed species (Mihály & Botta-Dukát, 2004). The European Union's list of the most dangerous invasive species with the highest risk of spreading includes 24 terrestrial plant species (DAISE, 2009).

Some of the geographic factors determining the occurrence of invasive plants are related to physical geography, while others are related to human activities. In our previous publications, we have shown that anthropogenic factors such as linear transport infrastructure (road and rail networks), surface water courses and ecological networks can facilitate the migration of some invasive plant species (Szilassi et al., 2021). In this paper, we investigate the relationship between the distribution data of five invasive plant species - widespread in Hungary and throughout the Eurasian continent - and changes in land cover within the whole territory of Hungary (another process of typically anthropogenic origin) (Csiszár et al., 2020). Our basic hypothesis is that land cover changes may facilitate the spread of many invasive plant species. In many cases, changes in land cover (e.g. deforestation, road construction) disturb natural and semi-natural ecosystems, and these disturbed - often barren - areas are more successfully and rapidly invaded by invasive species than by native plant species (Kálmán, 2014). In addition, changes in land cover are often associated with changes in soil characteristics, light conditions and microclimate (Csontos et al., 2009; DAISE, 2009; Dukes, 2004; Follak et al. 2021; Pyšek et al., 2009).

Here we compared the Euclidean distances between the invaded and uninvaded points of the five invasive plants and the nearest polygons of the land cover on a national-scale in Hungary. The aim of our research is to answer, how changes in land cover influence the occurrence of the five invasive species?

Materials and methods

Study area

Our investigations were conducted in Hungary. The country has a humid continental climate in Central Europe. The average annual temperature is 10.5 °C and the average annual precipitation is 550 mm. Climate change increases weather extremes, with a high probability of summer drought. The lowland areas of the Carpathian Basin are characterised by high soil fertility (mainly chernozem soils) (Dövényi et al., 2008). Arable land is the dominant land use type (about 50%). The proportion of the forested areas is 21% in Hungary, however, *Robinia pseudoacacia* has a considerable proportion, accounting for about 5% of the total area of the country. Biological invasions have severely damaged natural or semi-natural habitats about 13.1% of these habitats being invaded by alien species (Csiszár et al., 2020). In Hungary, the main types of land cover change are the loss of grassland due to the increase in artifical surfaces and forest cover, and the land abandonment in areas of lower soil fertility (Bíró et al., 2013,a,b).

Digital databases

Based on the 2015 field survey points for Hungary from the EUROSTAT Land Use and Coverage Area frame Survey (LUCAS) database, we produced a list of five invasive plant species -*Ailanthus altissima, Asclepias syriaca, Elaeagnus angustifolia, Robinia pseudoacacia* and *Solidago* spp. that are widespread in Europe and in Hungary (Fig1).

The spatial distribution of these invasive species shows large variation in Hungary, and the relationship of this spatial pattern with recent (2012-2018) land cover changes is not yet sufficiently clear (Fig1). The above species were mapped based on visual interpretation of more than 25 000 ground photographic images taken at 5169 field sites in about 5000 LUCAS surveys in Hungary. During the 2015 LUCAS survey, the predefined network of designated field survey points was surveyed based on visual interpretation of more than 25 000 ground photographs taken at 5169 field sites in about 5000 Hungarian LUCAS 2015 locations (Gallego et al., 2015; Szilassi et al., 2021). During the 2015 LUCAS survey, the predefined network of designated field survey points was located on average 3 km from each other. If we were able to identify at least one of the plant species we surveyed in one of the photographs taken at the points, we considered that LUCAS point is infected with that species (Szilassi et al., 2019). *Solidago canadensis* and *Solidago gigantea* were identified only at genus level as *Solidago* spp. (Szilassi et al., 2021).

The spatial patterns of land cover change between 2012-2018 were analysed using the CORINE digital map database. The CORINE Land Cover (CLC) database is a regional scale (1:100 0000) land cover database for the European Union, using a uniform mapping methodology, which describes land cover changes, including between 2012 and 2015, based on a consistent nomenclature (Büttner & Koszta, 2011).

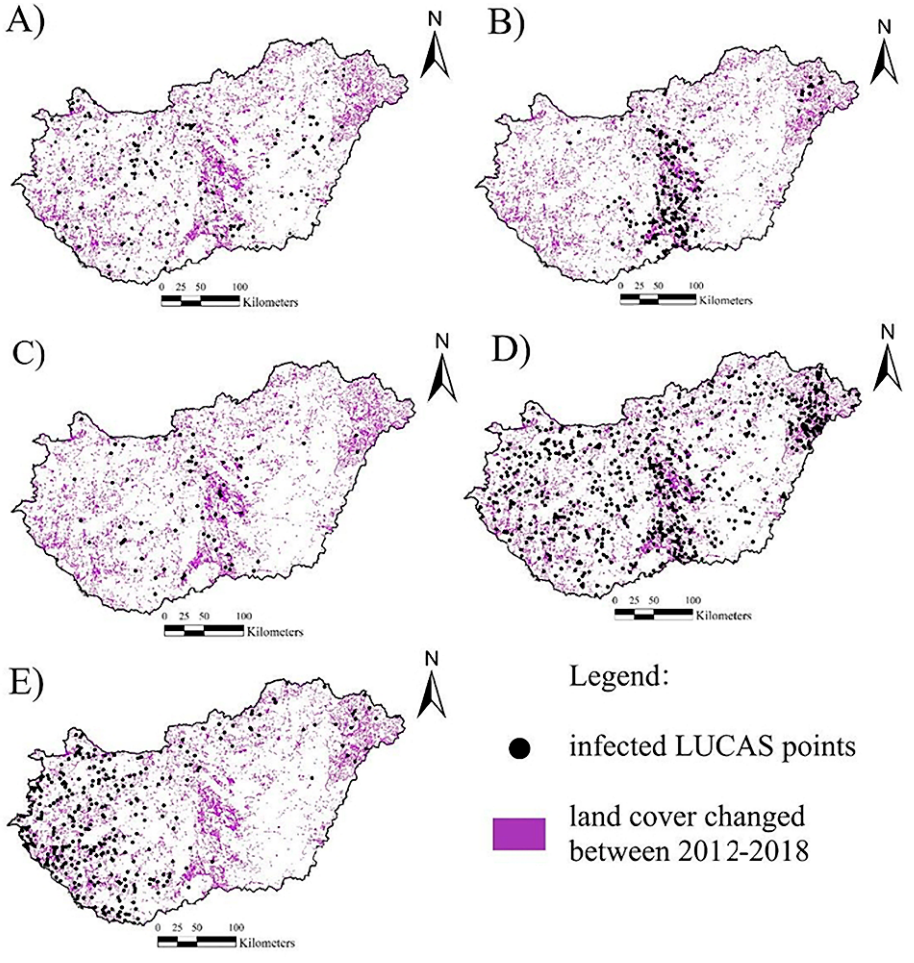

Figure 1. The areas with changed land cover, and the country-scale distribution of the investigated five invasive plants

2.3 GIS and statistical analysis

Using the spatial analysis tool of ArcGIS 10.7 software, we calculated the Euclidean distances between the LUCAS points of the five plant species (both infected and uninfected) and the nearest land cover change polygons. The resulting distance values were compared with each other using boxplot diagrams for each invasive plant, divided into infected and uninfected LUCAS point groups, using R-software. The

average, median, and standard deviation of the distances of LUCAS points from CLC change polygons of LUCAS points for each investigated plant species were calculated separately for those infected by the plant (where the plant occurs) and those not infected by the plant (where the plant does not occur). We also calculated, for each of the five studied plants, how much closer the LUCAS points infected with a given species are to the CLC land cover change polygons than the LUCAS points not infected with a given species. We subtracted the mean distances, standard deviation and median values of the distances of the non-infected points to the CLC change polygons from the mean distances, standard deviation and median values of the infected LUCAS points. If the value of the difference thus obtained has a positive sign, it means that individuals of the species are located closer to the CLC change polygons than to the uninfected points, i.e. the occurrence of the species is dependent on the change in the surface cover.

Statistical analyses were carried out using R studio software. For statistical analysis, we used the one-way ANOVA model with the function *aov*() (Fisher, 1925). In the model, distances of infected LUCAS points was the dependent variable and species was the independent variable. The pairwise comparison of LUCAS points infected with each species was performed with a Tukey post-hoc test with the function *TukeyHSD*().

Results

In the distribution map produced from the 2015 LUCAS survey, there were significantly fewer LUCAS points infected with the species than uninfected points. *Robinia pseudoacacia* has the highest and *Ailanthus altissima* the lowest proportion of infected points. An intermediate value was obtained for *Asclepias syriaca, Elaeagnus angustifolia, Solidago* spp. (Table 1).

The means and medians of the Euclidean distances of non-invaded LUCAS points from areas of changed land cover show similar values for all plants. However, there is significant variation among the invasive species when comparing the means and medians of the distances of infected points from CLC change polygons (Table 1).

The most significant relationship between land use change and the presence or spread of the species was found for *Asclepias syriaca* (1214.5 m) and the LUCAS points infected with it were spatially closest on average to the land cover change polygons. The distribution of the other investigated invasive plant species (*Ailanthus altissima*, *Robinia pseudoacacia*, and *Soli-*

Table 1. Summary statistics of the Euclidean distances between the LUCAS survey (2015) points and the nearest CLC (2012-2018) polygons

Species name	LUCAS point type	Number of LUCAS points	Distance between the LUCAS survey (2015) points and the nearest CLC (2012-2018) polygons		
			Average (m)	Median (m)	SD
Ailanthus altissima	Uninfected	5098	2257.3	1747.5	1976.3
	Infected	71	1594.7	1155.4	1473.0
	Difference*	-	662.7	592.2	503.2
Asclepias syriaca	Uninfected	4974	2298.4	1793.8	1979.8
	Infected	195	1083.9	634.7	1305.3
	Difference*	-	1214.5	1159.1	674.4
Elaeagnus angustifolia	Uninfected	5001	2248.2	1739.1	1967.6
	Infected	168	2220.3	1661.2	2063.0
	Difference*	-	27.9	77.9	-95.3
Robinia pseudoacacia	Uninfected	4538	2342.9	1852.7	1995.9
	Infected	630	1639.7	1105.9	1684.6
	Difference*	-	703.2	746.8	311.2
Solidago spp.	Uninfected	4844	2290.8	1768.6	2005.2
	Infected	324	1670.2	1364.3	1321.5
	Difference*	-	620.6	404.3	683.7

**Distance of uninfected points: Euclidean distance from the land cover changed areas minus Euclidean distance of infected points from the land cover changed areas*

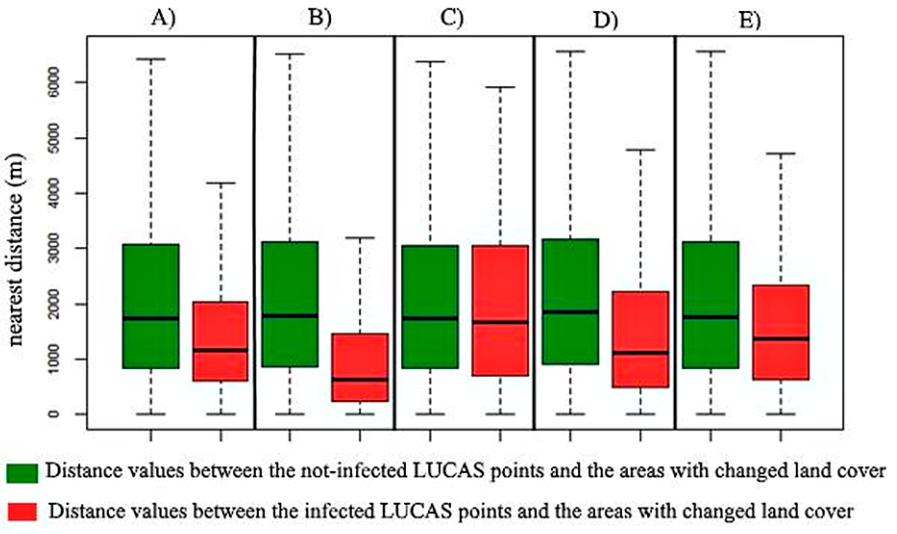

Figure 2. The distribution of Euclidean distances between the uninfected LUCAS points and the changed land cover areas. The distribution of Euclidean distances between the infected points and the changed land cover areas of the investigated invasive plants in a boxplot diagram

dago spp.) was also connected with land cover change. However, no relationship between landscape change and the distribution of the species was found for *Elaeagnus angustifolia*, as infected points were only marginally closer to CLC polygons, averaging only 27.90 m, compared to the average distances of LUCAS points uninfected with this species to CLC polygons (Table 1).

The distances of non-infected and infected LUCAS points from CLC polygons of the species studied differed in their median values to a similar extent as was seen for the mean values. Thus, it is clear from the differences in median values that while there is a significant difference in the Euclidean distances of infected and non-infected points from CLC polygons for the common milkweed (*Asclepias syriaca*), goldenrod (*Solidago* spp.), black locust (*Robinia pseudoacacia*), and tree of heaven (*Ailanthus altissima*). Nevertheless, the difference in both median and mean values for Russian olive (*Elaeagnus angustifolia*) is negligible, it is below 100 m (Table 1).

The fact that occurrence of *Elaeagnus angustifolia* is not related to changes in land use can also be concluded from the fact that the distance values of LUCAS points not infected with *Elaeagnus angustifolia* in 2015 show a much smaller spatial variance (spatial diversity) than those of the infected points compared to the areas with a change in land cover between 2012 and 2018. Therefore, the standard deviations of these distances is only negative for this species (Table 1, Fig 2).

Pairwise comparison of distances between infected LUCAS points show, a significant difference was obtained when Elaeagnus angustifolia and Asclepias syriaca (p< 0,001), *Robinia pseudoacacia* and *Asclepias syriaca* (p< 0,001), *Solidago* spp. and *Asclepias syriaca* (p<0,001), *Robinia pseudoacacia* and *Elaeagnus angustifolia* (p< 0,001) and *Solidago* spp. and *Elaeagnus angustifolia* (p= 0,003) pairs were compared (Table 2).

Table 2. Statistical analysis of the distances between LUCAS points infected with each species

Pairwise comparison of distances between infected LUCAS points for each species	p-value
Asclepias syriaca - Ailanthus altissima	0.146
Elaeagnus angustifolia - Ailanthus altissima	0.047
Robinia pseudoacacia - Ailanthus altissima	0.999
Solidago spp. *- Ailanthus altissima*	0.996
Elaeagnus angustifolia - Asclepias syriaca	< 0,001
Robinia pseudoacacia - Asclepias syriaca	< 0,001
Solidago spp. *- Asclepias syriaca*	< 0,001
Robinia pseudoacacia - Elaeagnus angustifolia	< 0,001
Solidago spp. *- Elaeagnus angustifolia*	0.003
Solidago spp. *- Robinia pseudoacacia*	0.999

Discussion

There is considerable variation between all investigated invasive species in relation to the type and weight of geographical factors influencing their occurrence. The presence or absence of a given invasive plant species is strongly related to different environmental (soil, climatic etc.) factors. One of these geographic and environmental factors is land cover, which is most often the result of anthropogenic processes. In our research, we found that changes in land cover may play different roles and have different importance in the distribution of the five studied invasive plant species.

The variation in adaptability of invasive plants may be related to the fact that the species studied are all broadly tolerant, occupying similar yet slightly different ecological niches in many aspects. For example, the tree of heaven is more commonly found in the urban environment around landfills and construction sites. The connection of the tree of heaven with land cover change, supported by our research results, is well explained, as its occurrence is linked to urbanisation and land cover changes in suburban areas (Knapp et al., 2000; Kowarik & Säumel, 2007; Kowarik, 2011).

The fact that *Elaeagnus angustifolia* does not show any relationship with land cover change has been confirmed in previous studies. The spread of *Elaeagnus angustifolia* is closely linked to urbanisation, water and cannel networks, and it prefers soils with salt accumulation. (Kitka & Szilassi, 2016; Szilassi et al., 2021).

Our results show that *Asclepias syriaca* is the most successful of the five invasive plants studied in colonising new habitats, such as open spaces, which are transformed by land cover change (Kitka & Szilassi, 2016; Bakacsy & Bagi, 2020). The occurrence of *Asclepias syriaca* mainly in disturbed habitats where natural competitors are absent. In these habitats, disturbance is a more important environmental factor than soil conditions (Mihály & Botta-Dukát, 2004). However, *Robinia pseudoacacia, Ailanthus altissima,* and *Solidago* spp. have the potential to easily conquer these new habitats as well (Török et al., 2003). The seeds of *Robinia pseudoacacia* can remain germinating for a very long time, for several decades. The initiation of germination is often triggered by human activities such as ploughing, burning or trampling, i.e. activities that lead to tangle. Land-use change is often accompanied by habitat disturbance, which favours the germination and spread of *Robinia pseudoacacia* (Csiszár, 2012).

As a result of land use change in many cases the agricultural fields turns into fallows. The best conditions for *Solidago* spp. and *Asclepias syriaca* seed germination are in abandoned agricultural fields, and it readily appears in fallow or neglected areas (Kitka & Szilassi, 2016; Szilassi et al., 2019).

The occurrence hotspots of *Ailanthus altissima* are located in cities, dumpsites, railway embankments and other devastated surfaces from here it spreads along road networks (Szilassi et al., 2019; Szilassi et al., 2021). To be able to settle, it needs soil disturbance and this often occurs as a result of land use change (Mihály & Botta-Dukát, 2004).

The barren surfaces created by construction sites are potential habitat for many pioneer weed species which are highly adapted to extreme environmental conditions (e.g. compact soil, drought, intense light). The impact of deforestation and plantations on biological invasion has been shown by several authors (Huebner, 2009; Warren et al., 2011). Our research has also shown that, in addition to common milkweed (*Asclepias syriaca*), the goldenrod (*Solidago* spp.) and black locust (*Robinia pseudoacacia*) also prefer spontaneously shrubby areas with changing land use (Csontos et al., 2009; Kelemen et al., 2016).

Deforestation and logging can also alter light, temperature and humidity conditions (Call and Nilsen, 2003), but can also significantly change the thickness of the topsoil layer. All of these factors result in changes in forest land cover that favour the occurrence of many invasive plant species (Webb et al., 2001). Our research supports Knapp & Canham's (2000) findings that clearcutting promotes the emergence and expansion of the tree of heaven.

Conclusions

For four of the five invasive plants studied in our research, we were able to show a strong correlation between changes in land cover and the distribution of the species. We have shown that land cover is one of the anthropogenic drivers of invasion and should be considered when invasion hazard maps are constructed. Our results can be used as input for land-use planning in protected areas, for the construction of distribution models for different invasive plants, and for a better understanding of the geographical background of biological invasion as an environmental risk (Genovesi et al., 2010).

The research methodology contributes to the understanding of the anthropogenic causes of biological invasions, and the relationship between land cover change and the distribution and spread of invasive plants. The results obtained can be used to model invasion risk and provide inputs for the assessment of invasion risk.

References

Bakacsy, L., & Bagi, I. (2020). Survival and regeneration ability of clonal common milkweed (Asclepias syriaca L.) after a single herbicide treatment in natural open sand grasslands. *Scientific Reports*, 10, doi:10.1038/s41598-020-71202-8

Bartha, D., & Csiszár, Á. (2012). Keskenylevelű ezüstfa (Elaeagnus angustifolia). In: Csiszár Á. (szerk.): Inváziós növényfajok Magyarországon. Nyugat-magyarországi Egyetemi Kiadó, Sopron, 115–120 pp.

Biró, M., Czúcz, B., Horváth, F., Révész, A., Csatári, B., & Molnár, Z. (2013a). Drivers of grassland loss in Hungary during the post-socialist transformation (1987–1999). *Landscape Ecology*, 28, 789-803. doi:10.1007/s10980-012-9818-0.

Biró, M., Szitár, K., Horváth, F., Bagi, I., & Molnár, Z. (2013). Detection of long-term landscape changes and trajectories in a Pannonian sand region: comparing land-cover and habitat-based approaches at two spatial scales. *Community Ecology*, 14, 219-230. doi:10.1556/comec.14.2013.2.12.

Büttner, Gy., & Koszta B. (2011). Manual of CORINE Land Cover changes EEA subvention 2011, Final Draft available online: https://land.copernicus.eu/user-corner/technical library/manual_of_changes_final_draft.pdf (13.05.2022).

Call, R. J., & Nilsen, E. T. (2003). Analysis of Spatial Patterns and Spatial Association between the Invasive Tree-of-Heaven (Ailanthus altissima) and the Native Black Locust (Robinia pseudoacacia). *The American Midland Naturalist*, 150(1), 1-14.

Csiszár, Á.(eds) (2012). Inváziós növényfajok Magyarországon. – Nyugat-magyarországi Egyetem Kiadó, Sopron, 364 pp.

Csiszár, Á., Kézdy, P., Korda, M., & Bartha, D. (2020). Occurrence and management of invasive alien species in Hungarian protected areas compared to Europe. *Folia Oecologica*, 47(2), 178. doi:10.2478/foecol-2020-0021

Csontos, P., Bózsing, E., Cseresnyés, I., & Penksza, K. (2009). Reproductive potential of the alien species Asclepias syriaca (Asclepiadaceae) in the rural landscape. *Polish Journal of Ecology* 57, 383-388.

Dövényi, Z., Ambrózy, P., Juhász, Á., Marosi, S., Mezosi, G., Michalkó, G., Somogyi, S., Szalai, Z., & Tiner, T. (2008). Magyarország kistájainak kataszterе [Inventory of Microregions in Hungary], 876 pp.

Dukes, J. S., & Mooney, H. A. (2004). Disruption of ecosystem processes in western North America by invasive species. *Revista chilena de historia natural*, 77(3), 411-437.

Follak, S., Bakacsy, L., Essl, F., Hochfellner, L., Lapin, K., Schwarz, M., Tokarska-Guzik, B., & Wołkowycki, D. (2021). Monograph of invasive plants in Europe N 6: Asclepias syriaca L. *Botany Letters*, 168(3), 422-451.

Gallego, F.J., Palmieri, A., & Ramos, H. (2015). Sampling system for LUCAS, 2015, JRC Technical reports: https://ec.europa.eu/eurostat/documents/205002/6786255/LUCAS+2015+sampling_20160922.pdf (13.05.2022).

Fisher, R. A. (1925). *Statistical Methods for Research Workers.* Edinburgh: Oliver & Boyd,

Genovesi, P., & Monaco, A. (2014). European guidelines on protected areas and invasive alien species | IUCN Available online: https://www.iucn.org/content/european-guidelines-protected-areas-and-invasive-alien-species (13.05.2022).

Genovesi, P., Scalera, R., Brunel, S., Roy, D., & Solarz, W. (2010). *Towards an Early Warning and Information System for Invasive Alien Species (IAS) Threatening Biodiversity in Europe.* Copenhagen: European Environment Agency. ISSN 1725-2237

Huebner, C.D. (2010). Spread of an invasive grass in closed-canopy deciduous forests across local and regional environmental gradients. *Biological In-*

vasions, 12(7), 2081-2089. doi:10.1007/s10530-009-9610-5

Hulme, P.E. (2021). Unwelcome exchange: International trade as a direct and indirect driver of biological invasions worldwide. *One Earth*, 4(5), 666-679. doi:10.1016/j.oneear.2021.04.015.

Kálmán, N. (2014). Inváziós növényfajok elterjedése a Duna-Tisza közi homokháton, felhagyott kisparcellásmozaikok területén. Tudományos diákköri dolgozat, Szent István Egyetem, Gödöllő, 44 pp.

Kelemen, A., Valkó, O., Kröel-Dulay, G., Deák, B., Török, P., Tóth, K., Miglécz, T., & Tóthmérész, B. (2016). The invasion of common milkweed (Asclepias syriaca) in sandy old-fields–is it a threat to the native flora? *Applied Vegetation Science*, 19, 218-224. doi:10.1111/avsc.12225.

Kézdy, P., Csiszár, Á., Korda, M., & Bartha, D. (2018). Occurrence and management of invasive alien species in Hungarian protected areas compared to Europe *Természetvédelmi Közlemények*, 24, 85–103. doi:10.20332/tvk-jnatconserv.2018.24.85

Kitka, D., & Szilassi, P. (2016). Geographic Factors Influencing the Spreading of Invasive Species A GIS-based Case Study in the Southern Great Plain of Hungary. *Tájökológiai Lapok*, 14, 168.

Kleinbauer, I., Dullinger, S., Peterseil, J., & Essl, F. (2010). Climate change might drive the invasive tree Robinia pseudoacacia into nature reserves and endangered habitats. *Biological Conservation*, 143, 382–390. doi: 10.1016/j.biocon.2009.10.024

Knapp, L. B., & Canham, C., D. (2000). Invasion of an Old-Growth Forest in New York by Ailanthus altissima: Sapling Growth and Recruitment in Canopy Gaps. *The Journal of the Torrey Botanical Society*, 127(4), 307-315, doi:10.2307/3088649

Kowarik, I. (2011). Novel urban ecosystems, biodiversity, and conservation. *Environmental Pollution*, 159(8–9), 1974-1983. doi:10.1016/j.envpol.2011.02.022

Kowarik, I., & Säumel, I. (2007). Biological flora of Central Europe: Ailanthus altissima (Mill.) Swingle. *Perspectives in Plant Ecology, Evolution and Systematics*, 8, 207–237. doi:10.1016/j.ppees.2007.03.002

Lundgren, R.M., Small, J. C., & Dreyer, D. G. (2004). Influence of Land Use and Site Characteristics on Invasive Plant Abundance in the Quinebaug Highlands of Southern New England. *Northeastern Naturalist*, 11, 313–332.

Manzoor, S., A., Griffiths, G., & Lukac, M., (2021). Land use and climate change interaction triggers contrasting trajectories of biological invasion. *Ecological Indicators*, 120, doi:10.1016/j.ecolind.2020.106936.

Mezősi, G., Bata T, Meyer, B., Blanka, V., & Ladányi, Zs. (2014). Climate Change Impacts on Environmental Hazards on Carpahtian Basin. *International Journal of Disaster Risk Sciences*, 5(2), 136-146. doi:10.1007/s13753-014-0016-3

Mezősi, G. (2022). *Natural Hazards and the Mitigation of their Impact.* Springer International Publishing AG, 260 pp. ISBN/Ean3031072251/9783031072253

Mihály, B., & Botta-Dukát, Z. (2004). *Biológiai inváziók Magyarországon. Özönnövények*, [Biological invasion in Hungary. Invasive plants]. Természetbúvár Alapítvány, 366 pp.

Pyšek, P., Lambdon, P.W., Arianoutsou, M., Kühn, I., Pino, J., & Winter, M. (2009). Alien Vascular Plants of Europe. In: *Handbook of Alien Species in Europe. Invading Nature - Springer Series in Invasion Ecology,* 3. doi:10.1007/978-1-4020-8280-1_4

Szilassi, P., Soóky, A., Bátori, Z., Hábenczyus, A. A., Frei, K., Tölgyesi, C., van Leeuwen, B., Tobak, Z., & Csikós, N., (2021). Natura 2000 Areas, Road, Railway, Water, and Ecological Networks May Provide Pathways for Biological Invasion: A Country Scale Analysis. *Plants*., 10(12), 2670. doi:10.3390/plants10122670

Szilassi, P., Szatmári, G., Pásztor, L., Árvai, M., Szatmári, J., Szitár, K., & Papp, L. (2019). Understanding the Environmental Background of an Invasive Plant Species (Asclepias syriaca) for the Future: An Application of LUCAS Field Photographs and Machine Learning Algorithm Methods. *Plants*, 8(12), 593. doi:10.3390/plants8120593

Török, K., Botta-Dukát, Z., Dancza, I., Németh, I., Kiss, J., Mihály, B., & Magyar, D. (2003). Invasion Gateways and Corridors in the Carpathian Basin: Biological Invasions in Hungary. *Biological Invasions*, 54(5), 349–356. doi:10.1023/B:BINV.0000005570.19429.73

Warren, R.J., Bahn, V., Kramer, T.D., Tang, Y., & Bradford, M.A. (2011). Performance and reproduction of an exotic invader across temperate forest gradients. *Ecosphere*, 2(2), 1-19. doi:10.1890/ES10-00181.1

Webb, S.L, Pendergast, P.H., & Dwyer, M.E., (2001). Response of Native and Exotic Maple Seedling Banks to Removal of the Exotic, Invasive Norway Maple (Acer platanoides), *The Journal of the Torrey Botanical Society*, 128(2), 141-149. doi:10.2307/3088736

ISSN 0354-8724 (hard copy) | ISSN 1820-7138 (online)

Climate Change as an Environmental Threat on the Central Plains of the Carpathian Basin Based on Regional Water Balances

Hop Quang Tran[A*], Zsolt Zoltán Fehér[B], Norbert Túri[C], János Rakonczai[A]

Received: April 03, 2022 | Revised: June 10, 2022 | Accepted: June 29, 2022
doi: 10.5937/gp26-37271

Abstract

Climate change is an essential environmental challenge nowadays. Its effects are already being felt in multiple ways. In the future, we will also have to adapt to its effects because of our farming and our daily lives. In our research, we assessed the climate sensitivity of the lowland areas of Hungary through the changes in landscapes and the changes in groundwater resources that have the greatest impact on agriculture, using data from more than half of a century. We have quantified that at the mid-territory level (5-10 thousand km^2) the groundwater resources show up to 3-5 km^3/year changes in both positive and negative directions due to climatic effects. This significantly exceeds the anthropogenic water uses (the total water use of Hungary is about 5 km^3 per year), so the effect of climate is the determining factor in the changes of regional water resources. Future changes in water circulation were modelled using the MIKE-SHE model in two micro-regions in Hungary. We have found that already at the level of the small catchments presented in our study, the water shortage increases by hundreds of millions of m^3 per year due to the expected increase in temperature (mainly due to the increase in evapotranspiration), which cannot be compensated by current water supply solutions. Model simulations have confirmed previous results showing that groundwater movements play a very important role even in lowland landscapes. Based on our research, we would like to draw the attention of decision-makers and agricultural experts to the fact that current methods (irrigation, regional water transfers) are not sufficient for successful adaptation to climate change. So, it is not the limited precipitation but the inappropriate agricultural practices that cause a real threat in a changing climate. Based on our research, we have made a proposal for the adaptation of agriculture to climate change.

Keywords: landscape sensitivity; shallow groundwater storage; GIS; modelling; MIKE-SHE

Introduction

Nowadays, we are increasingly confronted with the fact that climate change is one of the greatest challenges of our time. Scientists have been endorsing this more and more frequently and convincingly in recent decades (Intergovernmental Panel on Climate Change - IPCC, 1990-2022), and climate change is considered by renowned economists to be one of the most important threats (eg. World Economic Forum,

[A] University of Szeged, Faculty of Science and Informatics, Department of Geoinformatics, Physical and Environmental Geography; hoptran1207@gmail.com, j.rakonczai@geo.u-szeged.hu
[B] University of Debrecen, Faculty of Agricultural and Food Sciences and Environmental Management; feher.zsolt@agr.unideb.hu
[C] Hungarian University of Agriculture and Life Sciences, Institute of Environmental Sciences, Research Center for Irrigation and Water Management; turi.norbert@uni-mate.hu
[*] Corresponding author: Hop Quang Tran. Email: hoptran1207@gmail.com

2020, 2021[1]*). Global environmental policy has been in place since the 1990s (Rio Conference in 1992; Kyoto Protocol in 1997) to halt adverse change, but the reached agreements are weak and hardly implemented in practice. That is why the "Green Paper" of the European Union (EC, 2007) states that it is not enough to protect against the harmful effects of climate change (for example, by reducing greenhouse gas emissions), but that adaptation to inevitable changes is crucial.

In different parts of the world, the adverse effects of climate change can be experienced to very different degrees and at different rates. The global warming of the atmosphere and the change in precipitation patterns and annual distribution will affect the lives of most of humanity before long. The short-term effects of more extreme rainfall distribution appear more locally in nature. Furthermore, the effects of droughts tend to last longer, and could threaten the lives of hundred million (IPCC, 2021).

Climate change already has several consequences in the Carpathian Basin. The measured meteorological data (OMSZ, 2021), the evaluation of the historical data (Szalai, 2011; Sábitz et al., 2014) and the future forecasts made with different models (eg. Bartholy et al., 2008; Blanka et al., 2012; Csorvási et al., 2016; Pieczka et al., 2019) indicate increasing average temperatures, and more extreme precipitation with larger variation within a year (Bartholy & Pongrácz, 2017). Rising average temperatures are accompanied by increasing urban temperatures (eg. Unger et al., 2010; Gál et al., 2021; Fricke et al., 2022), increasing summer energy demand, spreading many invasive pests (eg. Szép, 2010; Janik et al., 2016), significant changes in forest water use (Tölgyesi et al., 2020), and increasing water demand in general. Precipitation, which is becoming more extreme, poses the greatest threat to agriculture with the formation of inland excess waters and droughts (Pálfai, 2004; Szatmári & van Leeuwen, 2013; van Leeuwen et al., 2019).

The current study attempts to present the main changes in the water circulation of the lowland areas of the Carpathian Basin in the context of climate change. Based on detailed monthly data of more than fifty years, the changes in groundwater resources were evaluated, which are of decisive importance for vegetation. Furthermore, using an integrated hydrological model (MIKE SHE), we forecast the changes in the water balance due to the expected climate change on two micro- regions on the plains. Unfortunately, farmers or decision-makers are not fully aware or underestimate of the magnitude of changes in water resources. Based on the research results, a proposal for adaptation to climate change in the context of agriculture is presented.

Data and methods

In previous studies by the contributing authors (Rakonczai, 2011; Rakonczai & Ladányi, 2012; Farkas et al., 2017), numerous comprehensive assessments of the most important consequences of climate change on the landscape of the Carpathian Basin have been already introduced. The study showed how changes in rainfall conditions affect, for example, the transformation of some soils and the complex consequences they can have for vegetation (Rakonczai & Ladányi, 2012; Ladányi et al., 2016;). Furthermore, the authors showed that the transformation of the water circulation of the landscape is the most important factor in the changes. In addition, the key role of shallow groundwater in assessing changes in water circulation has also been presented before (Fehér & Rakonczai, 2019). Shallow groundwater resources, for example, reflect the spatial and temporal variability of the precipitation (Garamhegyi et al., 2018) and reduce the impact of extremes.

Official temperature and precipitation series for more than a century are available nationwide for nearly eighty gauges in Hungary. In the current research, the monthly and annual precipitation data of the National Meteorological Service has been considered. The regional-scale systematic and scientific observation of shallow groundwater depth began in the early 1930s. After the Second World War, the number of measuring wells increased significantly. Nowadays, the data are collected and organised by the 12 regional water directorates and compiled by the National Water Administration. Based on more than 2 000 available data series, approximately 1 300 wells were considered reliable for our research in monthly detail.

Determination of the causes of groundwater changes is complicated because in addition to dynamic natural effects, they are also affected by several human activities. Assessment of the extent of environmental and anthropogenic impacts has long been the subject of professional debate. For example, when a significant decrease in the groundwater level on the sand ridge of the Danube–Tisza Interfluve was observed from the 1980s onwards, attempts were made through a multidisciplinary approach by several sciences to find an explanation for the process (Pálfai,

[1] Although the Covid and the war between Russia and Ukraine has changed the order of the threat to humanity in recent years.

1994). At the time, 50% of the reasons for groundwater discharge were attributed to the weather (scientists did not yet talk about climate change but rather about some unidentified shorter-term phenomena). Among the anthropogenic effects, the role of water extraction was estimated at 31% (25% for confined water, 6% for shallow groundwater). The role of land-use change (e.g. afforestation) has been estimated at 10%, and the effects of water management (sewerage, drainage) have been estimated at 7%. Another study by Szilágyi & Vörösmarty (1993) suggested that the extraction of confined groundwater might be the cause of the decline in water resources. The current research's first, most important goal was to find a measurable indicator that makes the different effects comparable.

From the beginning of the 2000s, the development of computers and GIS provided an opportunity for a new research direction (Geiger & Mucsi, 2005). Laborczi et al. (2020) found that the movement of groundwater cannot be studied itself, thus, the distinction between charge and discharge zones is proposed. We realised that instead of the traditional map-based assessment of groundwater changes (which did not allow for the examination of many essential elements of the changes), it is practical to examine the volumetric and spatial behaviour of water resources. To achieve this, the digital elevation model of the monthly groundwater level has shown the evolution of the water supply over time and was calculated based on the spatial differences of the successive periods. Monthly volumetric changes were corrected for an estimated average effective porosity of 30% in the sediments. Based on the analysis in the study areas, we found that traditional interpolation methods result in significant errors due to the greater distance between the wells measuring groundwater changes and the variability of the surface topography. Therefore, after comparing various geostatistical methods, we developed several advanced approaches (sequential Gaussian simulations in a space-time domain) (Fehér, 2015, 2019; Fehér & Rakonczai, 2019). In the first phase of these studies, to assess the effects of climate change more accurately, the boundaries of the sample areas were designed, taking into account the typical high-water levels of the larger rivers. These investigations were first carried out in the sub-areas of the Great Hungarian Plain, but in recent years the analysis was extended to the entire territory of Hungary, where the significant spatial extent of shallow groundwater can be found (Figure 1).

To investigate future impacts of climate change on water resources, two small catchments were modelled

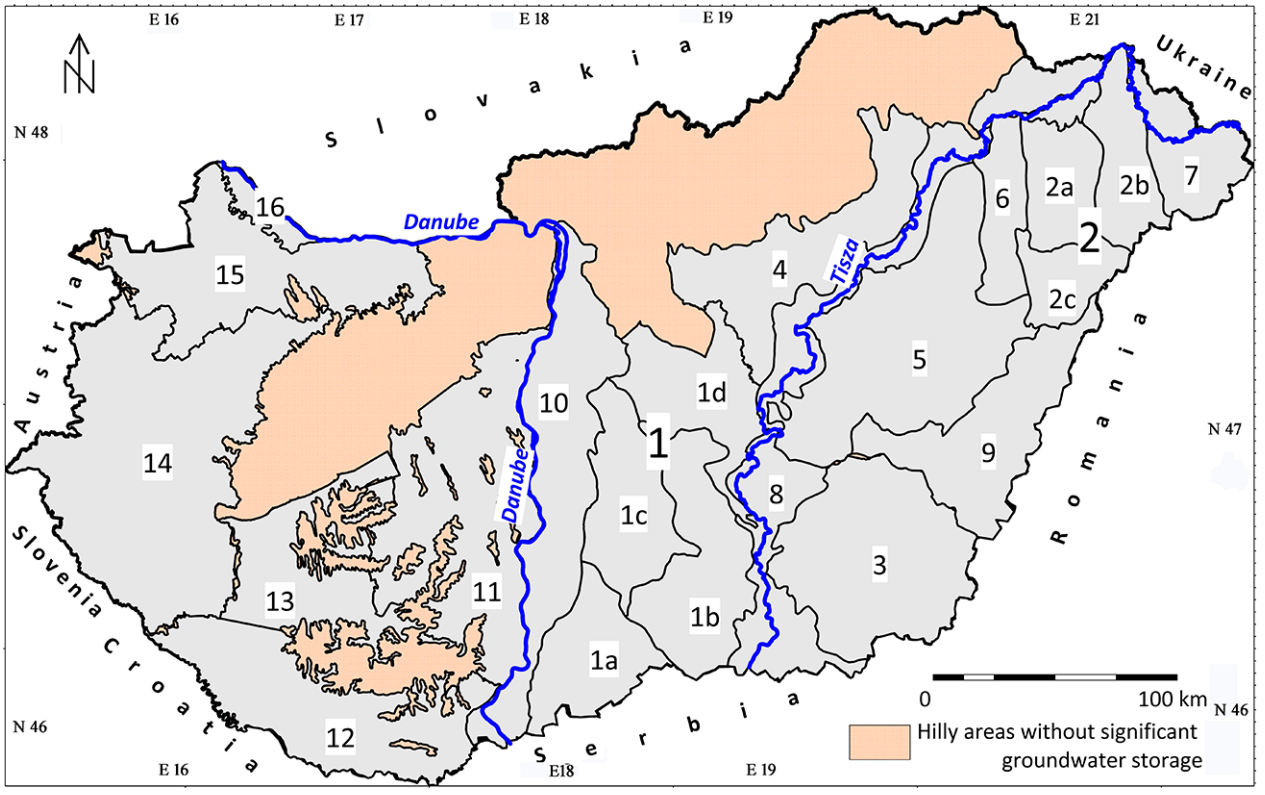

Figure 1. Areas included in the shallow groundwater resource assessment in Hungary
Regions and micro-regions: 1: Danube–Tisza Interfluve; 2: Nyírség; 3: Maros–Körös Interfluve; 4: North Periphery of Great Hungarian Plain; 5: Central Tisza Plain; 6: Hajdúság; 7: Upper Tisza Plain; 8: Tisza Valley; 9: Berettyó–Körös Plain; 10: Danubian Plain; 11: Mezőföld; 12: Dráva Plain; 13: Somogy Hills, 14: West Hungary; 15: Little Hungarian Plain; 16: Szigetköz. (For practical reasons, the boundaries of the assessed regions do not exactly match the natural geographical boundaries)

using the MIKE-SHE hydrological framework. This model includes a comprehensive, integrated water balance tool capable of completing local and entire catchment water balance calculations at any time interval, thus enabling the integration, mapping, and visualisation of water flow processes of the catchment components over the entire watershed (DHI Group, 2017; Graham & Butts, 2005). Two catchments were chosen for the current study, where sufficient spatial data was available to enable the calibration of a proper model (Nagy et al., 2019). The calibration was performed by the sensitivity analysis of the changing input parameters of the model (Tran, 2021). By considering the future climatic scenarios and past extreme precipitation conditions, future trends of water balances were simulated. Since such detailed spatial studies are very data-intensive (which can hardly be provided in sufficient detail in practice), methodologically significant analyses of the sensitivity of both spatial data requirements and some landscape features were also performed. The simplest methodology of sensitivity analysis (Hamby, 1994), the one-at-time method was used for the studies. This essentially means that the degree of sensitivity is determined by changing each parameter independently, while not changing any of the other parameters. The one-at-time methodology was applied with a comprehensive, spatially, and temporally integrated hydrological model, MIKE SHE, which can calculate each hydrological parameter and the water balance of the local or the entire catchment, and for any time interval.

Results

Groundwater resources as an indicator of climate change

A significant change can be observed when assessing climate change through the national rainfall conditions of the last 120 years. Based on the whole period, a decreasing trend can be observed; however, if we look only at the past 50 years, the trend is exactly the opposite. In addition, increasing precipitation extremes have developed over the last two decades (Figure 2). The changes are even more significant when looking at different parts of the country. A decreasing precipitation trend can be observed in the more humid Transdanubia while slightly increasing precipitation occurs in the eastern part of Hungary. The fact that annual rainfall is not the best climate indicator is reflected by the seemingly uncertain connection with the drought occurrence (Figure 3). It is not surprising that there is no significant drought in rainy years is. However, it is already more difficult to understand that in years of equal annual precipitation sum, some-

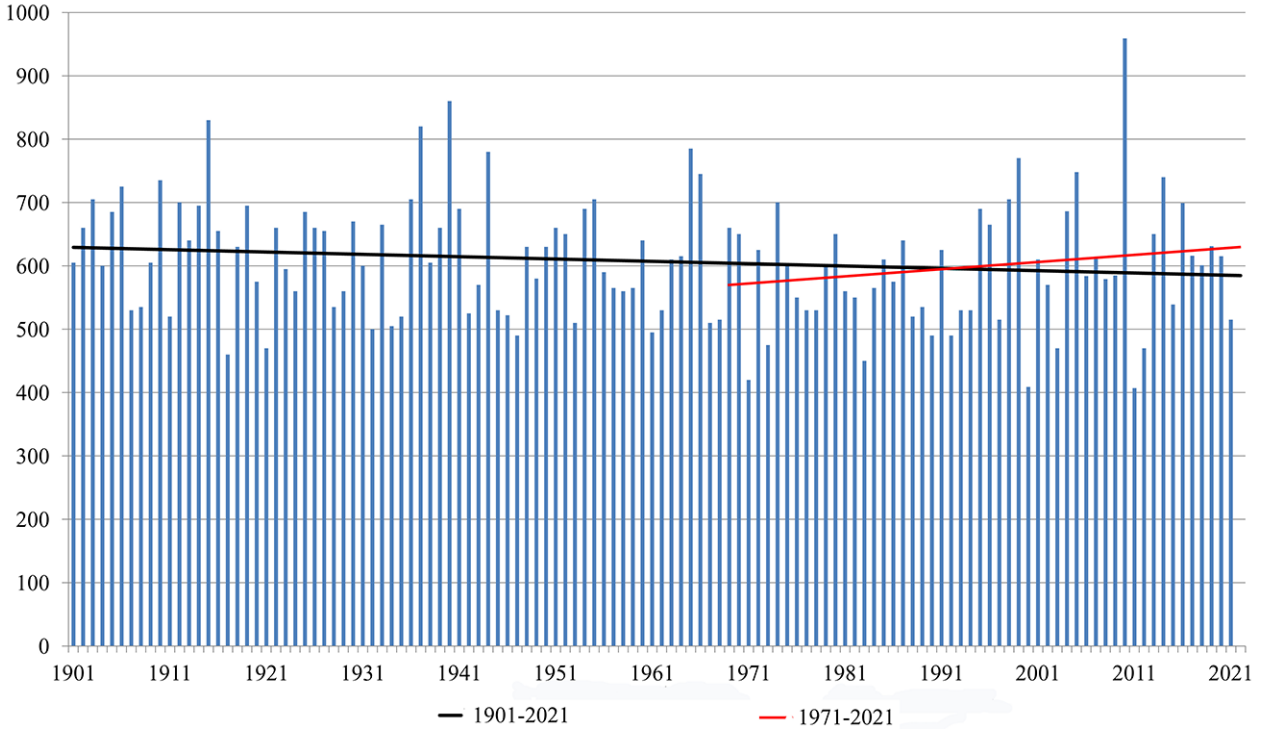

Figure 2. Annual rainfall (mm) in Hungary in 1901-2021 and its 120-year and 50-year trends (based on data of the Hungarian Meteorological Service)

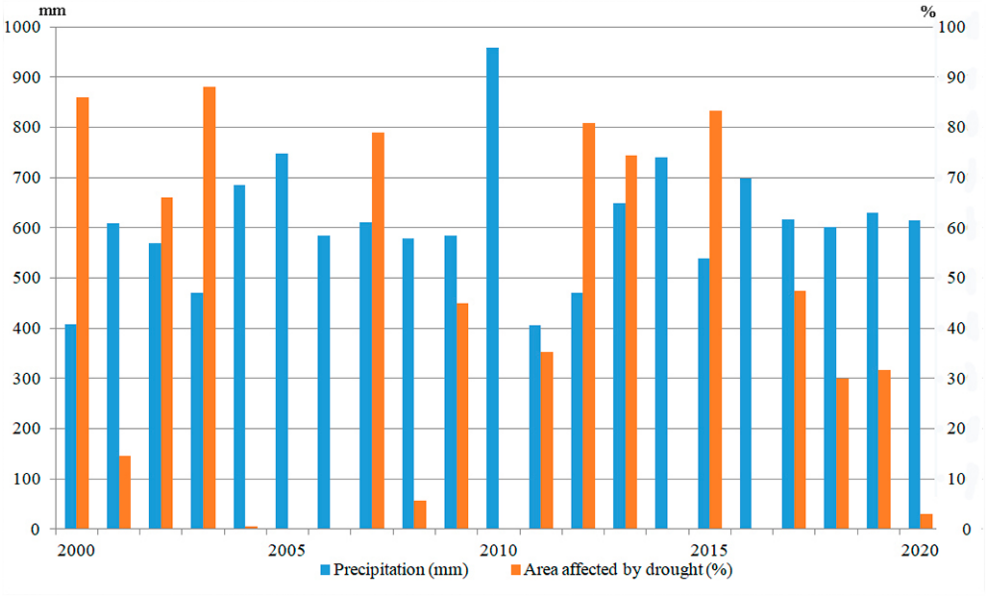

Figure 3. The relationship between the amount of annual precipitation and drought-affected areas in Hungary in the period 2000-2020 (based on the Hungarian Central Statistical Office)

times the area affected by drought is large, while other times it is much smaller. Examining the background of the phenomena, we can suppose that the water supply of the preceding period largely determines the intensity of drought of the given year. The best example of this is the rainy year of 2010, followed by one of the driest years of the century, yet only 1/3 of the country was under drought conditions in 2011. The next year was wetter than average, but at least 4/5 of the country was affected by drought in 2012. This can be explained by the decreased amount of water stored in the soils and the shallow groundwater in the previous year. Based on the above-observed processes, it was necessary to assess changes of a natural factor (shallow groundwater), which can express the environmental changes more accurately in a trend-like manner.

In the first stage of the research, taking advantage of the potential of geoinformatics, the quantitative changes in the groundwater supply as an environmental process were assessed on four regions on the Great Hungarian Plain (Figure 4) (Fehér & Rakonczai, 2019; Rakonczai & Fehér, 2015). These studies have clarified several essential questions. We have demonstrated that, at the landscape level, climatic effects are the decisive factors in the quantitative change of groundwater resources. For example, on the sand ridge of the Danube – Tisza Interfluve, the groundwater supply can change by as much as 3-4 km^3 in both positive and negative directions in just 1-2 years, depending on the amount of precipitation. Furthermore, during a 40-year period (between 1960 and 2000) only 2 km^3 of confined water was extracted. Consequently, the change in water resources is undoubtedly closely related to the amount of precipitation. Thus, the main reason for the decline in groundwater levels was not drinking water extraction.

We also succeeded to show that in Nyírség (the NE of the Great Hungarian Plain), which has similar geomorphological and hydrogeological characteristics to the ridge between the Danube and the Tisza (higher than its surroundings, and groundwater can only be replaced by precipitation), a similar decrease in groundwater resources has developed. The only difference in the water resources change in the two landscapes is that a lack of rainfall developed later in Nyírség and its volume was also slightly less. In these two landscapes, it was well demonstrated that due to the longer period of rainfall shortage, there is a significant runoff of the groundwater resources from the higher altitude areas to the lower ones. Thus, the decrease in groundwater levels is greater in higher altitudes, and even in very rainy years, the water shortage cannot be fully compensated.

The changes in the water resources of two additional landscapes (Maros-Körös Interfluve, and the North Periphery of the Great Hungarian Plain) were examined. Due to hydrogeological conditions, subsurface recharge from other (higher) landscapes is possible in these areas. During drier years, a slow decline in water supplies has been observed. Water scarcity could be quickly replaced during periods of high rainfall, so even in case of more extreme rainfall distribution, there is no permanent shortage of groundwater, if there are periods of high precipitation.

In the second phase of the research, the investigations have been extended to most of Hungary. The assessment of the landscapes mostly affected by groundwater depletion (Danube-Tisza Interfluve, Nyírség)

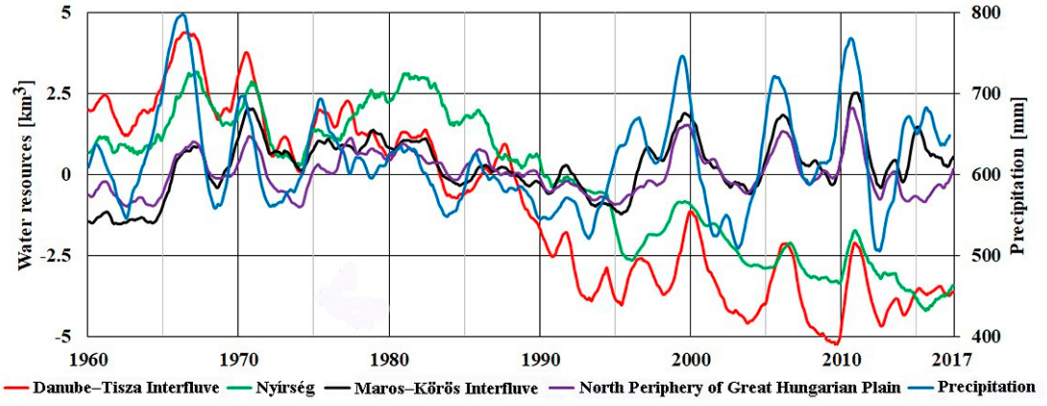

Figure 4. Precipitation and groundwater resources in four regions of the Great Plain 1960-2017*

** The volume of precipitation was displayed as the 24 months moving average of the annual precipitation. The reference „0" value of the shallow groundwater resources was determined as the mean of the estimated values for the period of 1950-2010*

has been further separated into sub-regions. The results highlight well that the landscape's geomorphological features and hydrogeological situation fundamentally determine the relationship between climate change and groundwater resources. In the Danube-Tisza Interfluve, shown as an example, the higher altitude landscapes reflect changes in precipitation well. Meanwhile, water level changes can hardly be observed on the Danubian Plain (Figure 5).

The analysis of the central, lower areas of the Great Hungarian Plain (Central Tisza Plain and Berettyó–Körös Plain) revealed a significant relationship between the change in water resources and the precipitation conditions. The magnitude of the changes is similar to that of the higher areas; meanwhile, no long-term trends could be identified. There might be several reasons for this. The eastern part of the area is hydrogeologically connected to the higher part of the basins through the river network. Thus, the region receives water replenishment by surface runoff and subsurface flow. There are remnants of the former riverbeds (paleo riverbeds) and many artificial canals in the landscape, allowing for more permanent surface infiltration. Agricultural production is assisted by irrigation with water supplies from nearby areas (mainly from the Tisza River). In addition, underground inflow is also coming from the direction of Nyírség.

The analysis of the areas west of the Danube (Figure 6) revealed several important findings. Similarly, to the Great Hungarian Plain, a close relationship between precipitation and groundwater resources can be observed. Still, the volume of the changes is smaller and regionally heterogeneous. The changes in the Mezőföld and Somogy hills show many similarities to those in the Danube–Tisza Interfluve and Nyírség, but they react to the extreme meteorological conditions abruptly. In some periods, groundwater resources of the western part of the country show striking changes that differ from the typical national trends and other Transdanubian areas. Examined in more detail, this may also be due to differences in precipitation distribution. For example, in 2010, when precipitation was 1.5 times higher than the long-term average in Hungary, only slightly above the long-term average precipitation was measured in the western part of the country. Still, the effects of the drought period in the early 2000s were also more pronounced.

In addition to the climatic effects, the dams of the Dráva River cause persistent low water levels in the Dráva Plain. Supposedly this may play a role in reducing water resources. Due to the closeness of the Dan-

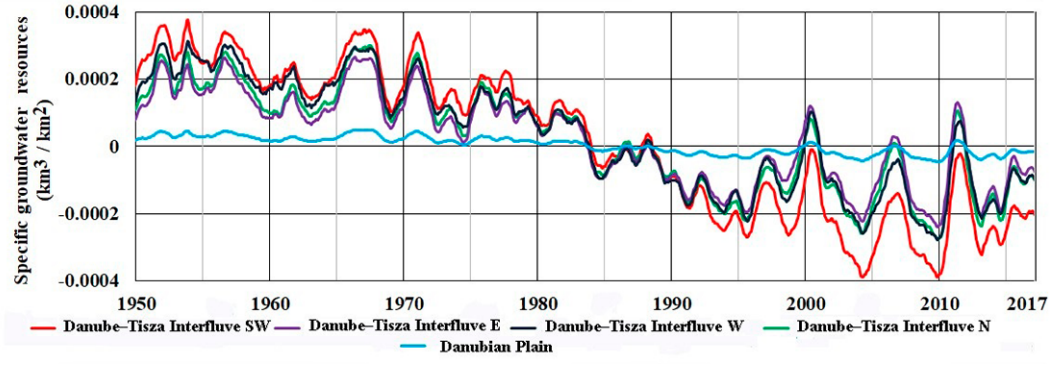

Figure 5. Changes in specific water resources in five sub-regions of the Danube-Tisza Interfluve 1950-2017

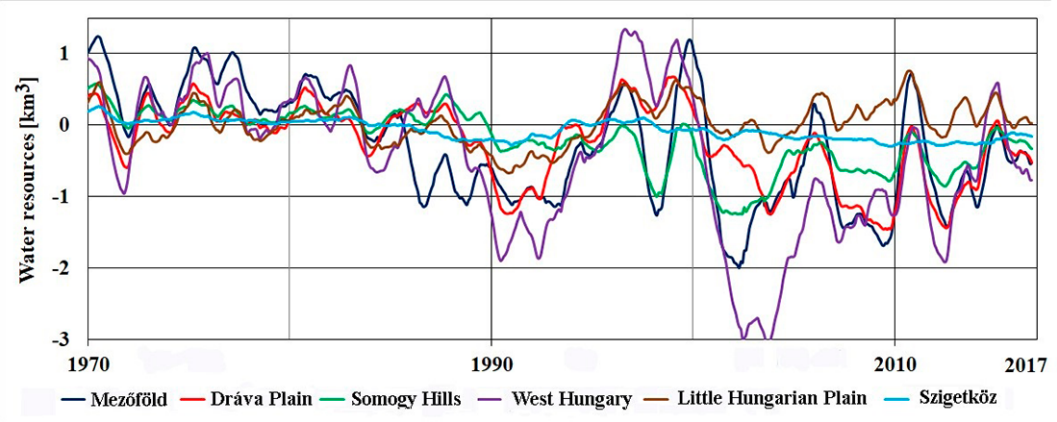

Figure 6. Changes in water resources in the areas west of the Danube 1970-2017

ube River in Szigetköz, the climatic effects can hardly be detected. However, the diversion of the Danube (due to the Gabčíkovo hydroelectric power plant) caused a 0.3-0.4 km³ discharge in the water resources.

Solutions to extreme climate events after World War II

The river regulations and water management interventions carried out in the second half of the 19th century fundamentally changed the hydrological conditions of the Carpathian Basin. After the drainage of the excess waters from the former floodplain areas, agricultural cultivation of more than ten thousand square kilometres of arable land began. Groundwater levels decreased in a large area over the summer season compared to the previous period. As a result, agriculture was more dependent on weather variability. To compensate for the water shortage in agriculture, several large-scale irrigation development programs were launched after World War II based on the water resources of the Tisza River. In contrast, inland excess water generated during hydrologically wet periods was discharged by surface or subsurface water management methods. Following the establishment of the large-scale agricultural farming structure of the socialist period, subsurface drainage programs came to the forefront in the early 1970s.

Subsurface drainage interventions were implemented as part of financial support by the State for agriculture and consisted mainly of field-level water management. By using tile drains, the goal was to achieve a balance in terms of water management in the areas to be treated. As a connecting link, the subsurface drains simultaneously serve the accelerated discharge of excess water from the soil into the recipient channel. Furthermore, it also regulated the groundwater level locally. In case of proper operation, the groundwater level could not rise above the installation depth of the drains within the treated agricultural plot. The implementation of the subsurface water management works already raised several problems during the construction. Due to the change of land ownership after the change of regime in the late 1980s, the subsurface drain networks were almost forgotten.

As one of our research objectives, we also surveyed the condition of the subsurface drained areas in the SE part of the Great Hungarian Plain and we also developed a complex methodology to analyse the detailed field-level studies along the River Hármas-Körös (Túri et al., 2021). Basically, our research results are quite unfavourable. The existence of subsurface drainage networks, once implemented with significant financial resources, has been almost forgotten over the decades. Often the networks are not properly maintained by the owner or operator. In many cases, they do not even know about their existence below the surface (Túri, 2021). Our detailed soil investigations have also revealed that the utilisation of tile drains on heavy texture soils is very limited. The main limiting factors for the operation of the tile drains are the lack of proper agrotechnics applied, the loss of the connection between the tile drains and the open recipient channel, and the insufficient water carrying capacity of the receiving channel system. The limited operation of tile drains installed decades ago has been found by researchers in other European countries as well (Tlapáková, 2017; Matcic & Steinman, 2007). Based on their experience Djurović & Stričević (2004), also pointed out that the functionality of an improperly maintained subsurface drain system deteriorated significantly in just over a decade.

Drought periods, which are becoming more frequent, regularly demonstrate the need to improve irrigation. Currently, irrigation is mostly possible from water resources taken from the Danube and the Tisza rivers. The extent of irrigated areas was the largest in the period of large-scale farming under the socialist era in the early 1970s (exceeding 300,000 hectares in some years) but barely exceeded 100,000 hectares in recent decades (Figure 7).

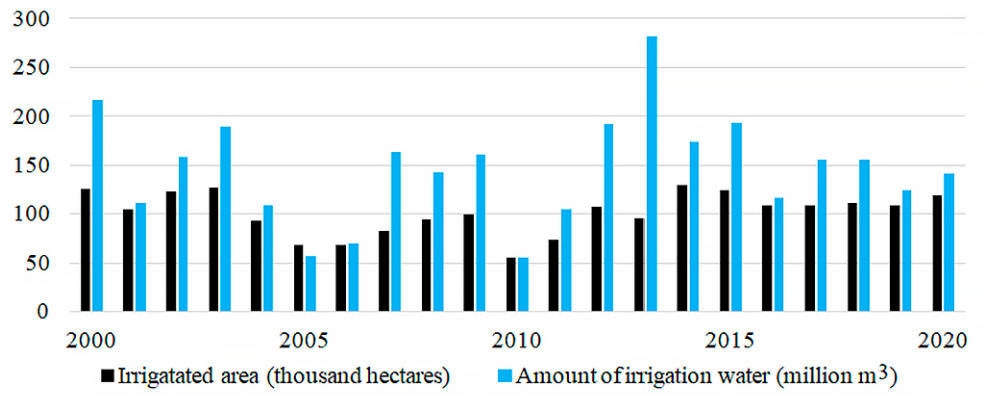

Figure 7. The extent of irrigated areas and the volume of irrigated water in Hungary between 2000 and 2020 (based on the Hungarian Central Statistical Office)

Assessment of impacts of future climate change on the water balance of micro-regions using the MIKE-SHE hydrological modelling framework

As previously introduced, diverse climatic effects may cause different effects on various landscapes due to their geographical location, and geomorphological and hydrogeological differences. The water balances of two micro-regions in one dry and one rainier year were selected to assess the future effects of climate change. Subsequently, the impact of the expected future temperature rise was also modelled. The spatial extensibility of our studies was also examined based on the extent to which reducing the data density of data-intensive models affects the accuracy of the water balance estimations.

Dong-ér catchment

The inland excess water protection management system of the Dong-ér main brook is located in the central-eastern part of the sand ridge of the Danube–Tisza Interfluve, about 50 km from the southern border of Hungary (Figure 8). The total area of the catchment is

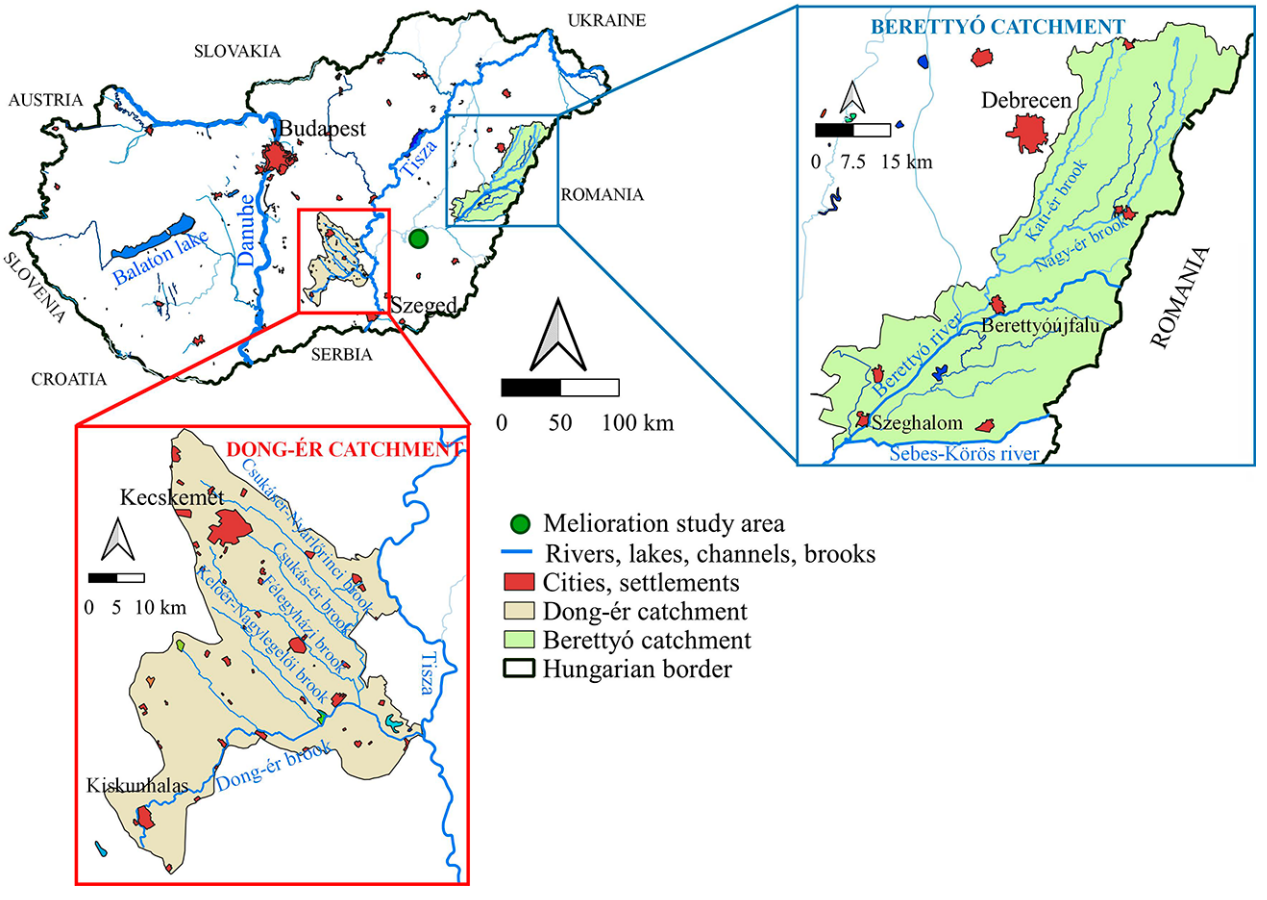

Figure 8. Location of the study areas

2 127 km², and it is characterised by a small relative relief (<2 m/km²) - the area slopes from west to east. The western, higher altitude area consists mainly of highly permeable sandy sediments. The eastern part is mainly covered by river sediments with minimal slope and lower hydraulic conductivity.

The effects of climate change on the water balance of the Dong-ér watershed were investigated by the following simulations:

- The simulations of the hydrological processes and water balance for 2018. The results of these simulations are considered a reference value for the comparison with further scenarios of extremely dry and extreme wet hydroclimatic conditions.
- Simulations of the unusually rainy year of 2014.
- Simulations of the effects of +1.5°C temperature rise, according to the forecasted IPCC scenarios (IPCC, 2018).

The comparison of simulation results performed for the years 2000 and 2014 with the results of the reference model of 2018, enabled us to examine the changes in hydrological parameters and water balance components in the context of the main characteristics of climate change. The results show that the deficit values of the unsaturated zone are much higher than the values of the other parameters (Figure 9). This means that the area is suffering from severe drought. A direct correlation can be found between the precipitation events and infiltration; nevertheless, the amount of water in the root zone and the unsaturated zone is negligible.

In addition, the actual evapotranspiration is higher than the amount of precipitation. The high sand content of the soil makes it highly permeable; meanwhile, the leakage coefficient of the sand is minimal, about 10-5 m/s. Consequently, during long periods of drought, most characteristically very intense, but short-term rain showers can hardly reach the deeper unsaturated zone. The results show that, besides evapotranspiration and precipitation, the subsurface inflows and surface runoff also have a high impact on the water balance of the entire catchment (Figure 10). This confirms our results obtained in the study of groundwater resources.

Based on the results, precipitation and infiltration are directly proportional (from 32 mm in 2000 to 138 mm in 2014). The water lost through evapotranspiration was more than precipitation in the studied years. It can be stated that the source of surface runoff in the Dong-ér catchment is primarily not precipitation or surface inflows. The question is, from where does the surface runoff get its water? The surface runoff is minimal due to the sandy surface, thus, infiltration of settlement's treated wastewater and groundwater resources into canals can be a source.

According to the results, it can be confirmed that there is a close relationship between the subsurface inflows and surface runoff components for the entire water balance of the catchment. Subsurface water flowing from the outside into the Dong-ér catchment provides ~90% of the water for the brooks, and this relationship mostly determines the water balance of the Dong-ér catchment. This is consistent with the results of a study by Kozák (2020). A comparison of the water balance results of extreme hydroclimatic conditions in 2000 and 2014 shows that the sensitivity in descending order to the following components is: infiltration (331%), overland flow to brooks (100%), subsurface water storage (-95%), evapotranspiration (75%) and overland water storage (58%) (Figure 10).

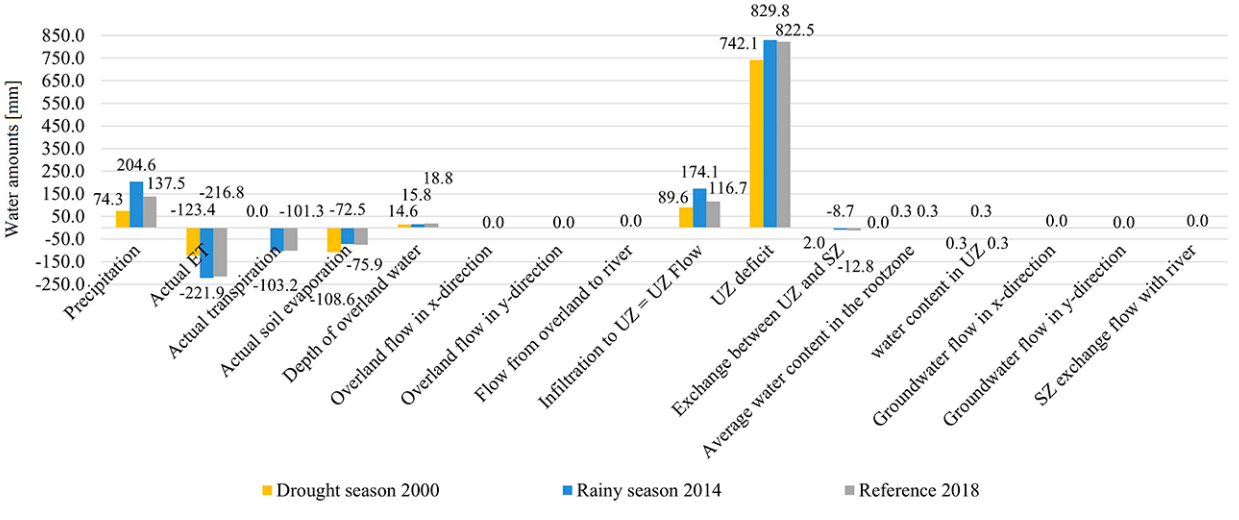

Figure 9. Average of simulated hydrological parameters from 1 March to 31 May in the drought year 2000, the rainy year 2014 and the reference year 2018
(ET: Evapotranspiration, UZ: Unsaturated zone, SZ: Saturated zone)

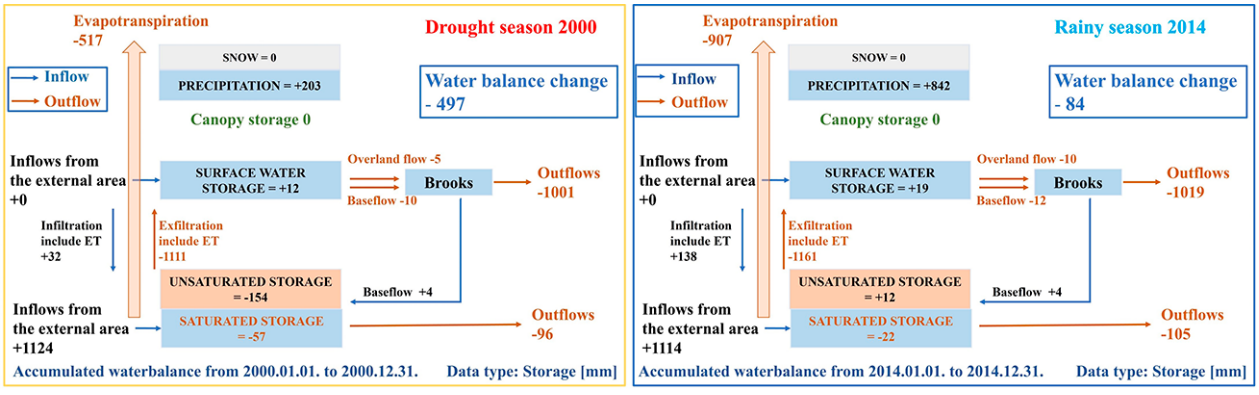

Figure 10. Water balance of the Dong-ér catchment in the drought year 2000 and rainy year 2014

Berettyó catchment

The Berettyó river originates from Romania. The current study was carried out for the 2 748.4 km² Hungarian part of the river basin area (Figure 8). Based on the topographical features, the catchment can be divided into two main parts. One-third of the basin in the NE is a sandy cone plain covered with wind-blown sand, where the surface is covered with sand and sandy loam soils. The altitude varies between 104 m and 159 m above sea level. The rest of the catchment has small relief intensity (approx. 2 m/km²) and is located at an altitude between 86 m and 101 m above sea level, sloping towards the SW. The surface features are predominantly of fluvial origin. Most of the surface contains clayey loam, clay, and loamy texture soils with low and extremely low hydraulic conductivity; thus, the infiltration properties of the surface are less favourable than in the Dong-ér catchment.

The simulated water balance of the catchment for 2018 has been presented in comparison with the Dong-ér catchment (Figure 11). In addition, a simulation was performed for a +1.5°C increase in mean temperature based on the IPCC climate scenario, and the model's sensitivity to the spatial density of cross-sections along the watercourses was investigated.

The analysis of the model outcomes highlights significant differences in the estimated water balance components, depending on the river cross-sections at every 0.5 km or 5 km. With a density of cross sections 5 km apart, the overland flow to brooks component is less than 98 mm, equivalent to nearly 270 million m³ of water. Besides, in the 5 km cross section data density model, the surface runoff exceeds 71 mm, and the water balance component shows a 27 mm surplus (80 million m³ water equivalent). Consequently, the selection of proper sampling density of river cross-sections plays a key role in the reliability of the hydrological model and thus indirectly on the water management strategies for the long-term adaptation to climate change.

The simulation results of the Berettyó river basin well reflect the low and extremely low hydraulic conductivity conditions of the soil. The surface water storage, surface runoff, and the water storage of the unsaturated zone exceed the values estimated for the Dong-ér catchment, made up of predominantly sandy sediments. The water balance of the Berettyó catchment – like the Dong-ér catchment – is highly dependent on the influence of subsurface boundary inflows from the neighbouring areas. Similar to the Dong-ér, the Berettyó river basin was also under water stress in 2018, but to a lesser extent.

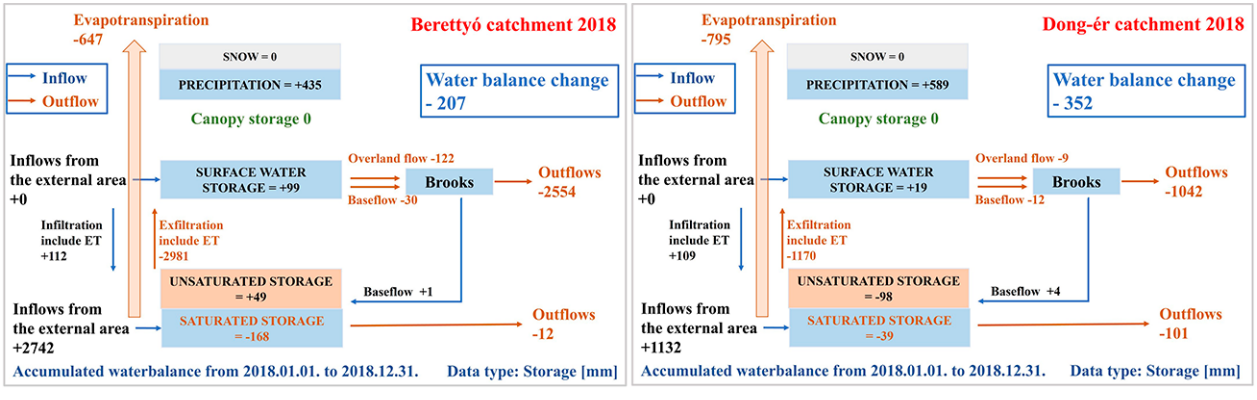

Figure 11. The water balance of the Berettyó and Dong-ér catchments in 2018

Discussion

As we have seen, the process of climate change over the last few decades has resulted in significantly different changes in water resources important to vegetation (and to agriculture in particular) across various landscapes. In smaller areas, adverse effects can be mitigated (irrigation, drainage), but long-term changes are determined by natural processes. Our study allowed us to assess the sensitivity of landscapes to climate change. Our assessment covered approximately 64 000 km² (68% of the territory of Hungary), and we separated six sensitivity groups (Figure 12).

a) *Landscapes at high risk to climate change.* These include the four sub-areas of the Danube-Tisza ridge and the three sub-areas of the Nyírség as well as the Hajdúság. Of the two contiguous areas, the longitudinal sand ridge of the Danube–Tisza Interfluve is more sensitive to drought periods because of its shape since the subsurface outflow is much more intense. The main reason for the significant water shortage in the area is the almost constant below-average rainfall from the late 1970s to the mid-1990s, when the volume of the accumulated rainfall deficit exceeded 1100 mm, and the intense rainy years were absent. The resulting water shortage of at least 5-6 km3 in the higher parts could not be compensated during the extremely rainy periods. This should be considered a long-term environmental condition. Water scarcity has been associated with significant landscape changes. The "restoration" of previous conditions is hardly conceivable and would result in substantial social conflicts since, although the majority is adversely affected by the landscape transformation, there are also beneficiaries. The development of irrigation in the region can only be economically profitable in small areas. On average, the landscape receives sufficient rainfall over many years that conscious conservation (especially in the soil, by increasing infiltration and reducing evaporation losses) can enable effective management. The area of Nyírség isdue to its shape better protected from the subsurface outflow. It is also slightly wetter, and sometimes it is even possible to regenerate the water resources in several heavily rainy years. However, a moderate depletion is more likely to persist.

b) *Regions threatened by climate change.* Mezőföld and Somogy hills were included in this category. Mezőföld has shown many similarities with the changes in the sand ridge of the Danube–Tisza interfluve since the 1970s. However, after a significant decline in resources, water resources appear to be normalising during the years with high precipitation of the 2000s.

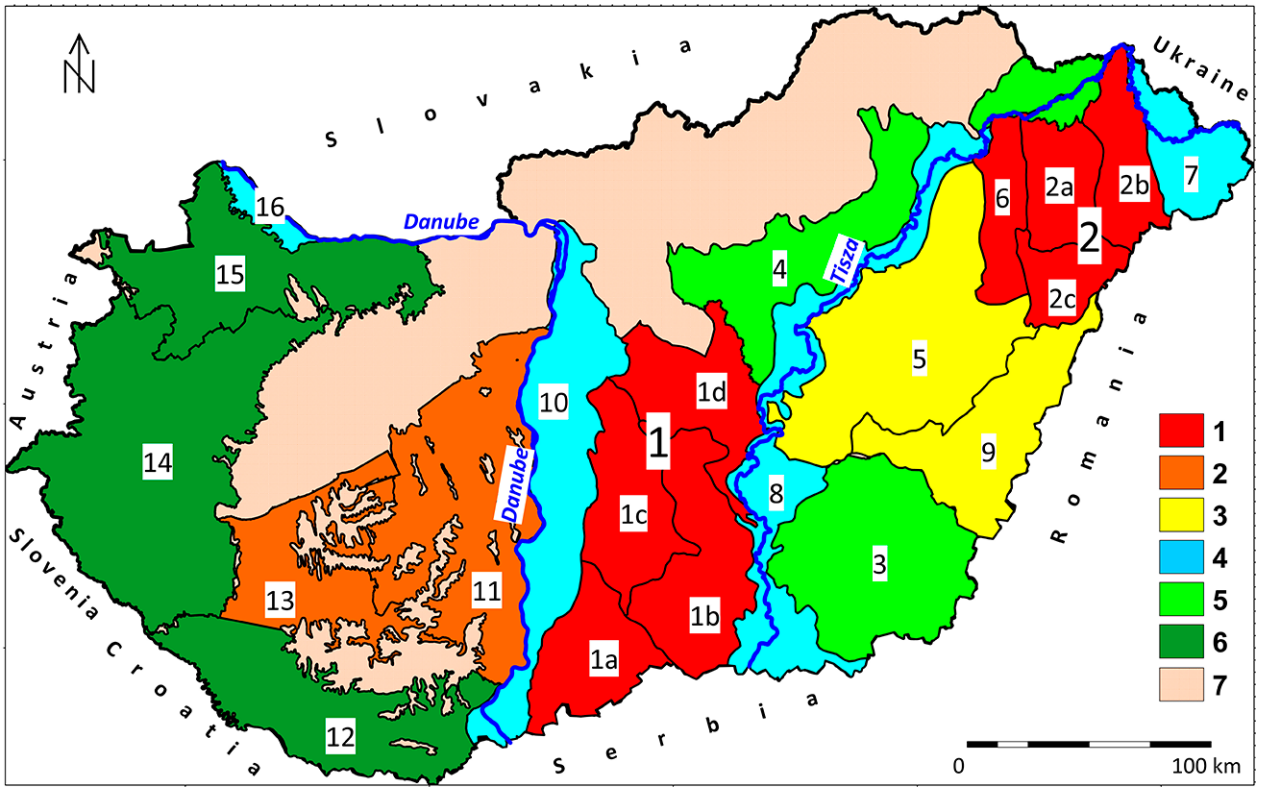

Figure 12. Climate sensitivity of Hungarian landscapes based on their water balance characteristics
a: Particularly vulnerable, b: vulnerable, c: moderately vulnerable, d: partially influenced by large rivers, e: less vulnerable, f: hardly vulnerable, g: not assessed

However, a considerable decrease that appears relatively quickly can be observed during dry periods. Several consecutive wet years would only provide an opportunity for water supplies to rise to a multi-year average. In the Somogy hills, the network of measuring wells is incomplete, and its topography is heterogeneous. Therefore, the classification of this area is somewhat uncertain. However, faster changes in water resources suggest significant climate sensitivity.

c) *Moderately endangered landscapes*. Although the landscapes in this group have been intensely exposed to climatic effects, water management interventions have significantly reduced this vulnerability. The Central Tisza Plain and Berettyó–Körös Plain classified here are characterized by significant water resources fluctuations. A period of depletion due to climatic reasons from the 1980s to the mid-1990s can be observed, but to a lesser extent than would be justified by climatic effects due to extensive irrigation in the area. In the wetter period that followed, there was a significant increase in the water resources, also due to substantial inland excess water inundations). Thus, we experience larger reserves at the end of the period than 30-40 years earlier. Consequently, due to water management interventions, the impact of climate change is not visible. Thereby, maintaining current water management practices can largely eliminate the effects of climate change. It should be noted, however, that in a landscape divided by canals and smaller or larger watercourses, interpolation can show significant uncertainty.

d) *Areas partially influenced by large rivers*. Four distant areas were included in this category. They are characterized by close hydrological links with the large rivers in their vicinity. The Danube Plain on the left bank of the Danube can receive significant water replenishment through the previously deposited gravel sediments and riverbed remnants of the river. The Szigetköz after the diversion of the Danube receives water through water replacement systems. In a significant part of the Tisza Valley, dams influence the minimum water level of the river. In the case of the Upper Tisza Plain, rivers and subsurface flow from higher areas can provide additional water replenishment. Although previous research has not considered the impact of rivers larger than a few km significant, this needs to be reconsidered in recent decades. The effects of persistently lower water levels and dams change these views. Except for the Tisza Valley, a slow to moderate decline in water resources can be observed in all areas. However, reserves are already declining since there has been no significant flooding of the Lower Tisza in the last 15 years.

e) *Areas less vulnerable to climate change, as long as there are regular periods of heavy rainfall*. Despite the alluvial plain of the North Periphery of Great Hungarian Plain and the flat surface of the Maros–Körös Interfluve, they are closely linked to the mountainous areas to the north and south-east of the micro-regions, from where groundwater recharge is ensured, not only for the confined groundwater but also for the shallow groundwater. Based on recent periods, it can be concluded that while extreme rainfall distribution sometimes results in significant precipitation, the amount of groundwater can be continuously replenished from neighbouring regions.

f) *Landscapes least threatened by climate change*. We classified three regions in Western Hungary into this category. These were characterized by significantly more precipitation and fewer extremes during the last half-century than the national average. In the case of Kisalföld and Western Transdanubia, the local rainfall is presumably supplemented by reserves from the subsurface flow. In the case of the Drava plain, the role of the river in increasing water resources is less pronounced due to the topography and the effect of the dams established on the river and therefore, they are not classified in category d. Since the spatial change in the distribution of precipitation due to climate change and the increasing evaporation, the classification of the vulnerability of the landscapes may even change in the long run. There are two signs of this process. Based on the observations of the last 80 years a trend in the change of the precipitation distribution of Hungary can be suspected, with increasing occurrence of extreme hydroclimatic conditions, the eastern parts are slightly increasing, the western ones are decreasing. Furthermore, 2010 was the wettest year measured so far. This year the Kisalföld and Western Transdanubia received much less rainfall.

Our hydrodynamic models for the two small catchments based on future climate change show that the 1.5 °C temperature rise in the Dong-ér catchment will probably cause more severe water shortages than what we experienced as the consequence of the drought conditions of 2000. In the case of the Berettyó catchment, a 1.5°C temperature rise may reduce the area's water resources by 13%, equivalent to almost 80 million m^3 of water. According to the results, the water leaves the hydrological system primarily through evapotranspiration. The topographical setting enables a sufficient amount of groundwater to flow into the region from higher altitudes, ensuring to largely compensate for the water deficit but is insufficient to keep the balance of the water resources permanently. The models highlighted that subsurface inflow and evapotranspiration are the two main driving forces regulating the catchments' water balance in the Carpathian Basin. Among the water balance factors of the two investigated small catchments, the sensitivity of the components to the

1.5°C temperature rise is the following (in descending order): infiltration, water balance change, subsurface water storage, overland flow to the brook, and evapotranspiration.

Conclusion

Both society and agriculture need to adapt to the changing climatic conditions. In the Carpathian Basin, the more extreme rain distribution results in less precipitation remaining in place. Some of the extremely high rainfall flows in the form of floods out of the rivers. At the same time, efforts should be made to keep as much water as possible in the landscape.

The presented results have shown that the most crucial shallow groundwater resources for vegetation and thus for crop production in the last fifty years are generally shaped by precipitation conditions instead of human activities. Using the presented method, we show that in the mid-region's with an extent of 5-10 thousand km², the climate can change the water resources in both positively and negatively direction by up to 2-4 km³ in 1-2 years of extreme rainfall, while in the Danube-Tisza Interfluve region with the highest groundwater depletion, the extraction of confined water over the past 40 years has been 2 km³.

Changes in climatic conditions significantly affect the landscapes to varying degrees due to their natural environmental conditions. Through social adaptation, we must mitigate this, for which the results of the current study can provide vital support. Recognizing this, the *presented results were also incorporated into Hungary's updated River Basin Management Plan* completed in 2021 (OVF, 2021). Furthermore, our results have been considered in drafting the Hungarian legislation on regulating water abstraction for irrigation purposes. The next important step would be to consider the results for agricultural policy. Unfortunately, the answer to the extreme weather conditions is still drainage and irrigation. Yet the comparison of the spatial extent of the irrigated areas and the trends of irrigation water consumption shows the limitations undeniably (see Figure 7). In the last twenty years, the extent of irrigated areas is typically 1 000-1 200 km², while the area of arable land is more than 43 000 km². Characteristically, the irrigation water usage does not exceed 0.2 km³ in most years. This volume is less than a tenth of the amount that climatic effects can cause to subsurface water resources annually.

In addition to irrigation, policymakers are seriously thinking about alleviating the problem of water-scarce regions through water replenishment. The other part of our research draws attention to the fact that this cannot be a satisfactory solution either. For example, 100-200 million m3 of water per year is planned to replenish the Danube-Tisza Interfluve sand ridge's water storages, which is no more than the amount that the small regions presented in our study lose through evapotranspiration due to the increasing temperature caused by climate change.

Considering landscape conditions in water management, efforts should be made to address water-balance conditions due to climatic effects. Soil scientists have long emphasized that soil is the largest natural reservoir, and that the top one meter can conserve up to one year of rainfall volume (Várallyay, 2007; Gálya et al., 2018). Therefore, improving soil structure and soil water balance properties might be the solution to the successful adaptation to climate change. Soil regeneration farming without deep plowing has proven that this can be successfully achieved in practice. Improved soil structure can retain more water in the soil layer during prolonged rainfall events, allowing for more efficient replenishment of the shallow groundwater. During drought, vegetation can access subsurface water resources easier. Unfortunately, yet only a few farmers are taking advantage of the versatile benefits of environmentally conscious and economical soil regeneration farming nowadays (, in addition to for example better water management, less fertilizer, and fuel use, less deflation, carbon sequestration, and significantly better crop yields). This type of farming is an essential step toward sustainable agriculture. Agricultural policy-makers should admit that it is a cheaper and easier solution to deliver the knowledge to the farmers than the water. However, the various compensation programs and financial support schemes do not encourage farmers to prioritise the prevention of drought and inland excess water damages. Part of agricultural subsidies should be realigned to assist farmers in more effective adaptation to the challenges of the changing climatic conditions by teaching them more sustainable agricultural production methods.

Acknowledgement

We are grateful to DHI Group for providing us with the MIKE SHE student license.

References

Bartholy, J. & Pongrácz, R. (2017). A közelmúlt és a jövő országos éghajlati trendjei. [Recent and future climate trends of Hungary]. *Erdészeti Lapok,* 152(5), 134–136. http://erdeszetilapok.oszk.hu/01824/pdf/EPA01192_erdeszeti_lapok_2017-05_134-136.pdf

Bartholy, J., Pongrácz, R., Gelybó, Gy. & Szabó, P. (2008). Analysis of expected climate change in the Charpathian Basin using the PRUDENCE results. *Időjárás/Quarterly Journal of the Hungarian Meteorogical Service,* 112(3-4), 249-264. https://www.met.hu/downloads.php?fn=/metadmin/newspaper/2013/07/055709504d11a1fe875754a267a7ef08-112-3-4-7-bartholy.pdf

Blanka, V., Mezősi, G., Loibl, W., Szépszó, G., Csorba, P., Burghard, M., Bata, T., Nagy, R. & Vass, R. (2012). Meso-region scale change of climate in the 21th century and its potential impacts on the environment in the Carpathian basin. In: Rakonczai, J. & Ladányi, Zs. (eds.). *Review of climate change research program at the University of Szeged* (2010–2012). 25–41. http://www.geo.u-szeged.hu/images/kutatas/kiadvanyok_tartalom/Review_of_climate_change/klimavaltozas_konyv.pdf

Csorvási A., Illy, T., Sábitz, J., Szabó, P., Szépszó, G. & Zsebeházi G., (2016). A jövőre vonatkozó projekciók eredményeinek együttes kiértékelése, bizonytalanságok számszerűsítése. [Joint evaluation of the results of the projections for the future, quantification of uncertainties] *RCMTéR* (EEA-C13-10.) https://www.met.hu/downloads.php?fn=/RCMTeR/doc/reports/D4.2_C13-10_kozos-kiertekeles_projekcio.pdf

DHI Group. (2017). MIKE SHE Volume 1: User Guide. https://manuals.mikepoweredbydhi.help/2017/Water_Resources/MIKE_SHE_Printed_V1.pdf

Djurović, N. & Stričević, R. (2004). Actual state of drainage system on the experimental field "Radmilovac" and priority works to be done for the improvement of its working characteristics. *Journal of Agricultural Sciences*, 49(2), 169-177. DOI: 10.2298/JAS0402169D

EC. (2007). Green Paper. Adapting to Climate Change in Europe – Options for EU Action. https://eur-lex.europa.eu/legal-content/EN/TXT/PDF/?uri=CELEX:52007DC0354&from=EN

Farkas, J. Zs., Hoyk, E. & Rakonczai, J. (2017). Geographical analysis of climate vulnerability at a regional scale: the case of the Southern Great Plain in Hungary. *Hungarian Geographical Bulletin,* 66(2), 129-144. https://doi.org/10.15201/hungeobull.66.2.3

Fehér, Zs. & Rakonczai, J. (2019). Analysing the sensitivity of Hungarian landscapes based on climate change induced shallow groundwater fluctuation. *Hungarian Geographical Bulletin,* 68(4), 355-372. https://doi.org/10.15201/hungeobull.68.4.3

Fehér, Zs. (2015). Talajvízkészletek változásának geostatisztikai alapú elemzése – a rendelkezésre álló információk természete és feldolgozása. [Geostatistical analysis of shallow groundwater fluctuations – the nature and processing of available informations] *Hidrológiai Közlöny*, 85(2), 15-31. (in Hungarian)

Fehér, Zs. (2019). A Dél-Alföld talajvíz idősorainak nagy léptékű, geostatisztikai alapú modellezése. Két megközelítés nem folytonos monitoring adatok együttes térbeli és időbeli sztochasztikus szimulációjára. [Large scale geostatistical modelling of the shallow groundwater time series on the Southern Great Hungarian Plain. Two approaches for spatiotemporal stochastic simulation of a non-complete monitoring dataset]. *PhD doctoral dissertation*. (in Hungarian) https://doktori.bibl.u-szeged.hu/id/eprint/10122/1/FeherZs_Disszertacio.pdf

Fricke, C., Pongrácz, R. & Unger, J. (2022). Comparision of daily and monthly infra-urban thermal reactions based on LCZ classification using surface and air temperature data. *Geographica Pannonica*. 26(1), 1–11. http://www.dgt.uns.ac.rs/dokumentacija/pannonica/papers/volume26_1_1.pdf

Gál, T., Skrabit, N., Molnár, G. & Unger, J. (2021). Projections of the urban and intra-urban scale thermal effects of climate change int he 21st century for cities in Carpathian Basin. *Hungarian Geographical Bulletin,* 70(1), 19–33. https://ojs.mtak.hu/index.php/hungeobull/article/view/4920/4466

Gálya, B., Tamás, J., Blaskó, L., Riczu, P., Nistor, S., Fehér, J., Bozsik, É. & Nagy, A. (2018). Water retention possibilities in soils – Hungarian part of Tisza-river basin. *Natural Resources and Sustainable Development,* 8(1), 35-40

Garamhegyi, T., Kovács, J., Pongrácz, R., Tanos, P. & Hatvani, I. G. (2018). Investigation of the climate-driven periodicity of shallow groudwater level fluctuations in a Cental-Eastern European agricultural region. *Hydrogeology Journal*, 26(3), 677–688

Geiger, J. & Mucsi, L. (2005). A szekvenciális sztochasztikus szimuláció előnyei a talajvízszint kisléptékű heterogenitásának térképezésében. [Advantages of the sequential stochastic simulation in mapping small-scale heterogeneity of the shallow groundwater level] *Hidrológiai Közlöny*, 85(2), 37-47. (in Hungarian)

Graham, D.N. & Butts, M. (2005). Flexible, integrated watershed modelling with MIKE SHE. In Singh,

V.P. & Frevert D.K. (Eds.) *Watershed Models*. CRC Press. 245-272. ISBN: 0849336090

IPCC. (1990, 1995, 2001, 2007, 2014, 2022). Synthesis Reports. https://archive.ipcc.ch/publications_and_data/publications_and_data_reports.shtml, https://www.ipcc.ch/ar6-syr/

IPCC. (2018). Global Warming of 1.5°C. Thematic Reports. https://www.ipcc.ch/sr15/

IPCC: Climate Change. (2021). The Physical Science Basis. Technical summary. https://www.ipcc.ch/report/ar6/wg1/downloads/report/IPCC_AR6_WGI_TS.pdf

Janik, G., Hirka, A., Koltay, A., Juhász, J. & Csóka, Gy. (2016). 50 év biotikus kárai a magyar bükkösökben [50 years biotic damages in the Hungarian beech forests]. *Erdészeti Tudományos Közlemények [Forestry Scientific Publications]*, 6(1). 45–60. https://www.researchgate.net/publication/310334682_50_ev_biotikus_karai_a_magyar_bukkosokben

Kozák, P. (2020). Felszíni lefolyások változása a Duna-Tisza közi Homokhátság dél-keleti lejtőjén a klímaváltozás tükrében [Changes in surface runoff on the south-eastern slope of the Danube-Tisza Interfluve Sand Ridge in the context of climate change]. In Farsang, A., Ladányi, Zs. & Mucsi, L. (Eds.) *Klímaváltozás okozta kihívások – Globálistól a lokálisig* [Climate change challenges – From global to local]. GeoLitera, 109-115. (in Hungarian)

Laborczi, A., Bozán, Cs., Körösparti, J., Szatmári, G., Kajári, B., Túri, N., Kerezsi, Gy. & Pásztor, L. (2020). Application of Hybrid Prediction Methods in Spatial Assessment of Inland Excess Water Hazard. *ISPRS International Journal of Geo-Information,* 9, 268. DOI:10.3390/ijgi9040268

Ladányi, Zs., Blanka, V., Deák, Á. J., Rakonczai, J. & Mezősi, Gábor. (2016). *Assessment of soil and vegetation changes due to hydrologically driven desalinization process in an alkaline wetland, Hungary. Ecological Complexity,* 25, 1–10. https://doi.org/10.1016/j.ecocom.2015.11.002

Maticic, B. & Steinman, F. (2007). Assessment of land drainage in Slovenia. *Irrigation and Drainage*, 56, 127-139. DOI: 10.1002/ird.338

Nagy, Zs., Pálfi, G., Priváczkiné Hajdu, Zs. & Benyhe, B. (2019). Operation of canal systems and multi-purpose water management – Dong-ér catchment. In Ladányi, Zs. & Blanka, V. (Eds.) *Monitoring, risks and management of drought and inland excess water in South Hungary and Vojvodina.* University of Szeged. 262-275. (In Hungarian, in Serbian and in English) http://www.geo.u-szeged.hu/wateratrisk/sites/www.geo.u-szeged.hu.wateratrisk/files/pdf/kotet.pdf

OMSZ (Hungarian Meteorogical Service). (2021). Magyarország éghajlata – éghajlati visszatekintő. [Climate of Hungary – climate retrospective]. https://www.met.hu/eghajlat/magyarorszag_eghajlata/eghajlati_visszatekinto/elmult_evek_idojarasa/

Országos Vízügyi Főigazgatóság – OVF [General Directorate of Water Management] (2021). Magyarország vízgyűjtő-gazdálkodási tervének második felülvizsgálata VGT3. [Second revision of the river basin management plan of Hungary] Vitaanyag és Aszálykockázat. (in Hungarian). https://vizeink.hu/wp-content/uploads/2021/05/VGT3_II_Vitaanyag.pdf, https://vizeink.hu/wp-content/uploads/2021/04/Aszaly_VGT3_2021.pdf

Pálfai, I. (1994). *A Duna–Tisza közi hátság vízgazdálkodási problémái* [Water management problems of Danube-Tisza interfluve]. A Nagyalföld Alapítvány Kötetei 3, 111-126. (in Hungarian)

Pálfai, I. (2004). Belvizek és aszályok Magyarországon [Inland excess waters and droughts in Hungary]. 492 pp

Pieczka, I., Bartholy, J., Pongrácz, R. & Szabóné, A. K. (2019). Validation of RegCM regional and HadGEM global climate model using mean and extreme climatic variables. *Időjárás/Quarterly Journal of the Hungarian Meteorogical Service.* 123(4), 409–433. https://www.met.hu/downloads.php?fn=/metadmin/newspaper/2019/12/e72da6e6a030f99e1e33e-56d8345a629-123-4-1-pieczka.pdf

Rakonczai, J. (2011). Effects and consequences of global climate change in the Carpathian Basin. In: Blanco, J. & Kheradmand, H. (eds.): *Climate Change – Geophysical Foundations and Ecological Effects.* 297-322. https://www.intechopen.com/books/climate-change-geophysical-foundations-and-ecological-effects/effects-and-consequences-of-global-climate-change-in-the-carpathian-basin

Rakonczai, J. & Ladányi, Zs. (eds.) (2012). Review of climate change research program at the University of Szeged (2010–2012). Szeged. 128 pp. http://www.geo.u-szeged.hu/images/kutatas/kiadvanyok_tartalom/Review_of_climate_change/klimavaltozas_konyv.pdf

Rakonczai, J. & Fehér, Zs. (2015). A klímaváltozás szerepe az Alföld talajvízkészleteinek időbeli változásaiban. [The role of climate change is the Great Hungarian Plain changes in groundwater resources over time]. *Hidrológiai Közlöny*, 95(1), 1–15. (in Hungarian)

Sábitz, J., Pongrácz, R. & Bartholy, J. (2014). Estimated changes of drought tendency in the Carpathian Basin. *Hungarian Geographical Bulletin,* 63(4), 365–378.

Szalai, S. (2011). Magyarország hidroklimatológiai jellemzése. [Hydroclimatological characterization of Hungary]. „Klíma-21" füzetek. 65, 17–28.

Szatmári, J. & van Leeuwen, B. (eds.). (2013). Inland excess water – Belvíz – Suvišne unutrašnje vode.

Szeged – Novi Sad. 154 pp. http://www.geo.u-szeged.hu/~joe/pub/Meriexwa/Konyv/Inland_Excess_Water_book_pdfx.pdf

Szép, T. (2010). A klímaváltozás erdészeti ökonómiai vonatkozásai. [Economic aspects of forestry in climate change]. PhD doctoral dissertation. http://ilex.efe.hu/PhD/emk/szeptibor/disszertacio.pdf

Szilágyi, J. & Vorosmarty, Ch. (1993). A Duna-Tisza közi talajvízszint-süllyedések okainak vizsgálata. [Investigation of the causes of ground water subsidence in the area between rivers Danube and Tisza]. *Vízügyi Közlemények*, 75(3), 280-294. (in Hungarian)

Tlapáková, L. (2017). Agricultural drainage systems in the Czech landscape – identification and functionality assessment by means of remote sensing. *European Countryside*, 1, 77-98. DOI: 10.1515/euco-2017-0005

Tölgyesi, Cs., Török, P., Hábenczyus, A. A., Bátori, Z., Valkó, O., Deák, B., Tóthmérész, B., Erdős, L. & Kelemen, A. (2020). Underground deserts below fertility islands? Woody species desiccate lower soil layers in sandy drylands. *Ecography*. 43(6), 848–859. https://onlinelibrary.wiley.com/doi/10.1111/ecog.04906

Tran, Q. H. (2021): Sensitivity Analysis for Effect of Changes in Input Data on Hydrological Parameters and Water Balance Components in the Catchment Area of Hungarian Lowland. *Journal of Environmental Geography,* 14(3-4), 1-13. DOI:10.2478/jengeo-2021-0007

Túri, N. (2021). Egy tiszántúli talajcsövezett mintaterület állapotfelmérési lehetőségeinek, valamint működési hatékonyságának vizsgálata [Investigation of the status assessment possibilities and operational efficiency of a Trans-Tisza tile-drained sample area]. *Hidrológiai Közlöny,* 101(2), 62-71. (in Hungarian)

Túri, N., Rakonczai, J. & Bozán, Cs. (2021). Condition Assessment of Subsurface Drained Areas and Investigation of their Operational Efficiency by Field Inspection and Remote Sensing Methods. *Journal of Environmental Geography,* 14(3-4), 14-25. DOI:10.2478/jengeo-2021-0008

Unger, J., Gál, T., Rakonczai., Mucsi., Szatmári, J., Tobak, Z., van Leeuwen, B. & Fiala, K. (2010). Modeling of the urban heat island pattern based on the relationship between surface and air temperatures. *Időjárás/Quarterly Journal of the Hungarian Meteorogical Service,* 114(4), 287–302. https://www.met.hu/downloads.php?fn=/metadmin/newspaper/2013/07/1388f16c6299008233bfae636208b56d-114-4-5-unger.pdf

van Leeuwen, B., Barta, K., Ladányi, Zs., Blanka, V., & Sipos, Gy. (2019). Talajnedvességen alapuló aszálymonitoring távérzékelés és terepi adatok alapján [Soil moisture based drought monitoring by remote sensing and field measurements]. In: *Aszály és belvíz monitoring és menedzsment, valamint a kapcsolódó kockázatok a Dél-Alföldön és a Vajdaságban [Monitoring, risk and management of drought and inland excess water in south Hungary and Vojvodina*]. University of Szeged. 23-33. http://publicatio.bibl.u-szeged.hu/17883/

Várallyay, Gy. (2007). A talaj, mint legnagyobb potenciális víztározó. [Soil as the largest potential reservoir] *Hidrológiai Közlöny*, 87(5), 33–36. (in Hungarian).

World Economic Forum, (2020, 2021). The Global Risks Report 2020, 2021. 102.p.,96 p. https://www3.weforum.org/docs/WEF_Global_Risk_Report_2020.pdf, https://www3.weforum.org/docs/WEF_The_Global_Risks_Report_2021.pdf

ISSN 0354-8724 (hard copy) | ISSN 1820-7138 (online)

Generation of a Flood Susceptibility Map of Evenly Weighted Conditioning Factors for Hungary

Noémi Sarkadi[A], Ervin Pirkhoffer[A*], Dénes Lóczy[A], László Balatonyi[B], István Geresdi[A], Szabolcs Ákos Fábián[A], Gábor Varga[A], Richárd Balogh[A], Alexandra Gradwohl-Valkay[A], Ákos Halmai[A], Szabolcs Czigány[A]

Received: July 04, 2022 | Revised: September 15, 2022 | Accepted: September 15, 2022
doi: 10.5937/gp26-39474

Abstract

Over the past decades, in the mountainous, hilly and/or urban areas of Hungary several high-intensity storms were followed by severe flash flooding and other hydrologic consequences. The overall aim of this paper was to upgrade the national flash flood susceptibility map of Hungary first published by Czigány et al. (2011). One elementary watershed level ($FFSI_{ws}$) and three settlement level flash flood susceptibility maps ($FFSI_s$) were constructed using 13 environmental factors that influence flash flood generation. FFSI maps were verified by 2,677 documented flash flood events. In total, 5,458 watersheds were delineated. Almost exactly 10% of all delineated watersheds were included into the category of extreme susceptibility. While the number of the mean-based $FFSI_s$ demonstrated a normal quasi-Gaussian distribution with very low percentages in the quintile of low and extreme categories, the maximum-based $FFSI_s$ overemphasized the proportion of settlements of high and extreme susceptibility. These two categories combined accounted for more than 50% of all settlements. The highest accuracy at 59.02% for class 5 (highest susceptibility) was found for the majority based $FFSI_s$. The current map has been improved compared to the former one in terms of (i) a higher number of conditional factors considered, (ii) higher resolution, (iii) being settlement-based and (iv) a higher number of events used for verification.

Keywords: flood potential; flash flood; susceptibility; ArcGIS; FFSI; conditional factors

Introduction

Over the past decades many hydrological and hydraulic engineering analyses have focused on the assessment of the socio-economic consequences of flash floods (Georgakakos, 1986; Lóczy et al., 2012). In Hungary these studies have mainly sought to assess flood hazards in the floodplains of large rivers, mainly the Danube and its largest left-bank tributary, the Tisza, and less attention has been paid to mountainous and hilly areas by the Hungarian water management policy (Lóczy, 2010).

A flash flood is commonly caused by heavy or excessive rainfall within a short period of time, generally interpreted as less than 6 hours in the US, following the onset of the rainfall event (Elkhrachy, 2015; Georgakakos, 1987). In the UK, concentration time for flash floods is less than 3 hours which is in the range of the times of nowcasting (Collier, 2007). Flash floods are characterized by extreme flow uncertainty which cannot be ignored in a reasonable estimation of flood risk or in the reliable mitigation of the haz-

[A] Institute of Geography and Earth Sciences, University of Pécs, Ifjúság u. 6, 7624 Pécs, Hungary; e-mail: sarkadin@gamma.ttk.pte.hu, loczyd@gamma.ttk.pte.hu, geresdi@gamma.ttk.pte.hu, smafu@gamma.ttk.pte.hu, gazi@gamma.ttk.pte.hu, brichard@gamma.ttk.pte.hu, valkays2@gamma.ttk.pte.hu, halmaia@gamma.ttk.pte.hu, sczigany@gamma.ttk.pte.hu
[B] General Directorate of Water Management, Márvány utca 1/D, 1012 Budapest, Hungary; e-mail: balatonyi.laszlo@ovf.hu
[*] Corresponding author: Ervin Pirkhoffer, e-mail: pirkhoff@gamma.ttk.pte.hu

ard. However, others, like Schwartz and Dingle (1980) adopted the term of "hybrid floods" with a lead time of 12 hours following the causative event. Localization of flash flood hot spots is of paramount importance to prevent or mitigate losses triggered by flash floods. Today, preliminary rapid screening of flash flood-prone localities is commonly done by GIS (Al-Juaidi et al., 2018; Stathopoulos et al., 2017). This approach is the susceptibility mapping of the parameters that influence the magnitude of runoff, in other words the partitioning of rainfall into infiltration and runoff (Czigány et al., 2009; Saleh et al., 2020). Rainfall-Runoff models are integrated systems of assessing possible impacts for severe flood events (Gioti et al., 2013).

Susceptibility models employed various assessment algorithms, like fuzzy rule algorithm (Bui et al., 2019), decision tree algorithms (Khosravi et al., 2018), analytical hierarchy processes (Youssef and Hegab, 2019) and bivariate and multivariate statistical methods (Youssef et al., 2016). Ngo et al. (2018) evaluated flash flood susceptibility by using machine learning techniques such as Firefly algorithm, Levenberg–Marquardt Backpropagation and classification tree.

Susceptibility or flood potential index (FPI) is defined as the probability that a risk occurs in a particular area and in a not determined date (Santangelo et al., 2011). Susceptibility mapping (a kind of potential natural hazard mapping) is usually based on the comparison of certain conditioning factors with the distribution of previous events, the latter used as model validation. In this sense, it is the degree to which an area can be affected by future flood hazards, i.e., an estimate of the location of future events. On the other hand, susceptibility does not consider the temporal probability of the event, i.e., when, or how frequently the hazardous events may occur. Nonetheless, mapping the most susceptible locations helps us understand flood trends and can aid appropriate planning and flood prevention (Tehrany, 2014).

In contrast to susceptibility, physical vulnerability (flood risk) assessment implies the identification of the elements at risk and commonly interpreted as the impact of natural disasters on physical, manmade structures (Aleotti & Chowdhury, 1999; Arrighi et al., 2020; Compton et al., 2013; Karagiorgos et al., 2016). In other words, vulnerability can be defined as a functional relationship between the magnitude of loss and the corresponding process intensity causing the damage (Fuchs et al., 2007; Fuchs et al., 2011; Khajehei et al. 2020; Totschnig et al., 2011).

A large number of techniques are available today for the susceptibility mapping of flash floods: traditional, empirical methods and various machine learning based methods. Statistical, rule-based and automated modelling approaches commonly outperform conventional flood models due to their suitability for hazard analyses (Tehrany et al., 2019). Numerous methods have coupled empirical models with Geographical Information Systems (GIS) with the purpose of flood susceptibility modelling (Saleh et al., 2020). Several papers focused on the impact of morphometric properties on flash flood susceptibility (Apaydin et al., 2006; Biswas, 2016; Fábián et al., 2016). Other papers quantified the impact of various conditioning factors, e.g.: topography, land use and soil hydraulic properties on the partitioning of rainfall into runoff and infiltration. The conditioning forces which are assumed to explain the flash floods by Abedi et al. (2021) were slope inclination and aspect, land use/land cover, hydrological soil type, lithology, topographic wetness index (TWI), topographic position index, profile curvature, convergence index and stream power index. Youssef and Hegab (2019) only used 7 flood factors - distance from streams, slope, curvature, lithological units, angle, elevation, and TWI. However, their results showed that the Analytical Hierarchical Process (AHP) provided a good estimation for flash flood susceptibility (83.3%). Tehrany et al. (2013) and Borga et al. (2014) combined bivariate probability and logistic regression for flood susceptibility analysis in Kelantan State of Malaysia.

Whereas warning systems for large riverine flooding are well applied all around the world, flash floods still represent prediction and detection challenges due to the large spatial heterogeneity of the influencing factors.

Although flash flood guidance (FFG) systems have been in operation since the 1970s in the United States and in many other countries across the globe, still, they prediction accuracy lags the accurateness of large riverine floods (Georgakakos, 2006; Norbiato et al., 2009). In Europe, where flash floods are also common (Gaume et al., 2009), there are also numerous efforts implementing FFG (for instance, in the Black Sea and Middle East regions). Although FFG provides a useful concept that simplifies communication between hydrologists to meteorologists as well as promotes mitigation, it does not predict flash flood timing (Collier, 2007).

Although the number of studies varies greatly, it can reflect that the field of flash floods has been widely studied by researchers in different countries (continents) to a certain extent. The have been collected 175 documents in the United States had carried out the most research in this field, followed by India by 77 documents, and then 71 documents Italy (Aronica et al., 2012; De Marchi et al., 2012; Forte et al., 2005; Heredia-Calderon et al., 1999, Miglietta et al., 2008). China ranked fourth (70 documents), and France ranked fifth, with 64 published documents (Yang et al., 2022).

Over the past decades, in the mountainous, hilly and/or in urban areas of Hungary several high-intensity storms were followed by severe flash flooding and other remarkable hydrologic consequences (Fábián et al., 2009; Gyenizse & Vass, 1998; Horváth, 2005, 2007; Horváth et al., 2007; Kovács et al., 2015; Vass, 1997). The highest frequency of occurrence of heavy storms was documented in the mountainous (Bakony, Mecsek, Börzsöny, Mátra and Bükk) and foothill regions (Alpokalja) of Hungary (Czigány et al., 2009, 2010, 2011; Pirkhoffer et al., 2009). Koris et al. (2021) have been collected and analyzed 28 flash flood events in Hungary since 1875 until 2020.

To assess the flash flood hazard in Hungary, especially following the floods in May and June 2010, in a collaboration between the General Directorate of Water Management and the University of Pécs a flash flood susceptibility index (FFSI) map was elaborated for Hungary (Czigány et al., 2011). However, in the wake of climate change and the increasing weather extremities in the headwaters of the hilly and mountainous areas of Hungary an upgrade of the first national FFSI map became necessary. With the advent of available environmental data and the increased GIS computation capacity an improved version of the FFSI map could be produced jointly by the two research institutes in 2021.

The overall aims of this paper were (i) to develop a national flash flood susceptibility map and (ii) illustrate the susceptibility conditions to flash floods in the hilly and mountainous areas of Hungary. Specifically, we aimed at evaluating the flash flood susceptibility of Hungary by evaluating a total of 13 topographical, hydrological, geological, pedological and land use parameters by means of GIS. The spatial goodness of the map was verified with reported and documented hydrological damages related to intense rainfalls and flash floods.

Methods

Data acquisition and processing

All derived topographic parameters and the delineation of watersheds were based on the 10-meter resolution DEM of Hungary. The land use model was generated using the CLC-50 and CLC-2012 and the Artificial Surfaces 2012 databases.

The Hungarian Stream network spatial database of VARGEO, provided by the Hungarian Water Directorate, was applied for stream network analyses (density, bottlenecks and confluences) and the generation of watersheds.

Lithological data were obtained from the 1:100,000 resolution geological database of the Mining and Geological Survey of Hungary. Soil data were obtained from the AGROTOPO (1:100,000 scale) and DoSoReMi (one-hectare resolution) soil databases, both developed by the Research Institute of Soil Sciences and Agricultural Chemistry (TAKI).

For rainfall data two datasets were used. Firstly, the interpolated and gridded dataset of 0.1° resolution of the Hungarian Meteorological Service (OMSZ). Secondly, rainfall data collected by an automated rain gage network over the period of 2013 to 2020.

All geospatial data were processed in ArcMap 10.7.1, ArcGIS Pro 2.8.0 and SAGA GIS software environments.

Delineation of areas of flash flood potential

Hilly and mountainous areas were delineated by calculating (a) range, (b) slope variety and (c) slope majority. The three parameters were then clustered to differentiate watersheds of various topographic characters using the K-means clustering algorithm of the Multivariate Clustering model of ArcGIS Pro (Figure 1).

The primary delineation was enhanced by defining valley widths at a height of 5 meters above the centerline of the channel by using the *Vertical Distance to Channel Network* function. The maximum search radius was set at 5 km. An area was considered a plain when no valley relief of at least 5 meters was found in the search radius of 5 km. Areas, prone to inland excess water were excluded from the delineation of hilly and mountainous areas.

By unifying methods 1 and 2 polygons of areas of potentially affected by flash floods were generated (Figure 1). For the optimization of calculation capacity, 5 areas were delineated. The total area of the potentially flash flood-prone areas was 32,759 km² covering 35% of the entire land area of Hungary.

Delineation of watersheds

Watersheds were delineated in a cumulative way identifying watersheds of about 3 to 8 km², with a mean of 6 km² as a minimum unit, which is a typical size of supercells of convective events, primarily responsible for flash flood generation. The number of unit watersheds and streams totalled 5,458 and 3,103, respectively, while the total length of streams was 18,561 km.

Generation of the watershed based FFSI

Elementary watersheds were delineated using the Hydrology tools (extension) of ArcGIS/ArcMAP 10.5.1. A total of 13 conditional factors, derived from the topographical, channel and flow properties, land use, ped-

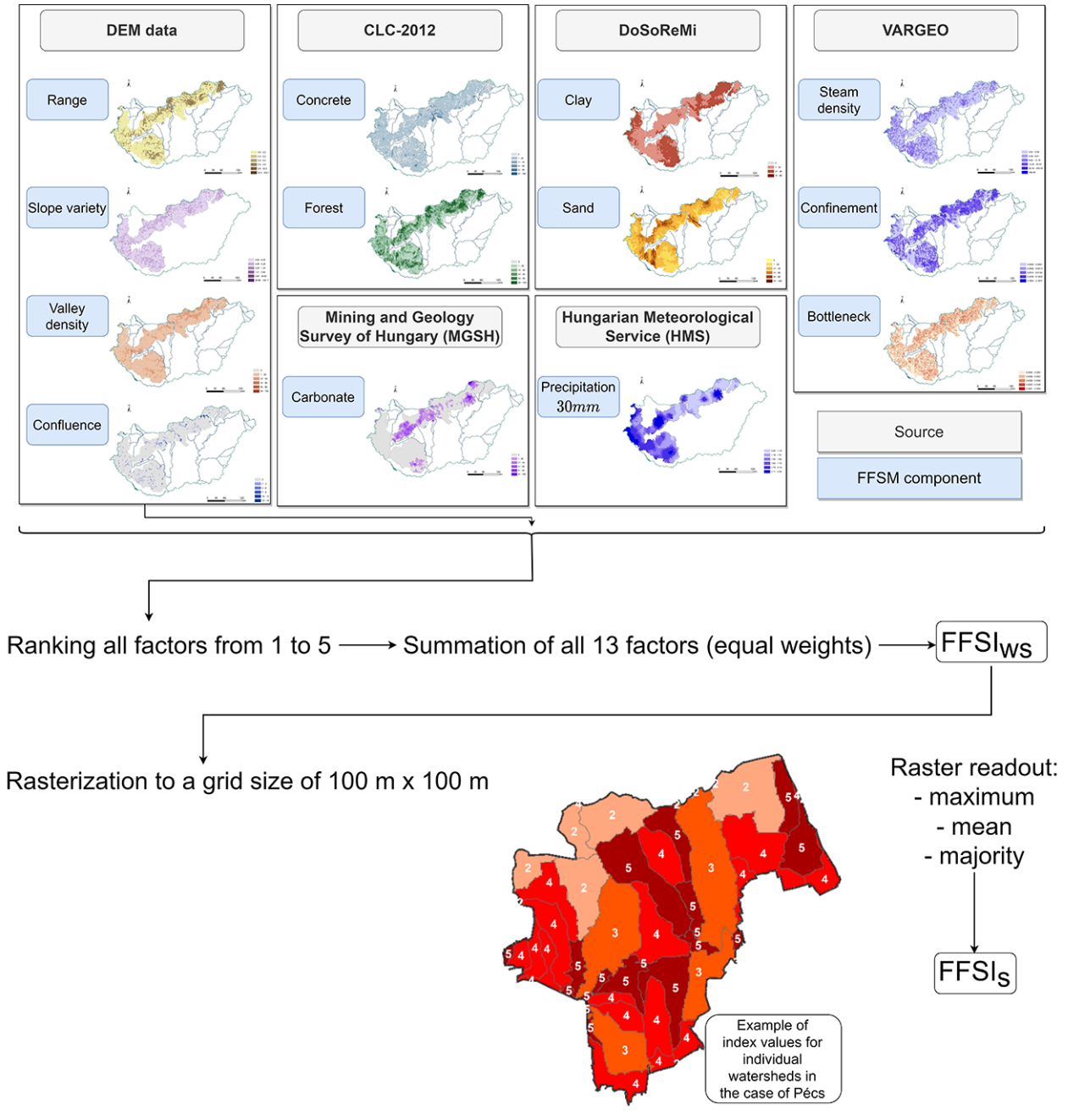

Figure 1. Flow chart visualization of the FFSIs generation

ological, geological and meteorological datasets were used for creating a watershed-based flash flood susceptibility map ($FFSI_{ws}$) of Hungary (Table 1).

The formation of flash floods is affected by several active (meteorological) and passive (morphological) parameters. These parameters (listed in Table 1) in the $FFSI_{ws}$ were selected and analyzed in terms of their impact on flash flood formation (see Table 1, influence on susceptibility). In our model only one active parameter was included, which is the annual average number of days with extreme precipitation (≥ 30 mm).

The passive factors were divided into two categories: (i) catchment characteristics (such as surface cover, lithological properties, slope variety and rate of change in range); (ii) river basin characteristics (e.g.: river density, confluence zones, bottleneck effect). All factors were ranked on a scale of 1 to 5 at watershed level (Fig. 1.), the higher the value, the higher the susceptibility. To calculate $FFSI_{ws}$ all 13 factors at a rank of 1 to 5 were summarized hence, counting each factor at an equal weight with a potentially maximum value of 65. The influence of the non-dynamic factors on flash flood susceptibility are listed below (Fig. 1 and Table 1):

- Artificial surfaces: Sealed surfaces are acting as impermeable surfaces, preventing the infiltration of precipitation and shorten the time of concen-

Table 1. Watershed scale input parameters for the FFSM.

General input category	Specific factor	Source	Influence on susceptibility
Topography	Specific relief	DEM	+
	Range of slope	DEM	+
	Valley density	DEM	+
Channel and flow parameters	Stream density	VARGEO	+
	Valley confinement	VARGEO	+
	Sinuosity	VARGEO	+
	Number of confluences per watershed	DEM	+
Land use data	Percentage of paved surfaces	CLC 2012	+
	Percentage of forests	CLC 2012	-
Pedology	Percentage of sand	DoSoReMi	-
	Percentage of clay	DoSoReMi	+
Lithology	Percentage of limestone and dolomite	MGSH*	-
Meteorology	Number of annual days with a >30 mm daily precipitation total	HMS**	+

**Mining and Geology Survey of Hungary*

***Hungarian Meteorological Service*

tration and increase runoff rate with increased yield;

- Karstic surfaces: this is the only lithological effect taken into account in this study. Limestone and dolomite surfaces were included in this category. Limestone areas typically have low surface drainage density and high infiltration rates.
- Forest cover: Canopy interception significantly delays and reduces intense runoff and provides time for early warning. Intensive forest management made the inclusion of this factor necessary.
- Valley density: from the point of view of the formation of flash floods the density of valleys, i.e., the dissection of the catchment area is really important. Note that valley density is not identical with river density, as intermittent valleys may act as linear conveyor paths facilitating water accumulation.
- Soil type: Clay and sand textured areas were calculated in all catchments. Clay and sand control runoff and infiltration adversely, i.e., clay promotes runoff, whereas sand enhances infiltration. This parameter accounts for two conditioning factors, namely (i) clay and (ii) sand percentage.
- Specific relief: the topographic conditions of the catchment, e.g., the height differences (relative relief) control the time of concentration and flow velocity. However, catchment areas with large relative relief are not necessarily hazardous. If the accumulating water does not reach an inflection point in the area, it cannot be classified as more dangerous than a catchment of lower relief. Areas that are "only" steep and have no inflection points will only conduct water through and this parameter will not indicate a hazard. In the model, we have calculated the difference between the highest and lowest points of the catchment and divided it by the catchment area.
- Slope variety: It demonstrates the ruggedness of the watershed, indicates the number of possible inflection points which dissect the terrain, and shows how many possible locations there are in the catchment where the accumulation process slows down.
- Bottleneck effect: in the case of heavy rainfall the valley bottlenecks impound runoff. On both sides of the river the valley height (up to 5 m) was examined to a horizontal distance of 5 km. Sections where the degree of constriction exceeded 50% in the flow direction compared to the previous point were sorted, and then their number in each catchment was counted and normalized to the catchment area.
- Confinement: valley morphology and asymmetry were calculated to account for blocking effect in the case of flooding. If the deviation from the center line exceeded the 50% asymmetry value, i.e., swinging left and right towards the valley sides, it was classified as a risk factor if the watercourse was closer than fifty meters to the valley edge on either side. The points in the catchment that meet this criterion were given and normalized to the catchment area.
- Drainage density: in connection with the valley density, the drainage densities of the catchments were also taken into the analysis. Lowland sections, artificial water networks, as well as watercourses shorter than 1 km have been removed from the dataset.
- Number of confluence points: We determined the confluence points (at least 2) within 500 meters'

distance, then we calculated how many confluence points are found in a given catchment area.

Except for the forested, paved and karstic areas (%) and the clay and sand percentages, all other eight factors were normalized and averaged to the catchment area.

Generation of $FFSI_s$ maps

To obtain the settlement level susceptibility indices ($FFSI_s$), feature polygons (watersheds) of each 13 conditioning factors were rasterized at a resolution of 100 × 100 m. $FFSI_s$ maps were calculated from the rasterized grid network by extracting the mean, maximum and majority raster values using the *Zonal Statistics* function of ArcGIS for the overlapping settlements. Each settlement was underlain by more than one watershed, hence calculating the majority was also an option for calculation. $FFSI_s$ was then calculated by evenly summing up each of the 13 values ranked on a scale of 1 to 5, having a maximum of 65 points potentially. Ranking was calculated using the *Geometric Intervals* extension of ArcGIS, commonly used for non-normal distribution datasets and producing results in a visually appealing and cartographically comprehensive way.

Data verification

$FFSI_s$ maps were validated using the locations of documented flash flood inventory data reported to insurance companies (Fig. 6). Database was provided by the General Directorate of Water Management of Hungary. Flash flood and intense rainfall related damages were selected from the database using the keywords "intense precipitation" and "flash flood". Accuracy of the susceptibility map was calculated for each of the quintiles by dividing the number of settlements with reported events by the total number of settlements:

$$Bin\ accuracy = \frac{S_e}{S} \cdot 100\%$$

where S_e is the number of settlements with reported events and S is the total number of settlements in the given bin.

Principal component analysis in MatLab was employed to calculate the level of influence of each of the 13 input parameters and assess the correlation of influence on flash flood generation. PC analysis showed that 10 components (out of the 13) explained 95% of all variability of our dataset. The first three component only explained 54.9% of all variations.

Results and Discussion

The watershed based $FFSI_{ws}$

In total, 5,458 watersheds were delineated. Almost exactly 10% of all delineated watersheds were included into the category of extreme susceptibility (Table 2). The highest flash flood susceptibility was found in the Southern Transdanubian region, along the western national border (the region of Alpokalja), and in the Börzsöny and the Mátra Mountains in the north central part of Hungary (Figure 2). Mean watershed area decreased to the direction of higher susceptibility demonstrating the increasingly headwater character of the watersheds. Most watersheds belonged to the category of moderate susceptibility.

In terms of the environmental factors on flash flood generation, artificial surfaces covered 5.9% of the studied river basins on average, whereas paved surfaces cover 20% of the area occurred at about 7.5% of the catchments. In comparison forest coverage was higher than 50% in 25% of the catchments, however, 32% of the studied area was afforested. The average proportion of carbonate surfaces in the studied catchments was 2.99%. 5.71% of them were covered with carbonate rocks in more than 20% of the total area. Clay and sand as physical soil type was measured on average 18.5% and 31.7%, respectively. 22.5% of the catchments showed valley density values higher than 20% (the average was 14.5%).

Settlement based susceptibility map ($FFSI_s$)

The distribution of the five susceptibility classes on the three $FFSI_s$ maps were rather different. While the

Table 2. Watershed statistics of the $FFSI_{ws}$.

Susceptibility class	Area (km²)	Mean area (km²)	Number of watersheds	%
Low	5,606	11.16	502	9.20
Moderate	16,022	8.06	1,987	36.41
Medium	6,226	5.21	1,195	21.89
High	4,039	3.28	1,229	22.52
Extreme	864	1.58	545	9.99
Total	32,757		5,458	100.00

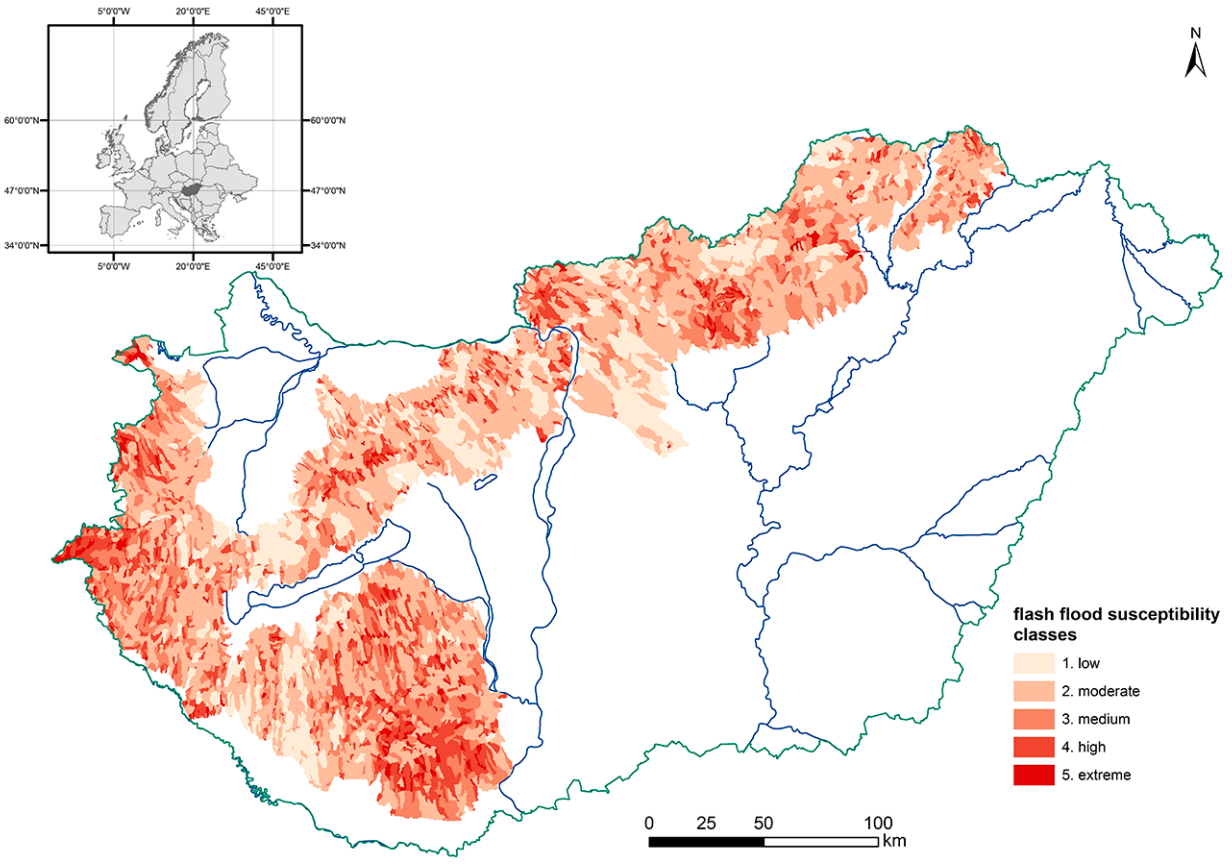

Figure 2. Elementary $FFSI_{ws}$ map of Hungary

number of the mean-based $FFSI_s$ demonstrated a normal quasi-Gaussian distribution with very low percentages in the quintile of low and extreme categories, the maximum-based $FFSI_s$ overemphasized the proportion of settlements of high and extreme susceptibility, accounting for more than 50% of both categories combined (Table 3). The number of the majority-based $FFSI_s$ again showed a normal distribution with less extreme values in the low and extreme quintiles than on the mean-based map.

The maximum based $FFSI_s$ hence showed a higher areal proportion of extreme susceptibility than the other two $FFSI_s$ maps (Figure 3). The lowest areal cover of the settlements of extreme susceptibility was found for the mean based FFSIs (Figure 5).

Data verification

The flash flood inventory data included a total of 2,677 events. On average, 62% of the analysed 1,912 settlements did not report any flash flood related losses. Hence, the average number of reported events per impacted settlement was 3.68.

According to the flood inventory, the highest absolute number of flash flood related events were reported from the city of Miskolc (38) and in the north central part of Hungary (Figure 6a). However, when the

Table 3. Statistics of the $FFSI_s$ rankings based on the mean, maximum and majority raster value

	Mean		Maximum		Majority	
Susceptibility class	Number of settlements	%	Number of settlements	%	Number of settlements	%
Low	103	5.39	316	16.53	265	13.86
Moderate	344	17.99	395	20.66	467	24.42
Medium	720	37.66	227	11.87	562	29.39
High	542	28.35	433	22.65	374	19.56
Extreme	203	10.61	541	28.29	244	12.76
Total	1912	100	1912	100	1912	100

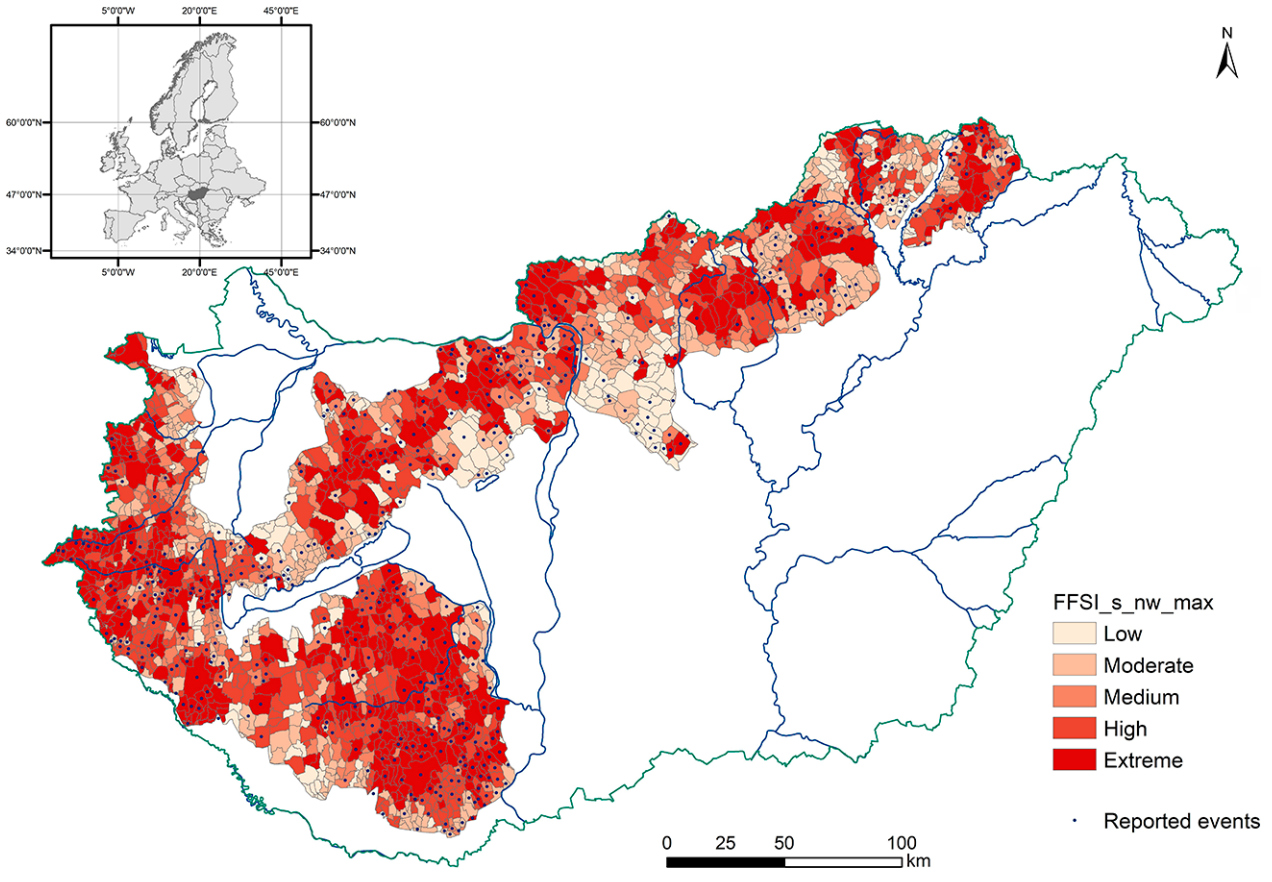

Figure 3. $FFSI_s$ map of Hungary with the maximum raster value used for susceptibility assignment

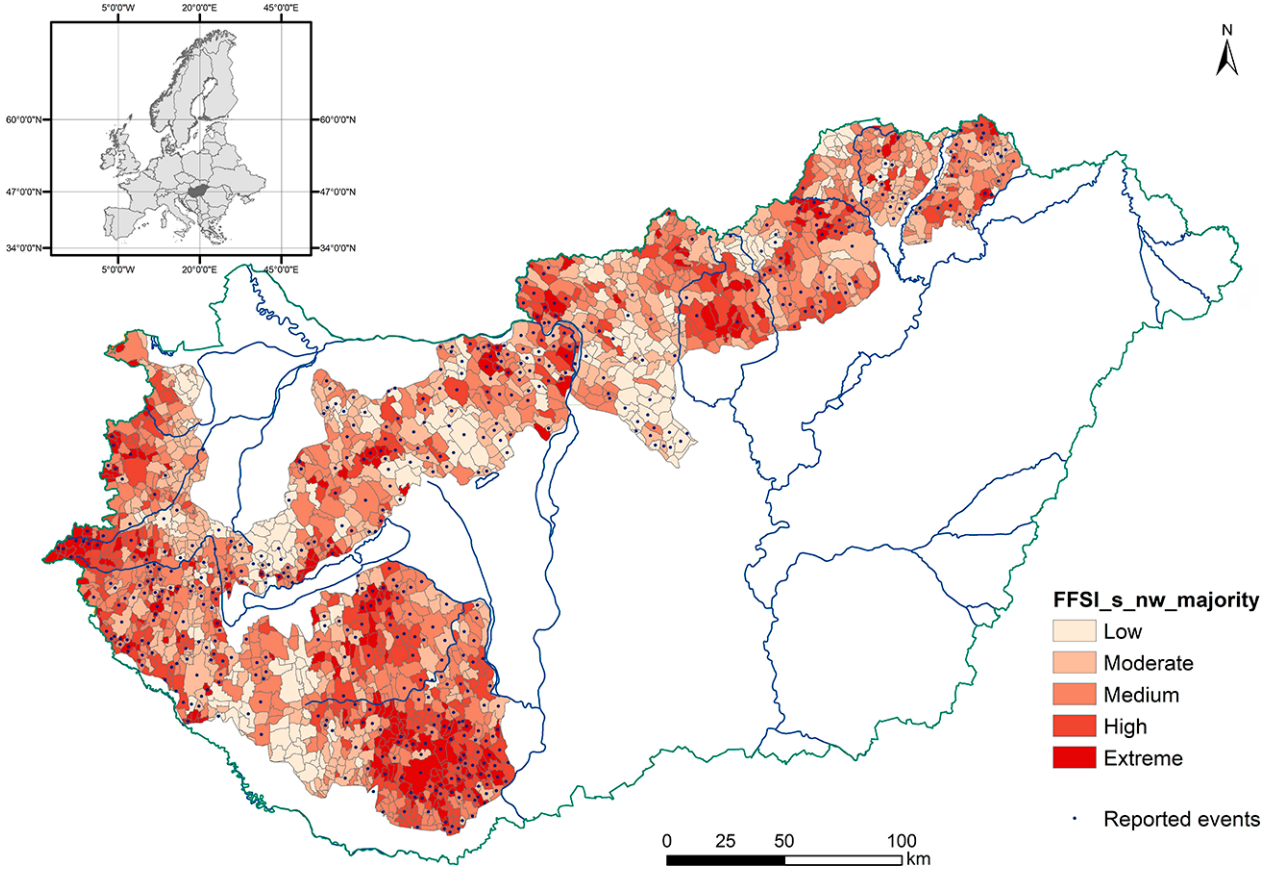

Figure 4. $FFSI_s$ map of Hungary with the majority raster value used for susceptibility assignment

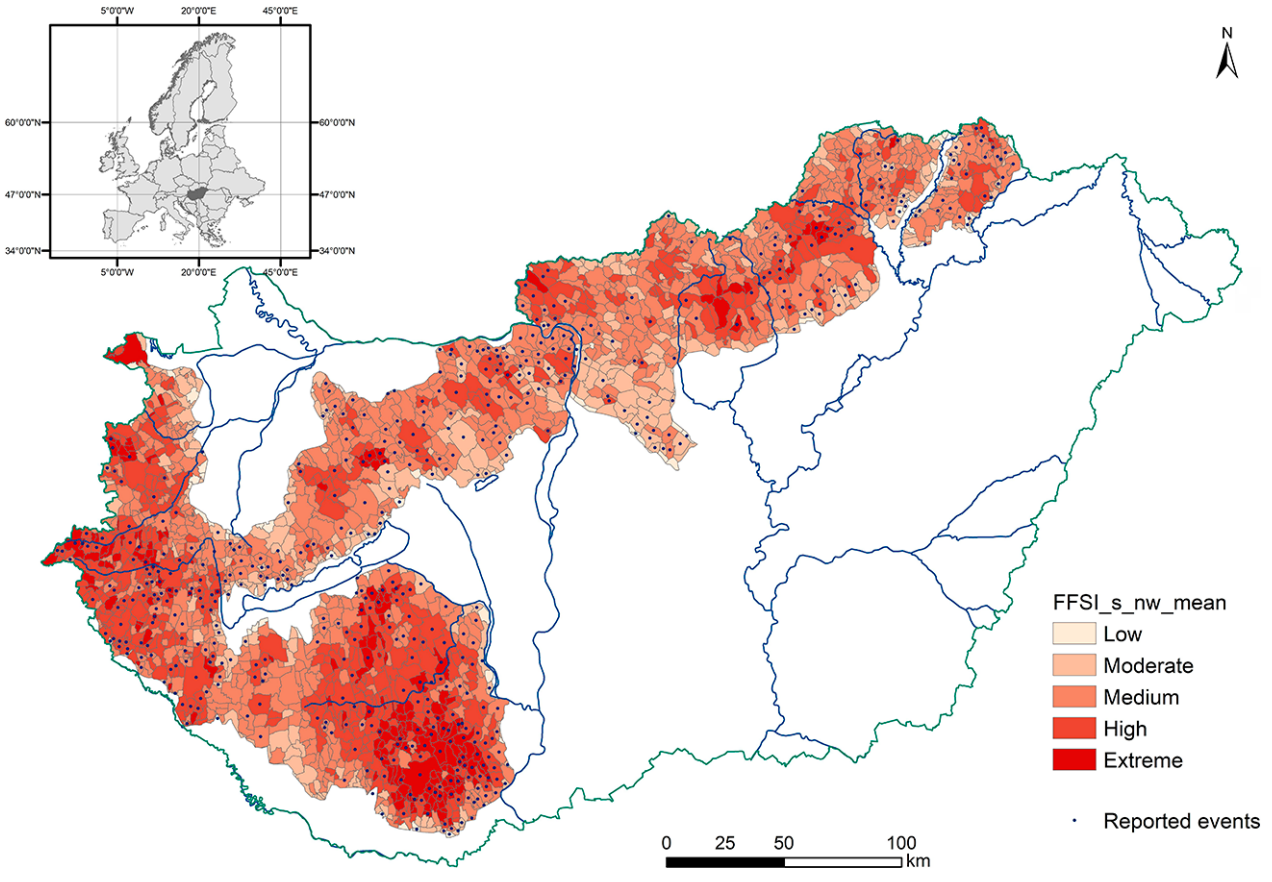

Figure 5. $FFSI_s$ map of Hungary with the mean raster value used for susceptibility assignment

number of reported events was normalized for the number of residents, the SW part of Hungary demonstrated a higher level of risk (Figure 6b). The contrasting differences in the distribution of reported events is partly due to the different settlement structures and the higher percentage of settlements of low population in the SW and NE parts of Hungary.

The accuracy of the three FFSIs maps was tested using the accuracy of the five susceptibility quintiles. Hence, the highest accuracy was expected for quantile 5 (highest susceptibility) and lowest for quantile 1 (lowest susceptibility). The highest accuracy at 59.02% for quintile 5 (highest susceptibility) was found for the majority based FFSIs, however for the same map the highest accuracy was also found here for the quintile of the lowest susceptibility (Table 4). The majority based FFSIs demonstrated the lowest accuracy for the quantile of high susceptibility (quintile 4), while FFSIs was the best at 50.74%. When accuracy of each quantile was considered, again the majority-based map performed the best at a mean accuracy of 48.41%, whereas the mean and maximum based FFSIs maps were almost identical at 46.33% and 46.29%, respectively.

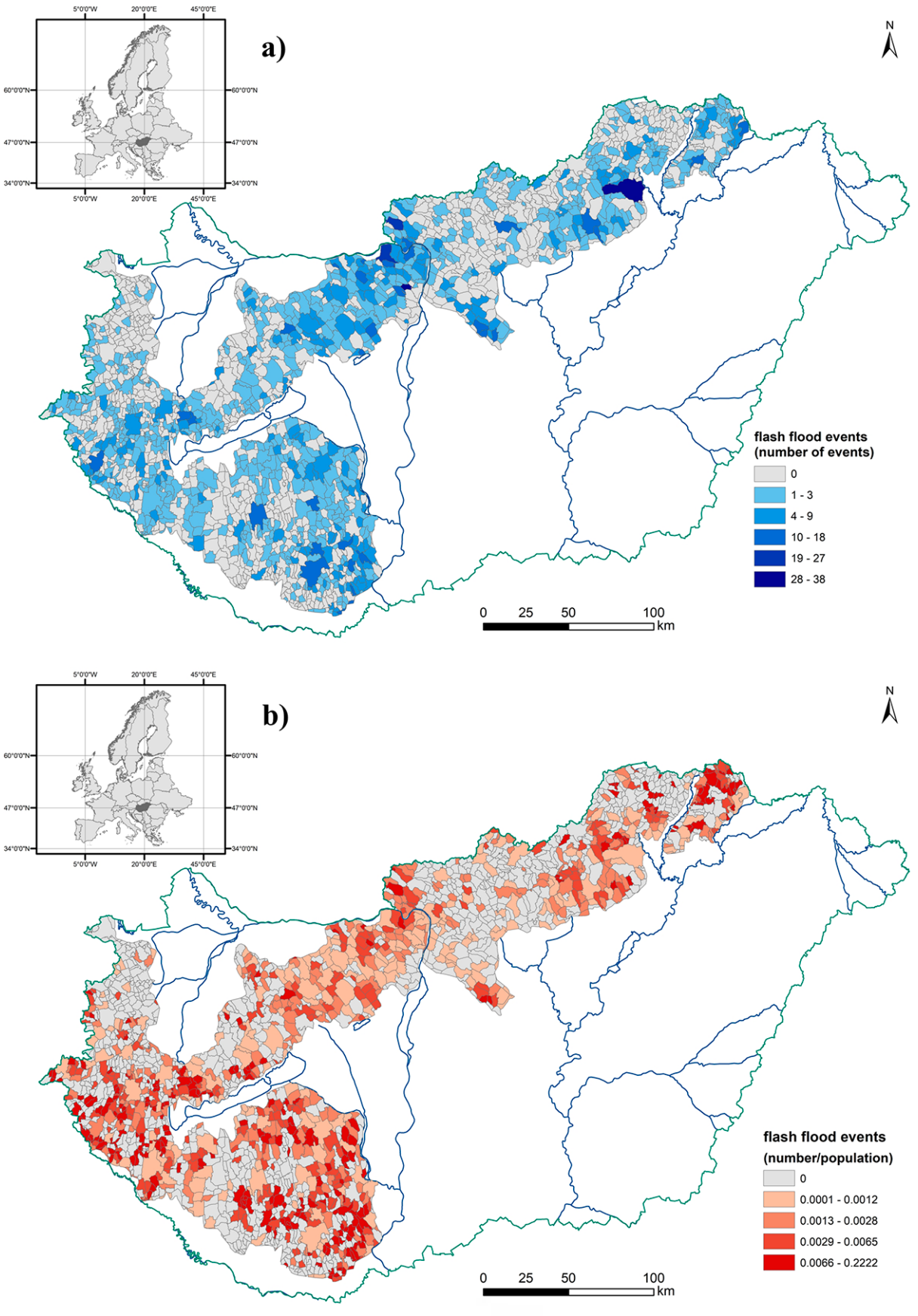

Figure 6. Reported flash flood events (a) and population normalized flash flood events (b) of Hungary

Table 4. Verification statistics for the FFSIs maps

	Mean	Maximum	Majority
Total number of settlements	1912	1912	1912
Total number of events	2677	2677	2677
Low, total number of settlements (S)	103	316	265
Low, settlement w/o reported event	66	202	157
Low, settlement with reported events (Se)	37	114	108
Low, accuracy (%)	35.92	36.08	**40.75**
Moderate, total number of settlements (S)	344	395	467
Moderate, settlement w/o reported event	205	223	257
Moderate, settlement with reported events (Se)	139	172	210
Moderate, accuracy (%)	40.41	43.54	**44.97**
Medium, number of settlements	720	227	562
Medium, settlement w/o reported event	368	128	287
Medium, settlement with reported events (Se)	352	99	275
Medium, accuracy (%)	48.89	43.61	**48.93**
High, total number of settlements (S)	542	433	374
High, settlement w/o reported event	267	215	193
High, settlement with reported events (Se)	275	218	181
High, accuracy (%)	**50.74**	50.35	48.4
Extreme, total number of settlements (S)	203	541	244
Extreme, settlement w/o reported event	90	228	100
Extreme, settlement with reported events (Se)	113	313	144
Extreme, accuracy (%)	55.67	57.86	**59.02**
Mean accuracy (%)	46.326	46.288	**48.414**

Conclusions

The currently proposed FFSIs maps comprise the second-stage development of the flash flood susceptibility map (flood potential map) of Hungary first generated and published by Czigány et al. (2011). In the present study a watershed based $FFSI_{ws}$ and three settlement level $FFSI_s$ maps were created. Using the maximum susceptibility value for statistical evaluation is a highly recommended approach, as this susceptibility level reflects the worst-case scenario for the relevant community. This approach enables decision makers to mitigate losses, however it increases the cost of flood prevention measures.

The current map, however, is a markedly improved version of the first susceptibility map. Improvements were done at the following four points:

a) The current map includes a larger number of conditional factors, specifically integrating multiple hydraulic factors that may influence channel flow.
b) The current map has a higher resolution. The current FFSI map was generated for 5,485 elementary watersheds in contrast to the 1,093 of the former FFSI map.
c) The prediction accuracy of the current map is verified by a much larger flood inventory dataset.
d) The current map focuses on settlement susceptibility/vulnerability, on the locations where damage happens.

A common number of conditioning factors used in the development of FFS maps is between 3 and 12 (Saleh et al., 2020; Tincu et al., 2018). As flash floods are generated by multiple conditioning factors, but in a site and climate specific manner, a multidisciplinary approach is needed forecasting such extreme hydrological phenomena and nowcasting the causative heavy rainfalls. However, reliable historical records are often too short. In addition, measuring peak rainfall or storm flow is subject to error. Thirdly, rainfall patterns have also changed over the past decades in the wake of climate change.

In addition to the above-discussed environmental factors, it is essential to incorporate and regularly monitor other, dynamic, non-steady environmental factors, like discharge, antecedent soil moisture contents, groundwater table depths, rainfall pattern and

canopy cover. The present model included 13 conditioning factors of even weight. A first option to improve the model of the current study is to perform a linear regression calculation to evaluate the weight of the conditioning factors, similarly to many previous studies on flood potential assessment. These papers used weighted parameters based on preliminary statistics and regression calculations. Secondly other classification methods and alternative raster resolutions may also be applied during ArcGIS processing and analyses. Consequently, a novel spatial statistical method and higher spatial resolution may be selected in GIS environment to convert watershed level data to settlement level data. Thirdly, the current susceptibility map could also be verified and compared with the susceptibility map developed for the headwater catchments of the Mecsek Hills by Fábián et al. (2016) on the basis of the morpho- and geometric properties of the studied watersheds.

Combining the current FFSIs maps with the extent of infrastructural damage the map may be further developed into a vulnerability map of advanced practical application for decision makers and end-users. For further refinement, other indirect factors may be included in the model. Khosravi et al. (2018) suggested the integration of the topographic wetness index (TWI) into FFS maps. (TWI was successfully employed in SW Hungary for the detection of soil moisture availability by Nagy et al. (2021)). Tincu et al. (2018) found a strong correlation between flow accumulation and flash flood susceptibility on a watershed of a surface area of 4,456 km².

Although the currently presented FFSI has a lower accuracy than most of the previously proposed ones, still it could serve as a useful tool for decision makers. A highlight of the current model is that it was verified with an independent dataset of flash flood related disasters and damage. The lower accuracy may also be explained by the size of the analysed area. Most studies performed flood potential analysis on drainage areas of relatively small areas, in some cases at city level (Tehrany et al., 2014), while others for areas of up to several thousands of square kilometres (Tincu et al., 2018) or the entire state of Pennsylvania (Ceru, 2012). Hence, the novelty of the current maps is their resolution compared to the dimensions of the modelled area. However, coming down to a resolution of a few km2s, vulnerability and risk mapping may also be enhanced by the actual forecasting and nowcasting of precipitation effects.

References

Abedi, R., Costache, R., Shafizadeh-Moghadam, H. & Pham, Q.B. (2021). Flash-flood susceptibility mapping based on XGBoost, random forest and boosted regression trees. *Geocarto International*, 36. https://doi.org/10.1080/10106049.2021.1920636

Aleotti, P. & Chowdhury, R. (1999). Landslide hazard assessment: summary review and new perspectives. *Bulletin of Engineering Geology and the Environment*, 58, 21–44. https://doi.org/10.1007/s100640050066

Al-Juaidi, A. E. M., Nassar, A. M. & Al-Juaidi, O. E. M. (2018). Evaluation of flood susceptibility mapping using logistic regression and GIS conditioning factors. *Arabian Journal of Geosciences*, 11, 1-10. https://doi.org/10.1007/s12517-018-4095-0

Apaydin, H., Ozturk, F., Merdun, H. & Aziz, N. M. (2006). Determination of the drainage basin characteristics using vector GIS. *Hydrology Research*, 37(2),129–142. https://doi.org/10.2166/nh.2006.0011

Aronica, G. T., Brigandí, G., & Morey, N. (2012). Flash floods and debris flow in the city area of Messina, north-east part of Sicily, Italy in October 2009: the case of the Giampilieri catchment. *Natural Hazards and Earth System Sciences*, 12(5), 1295–1309. https://doi.org/10.5194/nhess-12-1295-2012

Arrighi, C., Mazzanti, B., Pistone, F. & Catelli, F. (2020). Empirical flash flood vulnerability functions for residential buildings. *SN Applied Sciences*, 2(5), 904. https://doi.org/10.1007/s42452-020-2696-1

Biswas, S. S. (2016). Analysis of GIS based morphometric parameters and hydrological changes in Parbati River basin, Himachal Pradesh, India. *Journal of Geography & Natural Disasters*, 6(2), 175. https://doi.org/10.4172/2167-0587.1000175

Borga, M., Stoffel, M., Marchi, L., Marra, F. & Jakob, M. (2014). Hydrogeomorphic response to extreme rainfall in headwater systems: Flash floods and debris flows. *Journal of Hydrology*, 518,194–205. https://doi.org/10.1016/j.jhydrol.2014.05.022

Bui, D. T., Tsangaratos, P., Ngo, P. T., Pham, T. D. & Pham B. T. (2019). Flash flood susceptibility modeling using an optimized fuzzy rule based feature selection technique and tree based ensemble methods. *Science of the Total Environment*, 668, 1038–54. https://doi.org/10.1016/j.scitotenv.2019.02.422

Ceru, J. (2012). Flash Flood Potential Index (FFPI) for Pennsylvania. Proceedings, 2012 ESRI Federal GIS Conference. Available at: http://proceedings.esri.com/library/userconf/feduc12/papers/user/JoeCeru.pdf (29.06.2022)

Collier, C. (2007). Flash flood forecasting: what are the limits of predictability? *Quarterly Journal of the Royal Meteorological Society,* 133, 622A, 3–23. https://doi.org/10.1002/qj.29

Compton, K. L., Ermolieva, T., Linnerooth-Bayer, J., Amendola, A., Faber, R. & Nachtnebel, H.-P. (2013). Modeling Risk and Uncertainty: Managing Flash Flood Risk in Vienna. In, Amendola, A., Ermolieva, T., Linnerooth-Bayer, J. & Mechler, R. (Eds.) *Integrated Catastrophe Risk Modeling: Supporting Policy Processes*. Dordrecht: Springer. https://doi.org/10.1007/978-94-007-2226-2_2

Czigány, S., Pirkhoffer, E. & Geresdi I. (2009). Environmental impacts of flash floods in Hungary. In: Samuels, P., Huntington, S., Allsop, W. & Harrop, J. (Eds.) *Flood Risk Management: Research and Practice*, London: Taylor and Francis Group. pp. 1439-1447

Czigány, S., Pirkhoffer, E. Fábián, S. Á. & Ilisics, N. (2010). Flash floods as natural hazards in Hungary, with special focus on SW Hungary. Riscuri si Catastrofe, 8, 131-152.

Czigány, S., Pirkhoffer, E., Nagyváradi, L., Hegedűs, P. & Geresdi, I. (2011). Rapid screening of flash flood-affected watersheds in Hungary. Zeitschrift für Geomorphologie, 55, 1-13. https://doi.org/10.1127/0372-8854/2011/0055S1-0033

De Marchi, B. & Scolobig, A. (2012). The views of experts and residents on social vulnerability to flash floods in an Alpine region of Italy. *Disasters*, 36, 316–337. https://doi.org/10.1111/j.1467-7717.2011.01252.x

Elkhrachy, I. (2015). Flash Flood Hazard Mapping Using Satellite Images and GIS Tools: A Case Study of Najran City, Kingdom of Saudi Arabia (KSA). *The Egyptian Journal of Remote Sensing and Space Science,* 18, 261-278. https://doi.org/10.1016/j.ejrs.2015.06.007

Fábián, S. Á., Görcs, N. L., Kovács, I. P., Radvánszky B. & Varga, G. (2009). Reconstruction of flash flood event in a small catchment: Nagykónyi, Hungary. *Zeitschrift für Geomorphologie*, 53, 123-138. https://doi.org/10.1127/0372-8854/2009/0053S3-0123

Fábián, S. Á., Kalmár, P., Józsa, E., & Sobucki, M. (2016). Hydrogeomorphic exploration of a local headwater stream in low mountainous environment following detailed field survey protocol (Mecsek Mountains, Hungary). *Revista de Geomorfologie*, 18, 77-90. https://doi.org/10.21094/rg.2016.134

Forte, F., Pennetta, L. & Strobl, R.O. (2005). Historic records and GIS applications for flood risk analysis in the Salento peninsula (southern Italy). *Natural Hazards and Earth System Sciences*, 5, 833–844. https://doi.org/10.5194/nhess-5-833-20057

Fuchs, S., Heiss, K. & Hübl, J. (2007). Towards an empirical vulnerability function for use in debris flow risk assessment. *Natural Hazards and Earth System Sciences*, 7, 495-506. https://doi.org/10.5194/nhess-7-495-2007

Fuchs, S., Kuhlicke, C. & Meyer, V. (2011). Editorial for the special issue: vulnerability to natural hazards - the challenge of integration. *Natural Hazards*, 58, 609-619. https://doi.org/10.1007/s11069-011-9825-5

Gaume, E., Bain, V., Bernardara, P., Newinger, O., Barbuc, M., Bateman, A., Blaškovičova, L.; Bloschl, G., Borga, M., Dumitrescu, A., Daliakopoulos, I., Garcia, J., Irimescu, A., Kohnova, S., Koutroulis, A., Marchi, L., Matreata, S., Medina, V., Preciso, E., Sempere-Torres, D., Stancalie, G., Szolgay, J., Tsanis, I., Velascom, D. & Viglione, A. (2009). A compilation of data on European flash floods. *Journal of Hydrology*, 367(1), 70–78. https://doi.org/10.1016/j.jhydrol.2008.12.028.

Georgakakos K.P. (1986): On the design of national, real-time warning systems with capability for site specific flash flood forecasts. *BAMS*, 67, 1233-1239. https://doi.org/10.1175/1520-0477(1986)067<1233:OTDONR>2.0.CO;2

Georgakakos, K. P. (1987). Real-time flash flood prediction. *Journal of Geophysical Research*, 92, 9615–9629. ISSN 0148-0227

Georgakakos, K. P. (2006). Analytical results for operational flash flood guidance. *Journal of Hydrology*, 317, 81–103. https://doi.org/10.1016/j.jhydrol.2005.05.009

Gioti, E., Riga, C., Kalogeropoulos, K. & Chalkias, C. (2013). A GISbased flash flood runoff model using high resolution DEM and meteorological data. *EARSeL eProceedings*, 12(1), 33–43.

Gyenizse P. & Vass P. (1998) A természeti környezet szerepe a Nyugat-Mecsek településeinek kialakulásában és fejlődésében [The role of physical environment on the urban evolution of the settlements of the Western Mecsek Hills]. *Földrajzi Értesítő* 47, 131-148. (in Hungarian)

Heredia-Calderon, E. & Siccardi, F. (1999). Regional analysis of short duration precipitation annual maxima in Liguria (Italy). *IAHS Publ.*, 254, 71–78.

Horváth, Á. (2005). A 2005. április 18-i mátrakeresztesi árvíz meteorológiai háttere. [Meterological background of the Mátrakeresztes flash flood on April 18, 2005]. *Légkör*, 50, 6-10. (In Hungarian)

Horváth, Á. (2007). A légköri konvekció és a budapesti vihar. [Atmospheric convection and the Budapest Storm]. *Természettudományi Közlöny*, 138(5), 206-209. (in Hungarian)

Horváth, Á., Geresdi, I., Németh, P. & Dombai, F. (2007). The Constitution Day storm in Budapest: case study of the August 20, 2006 severe storm. *Időjárás / Quarterly Journal of the Hungarian Meteorological Service,* 111(1), 41-63.

Karagiorgos, K., Thaler, T., Maris, F. & Fuchs, S. (2016). Assessing flash flood vulnerability using a multi-vulnerability approach. FLOODrisk 2016 - *3 rd European Conference on Flood Risk Management*. E3S Web of Conferences 7, 08004. https://doi.org/10.1051/e3sconf/20160708004

Khajehei, S., Ahmadalipour, A., Shao, W. & Moradkhani, H. (2020). A Place-based Assessment of Flash Flood Hazard and Vulnerability in the Contiguous United States. *Scientific Reports*, 10, 448. https://doi.org/10.1038/s41598-019-57349-z

Khosravi, K., Pham, B. T., Chapi, K., Shirzadi, A., Shahabi, H., Revhaug, I., Prakash, I., Tien Bui, D., Shahabi, H., Chapi, K., Shirzadi, A., Pham, B. T., Khosravi, K. & Revhaug, I. (2018). A comparative assessment of decision trees algorithms for flash flood susceptibility modeling at Haraz watershed, northern Iran. *Science of Total Environment*, 627, 744–755. https://doi.org/10.1016/j.scitotenv.2018.01.266

Koris, K., Balatonyi, L., Bálint M., Filutás I., Horváth G., Kerék G., Koris K., Kovács P., Simonics L., Somogyi P., Takács Z., & Varga Gy. (2021). Magyarország kisvízfolyásainak árvizei, Budapest, Magyarország: Országos Vízügyi Főigazgatóság (OVF), 345 pp. ISBN: 9786155825026, Available online: https://vpf.vizugy.hu/reg/ovf/doc/koris_balatonyi.pdf

Kovács, I. P., Czigány, S., Józsa, E. Varga, T., Varga, G., Pirkhoffer, E. & Fábián, S. Á. (2015). Geohazards of the natural protected areas in Southern Transdanubia (Hungary). *Dynamiques Environmentales*, 35, 97-110. https://doi.org/10.4000/dynenviron.1182

Lóczy, D. (2010). Flood hazard in Hungary: a re-assessment. *Central European Journal of Geosciences*, 2, 537-547. https://doi.org/10.2478/v10085-010-0029-0

Lóczy, D., Czigány, Sz. & Pirkhoffer, E. (2012). Flash Flood Hazard. In: Muthukrishnavellaisamy, K. (Ed.): *Studies on water management issues*. Rijeka, Croatia: InTech. pp. 27-52.

Miglietta, M.M. & Regano, A. (2008). An observational and numerical study of a flash-flood event over south-eastern Italy. *Natural Hazards and Earth System Sciences*, 8, 1417–1430. https://doi.org/10.5194/nhess-8-1417-2008

Nagy, G., Lóczy, D., Czigány, S., Hrvatin, M., & Ciglič, R. (2021). Comparison of soil moisture indices and field measurements in hilly agricultural lands of SW Hungary. *Acta Geographica Debrecina Landscape and Environment,* 15, 50-57. https://doi.org/10.21120/LE/15/1/7

Ngo, P. T., Hoang, N. and Pradhan, B, Nguyen, Q. K., Tran, X. T., Nguyen, Q. M., Samui, P. & Bui, D. T. (2018). A Novel Hybrid Swarm Optimized Multilayer Neural Tropical Areas Using Sentinel-1 SAR Imagery and Geospatial Data. *Sensors*, 18, 3704. https://doi.org/10.3390/s18113704

Norbiato, D., Borga, M., & Dinale, R. (2009). Flash flood warning in ungauged basins by use of the flash flood guidance and model-based runoff thresholds. *Meteorological Applications*, 16, 65–75. https://doi.org/10.1002/met.126

Pirkhoffer, E., Czigány, S., Geresdi, I. & Nagyváradi, L. (2009). Impact of rainfall pattern on the occurrence of flash floods in Hungary. *Zeischrift für Geomorphologie*, 53, 139-157. https://doi.org/10.1127/0372-8854/2009/0053S3-0139

Saleh, A., Yuzir, A. & Abustan, I. (2020). Flash Flood Susceptibility Modelling: A Review. *IOP Conference Series: Materials Science and Engineering*, 712, 1–6. https://doi.org/10.1088/1757-899X/712/1/012005

Santangelo, N., Santo, A., Di Crescenzo, G., Foscari, G., Liuzza, V., Sciarrotta, S. & Scorpio, V. (2011). Flood susceptibility assessment in a highly urbanized alluvial fan: The case study of Sala Consilina (southern Italy). *Natural Hazards and Earth System Science*, 11, 2765–2780. https://doi.org/10.5194/nhess-11-2765-2011

Schwartz, G. & Dingle, D. R. (1980). The not quite flash flood—the hybrid. *Preprints of Second Conference on Flash Floods, American Meteorological Society*, Boston, MA. 254-258.

Stathopoulos, N., Kalogeropoulos, K., Polykretis, C., Skrimizeas, P., Louka, P., Karymbalis, E, & Chalkias, C. (2017). Introducing Flood Susceptibility Index Using Remote-Sensing Data and Geographic Information Systems, in: Petropoulos, G.P., & Islam, T. (Eds.): Remote Sensing of Hydrometeorological Hazards (1st ed.). CRC Press. https://doi.org/10.1201/9781315154947

Tehrany, M. S., Pradhan, B. & Jebur, M.N. (2013). Spatial prediction of flood susceptible areas using rule based decision tree (DT) and a novel ensemble bivariate and multivariate statistical models in GIS. *Journal of Hydrology*, 504, 69–79. https://doi.org/10.1016/j.jhydrol.2013.09.034

Tehrany, M.S, Lee, M.J., Pradhan, B., Jebur, M.N. & Lee, S. (2014). Flood susceptibility mapping using integrated bivariate and multivariate statistical models. *Environmental Earth Sciences*, 72, 4001–4015. https://doi.org/10.1007/s12665-014-3289-3

Tehrany, M. S., Kumar, L., Neamah Jebur, M. & Shabani, F. (2019). Evaluating the application of the statistical index method in flood susceptibility mapping and its comparison with frequency ratio and logistic regression methods. *Geomatics, Natural Hazards Risk*, 10(1), 79–101. https://doi.org/10.1080/19475705.2018.1506509

Tincu, R., Lazar, G. & Lazar, I. (2018). Modified Flash Flood Potential Index in order to estimate areas with predisposition to water accumulation. *Open Geoscience*, 10, 593–606. https://doi.org/10.1515/geo-2018-0047

Totschnig, R., Sedlacek, W. & Fuchs, S. (2011). A quantitative vulnerability function for fluvial sediment transport. *Natural Hazards*, 258, 681-703. https://doi.org/10.1007/s11069-010-9623-5

Vass, P. (1997). Árvizek a Bükkösdi-patak felső szakaszán. [Floods in the headwaters of the Bükkösd Stream]. In Tésits R. &Tóth J. (Eds.): *Földrajzi tanulmányok a pécsi doktoriskolából*. [Geographical studies from the Earth Sciences Graduate School of University of Pécs]. I. Bornus Nyomda, Pécs, 261-285. (in Hungarian)

Yang, Z., Yuan, X., Liu, C., Nie, R., Liu, T., Dai, X., Ma, L., Tang, M., Xu, Y. & Lu, H. (2022). Meta-Analysis and Visualization of the Literature on Early Identification of Flash Floods. *Remote Sensing*, 14, 3313. https://doi.org/10.3390/rs14143313

Youssef, A. M., Pradhan, B. & Sefry, S. A. (2016). Flash flood susceptibility assessment in Jeddah city (Kingdom of Saudi Arabia) using bivariate and multivariate statistical models. *Environmental Earth Sciences*, 75, 1–16. https://doi.org/10.1007/s12665-015-4830-8

Youssef, A. M. & Hegab, M. A. (2019). 10-Flood-Hazard Assessment Modeling Using Multicriteria Analysis and GIS: A Case Study—Ras Gharib Area, Egypt. *Spatial Modeling in GIS and R for Earth and Environmental Sciences*, 229–257. https://doi.org/10.1016/B978-0-12-815226-3.00010-7

ISSN 0354-8724 (hard copy) | ISSN 1820-7138 (online)

River Ice Monitoring of the Danube and Tisza Rivers using Sentinel-1 Radar Data

Boudewijn van Leeuwen[A*], György Sipos[A], Jenő Lábdy[B], Márta Baksa[B], Zalán Tobak[A]

Received: August 04, 2022 | Revised: September 21, 2022 | Accepted: September 21, 2022
doi: 10.5937/gp26-39962

Abstract

Due to extreme weather, occasionally Hungary's main rivers and lakes grow an ice cover causing severe damage to infrastructure and increased flood hazard. During cold periods in 2017 and 2022, a dangerous layer of ice developed on the main rivers in the country. Since river ice is rare in this region, no permanent ice monitoring system is in operation. Due to their all weather capabilities, active remote sensing instruments provide a good opportunity to monitor ice coverage. ESA's Sentinel-1 radar satellites acquire data with a relatively high spatial and temporal resolution. A method was developed to provide ice coverage information at a regular interval; depending on the satellite revisit, at least once every 5 days, but often also on a daily basis. In 2017, maps were created for sections along the Danube and in 2022 for another section of the Tisza river. The ice coverage was calculated with a spatial resolution of 10 metre and visualised with a spatial density of 100 metre along the rivers. The mapping procedure provides visual information to give a fast overview of the spatial extent of ice coverage and quantitative, tabular information for operational activities to mitigate the damage due to ice packs and ice jams.

Keywords: river ice; classification; Sentinel-1; flood; radar; Danube; Tisza

Introduction

January 2017 was the coldest month in Hungary in 30 years. The extreme temperatures were due to a Canadian High and Siberian anticyclone resulting in a large stationary high pressure area over Europe which caused cold air to flow from Scandinavia and Russia to Central and Eastern Europe (Horváth, 2017). The average daily temperature in Hungary in January was -5.8 °C, which is 4.5 °C lower than the long term annual mean. Due to a thin layer of snow and clear skies, the temperature dropped to its lowest point of -28.1 °C in Tésa on January 8. After a short, slightly warmer period in the middle of the month, a new, extremely cold period followed with average daily temperatures well below -6 °C (OMSZ, 2017). Due to the continuous low temperatures, ice developed on Hungary's main rivers and lakes (Gombás & Balatonyi, 2017; Liptay et al., 2021). From January 6 until February 3, 2017, everywhere along the Danube large patches and packs of river ice occurred (Takács & Kern, 2017). Although in the winter season of 2021/2022, the average monthly temperatures were not extreme (2.3 and 1.1°C in December and January at Szeged), there was a long cold period with average daily temperatures below 0°C from January 7 till January 25, 2022. (https://ogimet.com). The daily maximums were between 0-5°C, but the daily minimums were below freezing point, sometimes even below -10°C. These meteorological conditions resulted in river ice development on Tisza River.

The presence and frequency of floating or static ice on the largest rivers in the Carpathian Basin has changed a lot in the last 120 years (Takács et al., 2018; Keve, 2017b). While earlier floods caused by ice were

[A] Department of Geoinformatics, Physical and Environmental Geography, University of Szeged, 6722 Szeged, Egyetem str. 2-6. leeuwen@geo.u-szeged.hu; gysipos@geo.u-szeged.hu; tobak@geo.u-szeged.hu
[B] General Directorate of Water Management, 1012 Budapest, Márvány utca 1/d. labdy.jeno@ovf.hu; baksa.marta@ovf.hu
[*] Corresponding author: Boudewijn van Leeuwen; e-mail: leeuwen@geo.u-szeged.hu

a common phenomenon (at the Danube in 1838, 1839, 1850, 1876, 1878, 1883, 1891, 1920, 1923, 1926, 1929, 1940, 1941 and 1956, Keve, 2017b), from the second half of the 20th century, static ice cover occurred only sporadically (e.g. in 1962/1963 for a longer period and last time in 1984/1985, Takács & Kern, 2017). From 2000 not just static ice formation but also the occurrence and duration of ice floe periods decreased (Ionita et al., 2018). Since 2000, the ice floe period has never been longer than 20 days. Floating ice could be observed along the Danube (Budapest and Mohács) for more than 10 days in 2005/2006, 2011/2012 and 2016/2017 (Takács & Kern, 2017).

The development of river ice increases the risk of flooding, damage to infrastructure and transportation problems (Highs, 2009; Chu et al., 2015; Agafonova et al., 2017). The high pressure of the ice can cause problems in harbours, docks, buildings, and other flood defence structures. It can also damage the river bank and its vegetation. In Hungary, in addition to local protection measures, an icebreaker fleet is being deployed to combat river ice (Gombás & Balatonyi, 2017). Icebreakers are used to make rivers accessible for transport and reduce the pressure on infrastructure caused by ice collisions. It is important to map the ice coverage to optimize protection measures. However, as river ice does not occur often, no permanent monitoring system, covering the main rivers, is installed like in other countries with regular occurrence of river ice (Keve, 2014). The only attempt to monitor river ice in Hungary known to the authors is a network of five web cameras (four cameras, of which three on the Danube and one on the Tisza, were still operational in March 2022) on a 130 kilometer long segment of the Danube (Keve, 2017a). Permanent monitoring systems are expensive to maintain, restricted to a limited number of places and are technically challenging (Keve, 2017b; Keve 2020).

Active remote sensing data can be acquired at relatively fine spatial resolutions and operate in the microwave range. This circumvents the effect of haze and cloud cover and provides potential opportunities for the development of valuable automatic and periodic river-ice monitoring tools (Chu et al., 2015). Since 2015, ESA's Sentinel-1 radar satellites acquire data with a high spatial and high temporal resolution (Malenovský et al., 2012). This data provides new possibilities for the semi-permanent monitoring of ice coverage of large rivers and lakes (Van Leeuwen et al., 2018). Earlier research demonstrated that remote sensing data can be used to detect, classify and monitor ice on sea or on large lakes (Tom et al., 2020; Howell et al., 2021; Zhang et al., 2021; Lohse et al., 2020; Li et al., 2021). River ice monitoring in Arctic regions has been conducted by several authors: Weber et al. (2003) used active data, Altena et al. (2021) applied different optical data sets, Goldberg et al. (2020) worked with low resolution RS data to predict ice jams, and Zakharova et al. (2021) used altimetry to classify river ice. Our research is the first attempt to monitor river ice coverage in a continental climate using high resolution radar data. Our aim is to monitor the development of ice cover on the Danube and Tisza rivers in Hungary. Here, we present the validation, improvements and spatial extension of the algorithm introduced in our preliminary research on the Danube (Van Leeuwen et al., 2018). Other characteristics like thickness, chemical composition and typisation of the ice were not the scope of this research.

Data and methods

Study area

The study areas for this research cover a major part of the Middle Danube in the Carpathian Basin where most river ice is formed. The Danube study area stretches from Dunaföldvár in Hungary, via Croatia to Belgrade in Serbia. The Lower Tisza River study area extends from Algyő in Hungary to Kanjiza in Serbia (Figure 1). This section of the Tisza was selected because of the extend of ice coverage in 2022 and it was operationally easy to validate the ice detection methods at this location. The Danube is a major river in Europe with a mean discharge of 2350 m^3/s at Budapest and 5600 m^3/s at Belgrade (Mezősi, 2016). The Middle Danube is an alluvial river on the investigated reach and has a meandering pattern in general. However, numerous bends were cut-off artificially during the regulation works of the 19th century (Somogyi, 2001), and the originally ~540 km long reach was reduced to 400 km. The most affected sections were located between Paks and Baja, and between Mohács and Apatin (Fig. 1). A major motivation behind river training at that time was to prevent so called ice jam floods, developing by the ramping of ice floes at riffles and in meanders, which blocked river flow and caused serious upstream impoundment. Flood hazard was boosted by meteorological reasons as well, since general thawing advances from west to east in the region; thus, meltwater flood waves increased both ice ramping and inundation. Nevertheless, meander cut-offs just partly solved the problem, as the river channel is still shallow and wide, several islands exist, and riffles do also develop.

The Tisza is the second largest river in the Carpathian Basin and the largest tributary of the Danube. The

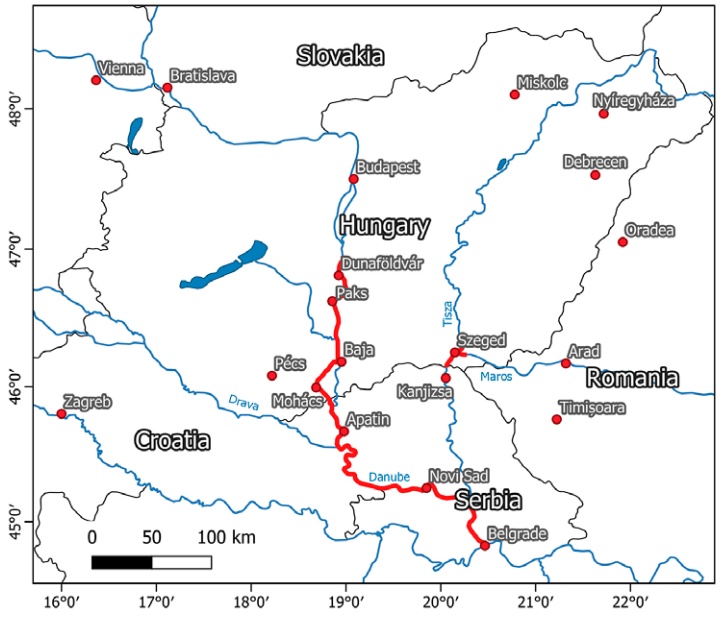

Figure 1. Study areas along the Danube and Tisza/Maros river

river is strongly regulated, i.e. its channel was shortened radically, by almost 40 % (Somogyi, 2001). Its mean discharge is 825 m³/s at Szeged (Kiss et al., 2019). The Tisza is less frequently endangered by ice jam floods. This is partly because on its catchment general spring thaw advances from southwest to northeast, i.e. opposite to its flow direction, and partly because the width/depth ratio of its channel is significantly lower than that of the Danube. The analysed river section is 40 km long and located at the Hungarian-Serbian border. The study area contains a short section of the Maros, which is the largest tributary of the Tisza.

Data

The identification of ice on the rivers is based on radar data from the Sentinel-1A and Sentinel-1B satellites. The satellites are equipped with identical 5.405 GHz C-band Synthetic Aperture Radar (SAR) instruments. In the presented workflow, we are using the Level-1 Ground Range Detected (GRD) product. Data is collected in the Interferometric Wide (IW) swath mode and has a 250 km swath width and a pixel spacing of 10 x 10 metre (Malenovský et al., 2012). The data product comes with VV and VH polarisation over land masses, but only the VV polarisation was used in our research. Data for the period from 1 January to 15 February 2017 and 19 January to 29 January 2022 was downloaded from Copernicus Open Access Hub. The data is free of charge and without restrictions of use.

The Sentinel-1 satellites form a constellation that provides an image of the area under investigation about every third day. The study areas are covered by three ascending and two descending paths, so the river sections are never covered by just one image; for each day, it is needed to mosaic different images. Since radar data is more or less independent from weather circumstances, atmospheric conditions do not disturb the data acquisition and every image that is acquired by the satellites can be used for information extraction. Unfortunately, due to a major anomaly, Sentinel-1B does not provide data since 23 December 2021, and only data from Sentinel-1A was used during the cold period in 2022.

Software

All preprocessing is carried out in ESA's SNAP open-source image processing software. Further processing and mapping are executed in ArcGIS Desktop. The processing is automated with a graph in SNAP and Python scripting in ArcGIS.

Data processing

Data preprocessing

To be able to extract useful information from the radar images, the raw radar GRD IW data need to be geometrically corrected and radiometrically calibrated. The process is presented in Figure 2. After downloading the image, the orbit state vector available from the metadata can be automatically updated, if a precise orbit file is available. In the next step, the image is calibrated to convert the raw pixel values to unbiased backscatter values. To reduce noise, which is inherent to radar images, a single image speckle filter is applied. The image is then geometrically corrected using the object-sensor geometry and a digital elevation mod-

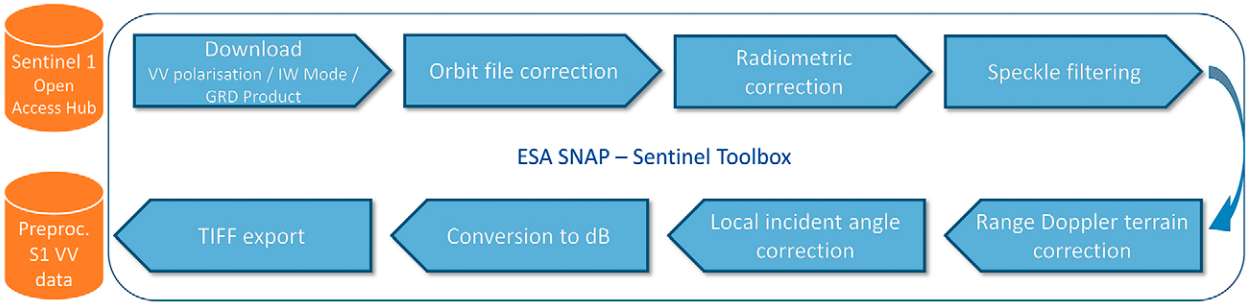

Figure 2. Raw data processing in ESA SNAP

el. In this step, also a map is created that stores the local incidence angle for each pixel in the image. Using this map, the backscatter values are normalised. Finally, the backscatter values are converted to decibel and stored as a GeoTIFF file for further processing in a geographic information system.

Creation of river polygons

The base data for the river polygon files was a 1:50,000 vector file acquired from the Hungarian General Directorate of Water Management. The file was clipped to both study areas. The resulting files for the Danube and Tisza areas were then draped over very high resolution GeoEye imagery in Google Earth and manually edited to reduce errors due to shadows, sandbanks, islands, and man-made structures. For both rivers, the centreline was extracted and perpendicular intersections with a spacing of 100 metre were calculated. For the Danube, the 405 km long polygon was split along its centreline into 4050 one-hundred-metre sections. The Tisza polygon map resulted in an approximately 40 km long polygon, with 371 one hundred metre sections along the Tisza and Maros. In both polygon files, islands, meanders, splittings and other problems were manually corrected, and the sectors were adjusted manually to coincide with the fluvial kilometre (fkm) markings of the Hungarian water directorate.

Ice detection

The strength of backscattered radar signals is highly dependent on the dielectric properties of the surface. The dielectric constant of clear and dry ice is between 2.0 and 3.2, while the dielectric constant of water is 80. Therefore, water results in a lower signal than dry ice. Ice with a rough surface gives the highest signal, while smooth non turbid water gives the lowest signal (Figure 3). A thawing ice layer with a higher dielectric constant and higher water and moisture content, produces a higher return signal compared to that of the layers with low dielectric constant, such as clear and dry snow/ice layers (Chu et al., 2015). The variation in ice roughness, water content and smoothness of the water makes it challenging to determine the boundary between water and ice.

After normalisation of the local incidence angle, the backscattered radar signal consists of two components: 1) surface scattering and 2) volume scattering. Smooth surfaces result in lower surface scattering, because the incoming radar signal is reflected away from the sensor, while rough surfaces have a higher signal due to diffuse surface scattering. Volume scattering is higher for ice surfaces with lots of cracks and impurities (Chu et al., 2015).

In this study, based on visual identification of the ice cover, we defined a threshold that - within the area of the river - separates surfaces below the threshold as water and above the threshold as ice (Figure 4). In this way, a binary raster map with ice and no ice pixels can be created. This raster is then converted to a polygon file and intersected with the river polygon file. For each of the 100 metre sections of the fkm file, the ratio between water and ice was calculated.

Mapping

The main goal of the mapping workflow was to create printed layouts with all information necessary for the operative decision making process. The image processing steps were conducted on individual satellite scenes.

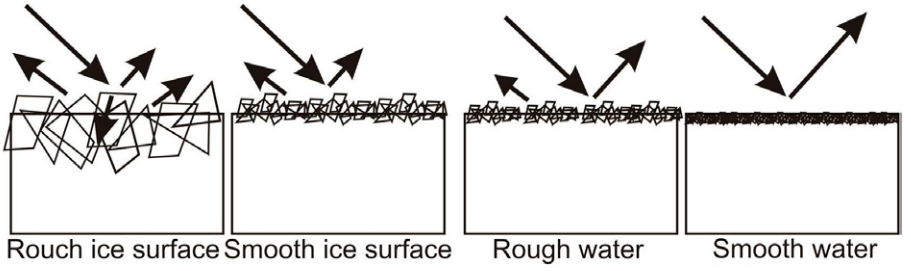

Figure 3. Relationship between ice surface and strength of the backscatter signal (Based on Unterschultz et al., 2009)

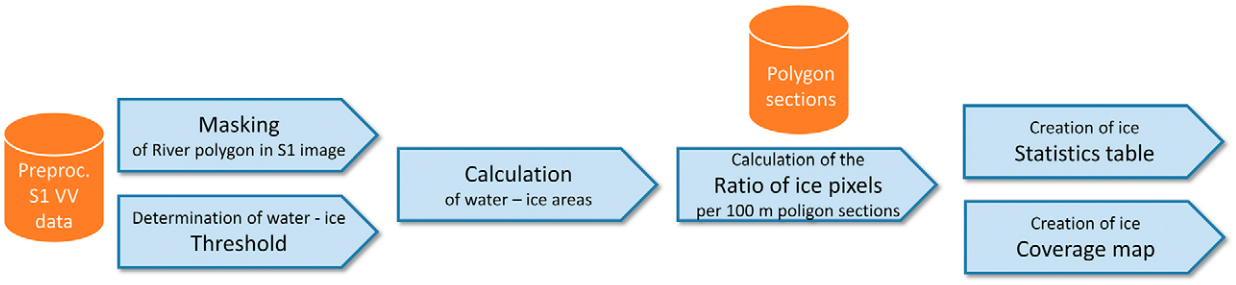

Figure 4. Processing workflow for determining ice cover from preprocessed satellite images

Therefore, the calculated ice cover maps of the same satellite path were merged, and the overlapping areas of ascending and descending satellite paths were mosaiced. The continuous ice cover dataset was aggregated into polygons covering 100 metre sections along the river. In this way, not only the actual position, but also the proportion of the ice cover is visualised.

Printable layouts were generated for each day when satellite data was available of the study area. In the case of the Danube, the whole 400 km section was divided into 8 smaller parts. This way the layouts could have better resolution when printed on A3 paper format. They contain multiple map frames to visualise the calculated ratio of ice cover in 100 metres sections, and the exact location of the identified ice blocks as well. The layers' symbology was generated based on the advice of the Hungarian General Directorate of Water Management to provide easily interpretable information. Optionally, the layouts can contain alphanumeric information in tabular form, presenting the exact ice cover ratio values in 100 metres sections. The dynamics of the ice cover can be visualised using the layouts of a selected river section on different dates.

Validation methods

There are no independent data sets that provide continuous information on the ice coverage of the Danube and Tisza, therefore quantitative validation of our results is problematic. Two methods have been applied to evaluate the quality of our methods. The first method is based on observations by inspectors of the Hungarian General Directorate of Water Management for the Danube River. The second method is based on comparison with independent data obtained from other optical satellites.

Comparison with ice watch data

Daily observations of ice coverage by inspectors of the Hungarian General Directorate of Water Management are aggregated to maps and tabular data with a spatial resolution of about 1 kilometre between the 1850 and 1440 fkm (Rajka, Hungary - Mohács, Hungary). This information is published on the hydroinfo webpage of the Hungarian General Directorate of Water Management (http://www.hydroinfo.hu/). A section to the south of Dunaföldvár with a length of 5 kilometres was selected to be compared to the satellite-derived ice coverage. The hydroinfo data is published in five ordinal classes: No ice, small ice cover, medium ice cover, large ice cover, completely covered. The radar derived ice coverage in percentage was aggregated to the same section as the observation.

Comparison with multispectral imagery

Multispectral data was evaluated as a source for validation of the presented method. Landsat 8 and Sentinel-2 data were considered, because they have similar resolution as Sentinel-1, they can be acquired free of charge and Sentinel-2 has a high temporal resolution. Landsat 8 and Sentinel-2 data are not acquired at the same time as Sentinel-1 data, but for the research, it was assumed that if data was acquired on the same day, the ice coverage should be comparable. Unfortunately, during the one and a half month long research period in 2017, only one usable Landsat 8 image was acquired on the same day as Sentinel-1. All other Landsat 8 or Sentinel-2 images were cloudy or collected on a different day. On January 22, 2017, a Landsat 8 image was acquired at 09:33 UTC, while a Sentinel-1 image was acquired at 16:33 UTC. The images overlap each other in a small area in Hungary. Obviously, the 7-hour difference between the image acquisitions limits the reliability of the validation. The validation at the Tisza in 2022 was conducted based on comparison between completely overlapping Sentinel-1 and Sentinel-2 images of the same day (January 24). The time difference was 5 hours. To evaluate the calculated ice cover map, the multispectral dataset was clustered into 15 classes using ISODATA algorithm and the corresponding classes were labelled as ice cover.

Data analysis

Beside developing, testing and validating an ice monitoring algorithm, the data obtained from the 2017 Danube ice survey was analysed in order to assess the temporal and spatial pattern of ice formation, and to determine what factors most severely affect the development of static ice cover on the river.

For the analyses the tabular data of those days were used when satellite coverage was complete for the entire section. In all, 11 full coverages could be assessed (3rd, 9th, 15th, 16th, 22nd, 27th, 28th of January and 3rd, 8th, 9th, 15th of February). For these days, first a mean daily ice cover ratio was determined, then a distance based mean ice cover graph was made, showing representative ice cover values for each 100 m polygon for the entire period. Daily mean temperature data were derived from the meteorologic station of Hódmezővásárhely, Hungary, being approximately at the centre of the study area.

Beside temperature, icing is also determined by channel geometry, reach scale and local changes in flow conditions, and by obstacles in the channel (Lal & Shen, 1993). As flow conditions could not be reconstructed for the entire section, we mostly focused on planform channel geometry data. Accordingly, the spatial distribution of ice cover data was first compared to channel width, and channel width variation. Width values were derived from the 100 m river polygons. Width variation was determined by subtracting each width data from the consecutive downstream value. A more negative value meant a more significant narrowing along the section and vice versa. Channel roughness can also be increased by the presence of mid-channel islands, therefore, these were mapped and overlaid on the ice data as well. Ice coverage was also assessed in relation with river sinuosity, taken from the arc/chord length ratio of river bends. Arc length was determined along the channel centreline in between two inflection points, while the chord length was taken as the straight-line distance of the points. Finally, ice cover was also compared to water surface slope conditions of the investigated reach, calculated from the absolute height of gauge stations (Dunaföldvár, Paks, Baja, Dunaszekcső, Mohács, Apatin, Novi Sad, Pancevo) and flood free low water data. We chose this approach to be able to determine which channel sections have below and above average channel slope.

Results and discussion

Ice coverage maps

For the complete ice periods in 2017 and 2022, maps were generated showing the ice coverage per pixel (at the resolution of the satellite data) and aggregated to the 100 metre sections of the rivers. Figure 5 shows a 36 kilometre long example of the ice coverage detection algorithm. The results show coverage and ratio of coverage per 100 metre section. The series of coverage maps and the 100 m resolution coverage ratio data also allowed the identification of reaches mostly affected by the formation of complete ice cover and ice jams and the evaluation of ice formation in relation with changes in river morphology. In general, ice packing was detected mostly at sections with fluvial islands or with mature meanders. Figure 6 shows the same type of result for the Tisza section in 2022. Here, the ice formed a blockage upstream of a sharp bend east of Szeged. As a result, a 3.8-kilometre-long stretch of the river was almost completely covered with ice.

In total 173 layouts in A3 format, with a scale of 1:100,000 were produced to visualise the ice coverage

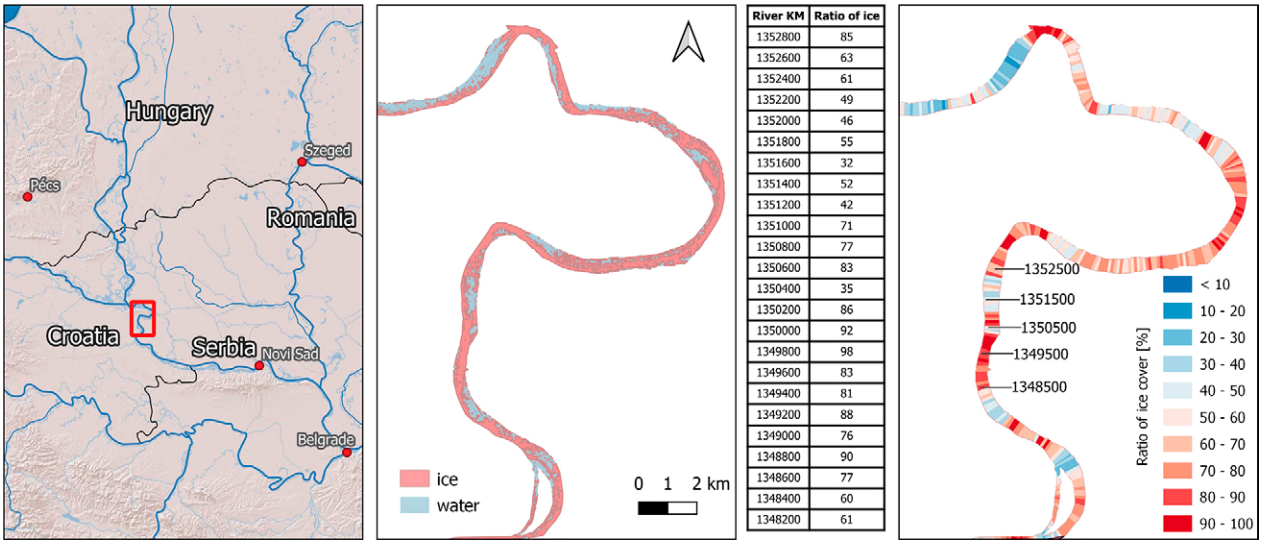

River KM	Ratio of ice
1352800	85
1352600	63
1352400	61
1352200	49
1352000	46
1351800	55
1351600	32
1351400	52
1351200	42
1351000	71
1350800	77
1350600	83
1350400	35
1350200	86
1350000	92
1349800	98
1349600	83
1349400	81
1349200	88
1349000	76
1348800	90
1348600	77
1348400	60
1348200	61

Figure 5. Results of the radar based ice coverage calculation of January 10, 2017 for a Danube river subsection in Croatia (left), the 10 x 10 metre resolution ice coverage (middle) and the polygon map showing the ratio of the river covered with ice per 100 metre section (right)

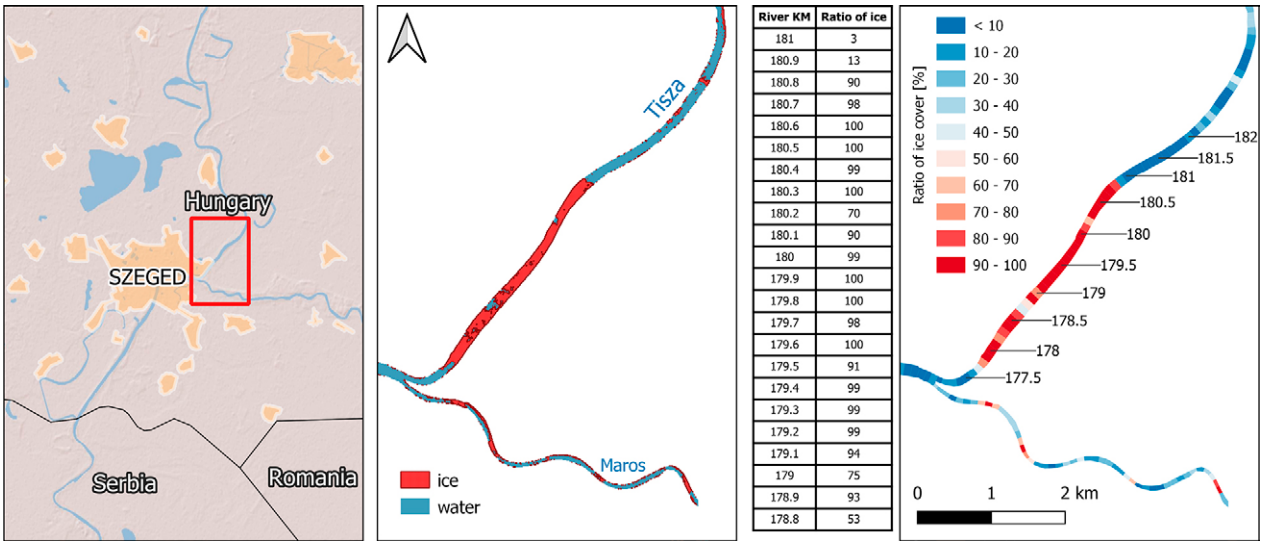

Figure 6. Results of the radar based ice coverage calculation of January 27, 2022 for a Tisza subsection near Szeged in Hungary (left), the 10 x 10 metre resolution ice coverage (middle) and the polygon map showing the ratio of the river covered with ice per 100 metre section (right)

on the Danube in 2017. Each layout shows a river section of around 50 km. The language of the layout is Hungarian because they are produced for operational activities of the Hungarian General Directorate of Water Management water management. An example of a printable map in Serbia is given in Figure 7.

Validation of results

The Sentinel-1 derived ice coverage maps were compared to the in-situ observations by the Hungarian General Directorate of Water Management for the long ice period in 2017 (Figure 8). The ice coverage pattern shown by in-situ observations is an in-

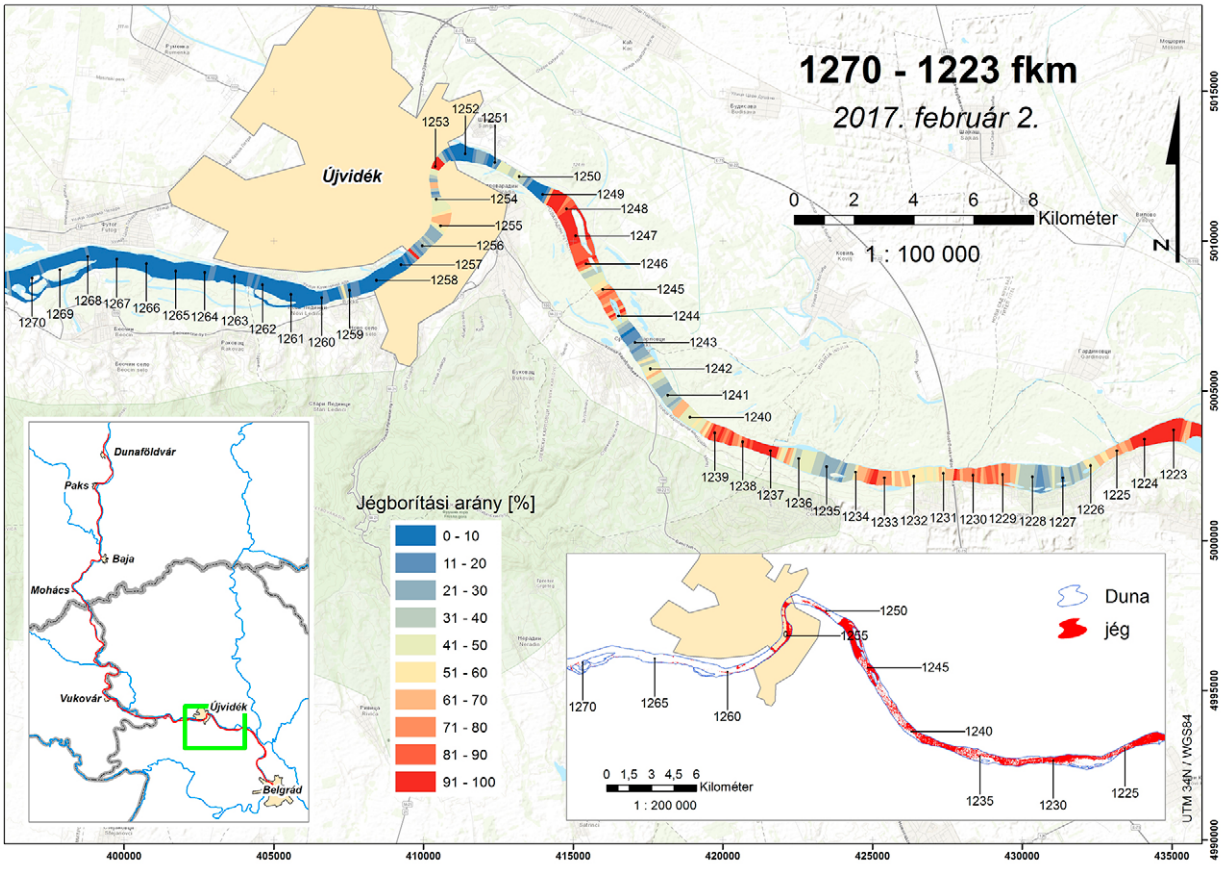

Figure 7. Sample layout of a selected Danube section (1270-1223 river km) on February 2, 2017

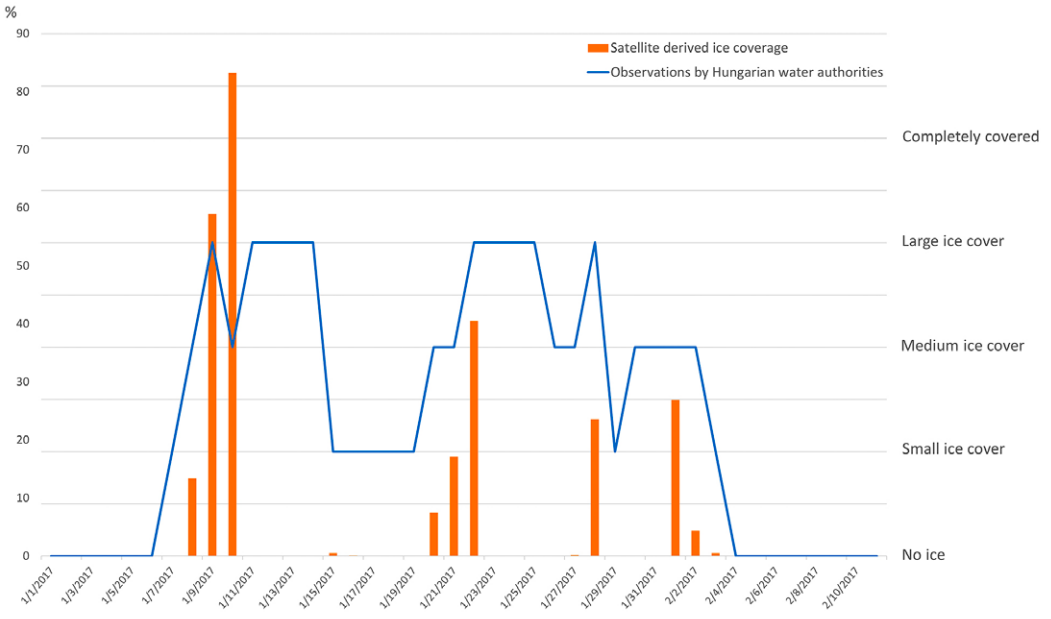

Figure 8. Comparison of satellite derived ice coverage in percentage and in situ observation by the Hungarian General Directorate of Water Management (https://www.hydroinfo.hu) for a section of the Danube between the cities of Dunaföldvár and Bölcske in 2017. Only dates when the satellite image was available are shown on the x -axis

terpretation of the amount of ice on the river as seen from the shore. There is some similarity to the patterns shown by the satellite derived ice cover, but it is not very strong. The large increase in ice coverage between the 8th and 10th of January can be clearly observed in both data sets. Also, the ice accretion on the 20th and 28th of January and the 1st of February seems to be detected in both data sets, but the limited number of observations by the satellite in the third week of January almost completely missed the small ice coverage observed during the in-situ observations.

In 2017, visual inspection of ice coverage on a Landsat 8 multispectral image clearly shows white-greyish areas at the East (left) bank of the river (Figure 9B), while ice coverage derived from a Sentinel-1 image of the same day shows ice on the same parts of the river (Figure 9C). It is not possible to quantify the correlation between the ice coverage, since the images are not from exactly the same time, but they clearly show the same pattern.

The amount of ice during the 2017 period on the Tisza near Szeged shows similarities between the two data sets as well (Figure 10A and B), although the spatial distribution is not as similar as in the validation period in 2017.

Temporal development of ice cover

During the study period the most extensive relative ice cover was experienced on the 9th of January, when 41% (~7700 ha) of the total 405 km long river reach was covered by ice. Based on the previous ice cover data (3rd of January) and the temperature curve, this intensive ice cover developed only in about 2-3 days, primarily due to the extreme cold period starting from the 6th of January (Fig. 11). However, by this time floating ice could develop on the river, as the ra-

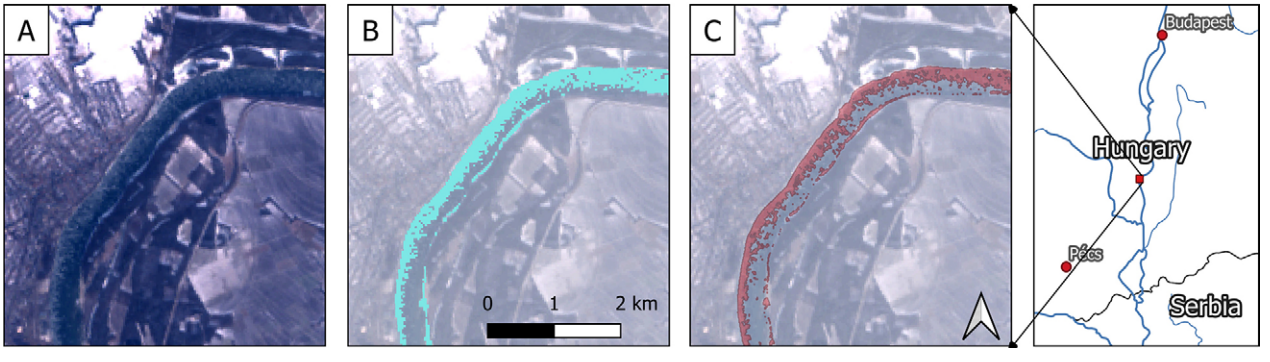

Figure 9. Validation of ice coverage derived from Sentinel-1 in 2017 on the Danube. Validation satellite image (Landsat 8 RGB432) (A), reference data derived by ISODATA clustering of Landsat 8 image (B), and ice coverage derived from Sentinel-1 satellite image (C). Sentinel-1 and Landsat 8 images were both acquired on January 22, 2017

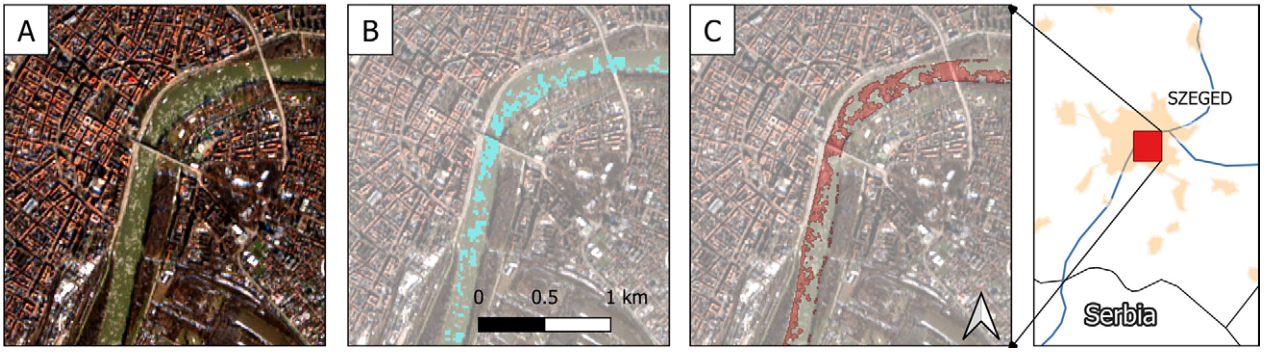

Figure 10. Validation of ice coverage derived from Sentinel-1 in 2022 on the Tisza. Validation satellite image (Sentinel-2 RGB843) (A), reference data derived by ISODATA clustering of Sentinel-2 image (B), and ice coverage derived from Sentinel-1 satellite image (C). Sentinel-1 and Sentinel-2 images were both acquired on January 24, 2022

tio of sections covered by static ice (ice cover ratio over 90%) was 1.1%. Although in the following days some warming was experienced, but daily means hardly reached 0°C, thus total ice cover did not increase, but the proportion of 100 m river polygons covered by static ice steadily increased (Fig. 11), even though, due to a short warming, the total ice cover decreased. In the next cold spell, the total ice cover remained 30-40 %. The maximum extension of static ice was experienced on the 28th of January. Total ice cover on the reach decreased by this time due to a slight warming (Fig. 11). This pattern refers to the pronounced formation of packed ice developing from an increased volume of ice floes on the river.

Due to a significant warming experienced from the beginning of February thawing advanced rapidly, ice cover halved in 2-3 days, and static ice cover dropped even more significantly.

Spatial pattern of ice development

Based on the time averaged 100 m ice cover data for the entire period, three zones of increased ice formation and ice floe congestion can be identified on the investigated river section. The first ice formation zone (Zone I.) is located between Dunaföldvár and Paks. In this zone, the time averaged data reached a maximum of 40%, except for a short section right upstream of the road bridge over the river at Dunaföldvár (Fig. 12). As on each survey day and at each bridge, a significant ice cover was detected, it is assumed that at bridges the designed algorithm gives false positive results, which is also supported by the fact that the dielectric constant of ice (ε=3–4) is very close to that of asphalt (ε=4–5) as opposed to that of water (ε=80).

The second ice formation zone (Zone II.) is located between Apatin and Vukovar on a 70–80 km long section of the Danube, where time averaged ice cover values reached a maximum of 50% on a roughly 10 km long section (1355-1345 fkm). The third and most extensive section favouring ice formation and ice packing (Zone III.) is situated between Novi Sad and Belgrade (~90–100 km), where time averaged ice cover reached up to 60%.

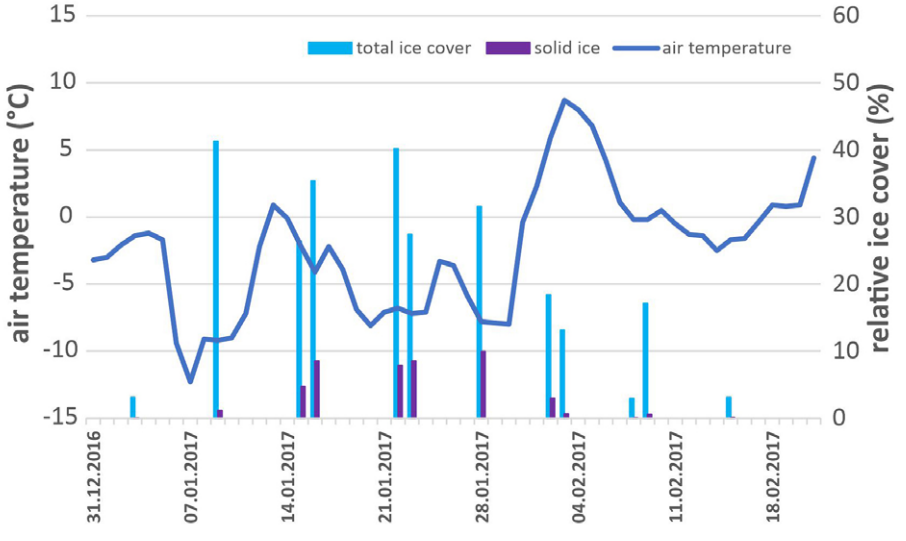

Figure 11. Daily mean air temperature between the period of 1st of January and 20th of February 2017, and the change of summed relative ice cover on the Dunaföldvár-Beograd section of the Danube River

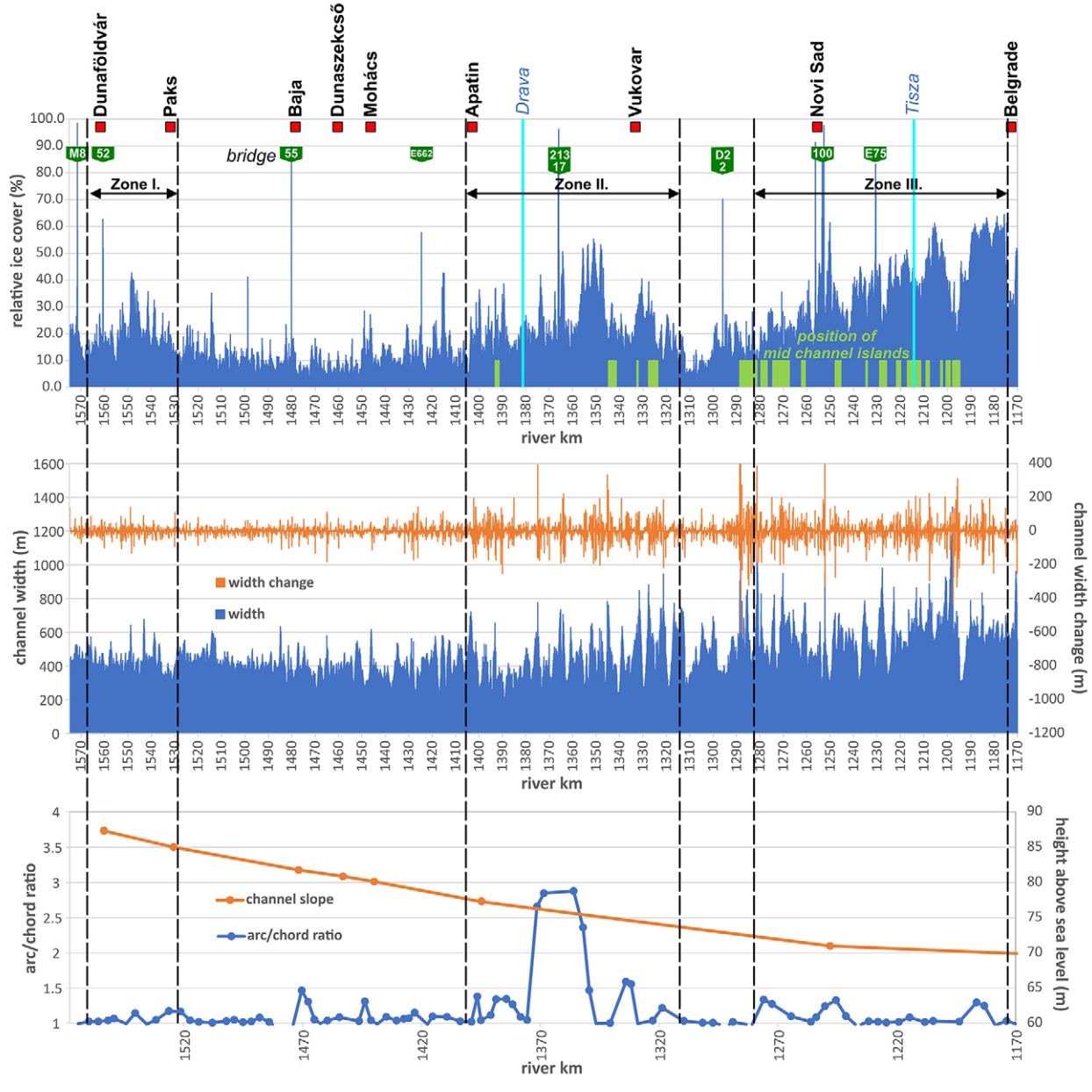

Figure 12. The time averaged distribution of ice cover on the investigated river reach, and the longitudinal change of channel geometric parameters (width, width change, meander arc/chord ratio, water surface slope at low water, position of islands)

The dynamics of ice transfer is also recognisable if the distribution of consecutive measurements is compared. On Figure 13, the survey made at the time of the largest ice cover (9th of January) is compared to the following surveys. It is clearly visible how floating ice moving from upstream is congested in the downstream ice zones, where full ice cover developed on several kilometre sections by this date, even though that day (15th of January) was right after the previously mentioned temporary warming (Fig. 11). On the next day (16th of January), as temperature decreased, ice formation, especially between Novi Sad and Belgrade, increased mostly because of local freezing. Ice transfer from upstream could have a secondary role in the increase of ice cover in the lack of time, as at an average velocity of the river (0.5 m/s) the transfer rate is 40-50 km/day. It must be also noted, that due to the temperature decrease, the ice formation started in ice zone I. as well (Fig. 13.).

Spatial variation of channel geometry

The average width of the river on the investigated section is 464 m. Downstream of the confluence with the Drava and further on with the Tisza, two major tributaries of the Danube, the average channel width increases first by 88 m (from 406 to 494 m) then 136 m (from 494 to 615 m) (Fig. 12). The upstream part of the investigated section, till Apatin (1405 fkm) exhibits a

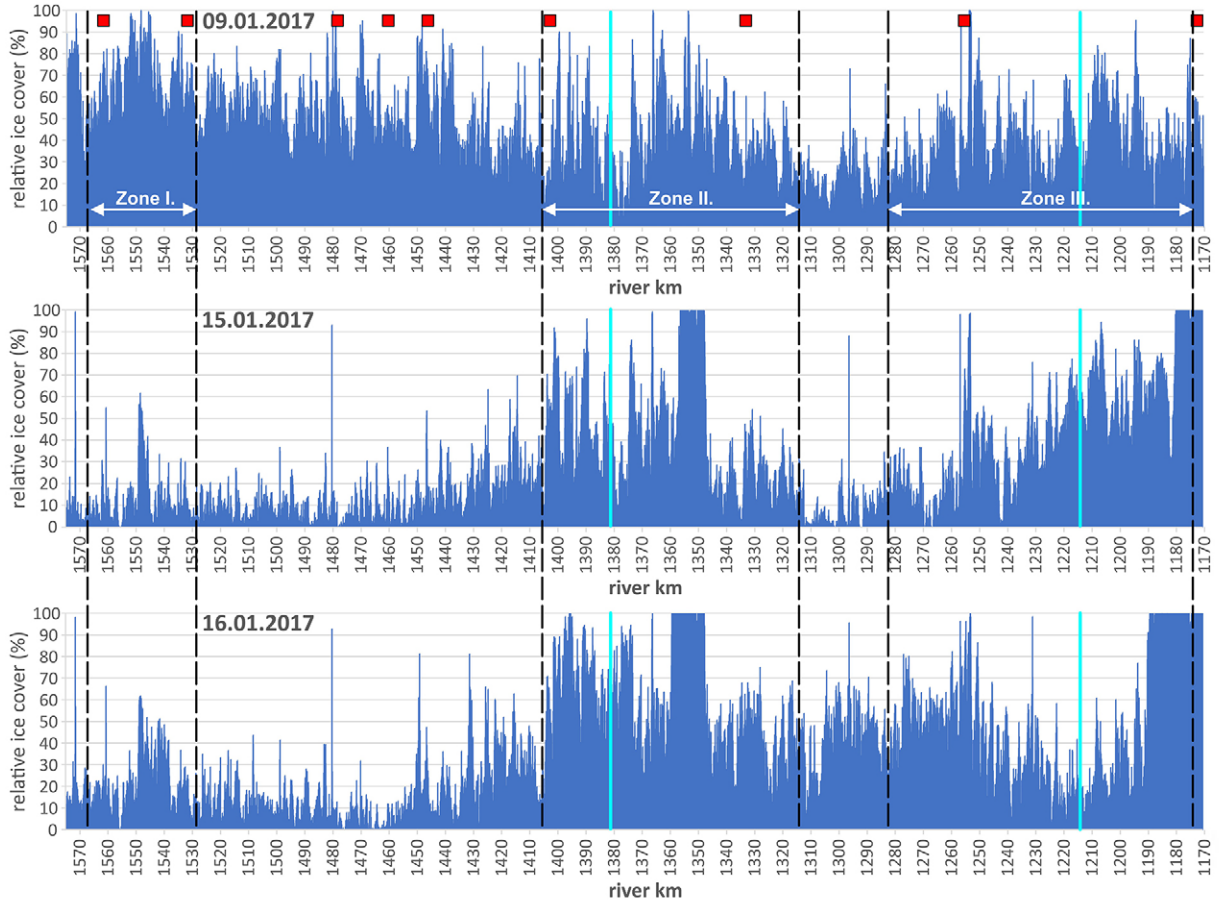

Figure 13. Changes in ice distribution on the study reach over three consecutive surveys. Red squares and cyan lines refer to the settlements and tributaries shown on Figure 12

lower variation in width values, being in average 19.5 m in absolute terms, equalling a roughly ±4.8% relative fluctuation. Going downstream, width variation increases, and a mean variation of 40 m can be observed, which even though the Danube gets wider corresponds to a ±8.4% mean fluctuation. However, there are longer sections, such as the one between 140 and 129 fkm, where fluctuation can reach a mean value of ±10% (Fig. 12).

An important feature affecting both width fluctuation and channel geometry in general is the presence of vegetated islands within the channel. In all 28 islands could be identified on the entire reach, most of them located on the lower section, between Vukovar and Belgrade. Their size shows a great variation; 13 out of them have a length below 1000 m, the rest are larger; their maximum length can reach 3000–4000 m.

Flow conditions are also affected by meanders and meander geometry. As the river has undergone significant regulations, the proportion of meandering sections is very limited. In total 91 river bends could be identified, but 70% of them is not a real bend (arc/chord length ratio < 1.1) (Fig. 12). The number of mature bends is only eight. Seven out of these are located between Apatin and Vukovar, which makes this the only meandering section of the study reach.

The mean slope of the river between Dunaföldvár and Belgrade (Pancevo) is 0.000044 m/m. Starting from 0.000079 m/m, between Dunaföldvár and Paks a generally decreasing trend can be seen in slope values in the downstream direction. The lowest value, 0.000014 m/m, was observed on the Novi Sad–Belgrade (Pancevo) section, which is under the impounding effect of the Iron Gate dam system (upper dam at 943 fkm).

Discussion

The presented approach based on slicing of radar backscatter values into water and ice is a straightforward method that can be applied to large areas, with high resolution and with reasonable accuracy. The advantage of the approach is that the freely available satellite data is processed uniformly with an interval of about three days. The threshold between ice and water is determined empirically. The signal of ice is affected by its structure and water content. The strength of the signal of water is influenced by the turbulence in wa-

ter, caused by wind or other factors (Chu et al., 2015). All factors result in uncertainty of the threshold, but the validation results provide confidence that the determined threshold gives satisfying results.

River ice does not frequently occur in Hungary; During the last 6 years, we could only create satellite based maps for two ice periods. In the latest period, it was only possible to detect ice on the Tisza River and not on the Danube. Climate change models predict an overall rise of temperature for the Carpathian basin, but also more extreme weather patterns, and periods with extreme cold are likely to occur more often (Mezősi et al., 2016). Remote sensing techniques provide a cost effective solution to monitor river ice and provide operational information to the authorities for mitigation of damage due to ice dams and floods.

Beside the potential for development of a basin wide monitoring activity and decision support system, the satellite based survey made during the 2017 ice event also allows to draw some general conclusions in terms of ice formation and congestion on the study reach.

Not surprisingly, based on the obtained data series, slope is among the most important determinants of ice development, since decreasing slope showed an extension of ice formation zones (Fig. 12). This is because lower velocity enables more effective freezing and also the congestion of ice floes. Due to the continuous downstream increase of width, parallel to the decrease of slope, a slight positive correlation can be observed between width and relative ice cover if the entire period and the entire section is considered (Fig. 14). However, if sectors, having similar but variable width all along, e.g. the one between 1315 and 1405 fkm (Zone II.) are analysed, then such a relationship cannot be observed (Fig. 14). This is partly because both narrowing (by congestion) and widening (by slower velocity) can contribute to ice cover development.

Considering the identified three ice formation zones, high relative ice cover ratios are the result of the interplay of several factors. In case of Zone I., ice jams and static ice cover could appear regularly because of two mild bends (arc/chord ratio < 1.5), which exhibit a slightly higher width variation than upstream. It must be noted that in a downstream direction more mature bends are situated, still, at a lower

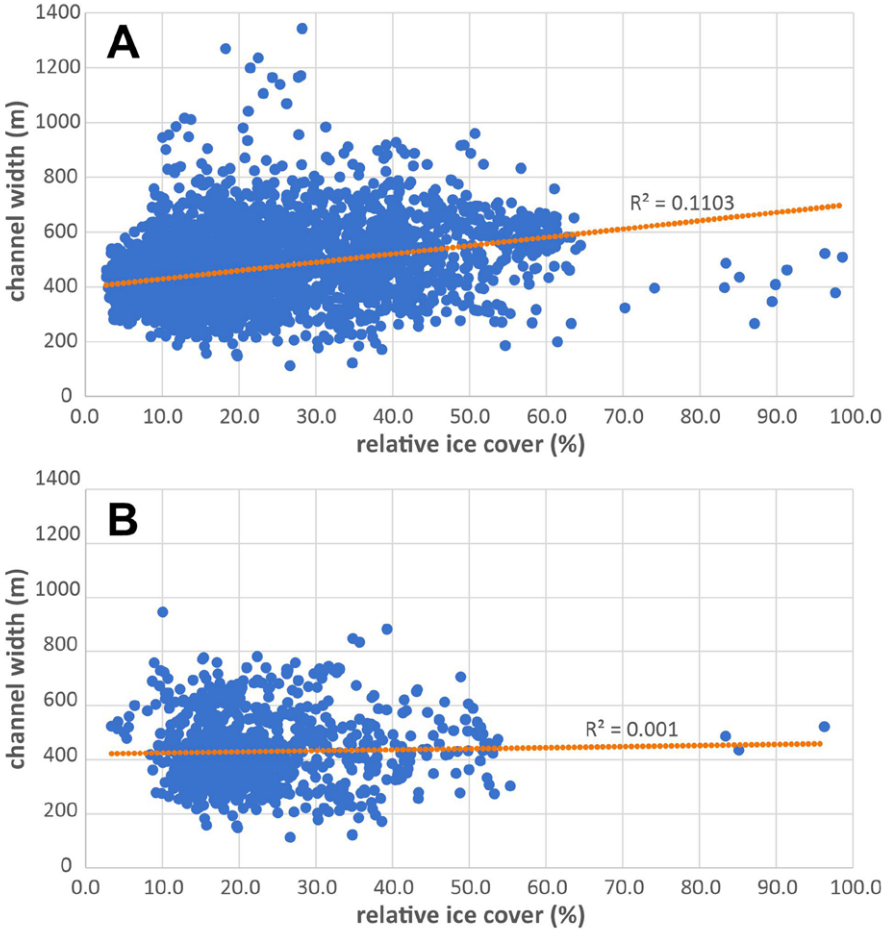

Figure 14. The relationship of width and ice cover A) on the entire study reach and B) on the reach of Zone II. with highly variable width conditions

width variation complete ice cover developed only in the coldest period.

Zone II. is the only true meandering section of the study area, besides, channel width variation is also significant here, and four mid channel islands obstruct the flow (Fig. 12). The formation of ice jams can clearly be related to four-five suddenly narrowing sections usually located at the apex of meanders, or at the confluence of anabranches at the downstream end of islands. Consequently, this was one of the sections where ice breaker ships had to intervene to avoid impoundment caused by piled up ice floes (Babic Mladenovic et al., 2017).

In accordance with Babic Mladenovic et al, (2017), the largest scale static ice formation occurred in Zone III., at Novi Sad and Belgrade. Here the most important drivers of static ice development were the backwater effect of the Iron Gate Dam I. and the resulting decrease of water surface slope and flow velocity (Fig. 12). However, based on Serbian ice cover reports, ice development downstream of Belgrade was less critical (Babic Mladenocic et al., 2017), which underlines the role of large tributaries, since the Sava River joining the Danube at Belgrade was not carrying much ice, whereas the Tisza, having its confluence in this zone, was heavily frozen. However, the impact of channel geometry must also be underlined in case of Zone III., since for example the significant narrowing at 1196 fkm, accompanied with the presence of some larger bends and mid-channel islands made the area ideal for the development of ice jams (Fig. 12).

Conclusion

Continuous monitoring of river ice is important not only for preventing and reducing floods, but also to prevent and decrease the impact of damage in river infrastructure. The presented method is a cost effective, remote sensing-based approach that can provide operational maps over large areas at high spatial (10 m) and relatively high temporal (2-3 days) resolution. The dataset complemented with field observations can aid interventions and support operational decision making.

Although the quantitative validation of ice cover detection results is problematic, the comparison with in-situ observations and other optical satellite data sets shows good comparability. Field observations are subjective, as they can mostly be made from the river bank. The radar-based ice coverage algorithm is objective and uniform over the total length of rivers. The algorithm is automated, provides robust results as long as Sentinel-1 data is available and can be applied in other regions as well. The application of other data sources, like IP cameras for continuous monitoring would help to refine and calibrate our satellite-based ice observation method.

The spatial and temporal evolution of ice coverage is very important for forecasting and analysing ice flow processes. Based on the 2017 data, the interplay of various parameters determines the location of ice jam development on the study reach. Among all, flow velocity, primarily governed by water surface slope, determines at most the intensity of ice accumulation and static ice cover formation. However, the role of channel geometry is also important, as increased channel width variability, high sinuosity or the presence of mid-channel islands are key parameters in the development of ice jams. The severity of the ice event is also greatly determined by the amount of ice arriving on the tributaries.

The present survey has also shown the dynamic character of ice formation and ice congestion. The appearance of ice floes on the upstream sections was quickly followed by the formation of packed ice on geometrically variable or low slope sections downstream. The data obtained in this study can help engineers to better identify critical cross-sections where preventive interventions are needed to better manage ice events in the future.

Acknowledgements

We are grateful for the General Directorate of Water Management of Hungary for their support of the research.

References

Agafonova, S., Frolova, N., Krylenko, I., Sazonov, A., & Golovlyov, P. (2017). Dangerous ice phenomena on the lowland rivers of European Russia. *Natural Hazards*, 88. http://dx.doi.org/10.1007/s11069-016-2580-x.

Altena, B., & Kääb, A. (2021). Quantifying river ice movement through a combination of European satellite monitoring services. *International Journal of Applied Earth Observation and Geoinformation*, 98, 102315, http://dx.doi.org/10.1016/j.jag.2021.102315

Babić Mladenović, M., Gombás, K., Liška, I., & Balatonyi L. (2017). Report on the ice event 2017 in the Danube River Basin. ICPDR-IKSD. available at: https://www.icpdr.org/main/sites/default/files/nodes/documents/report_ice_event_2017_0.pdf

Chu, T., Das, A., & Lindenschmidt K-E. (2015). Monitoring the variation in Ice-Cover Characteristics of the Slave River, Canada using Radarsat-2 data – A case study. *Remote Sensing*, 7, 13664-13691. https://doi.org/10.3390/rs71013664

Gombás K., & Balatonyi L. (2017). Extremities in winter season - outlook for mitigation measures. *Hidrológiai Közlöny*, 97(3), 81-85. available at: https://adt.arcanum.com/hu/view/HidrologiaiKozlony_2017/?pg=0&layout=s

Goldberg, M.D., Li, S., Lindsey, D.T., Sjoberg, W., Zhou, L., & Sun, D. (2020) Mapping, Monitoring, and Prediction of Floods Due to Ice Jam and Snowmelt with Operational Weather Satellites. *Remote Sensing*, 12(11), 1865. https://doi.org/10.3390/rs12111865

Hicks, F. (2009). An overview of river ice problems: CRIPE07 guest editorial. Cold Regions Science and Technology, 55, 175-185. http://dx.doi.org/10.1016%2Fj.coldregions.2008.09.006

Horváth, Á. (2017), 2017 jeges januárja [2017 ici january]. *OMSZ Tanulmányok*, http://www.met.hu/ismeret-tar/erdekessegek_tanulmanyok/index.php?id=1805&hir=2017_jeges_januarja

Howell, S.E.L., Brady, M., & Komarov, A.S. (2021). Large-scale sea ice motion from Sentinel-1 and the RADARSAT Constellation Mission. The *Cryosphere Discuss.*, https://doi.org/10.5194/tc-2021-223 (Preprint)

Ionita, M., Badaluta, C.A., Scholz, P., & Chelcea S. (2018). Vanishing river ice cover in the lower part of the Danube basin – signs of a changing climate. *Scientific Reports*, 8, 7948. https://doi.org/10.1038/s41598-018-26357-w

Keve, G. (2014). Jégészlelés a Duna magyarországi alsó szakaszán [Ice detection on the lower section of the Danube in Hungary]. Magyar Hidrológiai Társaság XXXII. Országos Vándorgyűlés. Szeged, Hungary, July 2-4,2014. Budapest: Magyar Hidrológiai Társaság (MHT), pp. 19

Keve, G. (2017a). Utilization of gained experiences based on ice observation by webcameras. XXVII Conference of the Danubian Countries on Hydrological Forecasting and Hydrological Bases of Water Management, Bulgaria. 68-78.

Keve, G. (2017b). Space-time ice monitoring of the Hungarian Lower-Danube. *Periodica Polytechnica-Civil Engineering*, 61(1). 27-38. https://doi.org/10.3311/PPci.9116

Keve, G. (2020). Determining accurate ice coverage on Danube by webcameras. In: *Proceedings of XXVII Conference of the Danubian Countries on Hydrological Forecasting and Hydrological Bases of Water Management,* https://doi.org/10.15407/uhmi.conference.01.03.

Kiss, T., Fiala, K., Sipos, Gy., & Szatmári, G. (2019). Long-term hydrological changes after various river regulation measures: are we responsible for flow extremes? *Hydrology Research*, 50(2), 417–430. https://doi.org/10.2166/nh.2019.095

Lal, A. W., & Shen, H. T. (1993). A mathematical model for river ice processes. *Journal of Hydraulic Engineering*, 117(7). http://dx.doi.org/10.1061/(ASCE)0733-9429(1991)117:7(851)

Li, X. -M., Sun, Y., & Zhang, Q. (2021) Extraction of Sea Ice Cover by Sentinel-1 SAR Based on Support Vector Machine With Unsupervised Generation of Training Data. *IEEE Transactions on Geoscience and Remote Sensing*, 59(4), 3040-3053, https://doi.org/10.1109/TGRS.2020.3007789

Liptay, Z., Czigány, Sz., & Pirkhoffer, E. (2021). River ice and water temperature prediction on the Danube. *Hungarian Geographical Bulletin*, 70, 201-214. https://doi.org/10.15201/hungeobull.70.3.1.

Lohse, J., Doulgeris, A., & Dierking, W. (2020). Mapping sea-ice types from Sentinel-1 considering the surface-type dependent effect of incidence angle. *Annals of Glaciology*, 61(83), 260-270. https://doi.org/10.1017/aog.2020.45

Malenovský, Z. Rott, H. Cihlar, J. Schaepman, M.E. García-Santos, G. Fernandes, R., & Berger, M. (2012). Sentinels for science: Potential of Sentinel-1, -2, and -3 missions for scientific observations of ocean, cryosphere, and land, *Remote Sensing of Environment*, 120, 91–101, https://doi.org/10.1016/j.rse.2011.09.026

Mezősi, G. (2016). *The physical geography of Hungary.* Springer International Publishing.

Mezősi, G. Blanka, V. Bata, T. Ladányi, Zs. Kemény, K., & Meyer, B.C. (2016). Assessment of future sce-

narios for wind erosion sensitivity changes based on ALADIN and REMO regional climate model simulation data. *Open Geosciences*, 8(1), 465-477. https://doi.org/10.1515/geo-2016-0033

OMSZ, Elmúlt évek időjárása (Weather in past years), 2017. https://www.met.hu/eghajlat/magyarorszag_eghajlata/eghajlati_visszatekinto/elmult_evek_idojarasa/

Somogyi, S. (2001). Természeti és társadalmi hatások a Duna mai vízrendszerében (Natural and social impacts in catchment of Danube). *Hungarian Geographical Bulletin/Földrajzi Értesítő*, 50(1-4), 299-310.

Takács, K., & Kern, Z. (2017): Long-term ice phenology records of Lake Balaton and the Danube River (East Central Europe). PANGAEA, *https://doi.org/10.1594/PANGAEA.881056*

Takács, K., Kern, Z. & Pásztor, L. (2018). Long-term ice phenology records from eastern–central Europe, *Earth System Science Data*, 10, 391–404, https://doi.org/10.5194/essd-10-391-2018

Tom, M., Aguilar,R., Imhof, P., Leinss, S., Baltsavias, E., & Schindler, K. (2020) Lake ice detection from Sentinel-1 SAR with deep learning, arXiv:2002.07040v2 [eess.IV]

Unterschultz, K.D., van der Sanden, J., & Hicks, F.E., (2009). Potential of RADARSAT-1 for the monitoring of river ice: Results of a case study on the Athabasca River at Fort McMurray, Canada, *Cold Regions Science and Technology*, 55(2), 238-248, https://doi.org/10.1016/j.coldregions.2008.02.003

Van Leeuwen, B., & Tobak, Z. (2018). Satellite data based river ice monitoring, In: Molnár, V. (Ed.), Az elmélet és a gyakorlat találkozása a térinformatikában IX.: Theory meets practice in GIS Conference, Debrecen, Hungary, Debreceni Egyetemi Kiadó. pp. 371-376. ISBN 978-963-318-723-4

Weber, F., Nixon, D., & Hurley, J. (2003). Semi-automated classification of river ice types on the Peace River using RADARSAT-1 synthetic aperture radar (SAR) imagery. *Canadian Journal of Civil Engineering*, 30, 11–27, https://doi.org/10.1139/l02-073

Zakharova, E., Agafonova, S., Duguay, C., Frolova, N., & Kouraev, A. (2021). River ice phenology and thickness from satellite altimetry: potential for ice bridge road operation and climate studies. *The Cryosphere*, 15, 5387-5407. https://doi.org/10.5194/tc-15-5387-2021

Zhang, Y., Zhu, T., Spreen, G., Melsheimer, C., Huntemann, M., Hughes, N., Zhang, S., & Li, F. (2021). Sea ice and water classification on dual-polarized Sentinel-1 imagery during melting season. *The Cryosphere Discuss.*, https://doi.org/10.5194/tc-2021-85 (Preprint)

ISSN 0354-8724 (hard copy) | ISSN 1820-7138 (online)

Alluvial Ridge Development and Structure: Case study on the Upper Tisza, Hungary

Tímea Kiss[A*], György Sipos[A], Róbert Vass[B]

Received: June 10, 2022 | Revised: July 24, 2022 | Accepted: July 28, 2022
doi: 10.5937/gp26-38365

Abstract

The juxtaposition of natural levees results in alluvial ridges with a unique fluvial record. Our aims were to (1) identify the alluvial ridges of the Upper Tisza (Hungary); (2) determine their morphological characteristics; and (3) reconstruct the Late Quaternary fluvial history of the region. The oldest paleo-meander was abandoned ca. 29 ka ago; referring to early avulsion of the Tisza. Five alluvial ridges were identified with intensive fluvial activity at ca. 12-13 ka, 7.7-8.6 ka, 6.1-6.6 ka, 4.8 and 2.9 ka ago. Moderate fluvial activity was indicated by early Atlantic and Subboreal paleosols. The sedimentation rate in the paleo-channels (0.3-0.5 mm/y) and on the alluvial ridges (0.3-0.5 mm/y) was slow, influenced by the reactivation of a paleo-channel.

Keywords: natural levee; alluvial ridge; overbank sedimentation; crevasse channel; pollen analysis; OSL dating

Introduction

Natural levees develop along concave banks (Allen, 1965) or straight reaches (Gábris 2003) during floods, when the flow velocity entering the floodplain decreases (Piégay et al., 2003; Steiger et al., 2005). The sediments of the natural levees are coarser than floodplain deposits, but finer than the bed-load (Cazanacli & Smith, 1998). Their material gets finer downstream (Kiss et al., 2018) and laterally too (Wolfert et al., 2002). Farther from the banks their sediment layers become thinner (Gábris 2016), and their slope becomes gentler (Cazanacli & Smith, 1998). The size of the levees is related to channel and sediment transport characteristics (Hudson & Heitmuller, 2003; Kiss et al. 2018), slope (Fryirs & Brierley, 2012), channel-bed material (Ostrowski et al., 2021), flood height and frequency (Brown, 1983; Adams et al., 2004), floodplain characteristics (Pierik et al., 2017), and riparian vegetation (Adams et al., 2004; Steiger et al., 2005). They control the lateral connectivity (Fryirs & Brierley, 2012) by regulating the inundations (Makaske et al., 2009).

The natural levees are dissected by crevasses and crevasse channels, which convey water to the low-lying floodplain areas, and they regulate the sedimentation processes and avulsions (Hajek & Wolinsky, 2012; Nicholas et al., 2018). When the flood breaches the natural levee, a small crevasse channel develops (Fryirs & Brierley, 2012), and the eroded material creates a lobe-shaped crevasse splay (Smith et al., 1989).

The *juxtaposition* of natural levees creates high surfaces along the channel, with an increasing elevation over time due to aggradation during floods (Florsheim & Mount 2002). Their height depends on channel conditions, sediment transport and flood history (Florsheim & Mount, 2002; Kiss et al., 2018; Balogh et al., 2020). During thousands of years, several kilometers-wide and high forms can develop. This complex form was defined as a "mega-levee" (Gábris, 2016), or

[A] Department of Geoinformatics, Physical and Environmental Geography, University of Szeged, Egyetem u. 2–6, 6722 Szeged, Hungary; kisstimi@gmail.com
[B] Institute of Tourism and Geography, University of Nyíregyháza, Sóstói út. 31/B, 4400 Nyíregyháza, Hungary
[*] Corresponding author: Timea Kiss; e-mail: kisstimi@gmail.com

as an "alluvial ridge" (Pierik et al., 2017). Their height is controlled by channel bed aggradation rate and suspended load (Nicholas et al., 2018). Conversely, alluvial ridges control the water and sediment delivery to the floodplain and regulate avulsions (Nicholas et al., 2018).

The modern and Holocene aggradation rates on natural levees are different. For example, during a flood, 70 cm accumulation was measured along the banks on the natural levees (Florsheim & Mount, 2002; Oroszi et al., 2006). In contrary, the long-term fluvial levee aggradation rate is just 0.6-2.3 mm/y (Stevaux & Souza, 2004; Makaske et al., 2009), though back loading through crevasses can increase it to 3.2-4.3 mm/y (Ishii et al., 2021). The long-term (Holocene) natural levee evolution is driven by sediment supply changes (Pierik et al., 2017; Ishii et al., 2021). After a levee reaches a threshold height, lateral growth will be dominant related to overbank flows and activity of crevasse splays (Ishii et al., 2021).

The rivers of the Carpathian (Pannonian) Basin filled up the sinking areas and created large alluvial fans (Kiss et al., 2014b; Gábris, 2020). The last accumulation phase was terminated by increased run-off and tectonic-driven incision in the Late Glacial (Borsy, 1995, 1998). In this way, for example, the Upper Tisza River in NE Carpathian Basin incised into its alluvial fan, and by lateral erosion it created floodplain segments (e.g. Szatmár Plain, Bereg Plain, Rétköz and Bodrogköz).

There are two unclarified key points in the development history of Upper Tisza region. (1) Here some alluvial ridges evolved, but their morphology or evolution history is not known. (2) During the Pleistocene the Tisza ran to SW (Borsy, 1995, 1998; Gábris, 2020); however, nowadays, its active course is towards NW, however the exact time of the avulsion is not known. We hypothesize that the sedimentary structure of mega-forms is closely related to the prevailing hydrological and environmental conditions; thus, they are good archives of Late Quaternary fluvial activity. The goals of this study are (1) to identify and characterize alluvial ridges in NE Hungary; (2) to investigate the spatial characteristics of their sediments; and (3) to evaluate their role in the fluvial development history of the region.

Study area

The Bereg Plain is located in the NE Carpathian Basin (Fig. 1), gradually sloping from SE to NW. The subsiding area of the Bereg Plain was filled up by ca. 150 m deep fluvial sediments (Gábris, 2020), deposited by the Tisza and its tributaries, which built a large alluvial fan. The alluvial fan was dissected by tectonic activity ca. 25-30 ka ago: the area of the present-day plains (i.e. Szatmár Plain, Bereg Plain) subsided, while the Nyírség

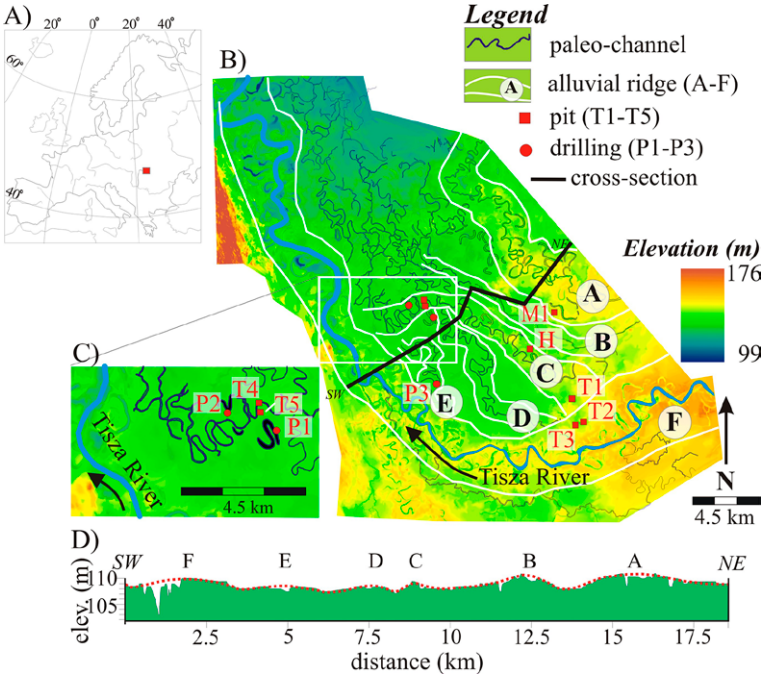

Figure 1. A) Bereg Plain is situated in NE Hungary. B-C) Its surface is densely covered by paleo-channels. Three of them (P1-P3) were sampled for pollen analysis. The alluvial ridges (A-F) were studied at mining pits (T1-T5). D) A cross-sectional elevation profile drawn along the black line on B.

elevated (Borsy, 1995). The Bereg Plain started to sink at the end of the Pleistocene (Borsy, 1998), forcing the avulsion of the Tisza River, which changed its course from SW to NE ca. 20-22 ka ago (Borsy et al., 1989). Subsequently, the Tisza eroded the alluvial fan, and later, it deposited clayey-silty materials along its courses and gradually reworked its floodplain (Sümegi, 1999; Magyari, 2002; Félegyházi et al., 2004; Vass, 2014).

Methods

To identify the forms a DEM (resolution 5 m) was created based on topographical maps (1:10,000). The paleo-meanders and alluvial ridges were identified, and their sizes were measured under ArcGIS 9.2.

Sediment samples were collected from the paleo-channels and their alluvial ridges (Fig. 1). The large clay and sand mine pits (T1-T5) provided a unique opportunity to study the fluvial sequence of alluvial ridges. At 25 points, we sampled the sediment layers for grain-size analysis. Paleosols were sampled for radiocarbon dating, and overbank deposits for OSL dating. Three paleo-channels (P1-P3) were sampled by drilling down to their coarse bed-load material (4.1-9.1 m) for grain-size and pollen analysis.

The preparation of samples for OSL dating followed Mauz et al. (2002), applying both the coarse- and fine-grain techniques. For the measurements a RISØ DA-20 TL/OSL luminescence reader and the single-aliquot regeneration (SAR) protocol was applied (Murray & Wintle, 2003). Environmental dose rate (D*) was determined by using Canberra XtRa Coaxial Ge detector, and applying the conversion factors of Liritzis et al. (2013).

On the organic-rich sediment samples radiocarbon dating was made. The standard AAA chemical treatment (Tans & Mook, 1980) was performed. The samples were converted to benzene using an Atomkomplex Prylad-type benzene synthesis line (Skripkin & Kovaliukh, 1998). Radiocarbon (^{14}C) activity was assessed by Liquid Scintillation Counting (LSC) using a Quantulus 1220 ultralow background LSC instrument (Skripkin & Buzinnyi, 2017). Calibration of conventional ^{14}C ages to calendar dates was performed using OxCal v.4.4.2 (Bronk Ramsey, 2009) in conjunction with the IntCal20 dataset (Reimer et al., 2020). The OSL and radiocarbon dating were made at the Geochronological Laboratory of the University of Szeged.

To provide data on the cut-off of the paleo-channels and environmental condition of the fluvial activity, pollen analysis was performed on 3 drilling cores. The pollen grains were extracted following the method of Zólyomi (1952). The identification was performed under 400-600x magnification on species, genus or family level. The visualization of the results was made under Tilia and TiliaGraph software.

The grain-size distribution of the dry, pulverized samples was determined by Fritsch Analysette 22.

Results

Geomorphology of the area

On the Bereg Plain, a dense paleo-channel network was identified (Figure 1B). In the eastern part of the study area, 6 paleo-channel courses were identified; however, in NW they create a net of paleo-channels, and it was impossible to classify them. The paleo-channels create 11-49 km long courses (Table 1), running north of the active channel belt of the Tisza (F course). Their mean channel width is 30-60 m; the widest channel (80-150 m) is the active channel of the Tisza. The sinuosity of most of the paleo-channels (D-F) is very similar (1.8-1.9); however, the B course has a very low sinuosity (1.2), whereas the A and C courses have a highly meandering pattern.

Table 1. Morphometric parameters of the paleo-channels and their alluvial ridges on the Bereg Plain

Channel course	Paleo-channel course				Alluvial ridge		
	length (km)	mean width (m)	sinuosity	mean slope (cm/km)	length (km)	relative height (m)	width (km)
A	47.2	30-60	2.3	12.7	21	1-2.5	2-3.5
B	19.5	30-60	1.2	10.3	17	0.5-2	0.5-1.6
C	22.2	30-50	2.2	6.6	17.4	1.5-2.5	0.8-2.0
D	23.6	25-60	1.8	8.5	13.1	0.5-1	0.8-2.5
E	11.1	20-40	1.8	9	6.1	0.3-0.5	0.3-0.7
F	49.5	80-150	1.9	14	26	2-3.5	2.5-4.0

The paleo-channels in the SE half of the study area are situated on elevated alluvial ridges (Figure 1D). The highest ridge (2-3.5 m) developed along the active Tisza (F course). Most of the ridges are 1-2.5 m high, but the E course has almost no alluvial ride. The width of these ridges is 2-3 km; however, the small E course is also very narrow (0.3-0.7 km). The ridges are the most elevated in their middle section, in the northwest they gradually lower to the floodplain level.

Results of the OSL and radiocarbon dating

Altogether 14 samples were collected for OSL dating from 6 sediment profiles, representing the sedimentary body of three alluvial ridges. Most of these samples were collected from the silty-clayey overbank deposits of alluvial ridges; however, two samples represent the first (T5/1) and the last member (T4/1) of a point-bar sequence. The paleosols between overbank sediments were dated by radiocarbon dating. The age of the sediments and the paleosols ranges between 2.9 and 24.7 ka, representing Late Pleistocene and Holocene fluvial activity (Table 2-3).

Description of sedimentary bodies

At four sites (T1-3, M1), the sedimentary sequence of ***alluvial ridges*** was revealed. The longest ***alluvial ridge sequence*** (300 m) was studied at site T1 (Fig. 1-2), which is ca. 1.5 km far from the paleo-channel C. The lowermost lacustrine sediments (≥1 m) were dated to 24.72±0.65 ka (T1/4). This layer is covered by fine-layered alluvial deposits (thickness: 200 cm), the topmost one is 13.23±0.35 ka old (T1/3). The fluvial activity repeatedly terminated, as it was reflected by paleosols. The lowermost paleosol (thickness: 30-40 cm) was represented all along the pit. It was covered by a silty-clayey layer (5-20 cm), which got thinner towards the distal edge of the alluvial ridge. The middle paleosol (thickness: 10-20 cm) was identifiable just along 260 m, as it was getting thinner towards the edge of the alluvial ridge, and finally, it terminated. This paleosol was covered by another silty-clayey layer (15-30 cm) dated to 8.17±0.20 ka (T1/2). The uppermost paleosol got thicker towards the distal part of the alluvial ridge (thickness: 20-60 cm) as it merged with the lowermost paleosol. The uppermost paleosol was dated to 6880-7620 cal BP (T1carb). This uppermost paleosol layer was buried by 90-120 cm thick silty-clayey deposits ca. 7.69±0.19 ka ago. The thickness of this sediment layer, just like the previous ones, got thinner towards the distal edge of the alluvial ridge.

A ***point-bar series*** buried by overbank fine-grained sediments were presented at the T4-5 sites (C paleo-

Table 2. Results of the OSL dating. W: water content, D*: environmental dose rate, De: equivalent dose.

Field ID	Course	Lab ID	Depth (cm)	W (%)	U (ppm)	Th (ppm)	K (%)	D* (Gy/ka)	De (Gy)	Age (ka)
T1/1	C	1129	60	23.9±2.4	3.05±0.02	11.39±0.08	2.62±0.06	3.95±0.09	30.33±0.28	7.69±0.19
T1/2	C	1120	100	29.9±3.0	2.56±0.02	9.80±0.07	3.00±0.09	3.79±0.09	30.94±0.28	8.17±0.20
T1/3	C	1126	125	23.4±2.3	1.59±0.02	6.86±0.06	1.57±0.04	2.38±0.06	31.52±0.27	13.23±0.35
T1/4	C	1132	345	25.5±2.6	3.24±0.02	11.03±0.08	2.49±0.06	3.81±0.09	94.2±1.04	24.72±0.65
T2/1	F	1334	135	10.4±2.1	3.32±0.02	12.72±0.08	2.73±0.06	4.80±0.11	15.88±0.34	3.31±0.10
T2/2	F	1128	245	17.3±3.4	3.30±0.02	12.30±0.09	2.82±0.06	4.48±0.11	21.46±0.20	4.80±0.12
T2/3	F	1331	300	12.8±2.6	3.33±0.02	11.83±0.08	2.63±0.06	4.50±0.11	28.34±0.29	6.30±0.16
T3/1	F	1121	150	10±2.0	2.02±0.02	6.62±0.05	1.67±0.04	2.51±0.04	9.94±0.79	3.96±0.33
T3/2	F	1127	215	16.6±3.3	1.80±0.01	5.51±0.04	1.67±0.04	2.24±0.05	9.29±0.66	4.14±0.31
T3/3	F	1124	315	30.0±5.0	2.30±0.02	9.04±0.06	1.68±0.04	2.67±0.08	32.46±0.29	12.15±0.40
T4/1	C	1130	250	16.4±3.3	1.77±0.01	5.54±0.04	1.39±0.03	2.01±0.05	5.89±0.69	2.93±0.35
T5/1	C	1123	225	17.2±3.4	2.17±0.02	7.15±0.06	1.59±0.04	2.34±0.05	9.88±0.38	4.23±0.19
M1/1	A	1125	65	20.1±2.0	3.23±0.02	11.66±0.08	2.60±0.06	4.15±0.09	25.37±0.41	6.11±0.17
M1/2	A	1122	130	14.0±2.8	2.78±0.02	10.34±0.08	2.34±0.05	3.93±0.10	33.98±0.42	8.65±0.23

Table 3. The radiocarbon age of the dated paleosols.

Field ID	Course	Lab ID	Depth (cm)	Conventional age (BP)	Calibrated age (cal BP) (2 sigma, 95.4 %)
T1carb	C	CSZ_45	80	6396±180	6880-7620
T2carb	F	CSZ_46	290	6837±140	7460-7950
T3carb	F	CSZ_47	280	4082±370	5492-3690
Hcarb	C	CSZ_39	190	5872±180	7158-6385
M1carb	A	CSZ_37	90	6171±200	6620-7470

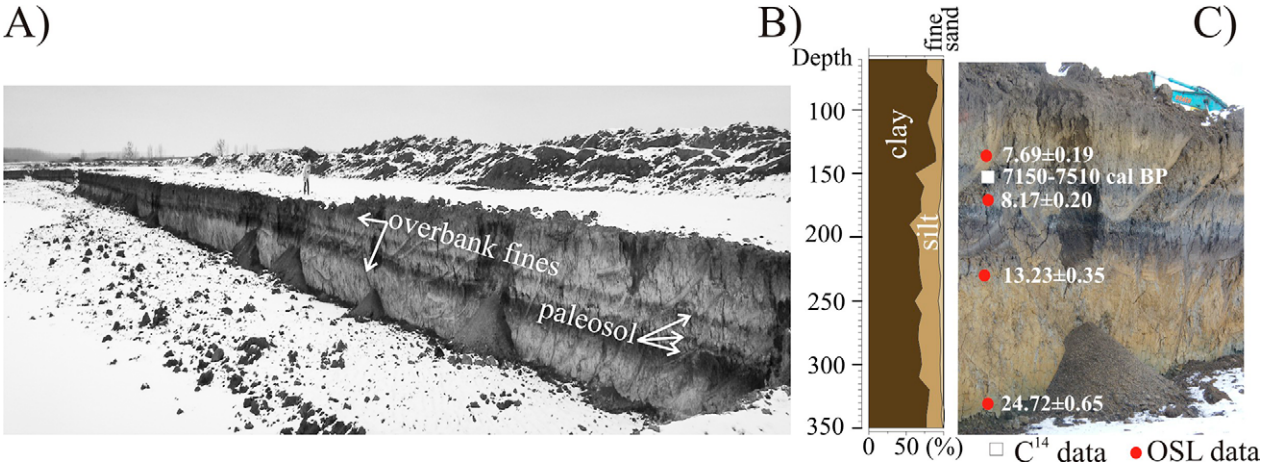

Figure 2. A) Typical alluvial ridge sequence at the T1 site. B) Grain-size distribution of the layers. C) OSL and radiocarbon age of the sediments.

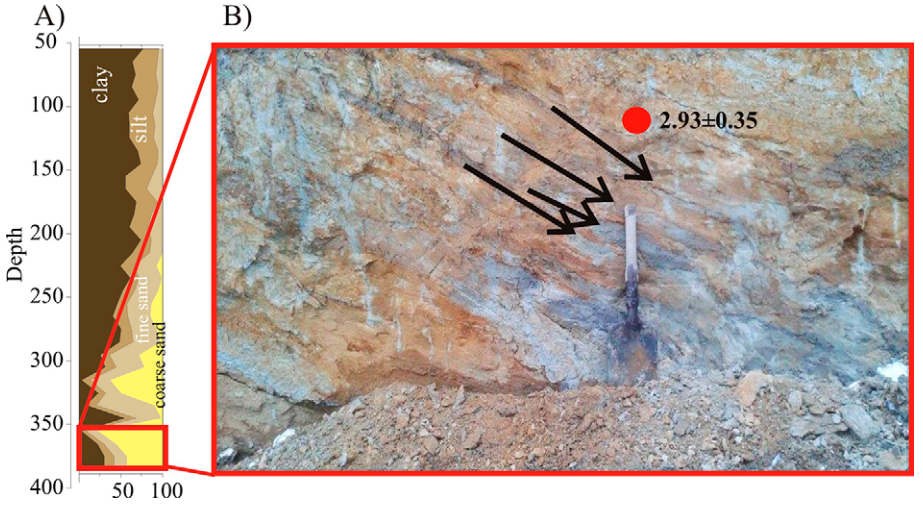

Figure 3. A) Point-bar sequence buried by fine-grained overbank material between the T4/1 and T5/1 sites. B) Within the point-bar sediments sandy and silty (indicated by arrows) alternate. The younger most point-bar layer was dated by OSL measurement.

channel course). The sandy material of the point-bar series (Fig. 3) was revealed along 340 m. The material of the oldest point-bar (T5) deposited 4.23±0.19 ka ago (T5/1), and the youngest point-bar was active 2.93±0.35 ka ago (T5/1). The point-bar series was covered by fine overbank deposits (200-220 cm), which got thinner towards the distal part of the alluvial ridge.

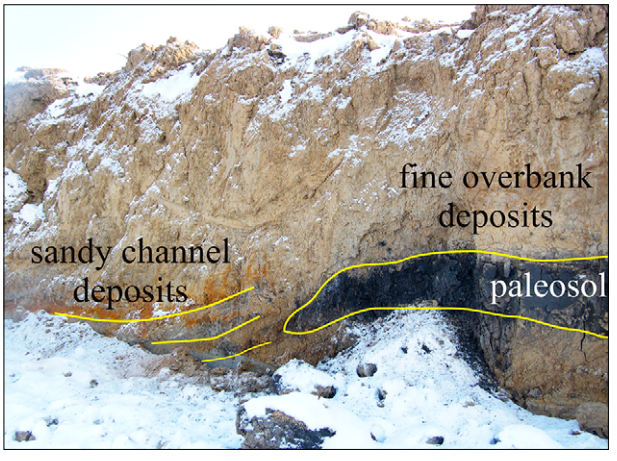

Figure 4. During the activity of the crevasse the overbank fluvial processes were limited, thus a thick paleosol developed.

A ***crevasse channel*** was visible on alluvial ridge C. The crevasse started at the apex of the 105 m-wide paleo-channel. The cohesive material of the paleosol overhung the bank of the crevasse, referring to their co-existence at 7158-6385 cal BP (Hcarb) (Fig. 4). The crevasse was 31 m wide and ca. 4 m deep, and its bottom was filled with 1 m thick fine sand, referring to active bed-load movement. Later the crevasse channel and the paleosol were buried by silty-clayey material.

Pollen analytical results

Not all the drillings contained enough pollen for statistical analysis; thus only 3 drill cores could be used. Here the deepest (910 cm) P1core is introduced in detail.

The lowermost samples (860-910 cm) contained medium sand (70-85%), representing the bedload (Fig.

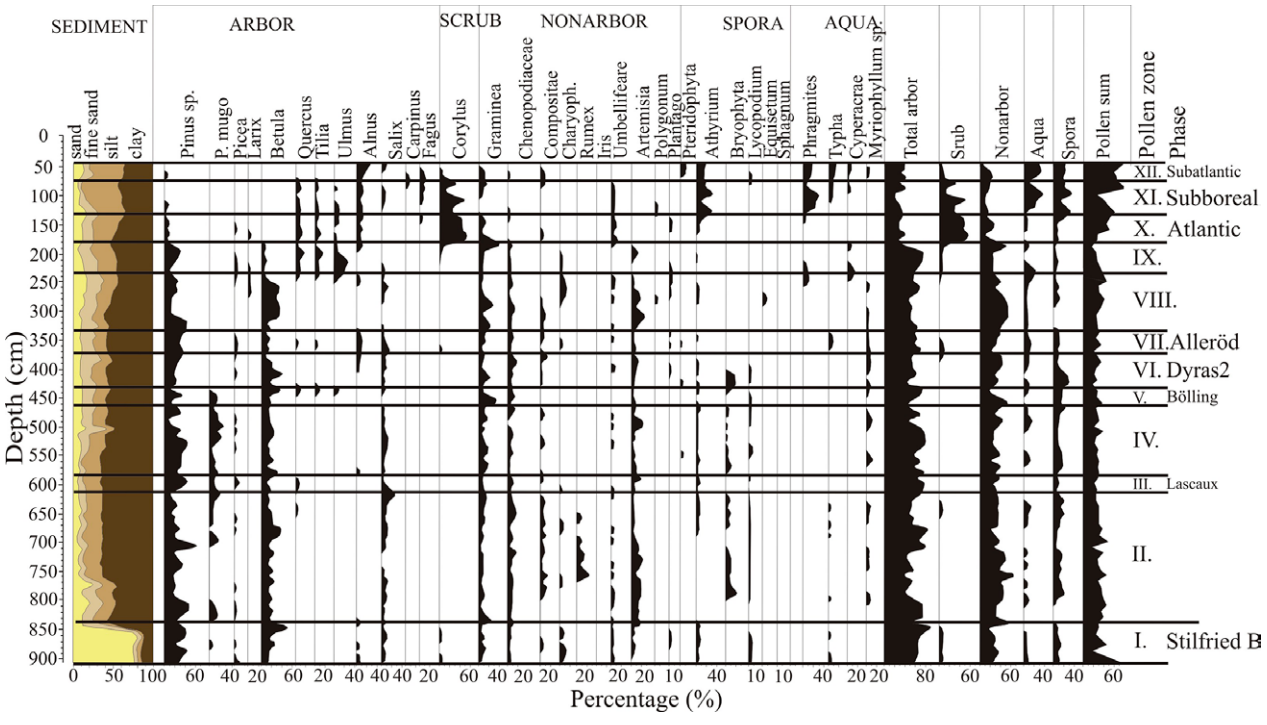

Figure 5. Sediment and pollen profile of the P1 paleo-channel, representing a paleo-channel in a back-swamp area between alluvial ridges

5). Upwards (860-780 cm) the proportion of sand decreased (15-30%), and the amount of silt (50-60%) and clay (10-20%) increased, reflecting a temporal connection to the main channel during floods. These sediments were covered by an almost homogenous silty-clayey layer (520-780 cm) deposited in an almost uniform sedimentary environment. In the next zone (0-520 cm), small sand peaks appeared, referring to sediment transport from a nearby active channel.

Altogether, 12 pollen zones were identified (Fig. 5). In the lowermost zones (I-VIII: 230-910 cm), *Pinus, Betula* and *Salix* dominated the arbor pollen, and the herbs were mainly represented by *Artemisia sp., Chenopodiaceae, Poaceae* and *Compositae*. In some samples (870-910 cm, 570-610 cm, 430-450 cm and 350-370 cm) deciduous tree pollen (e.g. *Quercus*, and *Alnus*) also appeared, referring to a milder climate. The *Sphagnum* indicates the existence of a peat (360-750 cm), and the algae refer to a cold lake (e.g. 440-450 cm: *Pediastrum kawrayskyi, Mallomonas teilingii*). These pollen refer to cold climate with taiga-like vegetation; however, the deciduous trees suggest short, warm periods. The channel was abandoned in the Stillfried B or Denekamp Interstadial. Similar pollen profile was found nearby, where the *Sphagnum* peat was dated to 29790±870 y BP (Félegyházi et al., 2004).

In the upper zones (IX-XII zones: 0-230 cm), the coniferous plant pollen disappeared, and deciduous trees became dominant (e.g. *Tilia, Quercus*, and *Corylus*). Based on the appearance of *Carpinus* and *Fagus* pollen, the material of the X zone (130-180 cm) deposited during the Atlantic Phase, while the XI zone (80-130 cm) represents the Subboreal, and the XII zone (0-80 cm) refers to the Subatlantic Phase. In these Holocene phases, the sedimentation rate was 0.2-0.3 mm/y, being the highest in the Atlantic and Subatlantic Phases, indicating that the nearby alluvial ridges were reactivated, and an extra amount of fine material was transported into this deep, back-swamp area.

Discussion

Formation of the Bereg Plain and the avulsion of the Tisza River

At the bottom of a back-swamp between alluvial ridges the oldest paleo-channel (P1) was identified, belonging to large river (ca. 9 m deep). It was already abandoned ca. 29 thousand years ago. The oldest OSL age of lacustrine sediments (24.72±0.65 ka) also supports the idea, that by this time the tectonic depression of the Bereg Plain already existed. The subsidence forced the rivers of the NE Carpathians to enter the area, so the avulsion of the Tisza was probably much earlier than it was expected (Somogyi, 1967; Borsy et al., 1989; Borsy, 1995; Tímár et al., 2005).

Temporal development of the alluvial ridges

According to our hypothesis, the paleosols reflect periods when the fluvial activity was moderate; thus, the overbank aggradation did not disturb the pedogenesis, just like in the case of loess profiles (Marković et al. 2007). On the other hand, the silty-clayey overbank deposits above paleosols refer to an increased fluvial activity when the aggradation impeded soil formation (Fig. 6). The identified paleosols refer to moderate fluvial activity in the first half of the Atlantic and in the Subboreal Phase. The beginning of the Atlantic was humid (Gábris, 1995), and the entire catchment was forested by closed oak and beech forests (Járainé-Komlódi, 1969, 2000; Sümegi et al., 2008); thus, the run-off and the sediment discharge decreased. These Atlantic paleosols were found in all dated alluvial ridges (A, C and F); thus, the declining fluvial activity was probably typical for the entire system. On most alluvial ridges, no younger paleosol was found above the Atlantic one, so the fluvial aggradation was still intensive; because the Subboreal Phase was more humid than the Atlantic Phase (Gábris, 1995, 2003). However, in the southernmost (F) alluvial ridge a Subboreal paleosol was identified, referring to a local sediment decline.

In the Late Glacial, ca. 12-13 ka ago, thick overbank fines deposited in C and F alluvial ridges (at the A ridge they were not revealed, probably because there the pit was not deep enough: its bottom sediments are 8.65 ka old). This increased fluvial activity could be related to the last deglaciation of the Carpathians (Bartyik et al., 2021), and the cool and dry climate during the Younger Dryas when the vegetation became sparse and the run-off intensified (Járainé-Komlódi, 1969).

During the next intensive fluvial period at the end of the Boreal Phase (ca. 7.7-8.6 ka) new overbank deposits were accumulated (A and C alluvial ridges), and one of the dated paleo-meanders (P2) was abandoned. In the late Atlantic Phase (6.1-6.6 ka), overbank aggradation was detected on the A and F alluvial ridges. The sandy bedload of the excavated crevasse also suggests intensive sediment transport. In contrary, on ridge C the paleosol formation continued. The high flood magnitudes in the active channels were also supported by the palynological data of the P1 paleo-channel situated between two alluvial ridges, as its sedimentation rate increased in the Atlantic Phase.

The next period of intensive fluvial formation (2.9 and 4.8 ka) was verified on all dated alluvial ridges: in the Subboreal Phase thick overbank sediments were deposited. The lateral reworking of floodplain sediments was also intensive, as the dated meander of the C ridge intensively migrated. It is in accordance with the cooler and more humid climate of the Subboreal Phase (Gábris, 1995, 2003; Nádor et al., 2007).

In the Subatlantic Phase the former point-bar series (T4-T5) were covered by fine overbank sediments, referring to a high (0.5-0.8 mm/y) aggradation rate. The intensive, general aggradation is also supported by the high sedimentation rate of the back-swamp area (P1).

Thus, the paleo-channels on the alluvial ridges drained water almost during the entire Holocene, and they were active simultaneously. It is a different paleohydrological model than found on other rivers of the Great Hungarian Plain, as usually, the paleo-channel courses represent distinct channel generations (Borsy et al., 1989; Kiss et al., 2014ab; Gábris, 2020). The paleo-channel courses probably developed via avulsions. After the avulsion the channel had low-sinuosity and slightly developed alluvial ridge. This first development stage is represented by paleo-channel course B. Later the channel started to meandering, gradually increasing the size of the alluvial ridge (course E). As the activity of a paleo-channels was longer, its alluvial ridge progressively grew (course A and F).

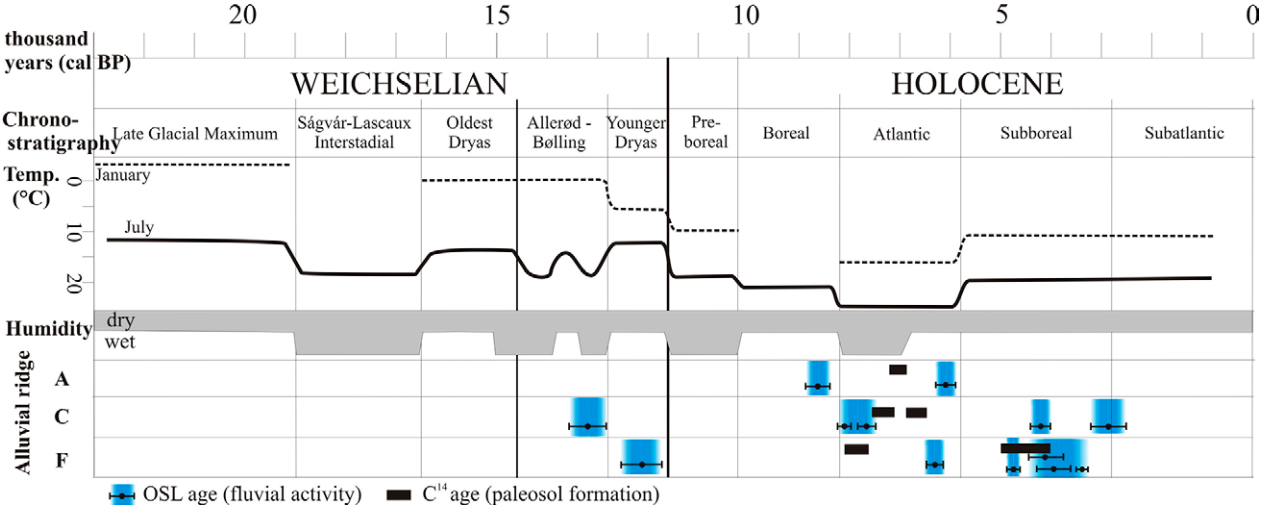

Figure 6. Formation of overbank deposits and paleosols compared to climate elements (source: Borsy et al., 1989; Gábris & Nádor, 2007, Hernesz & Kiss, 2013; Sümeghy et al., 2013; Kiss et al., 2014ab)

Architecture of the alluvial ridges and backswamps

The ridges are gently sloping towards the back-swamps: near the paleo-channel several overbank sediment layers were identified between the paleosols. However, the overbank layers wedge toward the distal areas, and the number of paleosols decreases as they merge into the back-swamp. The ridges are built of only fine-grained material, probably because sandy material was deposited just in a narrow strip along an active channel (Oroszi et al., 2006), and our sampling areas located further on.

The sedimentation rate in the paleo-channels and on the alluvial ridges was quite slow. Since the Late Pleistocene in the paleo-channels the mean aggradation rate was 0.3 mm/y. Usually, the paleo-channels had the highest sedimentation rate (0.5-1.2 mm/y) right after their cut off. During the Holocene the sedimentation rate was uneven, being the highest in the Atlantic Phase (0.3-0.5 mm/y), then it dropped in the Subboreal (0.2-0.3 mm/y), and slightly increased in the Subatlantic Phase (0.3-0.4 mm/y). Similar temporal pattern was revealed by Sümegi (1999), Magyari (2002) and Félegyházi et al. (2004).

The overbank accumulation rate (0.1-0.8 mm/y) on the alluvial ridges are dependent on the re-activation of a given paleo-channel and by the location of the sampling point relative to the channel. For example, in the case of the A alluvial ridge, until ca. 6 ka ago the aggradation rate was 0.27-0.28 mm/y, but then it decreased to 0.1 mm/y, referring to the Late Holocene abandonment or very low activity. Similar overbank accumulation (0.2-0.27 mm/y) was measured along the C paleo-channel in the first half of the Holocene; however, at the end of the Holocene, the aggradation rate increased (0.5-0.8 mm/y) referring to the re-activation of the paleo-channel and its alluvial ridge. Throughout the studied period, the highest aggradation rates (0.36-0.7 mm/y) were revealed from the F paleo-channel, suggesting that it served as the main channel of the Tisza continuously.

The aggradation rate alters laterally too: close to the former channel it was 0.8 mm/y, whereas 340 m further, it dropped to 0.5 mm/y, referring to rapidly declining sedimentation. The spatial pattern of the aggradation was also influenced by the distance from crevasses, which conveyed sediment to the distal floodplain areas. It is well-reflected by the P2 site, which had a higher sedimentation rate (0.5 mm/y) until the neighboring C paleo-channel actively conveyed floods. However, as this channel gradually lost its conveyance capacity due to its slow aggradation, the sedimentation rate also declined (0.3 mm/y).

Conclusions

The juxtaposition of natural levees results in large, convex forms, defined as alluvial ridges. In the Upper Tisza region, on the Bereg Plain, 5 alluvial ridges were identified (max width: 4.0 km, max. height: 3.5 m), providing detailed sedimentary archive on the fluvial history of the area. Based on the sedimentary profiles of the alluvial ridges, several periods with high fluvial activity were identified. According to the results the Tisza appeared in the region much earlier than it was expected, and the paleo-channels co-existed simultaneously conveying water. This paleo-channel network could be utilized in the future during large floods, as they could store and drain large quantities of water. In contrast, during droughts, they could provide water for irrigation.

Acknowledgement

We are grateful for Prof. Gábor Mezősi, who provided a stimulating research environment for the study. We are thankful for Dr. E. Félegyházi (Debrecen University) for the palynological analysis, and for Dr. P. Hernesz (University of Szeged) for the radiocarbon dating.

References

Adams, P.N., Slingerland, R.L., & Smith, N.D. (2004). Variations in natural levee morphology in anastomosed channel flood plain complexes. *Geomorphology*, 61, 127-142. 10.1016/j.geomorph.2003.10.005

Allen, J.R. (1965). A review of the origin and characteristics of recent alluvial sediments. *Sedimentology*, 5, 89-191. 10.1111/j.1365-3091.1965.tb01561.x

Balogh, M., Kiss, T., Fiala, K., & Fehérváry, I. (2020). Floodplain forms along the Lowland Maros River, Hungary. *Geographia Polonica*, 93, 51-68. 10.7163/GPol.0162

Bartyik, T., Sipos, Gy., Filyó, D., Kiss, T., Urdea, P., & Timofte. F. (2021). Temporal relationship of increased palaeo-discharges and Late Glacial degla-

ciation phases on the catchment of River Maros/Mureş, Central Europe. *Journal of Environmental Geography*, 14, 39-46. 10.2478/jengeo-2021-0010

Borsy, Z. (1995). Evolution of the NE part of the Great Hungarian Plain in the past 50,000 years. *Questiones Geographicae*, 4, 65-71.

Borsy, Z. (1969). A Felső-Tiszavidék [The Upper Tisza Region]. In: Pécsi, M. (ed): A Tiszai Alföld. Akadémiai Kiadó, Budapest, 27-66.

Borsy, Z. (1989). Az Alföld hordalékkúpjainak negyedidőszaki fejlődéstörténete. [Quaternary evolution of the alluvial fans of the Alföld]. *Földrajzi Értesítő*, 38, 211-224.

Borsy, Z., Félegyházi, E., & Csongor, É. (1989). A Bodrogköz kialakulása és vízhálózatának változásai. [Fluvial evolution of the Bodrogköz]. *Alföldi Tanulmányok*, 13, 65-81.

Brierley, G.J., Ferguson, R.J., & Woolfe, K.J. (1997). What is a fluvial levee? *Sedimentary Geology*, 114, 1-9. 10.1016/S0037-0738(97)00114-0

Bronk Ramsey, C. (2009). Bayesian analysis of radiocarbon dates. *Radiocarbon*, 51, 337-360. 10.1017/S0033822200033865

Brown, A.G. (1983). An analysis of overbank deposits of a flood at Blandford-Forum, Dorset, England. *Revue. Geomorphologie Dynamique*, 32, 95-99.

Cazanacli, D., Smith, N.D. (1998). A study of morphology and texture of natural levees, Cumberland Marshes, Saskatchewan, Canada. *Geomorphology*, 25, 43-55. 10.1016/S0169-555X(98)00032-4

Félegyházi, E., Szabó, J., Szántó, Zs., & Tóth, Cs. (2004). Adalékok az északkelet-Alföld pleisztocén végi, holocén felszínfejlődéséhez újabb vizsgálatok alapján. [Late Pleistocene and Holocene evolution of NE Great Plain] II. Magyar Földrajzi Konferencia, Szeged, 1-10.

Florsheim, J.L., & Mount J.F. (2002). Restoration of floodplain topography by sand-splay complex formation in response to intentional levee breaches, Lower Cosumnes River, California. *Geomorphology*, 44, 67-94. 10.1016/S0169-555X(01)00146-5

Fryirs, K.A., & Brierley, G.J. (2012). *Geomorphic analysis of river systems: An approach to reading the landscape*. Chichester: Wiley-Blackwell, 360. 10.1002/9781118305454

Gábris, Gy. (2016). A Körös-medence folyóvízi formavilága. [Geomorphology of the Körös Basin] *Acta climatologica*, 50/B, 47-53. http://acta.bibl.u-szeged.hu/44009/

Gábris, Gy. (2020). A folyóvíz felszínformáló tevékenysége Magyarországon. [Fluvial activity in Hungary] ELTE, Budapest, p. 181. ISBN-10:6202486759

Gábris, Gy. (1995). A folyóvízi felszínalakítás módosulásai a hazai későglaciális-holocén őskörnyezet változásainak tükrében. [Late Glacial-Holocene fluvial activity in Hungary] *Földrajzi Közlemények*, 119, 3-10.

Gábris, Gy. (2003). A földtörténet utolsó 30 ezer évének szakaszai és a futóhomok mozgásának főbb periódusai Magyarországon. [Aeolian activity of the last 30 ka in Hungary] *Földrajzi Közlemények*, 127, 1-14.

Gábris, Gy., & Nádor, A. (2007). Long-term fluvial archives in Hungary: response of the Danube and Tisza rivers to tectonic movements and climatic changes during the Quaternary. *Quaternary Science Reviews*, 26, 2758-2782. 10.1016/j.quascirev.2007.06.030

Hajek, E.A., & Wolinsky, M.A. (2012). Simplified process modeling of river avulsion and alluvial architecture: Connecting models and field data. *Sedimentary Geology*, 257-260, 1-30. 10.1016/j.sedgeo.2011.09.005

Hudson, P.F., & Heitmuller, F.T. (2003). Local and watershed-scale controls on the spatial variability of natural levee deposits in a large fine-grained floodplain: lower Pánuco Basin, Mexico. *Geomorphology*, 56, 255-269. 10.1016/S0169-555X(03)00155-7

Ishii, Y., Tamura, T., & Ben, B. (2021). Holocene sedimentary evolution of the Mekong River floodplain, Cambodia. *Quaternary Science Reviews*, 253, 106767. 10.1016/j.quascirev.2020.106767

Járainé-Komlódi, M. (1969). Adatok az Alföld negyedkori klíma-és vegetációtörténetéhez II. [Quaternary climate and vegetation history of the Great Hungarian Plain]. *Botanikai Közlemények*, 56, 43-55.

Járainé-Komlódi, M. (2000). A Kárpát-medence növényzetének kialakulása. [Vegetation history of the Carpathian Basin] *Tilia*, 9, 5-59.

Kiss, T., Hernesz, P., Sümeghy, B., Györgyövics, K., & Sipos, Gy. (2014a). The evolution of the Great Hungarian Plain fluvial system – fluvial processes in a subsiding area from the beginning of the Weichselian. *Quaternary International*, 388, 142-155. 10.1016/j.quaint.2014.05.050

Kiss, T., Sümeghy, B., & Sipos, Gy. (2014b). Late Quaternary paleodrainage reconstruction of the Maros River alluvial fan. *Geomorphology*, 209, 49-60. 10.1016/j.geomorph.2013.07.028

Kiss, T., Balogh, M., Fiala, K., & Sipos, Gy. (2018). Morphology of fluvial levee series along a river under human influence, Maros River, Hungary. *Geomorphology*, 303, 309-321. 10.1016/j.geomorph.2017.12.014

Liritzis, I., Stamoulis, K., Papachristodoulou, C., & Ioannides, K. (2013). A re-evaluation of radiation dose-rate conversion factors. *Mediterranean Archaeology and Archaeometry*, 13, 1-15.

Magyari, E. (2002). Climatic versus human modification of the Late Quaternary vegetation in Eastern Hungary. PhD dissertation, University of Debrecen, Debrecen.

Makaske, B., Smith, D.G., Berendsen, H.J., de Boer, A.G., van Nielen-Kiezebrink, M.F., & Locking, T. (2009). Hydraulic and sedimentary processes causing anastomosing morphology of the upper Columbia River, British Columbia, Canada. *Geomorphology*, 111, 194-205. 10.1016/j.geomorph.2009.04.019

Marković, S.B., Bokhorst, M.P., Vandenberghe, J., McCoy, W.D., Oches, E.A., Hambach, U., Gaudenyi, T., Jovanović, M., Zöller, L., Stevens, T., & Machalett, B. (2007). Late Pleistocene loess-palaeosol sequences in the Vojvodina region, north Serbia. *Journal of Quaternary Science*, 23, 73-84. 10.1002/jqs.1124

Mauz, B., Bode, T., Mainz, E., Blanchard, H., Hilger, W., Dikau, R., & Zöller, L. (2002). The luminescence dating laboratory at the University of Bonn: Equipment and procedures. *Ancient TL*, 20, 53-61.

Murray, A.S., & Wintle, A.G. (2003). The single aliquot regenerative dose protocol: Potential for improvements in reliability. *Radiation Measurements*, 37, 377-381. 10.1016/S1350-4487(03)00053-2

Nádor, A., Thamó-Bozsó, E., Magyari, Á., & Babinszki, E. (2007). Fluvial responses to tectonics and climate change during the Late Weichselian in the eastern part of the Pannonian Basin (Hungary). *Sedimentary Geology*, 202, 174-192. 10.1016/j.sedgeo.2007.03.001

Nicholas, A.P., Aalto, R.E., Sambrook Smith, G.H., & Schwendel, A.C. (2018). Hydrodynamic controls on alluvial ridge construction and avulsion likelihood in meandering river floodplains. *Geology*, 46, 639-642. 10.1130/G40104.1

Oroszi, V., Sándor, A., & Kiss, T. (2006). A 2005. tavaszi árvíz által okozott ártérfeltöltődés a Maros és a Közép-Tisza egy rövid szakasza mentén. [Floodplain aggradation of the Maros and Tisza after the 2005 flood]. In Kiss, A, Mezősi, G., Sümegi, Z. (edts): Táj, környezet és társadalom. SZTE, Szeged, 551-561.

Ostrowski, P., Falkowski, T., & Utratna-Zukowska, M. (2021). The effect of geological channel structures on floodplain morphodynamics of lowland rivers: A case study from the Bug River, Poland. *Catena*, 202, 105209. 10.1016/j.catena.2021.105209

Piégay, H., Arnaud, D., & Souchon, Y. (2003). Effects of riparian vegetation on river channel geometry: case studies from the Massif Central (France). *Géomorphologie*, 9, 111-128.

Pierik, H.J., Stouthamer, E., & Cohen, K.M. (2017). Natural levee evolution in the Rhine-Meuse delta, the Netherlands, during the first millennium CE. *Geomorphology*, 295, 215-234. 10.1016/j.geomorph.2017.07.003

Reimer, P., Austin, W., Bard, E., Bayliss, A., & Bronk Ramsey, C. (2020). The IntCal20 Northern Hemisphere Radiocarbon Age Calibration Curve (0–55 cal kBP). *Radiocarbon*, 62, 725-757. 10.1017/RDC.2020.41

Skripkin, V.V., & Buzynnyi, M.G. (2017). Teflon vials for precise C-14 in benzene measurements by LSC technique. *Biological and Chemical Research*, 4, 229-233.

Skripkin, V.V., & Kovaliukh, N.N. (1998). Recent developments in the procedures used at the SSCER Laboratory for the routine preparation of lithium carbide. *Radiocarbon*, 40, 211-214. 0.1017/S0033822200018063

Smith, N.D., Cross, T.A., Dufficy, J.P., & Clough, S.R. (1989). Anatomy of an avulsion. *Sedimentology*, 36, 1-23. 10.1111/j.1365-3091.1989.tb00817.x

Somogyi, S. (1967). Ősföldrajzi és morfológiai kérdések az Alföldről. [Paleo-hydrography of the Great Plain] *Földrajzi Értesítő*, 16, 319-337.

Steiger, J., Tabacchi, E., Dufour, S., Corenblit, D., & Peiry, J.L. (2005). Hydrogeomorphic processes affecting riparian habitat within alluvial channel-floodplain river systems: a review for the temperate zone. *River Research and Applications*, 21, 719-737. 10.1002/rra.879

Stevaux, J.C., & Souza, I.A. (2004). Floodplain construction in an anastomosed river. *Quaternary International*, 114, 55-65. 10.1016/S1040-6182(03)00042-9

Sümegi, P. (1999). Reconstruction of flora, soil and landscape evolution, and human impact on the Bereg Plain from Late Glacial up to the present, based on paleoecological analysis. In: Hamar, J., & Sárkány-Kiss, A. (edts): The Upper Tisza valley. Szeged, 173-204.

Sümegi, P., Juhász, I., Magyari, E., Jakab, G., Rudner, E., Szántó, Zs., & Molnár, M. (2008). A keleméri Mohos-tavak fejlődéstörténetének rekonstrukciója paleobotanikai vizsgálatok alapján. [Development of the Mohos Lakes at Kelemér based on paleobotanical methods] In: Boldogh, S., & Farkas T. (eds). A keleméri Mohos-tavak. ANP, Jósvafő, p. 334

Tans, P.P., & Mook, W.G. (1980). Past atmospheric CO2 levels and 13C/12C ratios in tree rings. *Tellus*, 32, 268-283.

Timár, G., Sümegi, P., & Horváth, F. (2005). Late Quaternary dynamics of the Tisza River: evidence of climatic and tectonic controls. *Tectonophysics*, 410, 97-110. 10.1016/j.tecto.2005.06.010

Vass, R. (2014). Ártérfejlődési vizsgálatok felső-tiszai mintaterületeken [Floodplain development of the

Upper Tisza]. PhD Dissertation, Debrecen University, Debrecen, p. 184.

Wolfert, H.P., Hommel, P.W.F., Prins, A.H., & Stam, M.H. (2002). The formation of natural levees as a disturbance process significant to the conservation of riverine pastures. *Landscape Ecology*, 17, 47-57. 10.1023/A:1015229710294

Zólyomi, B., 1952. Histoire de 1'évolution du tapis végétal de la Hongrie depuis la derniére époque glaciaire. MTA *Biol. Oszt. Közl*. 1, 491-530.

ISSN 0354-8724 (hard copy) | ISSN 1820-7138 (online)

Plot-level Field Monitoring with Sentinel-2 and PlanetScope Data for Examination of Sewage Sludge Disposal Impact

Ferenc Kovács[A*], Zsuzsanna Ladányi[A]

Received: May 19, 2022 | Revised: August 04, 2022 | Accepted: August 10, 2022
doi: 10.5937/gp26-37964

Abstract

Agricultural use of sewage sludge is one of the means of sustainable environmental management. In order to monitor the short-term effects of sludge disposal a multi-year, high-resolution data collection was planned on arable land in south-eastern Hungary. Data acquisition was applied at the highest temporal and spatial resolution using Sentinel-2 and PlanetScope satellite imagery observing the vegetation period based on vegetation indices (EVI, NDVI) from 2016 to 2021. There were statistical differences in the case of sunflower and maize biomass productions but the spatial and statistical deviations between the affected and non-affected areas of sludge disposal were generally not significant. The sensitivity of EVI in the dense vegetation period and its applicability might be emphasized in a comparative analysis.

Keywords: sewage sludge; agricultural monitoring; Sentinel-2; PlanetScope; spectral index

Introduction

The macronutrient content in the sewage sludge, disposed to the soil and complying with public health and environmental requirements and legislation (biosolid), is similar to that found in animal manure, where the N, P, and organic nutrient content, can be used by plants, can reach 50% (Sagasta et al., 2015; Tomócsik et al., 2016). Field disposal also addresses the problem of disposing of sludge treated as waste, moreover, results in increased crop yields. The increase in humus quality and quantity improves soil water holding capacity and compactness, thus, resulting in a more balanced, stronger vegetation (Simon & Szente, 2000). According to Markowicz, et al. (2021), wastewater disposal up to 15 t/ha is the most efficient way to recultivate certain soils having a nutrient deficit. The use of sewage sludge is encouraged by also the European Union and the Hungarian regulations (e.g. 91/271/EEC, 36/2006 (V.18.)), 40% of the sewage sludge is utilized in agriculture in Hungary (Sewage Sludge Treatment and Utilization Strategy 2014-2023).

On a plot treated with sewage sludge, compared to the other areas, the development of vegetation is more dynamic in principle and has a higher biomass production. Obtaining data and information on vegetation development on regional scale is easy owing to the development of remote sensing in the past 40 years. Multispectral data content of new sensors, of different resolutions which also distinguishes the main cultivated field crops based on the time series, allows the continuous spatial and temporal evaluation locally too, which is greatly supported by the increased number of sensors (Kuenzer et al., 2015; McCabe et al., 2017). The problem is more complex; the different soil types are only allowed to filter and transform sewage sludge by

[A] Department of Geoinformatics, Physical and Environmental Geography, Faculty of Science and Informatics, University of Szeged; 6722, Szeged Egyetem utca 2; kovacsf@geo.u-szeged.hu
[*] Corresponding author: Dr. Ferenc Kovács (PhD, habil), kovacsf@geo.u-szeged.hu

biological and chemical processes up to a certain load; furthermore, it is difficult to analyze the small changes in the quantity and quality of organic matter and the yield during 1-2 years. Thus, several years or decades of observation are necessary to assess its effect on soil improvement (Banerjee et al., 1997). Moreover, the land use changes or the climatological parameters influencing the development of plants can also not be omitted (Erdődiné & Kovács, 2021).

In this study, our aim was to observe the effect of sewage sludge disposal on biomass production on arable land plots with the highest possible temporal and spatial resolution, which is a continuation of the earlier evaluation process (Kovács & Ladányi, 2021). The original studying period was broadened to 6 years between 2016 and 2021, and the data of a new sensor was also applied when observing the extended vegetation period from March 1 to September 30.

Data and methods

In addition to multispectral monitoring assessments of land use, damage estimation, and agricultural science applications for yield estimation, there are an increasing number of users that collect very high-resolution precision agricultural data to optimize farming (Kovács et al., 2019; Segarra et al., 2020; Weiss et al., 2020). Regular and detailed examination on plot level requires high- and very high-resolution multispectral recordings (cell size <= 2 m), where remote sensing – e.g. WorldView – can only be implemented extremely costly and in a programmed manner (Kuenzer et al., 2015). Liu et al. (2018) show that archive data collection of high temporal resolution is not feasible with even more sensors. Dove PlanetScope (Planet) recordings, which regularly provide higher temporal resolution than ever before and are available for free after registration in Europe from 2017, are currently being addressed (Roy et al., 2021).

Sentinel-2A and -2B (S2) multispectral satellite images were used primarily for the entire investigated period in our study having a spatial resolution of 10 m and a temporal resolution of 3–5 days (Table 1). A total of 145 pieces of images were evaluated, that were all atmospherically corrected, Level-2 processed, cloud-free recordings. On the Tile 34TDS, all sample areas are covered. In 2018-2019-2020, and mostly in August and September, more recordings than average could be expected. Monitoring was limited by the higher cloud cover typical in spring and early summer periods, thus, only 24-40% of all possible summer semester recordings could be used in certain years. There were no satellite images to be evaluated in July 2016 and also for several areas in 2018, and in June 2017.

It is risky to use one single sensor to assess one geophysical variable, thus, all available Level 3A, surface reflectance 4 band Planet data for 2020 were evaluated to monitor vegetation dynamics in more detail, as well as for the verification and validation of S2-based results. In addition to the daily time resolution, 64 pieces of cloud-free satellite images with 3 m resolution were available, furthermore, data from 21 dates were available to compare the results of the two sensors between March 1 and September 30.

Table 1. Applied Sentinel-2 and PlanetScope imagery and their parameters

Satellite / sensor	Multispectral imagery / year	Applied spectral bands, middle of wavelengths	Spatial resolution
Sentinel-2A and 2B	20 images / 2016 14 images / 2017 34 images / 2018 29 images / 2019 26 images / 2020 21 images / 2021	B2: 492.4 / 492.1 nm B4: 664.6 / 665 nm B8: 832.8 / 833 nm	10 m
PlanetScope	64 images / 2020	B1: 485 nm B3: 630 nm B4: 820 nm	3 m

*Data: Copernicus Open Access Hub (*https://scihub.copernicus.eu/dhus/*),*
*Planet Explorer (*https://www.planet.com/explorer/*)*

Less cloudless images were available from LANDSAT-8 (L8) database. L8 and S2 were recorded 15 times on the same days in the summer semesters between 2016 and 2019. The statistical relationship (R2EVI >= 0,8), interpreted by Kovács and Ladányi (2021) when comparing the satellite images, does not allow the values of the two sensors to be used in one time series, while the Planet data are more suitable for validation purposes.

It is advisable to plan the timing of the recording for months determining the development of the giv-

en plant (the harvest and 2-3 months before), which is different for each plant species (winter wheat: III-VI months, maize: V-VIII months). The plots in our sample area were usually cultivated with different crops every year, which, together with the high cloud cover that caused problems in image data collection, increases the limitations of the comparison.

The commonly used Normalized Difference Vegetation Index (NDVI) and the improved Enhanced Vegetation Index (EVI), which reduces the impact of the soil and the atmosphere, are applied to measure the photosynthetic activity and the changes in biomass production for decades (Bannari et al., 1995). These indices (VI) are determined by plant wetness and chlorophyll content (Equations 1 and 2).

$$NDVI = \frac{NIR - Red}{NIR + Red} \quad (1)$$

$$EVI = G\frac{NIR - Red}{NIR + C1 \cdot Red + C2 \cdot Blue + L} \quad (2)$$

where NIR indicates the near-infrared band, Red indicates the visible red band, Blue indicates visible blue band, L = 1, C 1 = 6, C 2 = 7.5, and G = 2.5.

According to Huete et al. (2002) EVI is more sensitive in areas more densely covered with vegetation. Differences between plant species, physiological and leaf structure differences can be better indicated. The general overview of NDVI values is useful in observing low vegetation coverage and the temporal dynamics, however, but a value higher than EVI will saturate sooner, and even though phytomass increases, reflectance no longer increases, underestimating biomass production. This may make it difficult to assess the response during the developmental phase of maximum vegetation coverage. The use of EVI or the Red Edge (RE) bands with lower chlorophyll absorption instead of reflectance in the red band is a solution to the latter problem (Clevers & Gittelson, 2013), however, such bands are only available at S2 among the sensors applied in this study. Based on the comparison with reference measurements, the indices made from S2 spectra are well representative of the areas (Plug & Louis, 2020). NDVI can not be omitted from the long-term regional monitoring (Tran et al., 2017), and the EVI and NDVI index values in small and medium-scale studies are able to show the dates and periods of agricultural management (Kovács & Gulácsi, 2019; Szabó et al., 2019). Locally, the main cultivated field crops can be well distinguished, although they can differ significantly from year to year due to local environmental factors (water supply, harvest time, etc.). The values depend on the vegetation density: on those plots where plants hatched rarely, the NDVI values are lower throughout the developmental period (Erdődiné & Kovács, 2021). According to a high-resolution, decades-long multispectral analysis, the short-term effects observed after sewage sludge treatment within a few years are variable, while over a longer period (about 10 years), the change in plant growth is positive (Álvarez et al., 2014).

Study area

Data collection based on remote sensing methods was performed for 14 homogenous quadrates having a size of 50x50 m2 on three agricultural plots producing different crops, in parallel with the soil sampling according to Farsang et al. (2020). Certain quadrates represent areas treated with sewage sludge and the adjacent quadrates with very similar properties without treatment served as control areas for the study (Table 2). The sample areas are located in the Great Plain in Hungary, between the River Körös and Maros, near Újkígyós and Kardos settlements (Figure 1.). The quadrates were placed in pairs named the followings: in Újkígyós 1t-2t, 3t-4t, 6t-7t, 9t-10t (coordinates of the plot center: UTM (Zone 34N) X: 503400, Y: 5160000), in Kardos: 10t-11t, 12t-13t (X: 479020, Y: 5181700) and 14t-15t (X: 480630, Y: 5180200).

In the study area, which has been cultivated continuously for decades, mainly maize, winter wheat, sunflowers, furthermore colza, and oil radish are grown. Comparative examination of the yearly changing vegetation is difficult and uncertain, it seemed better to show only the significant differences.

In the Újkígyós study area, 1t-4t quadrates were sampled as treated areas, where sewage sludge was disposed in October 2017. 6t-7t were control areas and partly treated areas, as one year later, in autumn 2018, sewage sludge was dumped here too. Quadrates 9t-10t were untreated, in control areas. Between 2016 and 2021, the surface coverage of the 1t-4t samples, situated on the same agricultural plot in Újkígyós, was different every year, only in 2018 and 2020 the produced crop was the same: winter wheat. In the 6t-7t and 9t-10t quadrates, located on different plots, the same crop, corn, was found in 2017, 2018, and 2020 to facilitate our comparative study, and winter wheat occurred in 2019 and 2021. In the knowledge of the autumn sewage sludge disposal in 2017 and 2018 and the management, the following comparisons were planned in Újkígyós sample areas:

- maize: observation of 6t-10t quadrates as control areas between 2017 and 2018, followed by measures on the 6t-7t in 2020 after sludge disposal and their comparison
- winter wheat: observation of 1t-4t quadrates between 2018 and 2020 show the vegetation development after the sewage sludge disposal in 2017.

Table 2. Crops produced in quadrates of Kardos and Újkígyós parcels between 2016–2021

Újkígyós / quadrates	2016	2017	2018	2019	2020	2021
1t	maize	oil radish[1]	winter wheat	colza	winter wheat	sunflower
2t	maize	oil radish[1]	winter wheat	colza	winter wheat	sunflower
3t	maize	oil radish[1]	winter wheat	colza	winter wheat	sunflower
4t	maize	oil radish[1]	winter wheat	colza	winter wheat	sunflower
6t	colza	maize	maize[2]	winter wheat	maize	oil radish
7t	colza	maize	maize[2]	winter wheat	maize	oil radish
9t	sunflower	maize	maize	winter wheat	oil radish	winter wheat
10t	sunflower	maize	maize	winter wheat	oil radish	winter wheat
Kardos / quadrates	**2016**	**2017**	**2018**	**2019**	**2020**	**2021**
10t	sunflower	winter wheat[1]	sunflower	winter wheat	maize	sunflower
11t	sunflower	winter wheat[1]	sunflower	winter wheat	maize	sunflower
12t	sunflower	winter wheat	sunflower	winter wheat	maize	sunflower
13t	sunflower	winter wheat	sunflower	winter wheat	maize	sunflower
14t	sunflower	winter wheat[1]	maize	maize	maize	maize
15t	sunflower	maize	maize	maize	maize	maize

[1] - 2017 autumn: sewage sludge placement; [2] - 2018. October: sewage sludge placement

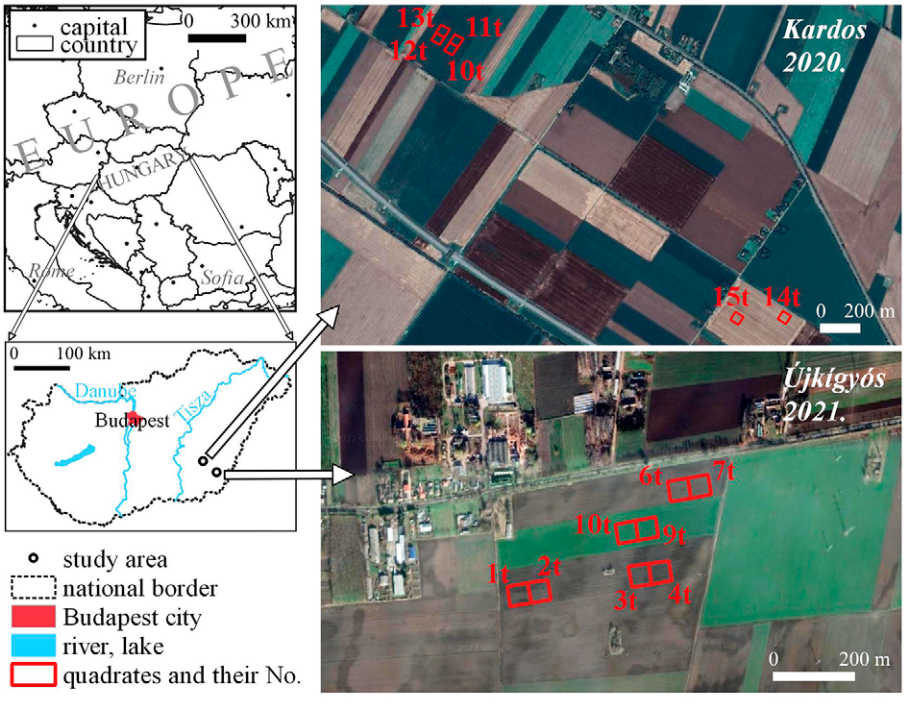

Figure 1. Sample quadrates near Kardos (No. 10t-15t) and Újkígyós settlements (No. 1t-4t, 6t-7t, 9t-10t) located on the Great Hungarian Plain, Hungary (background: GoogleEarth)

Regarding the control areas, the investigation possibilities are limited, as only 9t-10t were without sewage sludge disposal in 2019 and 2021that could be assessed.

- sunflower: control quadrates (9t-10t) in 2016 can be compared with the values of the 1t-4t in 2021 showing the effect of the 2017 sewage sludge disposal.
- colza: observations in 6t-7t as controls in 2016 can be compared to the 1t-4t areas following the disposal in 2019.

Planet images applied in this area in 2020 are good additional data for several crops; e.g. for maize, winter wheat, and oil radish.

In the Kardos study area, 10t-11t and 12t-13t quadrates are within a plot as shown in Figure 1, with the same management pattern varying from year to year; sunflowers were produced in 2016, 2018, and 2021, and winter wheat in 2017 and 2019. The land use in 14t and 15t quadrates in 2016 was still sunflower, but in 2017 only 14t had winter wheat cover while in 15t corn

was grown. Between 2018 and 2021, maize production was already uniform. 10t-11t and 14t were allocated on plots where sewage sludge was disposed in autumn 2017, 12t-13t and 15t were used as control areas. The following comparisons were planned in the Kardos sample areas (three types of plants were grown during the study period):

- maize: after the disposal in 2017, the differences with 10t-11t in 2020 are assessed and 12t-13t quadrates are used as a control. As a consequence of the disposal of sewage sludge, between 2018 and 2021, the values of the parcels according to 14t must deviate from the values of 15t
- winter wheat: in the case of 10t-13t quadrates the biomass production of the year 2017 can be compared with 2019. In the 10t-11t, the impact of the sewage sludge disposal in 2019 can be assessed
- sunflower: the control value in 2016 on the 10t-13t quadrates might be compared with the values of 2018 and 2021 showing the effect of placement.

The Újkígyós quadrates are located on the alluvial fan of the Mureş 90-92 m above sea level, while the Kardos sample areas are situated on the edge of the alluvial fan at an elevation of 84-85 m above sea level (Mezősi, 2017). The soil type is the same on all study areas: calcareous Chernozem which makes comparison possible. Based on the digital soil maps (DOSoReMI[1]), the particle size fraction of the upper 0–30 cm soil layer is 10% -10% -25% for clay, loam, and sand in the Újkígyós plots, respectively, meaning that soil water retention capacity is poor. The topsoil texture is loam (sandy loam) having an organic matter content of 2-3%. In the Kardos plots, soils have a good water retention capacity due to more clay and loam fractions but less sand: 30% -35% -5%, and the organic matter content is higher here: 3-4%. The value expressing natural soil fertility for the study areas is 70-80% in Kardos compared to 50-60% in Újkígyós study areas. There were no significant changes in the basic soil parameters in the Újkígyós sample area in the last 5 years besides the sewage sludge discharges, only N and P content increased (Ladányi et al., 2020).

Agricultural production is affected by climate change in the sample area. Between 1981 and 2020, the average annual temperature increased by + 1.8–1.9 °C, and the number of heat-wave days increased by more than 14 days. In the last 40 years the precipitation showed a 10% increase in the annual amount, and extreme rainy days, having more than 20 mm precipitation, dominate. As a result, the longest dry periods appear to be shortened (Lakatos et al., 2021). In Hungary, there is a moderate drought every second year and a strong drought every third year (Buzási et al., 2021) and according to Mezősi et al. (2016) as a result of the increasing impact of drought, the role of tillage will come to the fore in the next 2-3 decades. The farming and tillage of the near future are basically determined by the rapid changes in the seasons. By 2100, half-year-long summers can be expected in the northern hemisphere (Wang et al., 2021).

In our sample area, the average temperature of the summer semester is + 0.8–2 °C higher each year compared to the period between 1970 and 2000. 2017-2018-2019 was the hottest period; the deviation from the average exceeded even +3 °C in several months. Although the climate was cooler than average in the spring of 2020-2021, the positive difference was still significant in the summer months (July 2021: +4.6 °C). Precipitation amount only exceeded the 30-year average (368.4 mm) in 2019 (453 mm), while 13% less precipitation than the average fell in the 6 studied years. A longer, continuous dry period from March to July 2017 and throughout the first half of 2021; in the last year, only 45% of the average has fallen (Figure 2). There are outstanding rainy months every summer for the rest of the years; June 2016, March 2018, May and July 2019, and March and June 2020.

The daily meteorological drought index (HDI) shows the same as the climatic data presumed (Fiala et al., 2018); more than 30% of the studied period is characterized by drought; 6.5% by severe drought (HDI>=2), and 25% by moderately drought (HDI> = 1.5). In the study area, 2018, 2019, and 2020 were the least dry years; it was only August 2018 and April 2019 that were characterized by moderate droughts, and June and July in 2017 also showed moderate droughts with slightly higher values. The driest year was 2021 when a continuous moderate drought was experienced between June and September, moreover, August and September showed high drought. The sensitivity of the groundwater level to climatic effects, which determines the water supply, increases towards the central part of the alluvial fan (Újkígyós), while towards the edge of that (Kardos) it decreases (Rakonczai & Fehér 2015).

[1] https://dosoremi.hu/maps/

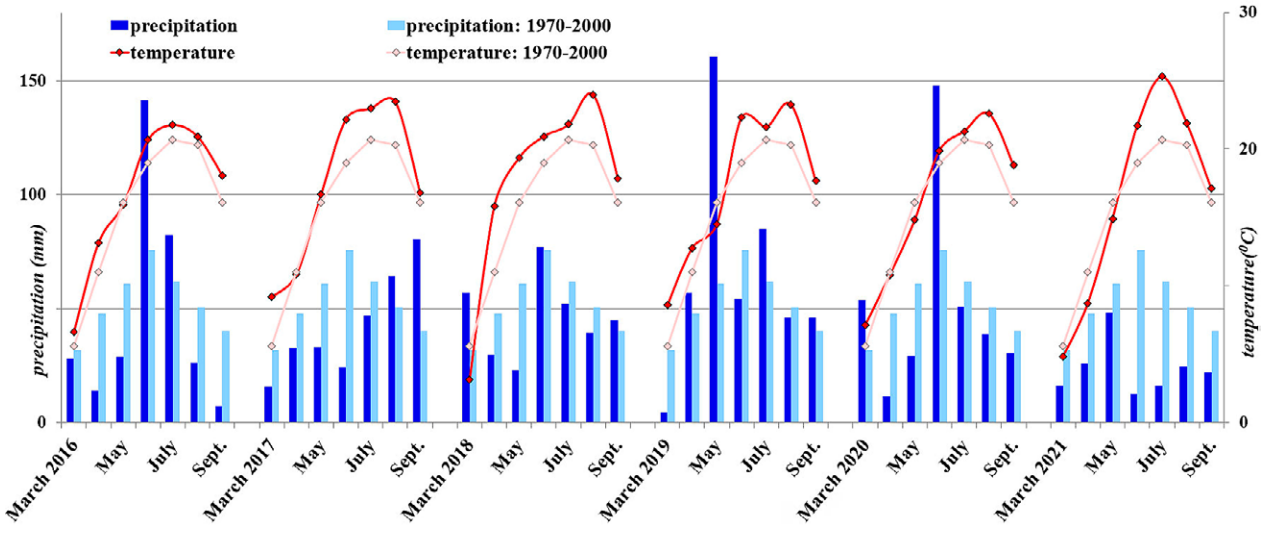

Figure 2. Precipitation and temperature in Békéscsaba station in the period of 2016–2021
Data: Ogimet.com (http://www.ogimet.com/gsynres.phtml.en); Operatív Vízhiány Értékelő és Előrejelző Rendszer (http://aszalymonitoring.vizugy.hu/)

Results and Discussion

The difference in the growing cycle of the crops and the changes in land use in the plots are clearly visible in the VI values, and the curves follow the vegetation development well (Figures 3–6).

In a data set of quadrat-pairs with identical land-use values, the sensitivity of the index means that EVI shows significant differences within the plot, while NDVI rarely does. We also see a difference between 1t-2t and 3t-4t pairs in the same plot, which can be as high as 0.15 NDVI and 0.2 EVI in the June 2016 maize crop. In the same area, the average EVI difference for the 2017 oil radish crop is 0.1-0.15 in May-June, and a difference of 0.15 EVI is found in September after the 2020 harvest. This includes the difference between the May-June 2021 EVI of 0.1 and the August 2021 EVI of 0.15-0.2 for the sunflower crop. Interestingly, in the 10t-13t quadrates of the Kardos sample area, we observed 0.1-0.15 EVI differences already in August and September, but only in 2017, 2020, and 2021. Similarly, August shows a larger – 0.15-0.2 – EVI and NDVI divergence for 14t-15t in 2018.

The highest average VI values above 0.9 (up to 0.98) occur in June in almost all cases, regardless of the crop. Many NDVI averages above 0.9 were observed in sunflower, winter wheat, and maize growing areas in June 2017 and 2021, the summer months of the driest years. Only the high average EVI values were deviated from this and only in Újkígyós study site, where they were approximately 0.1 lower and only in May (2016 and 2020) in colza and oil radish areas. For the whole analyzed period 2016-2021, neither Újkígyós nor Kardos study areas show a significant change in biomass product for either index. The time series of treated by sewage sludge and non-treated parcels could be compared for the months of May-July 2018-2021 in Kardos study area thanks to the plots producing similar crops. Small extent, but both NDVI and EVI show systematically higher average values in the sludge-treated plots.

The EVI is very rarely higher than the NDVI value, only in the case of dense vegetation. The difference is typically around +0.08-0.2, which can be as high as +0.35-0.4 during the peak biomass production period; the difference between NDVI and EVI in Újkígyós study area is larger and typically smaller in areas treated with sewage sludge. Dense vegetation should be interpreted in terms of EVI, but the increase in biomass production can be well distinguished by NDVI, and sometimes the difference between vegetation types can be also better assessed. It makes sense to use the two indices together in the assessment, as exemplified by the different VI values of the 6t-7t areas in 2016 and 2017.

The effect of sewage sludge disposal on maize has been investigated in several locations. On the 14t quadrate of Kardos, values of the 15t were used as controls for 2018, 2019, and 2021[2] VI values after the year 2017 sewage sludge placing (Figure 7.). For the 6t-7t quadrates of Újkígyós, we compare the years that precede (2017, 2018) and the years that follow (2020) the placement in 2018.

[2] Despite Table 2 data in 14t, 15t quadrates no maize was grown in 2020 as clearly shown in VI data series.

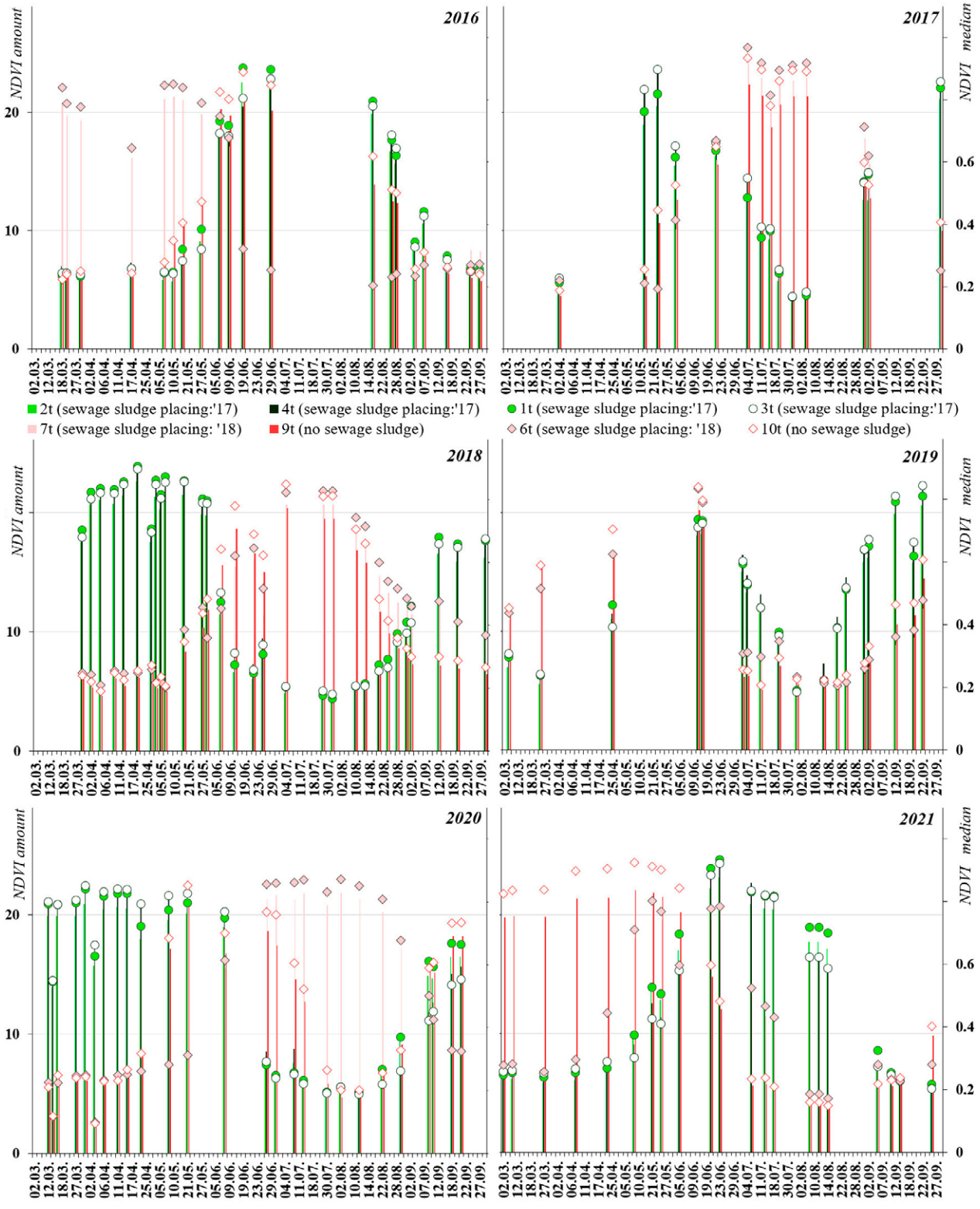

Figure 3. NDVI values of quadrates of Újkígyós study site between 2016 and 2021 (points: NDVI median, columns: NDVI total) (1t-4t: sewage sludge placing in 2017; 6t-7t: sewage sludge placing in 2018; 9t-10t: no sewage sludge)

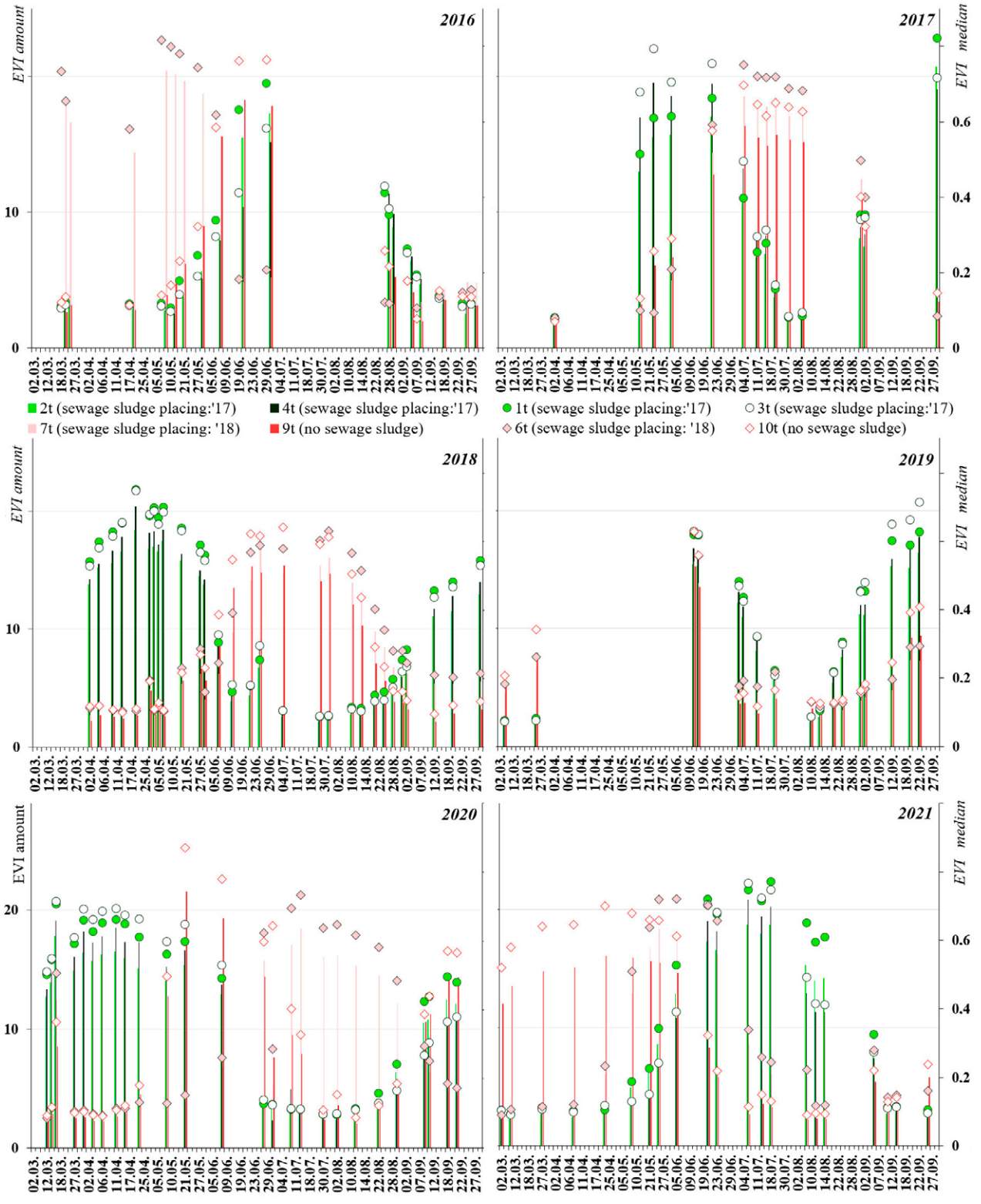

Figure 4. EVI values of quadrates of Újkígyós study site between 2016 and 2021 (points: EVI median, columns: EVI total) (1t-4t: sewage sludge placing in 2017; 6t-7t: sewage sludge placing in 2018; 9t-10t: no sewage sludge)

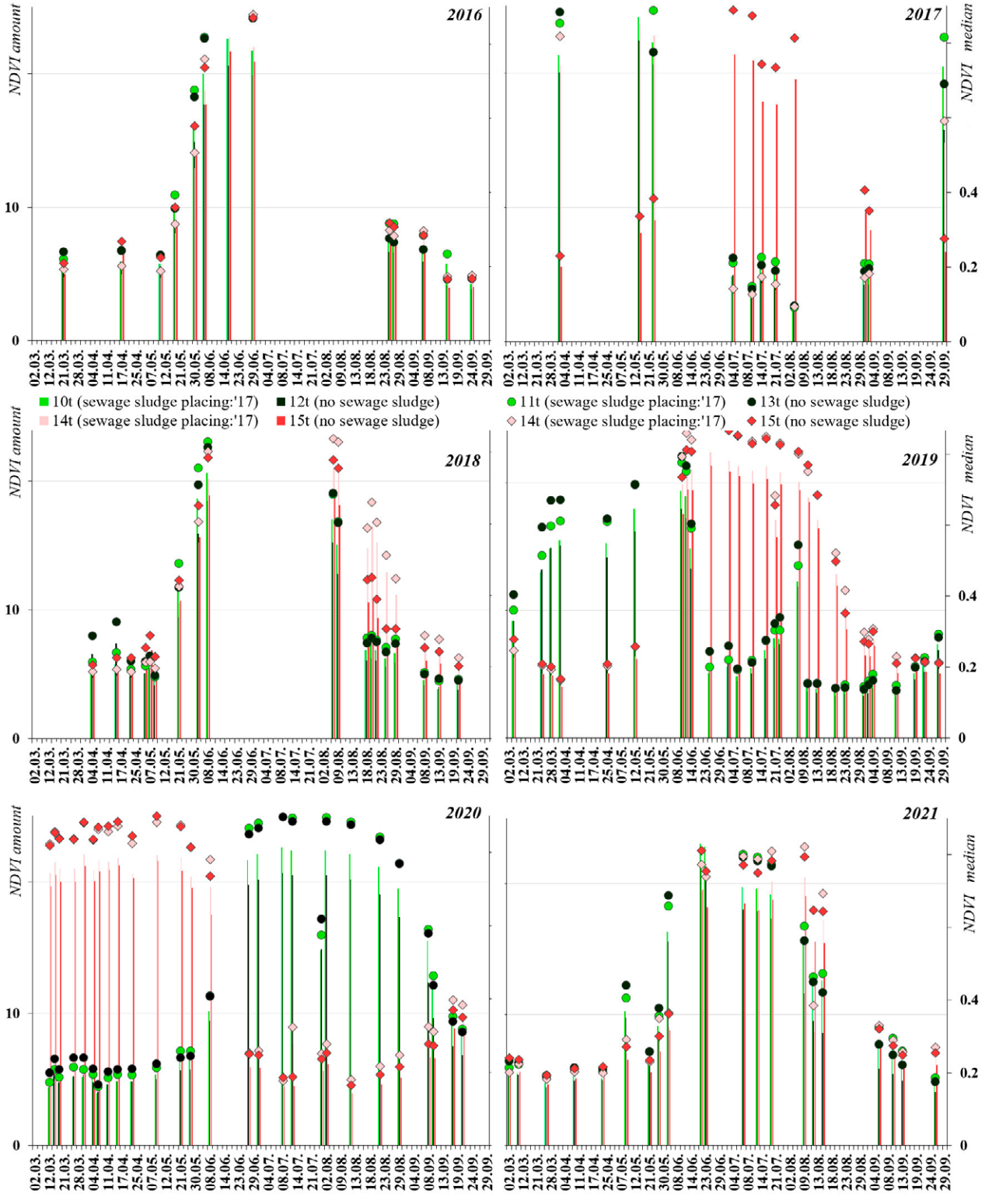

Figure 5. NDVI values of quadrates of Kardos study site between 2016 and 2021 (points: NDVI median, columns: NDVI total) (10t-11t and 14t: sewage sludge placing in 2017; 12t-13t and 15t: no sewage sludge)

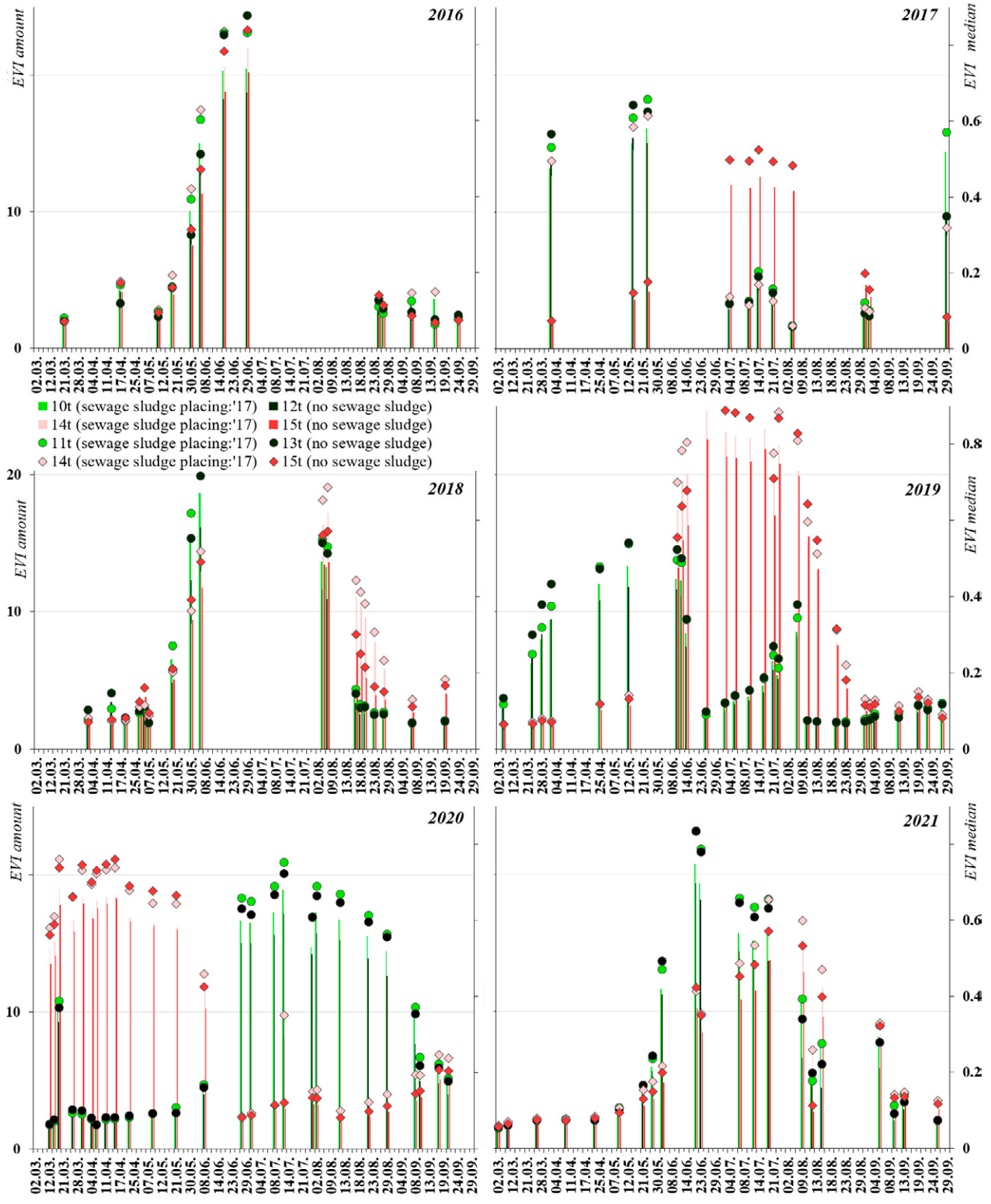

Figure 6. EVI values of quadrates of Kardos study site between 2016 and 2021 (points: EVI median, columns: EVI total) (10t-11t and 14t: sewage sludge placing in 2017; 12t-13t and 15t: no sewage sludge)

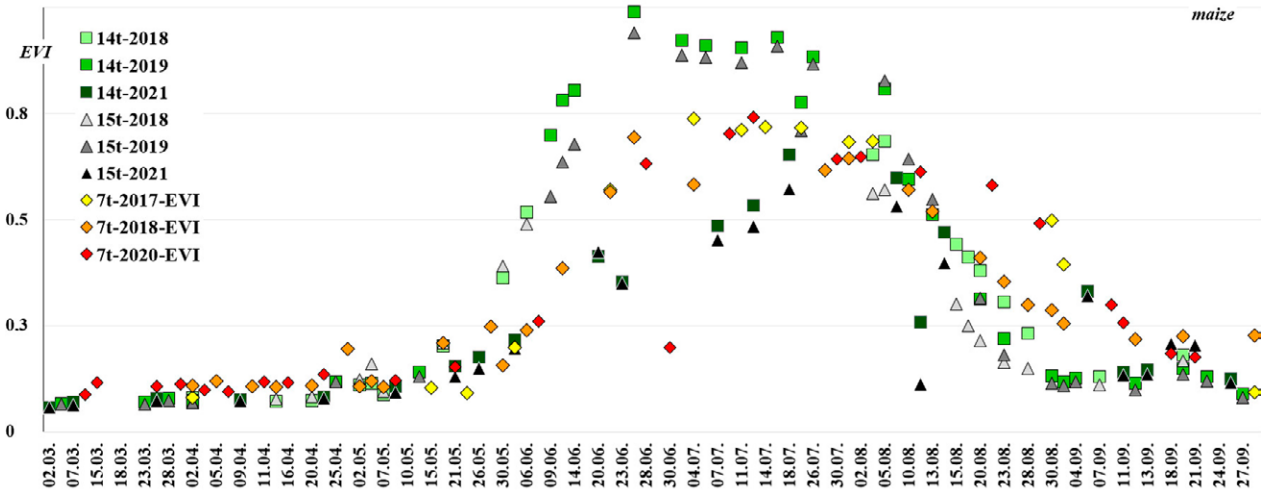

Figure 7. Effect of sewage sludge deposition based on maize Sentinel-2 EVI values on the example of 14t quadrat by comparing 15t, 7t control areas

The spring EVI and NDVI data for 14t 2018 are still in line with 15t quadrat, but before the harvest, the area treated in the previous year shows continuous VI values of at least 0.1 higher throughout August. NDVI value of the treated area is higher, even exceeding the untreated 15t maize production by up to 0.2. In 2019, the difference between 14t-15t can now be tracked throughout the year. The EVI difference in June-July is consistently between 0.05-0.15 in favour of 14t and the two curves only level out towards the end of July. This difference in 2019 is not present at all in the NDVI, the values of the two quadrates are actually the same. The 2019 14t maize EVI values are the highest index values for the whole study period, with average values above 0.8 from the second half of June and above 0.9 in July. This is a striking phenomenon, as the NDVI is otherwise known as a higher index prone to saturation (Huete et al., 2002). In 2021, we basically get different VI's, which is also due to the moderately droughty summer semester and the rainless June (2 mm of precipitation fell at the drought monitoring station). The NDVI curve matches the values observed in previous years, but shows the lowest biomass production in both the growth and maturation phases in the period 2018-2021; between May and August, with biomass production typically 10-40% lower than in previous years. There is no typical NDVI difference between the 14t and 15t areas, but rather the untreated area has the higher index value. EVI shows the difference in a more sensitive way when comparing; the values for June 2021 are only half of those for the same period in previous years, with the difference closing in August, probably also due to the late harvest in 2021. Even the summer peak is almost 30% lower than in 2019. The EVI of the 14t treated area in 2021 is slightly, but typically higher (+10-12%) than the untreated 15t sample area. The EVI values for maize in the 15t control area in 2017 - also droughty - are similarly only 55-60% of the 2019 data.

There is no typical change in the Újkígyós maize fields (6t-7t); the 2017 and 2018 VI values before planting coincide almost perfectly with the 2020 data after planting. Compared to the very high EVI values of 14t, lower values of between 0.56 and 0.73 were also found here. In the case of maize, a comparative evaluation of the EVI values for the 14t quadrat suggests that sewage sludge disposal may have played a role in the evolution of biomass, while such a relationship was not observed in the Újkígyós area.

The impact of placement on winter wheat production at Újkígyós could be assessed on the basis of data of 1t-4t for 2018 and 2020. As a control, the 9t-10t could only be compared indirectly with the VI for 2019 and 2021. Our observations show that the VI values for different years are either the same or possibly even higher in the control areas. As a control for the 2019 crop of 10t-11t of Kardos, we used the previous values of the same quadrates from 2017 and the data of 12t-13t from 2017 and 2019, free of placement. The VI values in the different quadrates are the same in the different years, and despite the treatment, the values in May-June 2017 are higher. It can be concluded that for this crop, the effect of sewage sludge placement is not noticeable.

For the evaluation of sunflower, the VI values for 2018 and 2021 for the 10t-11t in Kardos study area were used, with the control values for the same years being the 12t-13t and the 10t-13t for 2016. The similar small April values compared to 2016 increased very intensively in May 2018 – producing a nearly 3-fold increase in VI during one week – and by the beginning of June the EVI value was 0.08 higher in the area of sludge disposal (Figure 8.), a difference that is also – to a lesser extent – characteristic of the NDVI. The

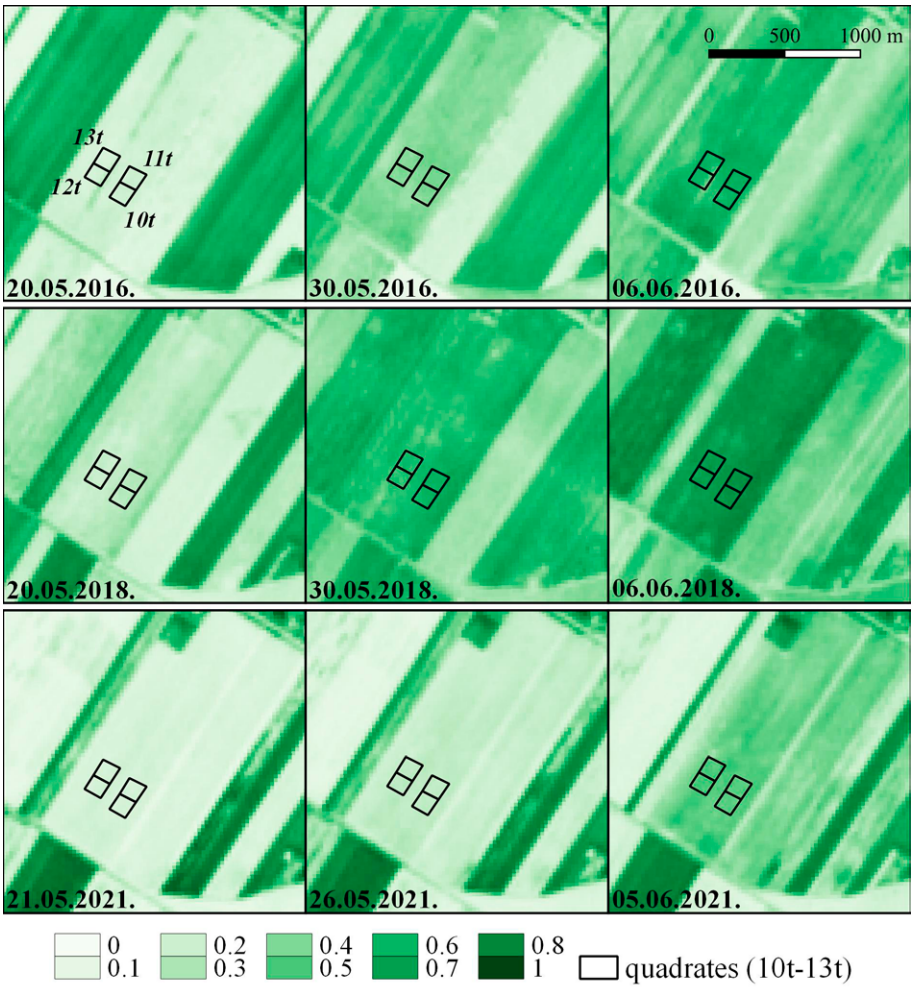

Figure 8. Short-term impact of sewage sludge disposal in 2017 on sunflower yield based on Sentinel-2 EVI data

drought in 2021 seems to have set back yields and we get EVI values similar to 2016 in the first half of the year. NDVI is less sensitive, with no typical difference between years. The VI difference between treated and untreated areas during drought can be seen. In August and September, EVI and NDVI values were 1.2-1.5 times and 1.2-1.3 times higher in the 10t-11t compared to the control area, indicating improved soil water management characteristics.

The more constant NDVI value, which also characterise the quadrat despite the drought, may indicate more favourable soil water management. At Újkígyós we were able to compare 2016 and 2021 data, but only at different quadrates; 9t-10t versus 1t-4t. No difference was observed, but given the drought situation, it could be here also a sign of better water management, so the application of the sludge in 2017 could have played a role, given the climatic parameters.

The effect of treatment on colza production could only be studied in Újkígyós, comparing quadrates of different areas. The control values for the 1t-4t after sewage sludge placing (2019) were taken from the 6t-7t of 2016. In 2019, due to the approximately 1 month later greening and harvesting time, the VI values are of limited comparability. The peak of VI values in 2016 are higher, especially for EVI, and there is no difference in the run of the data, so the sewage sludge has no consequences for colza produce. The differences between August and September already indicate the next year's crop; in 2017 maize while in 2020 it is winter wheat.

The heterogeneity of the different crops is also well patterned spatially by quadrates. The columns in Figure 9. show the recording of nearly the same days of each month of each summer semester, plotted against the rows for each year. As in the diagrams, the spatial homogeneity of the VI generally shows homogeneity within quadrates, but also in such small sample areas, sampling with larger variance occurs; e.g. on 06.06.2018 and 05.06.2021. In particular, the remote sensing survey in June and August revealed the alluvial form which bisects the area from North-East to South, the curvature of which is determined by the soil conditions and the biomass product, causing differences in yields within a single plot. The VI values of the 2t, 3t, and 10t quadrates are influenced by the dif-

ferent physical nature of the soil resulting differences in water management. In the time series, the drought year 2021 is strikingly distinct from similar periods in other years, with perhaps only March 2017 indicating a more drought-like character. Looking at satellite imagery data from early June 2021, there are several years with lower VI categories, e.g. 04.06.2017.

Using PlanetScope imagery in 2020

Our Sentinel-2 EVI and NDVI results were verified using the method of comparison with satellite data with higher geometric and different spectral resolution. When using Planet and Sentinel-2 data taken on the same days in 2020, we typically observe a larger difference between the two sensors in the case of EVI. The standard deviation of the annual data is smaller for Planet, and for all three crops studied (Figure 10). The S-2 VI value is higher (up to +0.1) in the greening and ripening stage, while the Planet index is higher in the pre-harvest and post-harvest stages. According to the S-2 based results, the Planet VI mid-summer peaks are in decreasing order: oil radish, maize, winter wheat. The 21 common dates were compared for all crops in the different quadrates.

The value ranges of determination coefficient suggest a close relationship, especially for NDVI; $0.685 < R^2_{EVI} < 0.867$, and $0.8137 < R^2_{NDVI} < 0.921$. The higher NDVI coefficient is the result of saturation (typical of the index), as the difference between the Planet and S2 NDVI values of the soil or sparsely vegetated surface is often greater than 0.2. In the case of EVI, the relationship is consistent for both dense and sparse vegetation. On a crop-by-crop basis, we found greater similarity between the EVI for maize and the NDVI for winter wheat, while looking the two indices together most balanced was for oil radish. Based on the coefficients of determination, Sentinel-2 data with high temporal resolution and on homogeneous surface coverage of sufficient quality can be used for agricultural monitoring at the parcel level.

Conclusion

To observe the short-term effects of sewage sludge disposal, we planned a six-year, high-resolution monitoring study in continuously cultivated agricultural parcels, often covered with different crops from year to year. In 14 quadrates of 50 m x 50 m, Sentinel-2 satellite imagery-based data collection was applied at the highest temporal and spatial resolution. A database of 140 cloud-free images, supplemented with PlanetScope images was evaluated with vegetation indices (EVI, NDVI) to assess photosynthetic activity and biomass production changes in space and time during the summer semester.

Spectral index-based differences in the vegetation cycle can be used to determine the diversity of plant species produced in the area, and differences in land cover. Similar to the analyses of soil and shorter-term field vegetation monitoring (Ladányi et al., 2020; Kovács & Ladányi, 2021) prior to our studies, we could not detect a generally significant relationship between areas affected and unaffected by sludge placement, through statistical differences measured by EVI and NDVI. Among the four crops studied, the biomass products of sunflower and maize show index differences, which can be evaluated as the effect of sludge application within 1-4 years: more intensive greening, typically higher index values, and vegetation development not affected by drought. In the case of colza and winter wheat, the available data do not show a similar pattern, and in several cases the vegetation index values before the placement are higher. The spatial heterogeneity of the parcels, which is well represented by the quadrates, was not altered by the disposal of sewage sludge during the period studied.

The combination of two different vegetation indices is useful. In addition to the general advantages of the EVI, the accuracy of the assessment of the dense vegetation period, its sensitivity, and applicability in comparative analysis can be highlighted, while the NDVI can be a good complementary data in the dynamics of sparse vegetation, and in the differentiation of vegetation types. Interesting, that the difference between NDVI and EVI is smaller in areas treated with sewage sludge. As expected, in a study requiring a high spatial resolution, the Planet data are generally in close statistical correlation with the Sentinel-based index values and confirm the results of the assessment. Due to their temporal and spatial detail, they can also be presented as separate data, but only from 2017 onwards.

Despite the change in management, the objective of detecting significant differences justifies the continuation of monitoring and the inclusion of data from current years in further analysis, which will also help to narrow down the data gap periods; the extension of Planet data over time and space is already in progress.

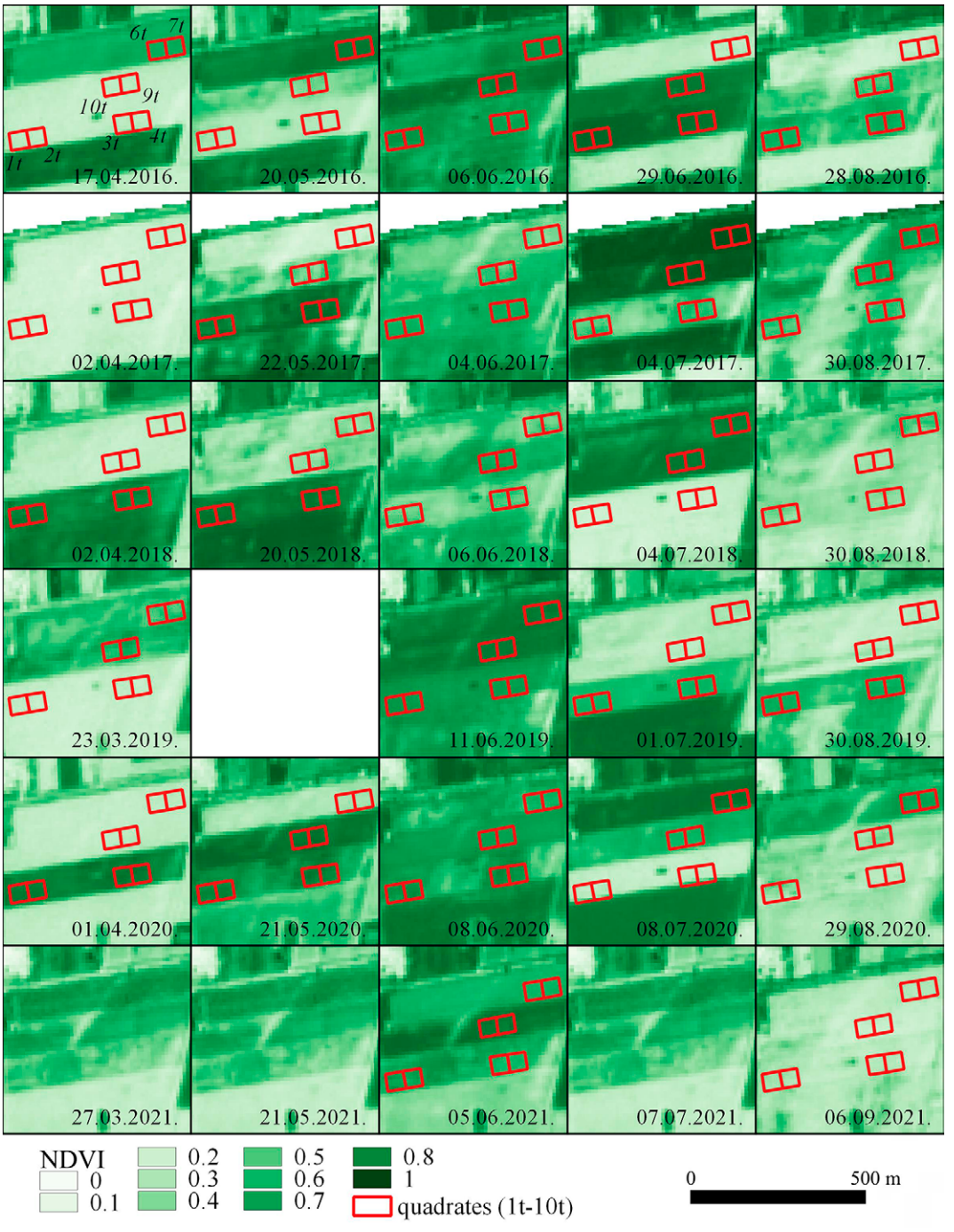

Figure 9. Spatial distribution of agricultural biomass production in the same summer periods of different years based on Sentinel-2 EVI in Újkígyós sample area between 2016–2021 (May 2019: lack of data)

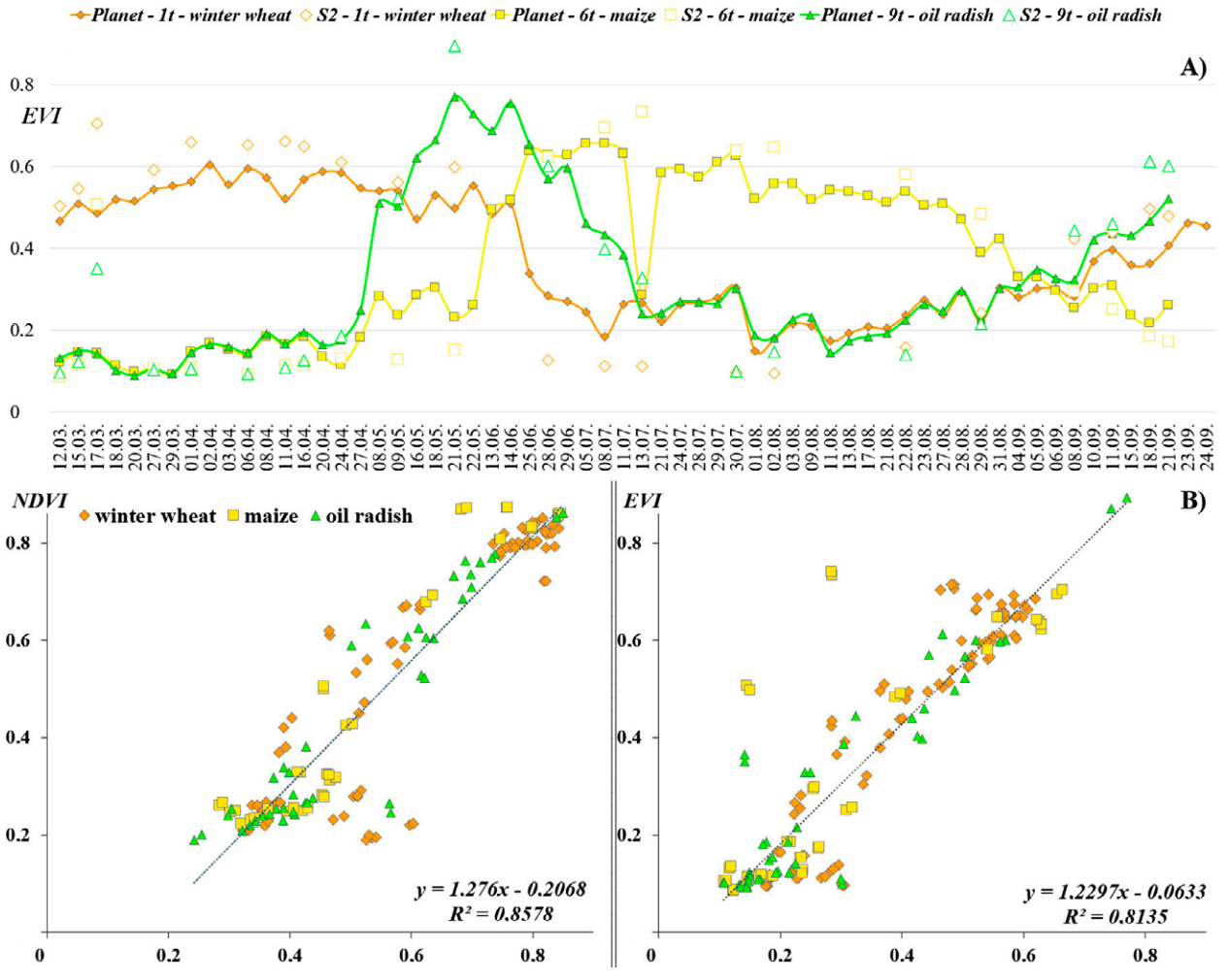

Figure 10. EVI time series of Planet and Sentinel-2 satellites for different crops in summer 2020 (A), and linear regression analysis based on EVI and NDVI for this period (B)

Acknowledgement

The research was funded by the 'RING2017' – EFOP-3.6.2-16-2017-00010 project. The paper is dedicated to Prof. Gábor Mezősi, Professor at the University of Szeged.

References

Álvarez, M.M.S., Brown, L.N., Lim, J.B., Ersahin, K., Borstad, G.A., Dickson, J. & Martell, P. (2014). Assessment of vegetation change after biosolids treatment: use of remotely sensed vegetation time series. *British Columbia Mine Reclamation Symposium*, 1–11. https://doi.org/10.14288/1.0042661

Banerjee, M.R., Burton, D.L. & Depoe, S. (1997). Impact of sewage sludge application on soil biological characteristics. *Agriculture Ecosystems and Environment*, 66(3), 241–249. https://doi.org/10.1016/S0167-8809(97)00129-1

Bannari, A., Morin, D., Bonn, F. & Huete, A.R. (1995). A review of vegetation indices. *Remote Sensing Reviews*, 13, 95–120. https://doi.org/10.1080/02757259509532298

Buzási, A., Pálvölgyi, T. & Esses, D. (2021). Drought-related vulnerability and its policy implications in Hungary. *Mitigation and Adaptation Strategies for Global Change*, 26(11), https://doi.org/10.1007/s11027-021-09943-8

Clevers, J.P.G.W & Gitelson, A.A. (2013). Remote estimation of crop and grass chlorophyll and nitrogen content using red-edge bands on Sentinel-2 and -3. *International Journal of Applied Earth Observation and Geoinformatics*, 23, 344-351. https://doi.org/10.1016/j.jag.2012.10.008

Copernicus Open Access Hub, https://scihub.copernicus.eu/dhus/

DOSoReMI, Hungarian Digital Soil Map Database: https://dosoremi.hu/maps/genetikus-tipus/

Farsang, A., Babcsányi, I., Ladányi, Zs., Perei, K., Bodor, A., Csányi, K. & Barta, K. (2020). Evaluating the effects of sewage sludge compost applications on the microbial activity, the nutrient and heavy metal content of a Chernozem soil in a field survey. *Arabian Journal of Geosciences*, 13, 982. https://doi.org/10.1007/s12517-020-06005-2

Fiala, K., Barta, K., Benyhe, B., Fehérváry, I., Lábdy, J., Sipos, Gy. & Győrffy, L. (2018). Operatív aszály- és vízhiánykezelő monitoring rendszer [Operational drought and water scarcity monitoring system]. *Hidrológiai közlöny*, 98(3), 14–24.

Huete, A., Didan, K., Miura, T., Rodriguez, E.P., Gao, X. & Ferreria, L.G. (2002). Overview of the radiometric and biophysical performance of the MODIS vegetation indices. *Remote Sensing of Environment*, 83, 195–213. https://doi.org/10.1016/S0034-4257(02)00096-2

Kovács, F. & Gulácsi, A. (2019). Spectral index-based monitoring (2000–2017) in lowland forests to evaluate the effects of climate change. *Geosciences*, 9(10), 411. https://doi.org10.3390/geosciences9100411

Kovács, F. & Ladányi, Zs. (2021). Szennyvíziszap kihelyezés rövidtávú következményeinek értékelési lehetősége Sentinel-2 alapú szántóföldi vegetációmonitoring alapján [Evaluate the short-term effects of sewage sludge disposal based on Sentinel-2 vegetation monitoring]. *Agrokémia és Talajtan*, 70(1), 25–43. https://doi.org/10.1556/0088.2021.00073

Kovács, F., Ladányi, Zs., Blanka, V., Szilassi, P., van Leeuwen, B., Tobak, Z., Gulácsi, A., Szalma, E. & Cseuz, L. (2019). Remote sensing data collection and analysis for vegetation monitoring since 2000 at various scales in Southeast Hungary and Vojvodina. In: Ladányi, Zs. & Blanka, V. (eds.) *Monitoring, risks and management of drought and inland excess water in South Hungary and Vojvodina*. Szeged: SZTE TFTG, pp. 212–226.

Kuenzer, C. & Ottinger, M. (2015). Earth observation satellite sensors for biodiversity monitoring: potentials and bottlenecks. *International Journal of Remote Sensing,* 35(18), 6599–6647. https://doi.org/10.1080/01431161.2014.964349

Ladányi, Zs., Csányi, K., Farsang, A., Perei, K., Bodor, A., Kézér, A., Barta, K. & Babcsányi, I. (2020). Impact of low-dose municipal sewage sludge compost treatments on the nutrient and the heavy metal contents in a chernozem topsoil near Újkígyós. Hungary: a 5-year comparison. *Journal of Environmental Geography,*13(1-2), 25–30. https://doi.org/10.2478/jengeo-2020-0003

Lakatos, M., Bihari, Z., Izsák, B., Marton, A. & Szentes O. (2021). Megfigyelt éghajlati változások Magyarországon [Observed climate change in Hungary] *Légkör* 66(3), 5–11.

Liu, W., Huang, J., Wei, C., Wang, X., Mansaray, L.R., Han, J., Zhang, D., Chen, Y. (2018). Mapping water-logging damage on winter wheat at parcel level using high spatial resolution satellite data. *ISPRS Journal of Photogrammetry and Remote Sensing*, 142, 243–256, https://doi.org/10.1016/j.isprsjprs.2018.05.024.

Markowicz, A., Bondarczuk, K., Cycoń, M. & Sułowicz, S. (2021). Land Application of Sewage Sludge: Response of Soil Microbial Communities and Potential Spread of Antibiotic Resistance. *Environmental Pollution*, 271, 116317. https://doi.org/10.1016/j.envpol.2020.116317

McCabe, M.F., Rodell, M., Alsdorf, D.E., Miralles, D.G., Uijlenhoet, R., Wagner, W., Lucieer, A., Houborg, R., Verhoest, N.E.C., Franz, T.E., Shi, J., Gao, H. & Wood, E. F. (2017). The future of Earth observation in hydrology. *Hydrology and Earth System Sciences,* 21, 3879–3914. https://doi.org/10.5194/hess-21-3879-2017

Mezősi, G. (2017). Physical Geography of the Great Hungarian Plain. In: Mezősi, G. *The Physical Geography of Hungary*. Geography of the Physical Environment. Springer, Cham. 195–229. https://doi.org/10.1007/978-3-319-45183-1_7

Mezősi, G., Blanka, V., Ladányi, Zs., Bata, T., Urdea, P., Frank, A. & Meyer, B. (2016). Expected mid- and long-term changes in drought hazard for the South-Eastern Carpathian Basin. *Carpathian Journal of Earth and Environmental Sciences,* 11(2), 355–366.

OGIMET, Climate data: http://www.ogimet.com/gsynres.phtml.en

Operatív Vízhiány Értékelő és Előrejelző Rendszer [Operational drought and water scarcity monitoring system]: http://aszalymonitoring.vizugy.hu/

Plug, B. & Louis, J. (2020). Sentinel-2 L2A surface reflectance product compared with reference measurements on ground. *Quarterly*, 14(1), 11-14. https://doi.org/10.25923/enp8-6w06

Rakonczai, J. & Fehér, Zs. (2015). A klímaváltozás szerepe az Alföld talajvíz-készleteinek időbeli változásaiban [Function in change of climatic in the temporal change on the groundwater supply in the Hungarian Plain]. *Hidrológiai Közlöny*, 95(1), 1–15.

Roy, D.P., Huang, H., Houborg, R. & Martins, V.S. (2021). A global analysis of the temporal availability of PlanetScope high spatial resolution multi-spectral imagery. *Remote Sensing of Environment*, 264, 112586. https://doi.org/10.1016/j.rse.2021.112586

Sagasta, J.M., Sally, L.R. & Thebo, A. (2015). Global wastewater and sludge production, treatment and

use. In: Drechsel, P., Quadir, M. & Wichelns, D. (eds.) *Wastewater, Economic Asset in an Urbanizing World*. Springer Science+Business Media. pp. 15–38. https://doi.org/10.1007/978-94-017-9545-6_2

Segarra, J., Buchaillot, M.L., Araus, J.L. & Kefauver, S.C. (2020). Remote sensing for precision agriculture: Sentinel-2 improved features and applications. *Agronomy*, 10(5), 641. https://doi.org/10.3390/agronomy10050641

Simon, L. & Szente, K. (2000). Szennyvíziszap komposzt hatása a kukorica nitrogéntartalmára, néhány élettani jellemzőjére és hozamára [Effect of sewage sludge compost on nitrogen content, some physiological characteristics and yield of maize]. *Agrokémia és Talajtan*, 49, 231–246.

Szabó, Sz., László, E., Kovács, Z., Püspöki, Z., Kertész, Á., Singh, S. K. & Balázs, B. (2019). NDVI dynamics as reflected in climatic variables: spatial and temporal trends – a case study of Hungary. *GIScience and Remote Sensing*, 56(4), 624–644. https://doi.org/10.1080/15481603.2018.1560686

Szennyvíziszap kezelési és hasznosítási stratégia 2014–2023 [Sewage Sludge Treatment and Utilization Strategy 2014–2023], Országos Vízügyi Főigazgatóság.

Tomócsik, A., Makádi, M., Orosz, V. & Füleki, Gy. (2016). Effect of sewage sludge compost treatment on crop yield. *Agrofor International*, 1(2), 5–12. https://doi.org/10.7251/AGRENG1602005T

Tran, H. T., Campbell, J.B., Tran, T.D. & Tran, H.T. (2017). Monitoring Drought Vulnerability Using Multispectral Indices Observed from Sequential Remote Sensing (Case Study: Tuy Phong, Binh Thuan, Vietnam). *GIScience & Remote Sensing*, 54(2), 167–184.https://doi.org/10.1080/15481603.2017.1287838

Wang, J., Guan, Y., Wu, L., Guan, X., Cai, W., Huang, J., Dong, W., & Zhang, B. (2021). Changing lengths of the four seasons by global warming. *Gephysical Research Letters*, 48(6), e2020GL091753. https://doi.org/10.1029/2020GL091753

Weiss, M., Jacob, F., & Duveiller, G. (2020). Remote Sensing for agricultural applications: A meta-review. *Remote Sensing of Environment*, 236, 111402. https://doi.org/10.1016/j.rse.2019.111402

36/2006. (V. 18.) FVM rendelet a termésnövelő anyagok engedélyezéséről, tárolásáról, forgalmazásáról és felhasználásáról [Decree of the Ministry of Agriculture and Rural Development on the Authorization, Storage, Marketing and Use of Propagating Material and Plants in Hungary].

91/271/EEC, Council Directive concerning urban waste-water treatment.

ISSN 0354-8724 (hard copy) | ISSN 1820-7138 (online)

Assessing the Structure and Composition of Artificial Levees Along the Lower Tisza River (Hungary)

Diaa Sheishah[A,B], György Sipos[A*], Alexandru Hegyi[C], Péter Kozák[D], Enas Abdelsamei[A,B], Csaba Tóth[E], Alexandru Onaca[C], Dávid Gergely Páll[A]

Received: August 02, 2022 | Revised: September 16, 2022 | Accepted: September 17, 2022
doi: 10.5937/gp26-39474

Abstract

Levees are earth structures constructed along alluvial rivers and are considered to be one of the essential components of flood risk and natural hazard reduction. The preservation of their condition would require orderly monitoring. In Hungary, an over 4200 km long levee system was constructed from the 19th century on. Since then, many natural and anthropogenic processes, such as compaction, erosion, subsidence etc., could contribute to the slow but steady deformation of these structures. In the meantime, due to the lack of documentation, their structure and internal composition are still unclear in many sections. The present study uses different geophysical techniques to validate their efficiency in detecting the structure, composition and potential defects along a 3.6 km levee section of the Lower Tisza River, affected significantly by seepage and piping phenomena during floods. Measurements were made using Ground Penetrating Radar (GPR), Electrical Resistivity Tomography (ERT) and drillings. Information obtained by the different techniques was cross-checked and combined. This way, the potential of the applied survey strategy could be demonstrated, and the selected levee section could be assessed in terms of its structure and composition. Consequently, the major reasons for frequently occurring adverse flood phenomena at the site could be revealed. The survey approach outlined in the present paper can be applied extensively along lowland levee systems in the region and elsewhere.

Keywords: levee assessment; flood risk; Electrical Resistivity Tomography (ERT); Ground Penetrating Radar (GPR)

[A] Department of Geoinformatics, Physical and Environmental Geography, University of Szeged, 6722 Szeged, Egyetem u. 2-6., Hungary; geodiaa1311@gmail.com, gysipos@geo.u-szeged.hu, enasmuhammad1@gmail.com, pall.david.gergely@gmail.com
[B] National Research Institute of Astronomy and Geophysics, 11421, El Marsad st., Helwan, Cairo, Egypt; geodiaa1311@gmail.com, enasmuhammad1@gmail.com
[C] Applied Geomorphology and Interdisciplinary Research Centre (CGACI), Department of Geography, West University of Timisoara, 300223 Timisoara, Timis, Romania; alexandruhegyi@gmail.com, alexandru.onaca@e-uvt.ro
[D] Lower Tisza Water Directorate, 6720 Szeged, Stefánia 4., Hungary; kozakp@ativizig.hu
[E] Department of Highway and Railway Engineering, Budapest University of Technology and Economics, 1111 Budapest, Műegyetem rakpart 3., Hungary; toth.csaba@epito.bme.hu
[*] Corresponding author: György Sipos; e-mail: gysipos@geo.u-szeged.hu

Introduction

In a lowland, temperate zone environment floods have the greatest damage potential compared to other natural hazards (Mezősi, 2022). Earthen dams, such as artificial levees constructed along rivers, are essential for flood risk management. They have an important role in protecting human life, agricultural lands, urban areas and other infrastructure from regular inundations.

Flood protection in Hungary relies primarily on artificial levees: their total length is around 4200 km in the country. The Tisza River and its tributaries have a 65% share of this value, making the river system, in this respect, one of the most heavily engineered rivers on Earth (Nagy, 2010). Most of the levees along the Tisza were originally constructed in the 19th century in a relatively short period. The first levees were not high enough, and recurring floods overtopped them regularly. Consequently, their height and size continuously increased over time, usually after significant and destructive flood events. This resulted in the development of complex earth structures with spatially variable compositions (Galli, 1976, Schweitzer, 2001). Moreover, levees were then affected by various post-constructional processes, such as compaction, subsidence or water seepage during floods (Galli, 1976; Kovács, 1979; Sheishah, et al., 2022). Due to the reasons above, there is a lack of information concerning their structure and composition, making flood risk assessment and preparedness difficult (Tímár, 2020).

Although the external change of levees can be detected easily, the investigation of subsurface properties is challenging. Levees are critical and spatially extended infrastructures; thus, using invasive and time-consuming techniques, usually providing only local information, is not a viable option for assessment. Consequently, non-destructive shallow geophysical methods, allowing a fast and continuous assessment of physical parameters, have widely been utilised recently (see, e.g.: Perri, et al., 2014; Rahimi et al., 2018; Dezert et al., 2019; Jodry et al., 2019; Tresoldi et al., 2019; Lee et al., 2020).

Ground Penetrating Radar (GPR) and Electrical Resistivity Tomography (ERT) are the most widespread among these. The two methods offer advantages in different applications, and their combination with geotechnical assessment can provide a robust picture of levee conditions. Accordingly, GPR accompanied by permeability logging was successfully applied in locating seepage zones, e.g. by (Antoine et al., 2015). With a similar approach and by performing ERT surveys (Sentenac et al., 2017) mapped the structural heterogeneity and post-flood damages of historical earthworks. ERT is adequate not only for structural assessments but by long-term monitoring, it can also enable the identification of seepage zones and sections affected by intensive water saturation, as demonstrated by Tresoldi et al. (2019). Using ERT enabled the authors to assess the function between water content and resistivity values, which allowed the transformation of the resistivity profiles into water content maps. Perri et al. (2014) also applied geotechnical investigations to validate geophysical surveys. 2D DC electrical resistivity tomography and seasonal temperature profiles were applied by Jodry et al. (2019) to monitor the seasonal change of soil moisture in an earthen levee to produce seasonal resistivity change models.

Nevertheless, compositional and at-a-point defects can reduce the flood retention capacity of earthen structures. In this sense, contraction cracks and animal burrows can be a major issue and an important factor behind increased flood risk (Chlaib et al., 2014). Not only GPR but resistivity surveys and multichannel analysis of surface waves (MASW) were used by Rahimi et al. (2018) to detect cavities responsible for piping and the formation of sand boils on the protected side of levees. The cause and path of seeping in a damaged embankment were interpreted by Lee et al. (2020) using an integrated method of 3-D resistivity inversion.

Many authors agree that GPR has a limited investigation depth in most levee applications because of the usually high clay content of these earth structures, and they turn to ERT, providing a higher penetration depth and more information on the sedimentary composition of the levee structure (Perri et al., 2014; Busato et al., 2016). However, by using ERT, a serious compromise must be made regarding spatial resolution and measurement time. Besides, the shortage of geotechnical control in many cases, disables the validation of the quality of results (Dezert, et al., 2019, Lee, et al., 2020, Radzicki, et al., 2021).

In the present study, we aimed to combine the strength of two geophysical techniques (GPR and ERT) on a levee section characterised by recurring seepage and piping during floods along the Lower Tisza River. As mentioned above, GPR has a low penetration because of the conductive nature of levee materials; however, due to its high spatial resolution, it can be very useful in detecting small but shallow anomalies and interfaces. In the meantime, ERT has a high potential in detecting compositional differences and anomalies at greater depths, though at limited resolution. We also aimed to validate and improve our interpretation by drillings at the survey site. Finally, we intended to develop a measurement strategy which can be applied for more extensive surveys along the Tisza River.

Study area

The Tisza River is the largest tributary of the Danube: its present length is 962 km, the area of its catchment is 157 000 km², while its mean discharge at Szeged, close to the study site and not far from its confluence with the Danube, is 865 m³/s. Before the great-scale regulation works of the 19th century, the lowland section of the river was characterised by extensive floodplains (38 500 km²) inundated almost every year, thus making agricultural activity difficult (Kovács, 1979). Consequently, the major aim of river training was to increase the velocity of flood waves by making 112 cut-offs to reduce the length of the river and to decrease the extent of inundated areas by building 3555 km of artificial levees along the river and its tributaries (Szlávik, 2003).

Due to increasing flood heights and related flood risk, levees have been heightened several times in the past 150 years, resulting in very complex earthen structures with several layers and reaching relative heights between 5-8 m (Kovács, 1979, 1973; Nagy, 2000). Levees were mostly composed of nearby floodplain sediments. Their core is usually clayey, covered with compacted silty layers. Sandy layers frequently cover the protected side of levees to enable the draining of the levee core during floods (Szűcs et al., 2019).

Several issues may decrease the resistance of levees and hence increase flood risk. Water can pass through the levee body and weaken the structure internally at the interface between layers and in layers with coarser grain sizes (Casagrande, 1937; USACE, 2000). The process can be accelerated by cracks and animal burrows (Nagy, 2000). Seepage can also occur below the levee in higher porosity sediments, resulting in the development of sand boils (Li et al., 1996), which can easily lead to the failure of the structure (Desai, 1970; Ojha et al., 2001). Bearing in mind the above issues and the ageing of levees, it is ultimately important to map and survey their structure, composition and condition to prevent hazardous situations.

The study area is situated on the left bank of River Tisza, near the city of Szeged in the southern part of Hungary. A total of 3.6 km levee section, between 13 and 16.6 levee km (lkm), was chosen to conduct geophysical surveys and drillings (Fig. 1). The relative height of the levee on this section is ~6.5 m. The investigated levee was last reinforced in the 1970s, but not much is known of its internal structure and the composition of its layers. An important reason for selecting this study site was the high number of seepage phenomena recorded during the past few floods by levee watchers (Sheishah et al., 2022), which implies that there can be structural and compositional anomalies in the levee body.

Methods

Data collection

In the present study, two shallow geophysical techniques, Ground Penetrating Radar (GPR) and Electrical Resistivity Tomography (ERT), were compared and combined. At the same time, two boreholes were made to validate and interpret GPR and ERT results (Fig. 1)

GPR surveys were conducted by applying two systems (GSSI SIR 3000 and IDS) with different centre frequencies (200 MHz and 80 MHz) on the levee crown between 13 and 16.5 levee km (Figures. 2A and B). In the case of both systems, measurements were made using the survey wheel mode, and the survey track was dissected into 100 m sections. To enhance comparability, the starting and end points of each 100 m section were the same during both surveys. Data collection was made using a time range of 170 ns (200 MHz) and 300 ns (80 MHz), scanning frequency was 64 scans per second. Scans per unit (meter) were set to 60, and samples per scan were 1024. The applied dielectric permittivity value (12.5) was determined based on the depth of layers identified by drilling.

Electrical Resistivity Tomography profiling was made by using a GeoTom MK8E100 apparatus equipped with a multi-electrode system (50 electrodes) (Fig. 2C). Four profiles were measured: three longitudinal and one transverse (Fig. 2C), and the centre point of each profile was at 13.00 lkm. The Wenner electrode configuration was used for data collection since it is relatively sensitive to vertical changes in subsurface resistivity values below the array's centre. The three longitudinal profiles with the same centre point were measured using 2, 1.5 and 1 m electrode spacing to investigate differences in results as a matter of resolution. The transverse profile, perpendicular to the previous three, was measured using a 1 m electrode spacing. The number of depth levels was set to 16 in each case, and consequently, 384 data points were acquired per profile. Elevation data were collected at each odd number electrode along the survey line by a TopCon Hyper Pro RTK GPS to apply a topographic correction for the transverse profile.

For the validation of GPR and ERT measurements, two boreholes were drilled at 13 lkm on the riverside

edge of the levee crown (BH1) and the protected side slope of the levee (BH2). Drilling depths were 6.5 m and 4 m, respectively. Drilling was done using an Eijkelkamp drilling system with a 5 cm diameter drilling head (Fig. 2D). The coordinates and elevation data of the drilling locations were measured by TopCon Hyper Pro RTK GPS to locate them on ERT profiles correctly. With the help of the drillings, the structure of the levee and the main layers were identified on-site by the macroscopic description of the cores.

Simultaneously, at every 20 cm, samples were collected for grain size analysis, performed with a Fritsch Analysette 22 laser analyser, having a measurement range of 0.08-2000 µm. Samples underwent ultrasonic homogenisation, and all measurements were repeated three times to check if there was further disintegration. The D50 value was applied to identify the grain size category of samples using the Udden-Wentworth scale. Additional samples were collected at every 40 cm to assess the vertical change of gravimetric water content in the profiles. Samples were packed in airtight bags, and after measuring their wet weight in the laboratory, they were dried at 105 °C to obtain dry weights.

The resistivity of sedimentary layers and earthen structures depends primarily on the water content and the grain size (in close relation to porosity) of the deposit. In general, by increasing grain size, resistivity values increase (see, e.g. Oludayo, 2021; Siddiqui & Osman 2012; Cosenza et al., 2006; Sudha et al., 2009; Samouelian et al., 2005), whereas increasing water content has a reverse effect (Loke, 2004; Pozdnyakova & Pozdnyakova, 2002; Abu-Hassanein et al., 1996; Yoon & Park 2001; McCarter, 1984; Michot et al., 2000; Fukue et al., 1999). Goyal, et al. (1996); Gupta and Hanks (1972) proposed an empirical linear relationship between resistivity and water content. Consequently, we also investigated the effect of these parameters on the measured resistivity to see to what extent structural units can be separated. Specific resistivity values used for the analysis were obtained from the ERT profiles at the boreholes and the sampling depths.

Data processing

During the GPR surveys, no data filters were applied; thus, signals contained different types of noises, which had to be eliminated. Raw profiles acquired by the GSSI GPR system were processed by software RADAN 7 (GSSI, 2018). Processing included several steps: time zero correction, Finite Impulse Response

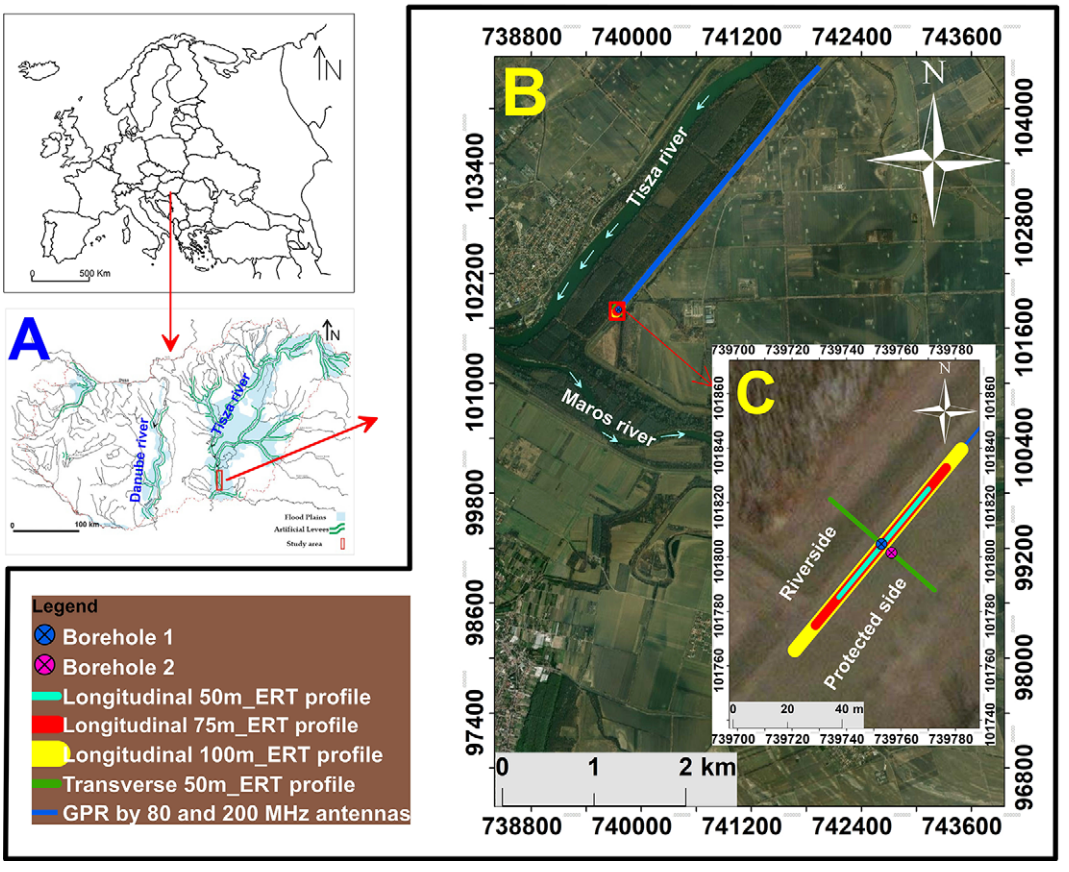

Figure 1. The location of the study area and the survey plan. A) Artificial levees and potential floodplains along the rivers of Hungary (modified after OVF 2014). B) Survey track of GPR profiles and the location of the ERT measurement site. C) Location of ERT profiles and boreholes

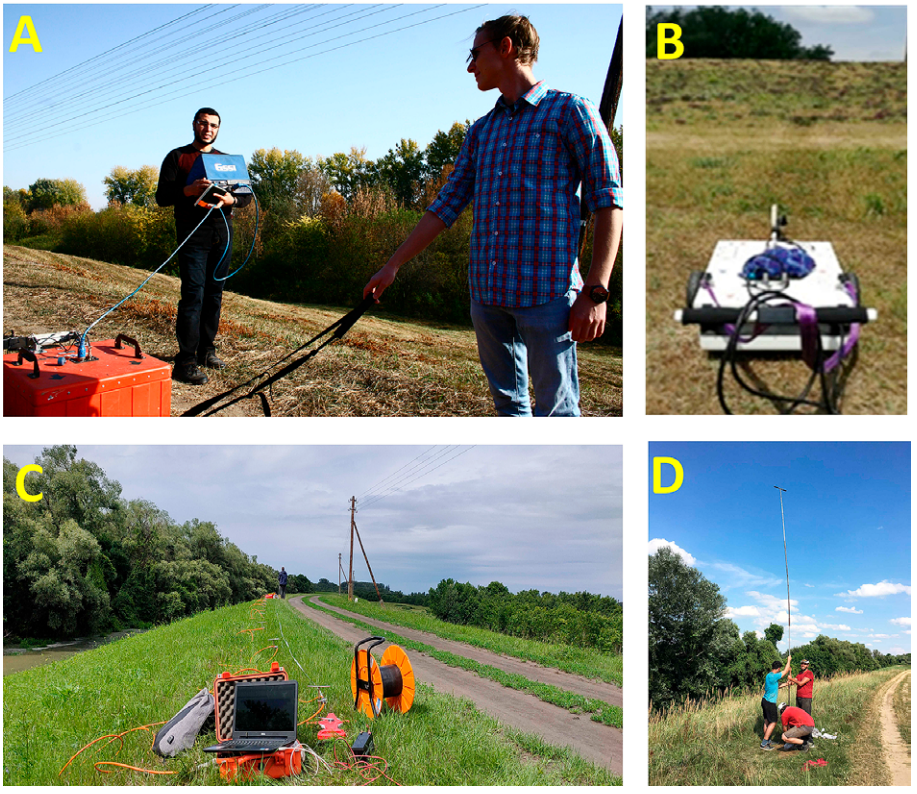

Figure 2. Data acquisition by A) GSSI SIR3000 GPR system with a 200 MHz antenna, B) IDS GPR system with an 80 MHz antenna, C) GEOTOM MK8E100 multi-electrode ERT system and D) drilling using an Eijkelkamp-type drilling equipment

(FIR) filtering, stacking, background removal, gain setting and migration. RADANn 7 was also used to pick positive peaks of the highest amplitudes of traces to enhance the detection of interfaces between different layers having different dielectric permittivity values. In the case of the profiles measured using the IDS system software RELEXW 8 (Sandmeier, 2016) was applied. Processing steps were time zero correction, subtraction of the mean (Dewow), 1D bandpass frequency filtering, running average, background removal and manual gain setting.

Apparent resistivity values obtained during ERT profiling were processed in RES2DINV 3.4 (Loke & Barker, 1996) to get the true resistivity values for the subsurface layers. During the process, erroneous outlying data points were removed before inversion. The inversion scheme was based on the least squares smoothness constrained iterative optimisation algorithm (Constable et al., 1987; De Groot-Hedlin & Constable, 1990). The transverse profile has also undergone a topographic adjustment. Data were then exported, and profiles were drawn and further analysed in Surfer v14.

Results and discussion

GPR measurements

Along the 3.5 km levee section investigated, the penetration depth of the 200 MHz GPR antenna ranged between 3.6 m to 4.4 m, with an average value of 3.9 m. In contrast, in the case of the 80 MHz antenna, the values ranged between 1.8 m and 5.6 m, with 4.0 m on average. Thus, irrespective of centre frequency, no significant difference was experienced between the two systems in average penetration. High variation in penetration depths concerning the 80 MHz antenna refers to considerable measurement uncertainty.

The relatively low penetration depth of GPR in fine grain media is well-known due to enhanced wave relaxation due to polarisation effects (Ishida & Makino, 1999; Santamarina et al., 2001, Bittelli et al., 2008). Polarisation results in larger dielectric permittivities and electrical conductivity values, dissipating GPR energy and causing weaker signal reflections. Besides, clayey soils and sediments are usually associated with high ion concentrations in the liquid phase, facilitating energy dissipation (Saarenketo, 1998, Ishida & Makino, 1999). However, the variation of penetration depth as a matter of variable dielectric properties can also refer to compositional changes in the levee material (Sheishah et al., 2022).

A remarkable change in dielectric values was clear at approximately 25% of the 100 m profiles. The two

antenna types identified dielectric changes approximately at the same locations (Fig. 3). Layers and interfaces within the levee body and smaller anomalies could only be detected using the 200 MHz antenna. The vertical resolution of the 80 MHz antenna was inadequate for these purposes. In general, three units were identified in most of the profiles (Fig. 3A). The thickness of the topmost unit was 1.09 m on average, while the thickness of the middle unit was 1.32 m. The vertical extension of the third unit could not be mapped as it reached below the depth of investigation.

Smaller anomalies within the topmost layer were interpreted as contraction cracks resulting from the desiccation of the levee material. By using the equation $\lambda = v/f$, where (λ) is the wavelength, (v) is transmission velocity, and (f) is the centre frequency of the antenna used for the survey, and the relationship that the size of the detectable target is approximately 10% of the wavelength (Utsi, 2017), we estimated the minimum size of anomalies the two antennae can detect. At a velocity of 8.5 cm/ns for the 200 MHz antenna, this value was 4.3 cm, while for the 80 MHz antennae, it was 10.6 cm. No voids could be identified using the 80 MHz antenna, so the width of the voids detected by the 200 MHz antenna was above 4.3 and below 10,6 cm. The identified cracks were in the topmost layer at a maximum depth of 1 m. Along the survey line, four profiles contained a high density of cracks, meaning that around 10% of the profiles are greatly affected by this defect.

A High-frequency antenna was used successfully by other authors as well to detect small-scale voids and discontinuities (anomaly size 0.1 m or less) in artificial levees (e.g. Di Prinzio et al., 2010, Chlaib et al., 2014). Contraction voids and cracks identified in our study mostly get closed by wetting the levee body during floods, though the largest ones may remain open (Szűcs et al., 2019), which means that their presence can increase the risk of damage. Leakage through cracks can lead to piping, being the main cause of levee failure events (Huang et al., 2014, Cleary et al., 2015). Besides voids, layer deformation and changes in levee composition, marked by sudden shifts in dielectric permittivity, are also very important regarding flood risk. They can contribute to considerable seepage during floods.

ERT measurements

ERT profiles exhibited low and moderate resistivity values. Along the longitudinal profiles, values ranged between 7 and 100 Ωm at 1 m electrode spacing, and the average value of specific resistivity was 22 Ωm. In terms of the transverse profile, values were considerably higher and reached a maximum at 640 Ωm, while the mean specific resistivity was 120 Ωm (Fig. 4).

Similarly to GPR measurements, ERT profiles also refer to the layered structure of the levee body. Since the resolution of ERT data is determined by the applied electrode spacing, i.e. the lower the distance is between electrodes, the thinner layers can be resolved, the topmost layer of the levee body could only be identified using a 1 m electrode spacing (Fig. 4A). In turn, at a larger spacing (1.5 and 2 m) it was possible to get information on the sedimentary base below the levee body (Fig. 4B and C). This way, along the longitudinal profile on the levee crown at a higher vertical resolution (1.0 m), a thin, low resistivity layer could be identified at the top, with resistivity values ranging between 7–20 Ωm. Below, a 1.5–2.0 m thick, slightly higher resistivity (23–32 Ωm) layer was found, then again, a lower resistivity unit (15–30 Ωm) (Fig. 4A). The maximum survey depth at this resolution was 7

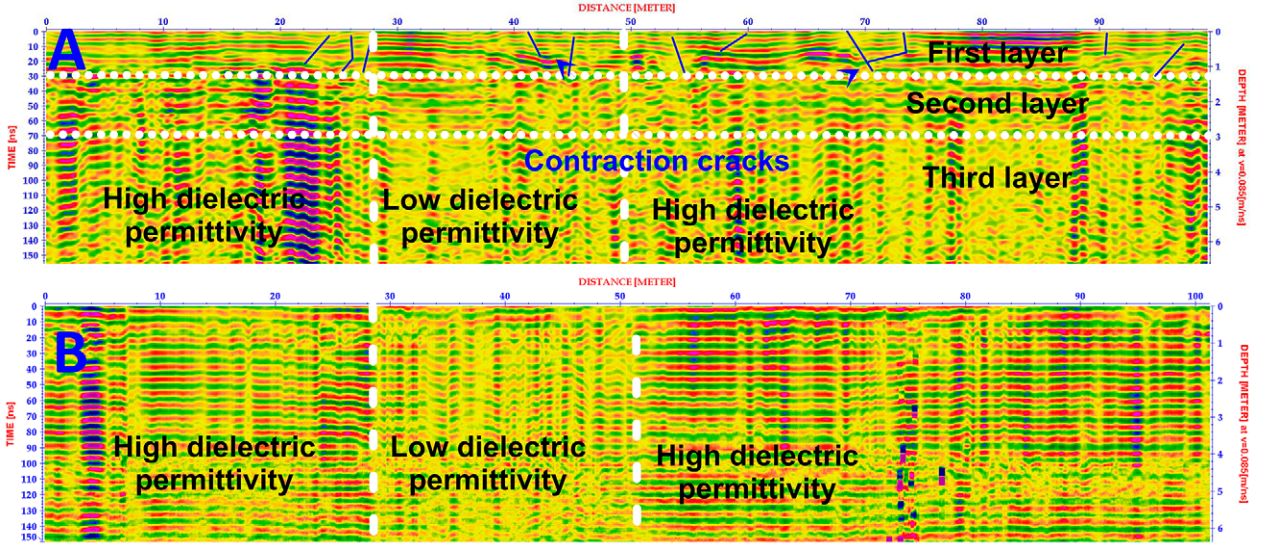

Figure 3. Interpretation and comparison of 100 m GPR profiles made by A) 200 MHz and B) 80 MHz antennae along the same survey line (16.2-16.1 lkm)

m, which is equal to the relative height of the levee. At a 1.5 m electrode spacing, a higher specific resistivity (30–40 Ωm) unit could be identified below the levee body, which was even more pronounced at a 2 m electrode spacing (35-50 Ωm).

Regarding the transversal profile, three ERT units were recognised for the levee crown. Still, the obtained specific resistivity values were different (Fig. 4D). At the top of the levee values were extremely high compared to the previous ones and reached 280–420 Ωm in the topmost, approximately 1 m thick layer. The next unit, with a thickness of 1.5–2.0 m, was characterised by a lower specific resistivity (70–240 Ωm) but was still significantly higher than those measured in the longitudinal profile. From a depth of 3 m, values decreased to 7–30 Ωm, which is like those shown by the longitudinal ERT profiles (Fig. 4). The remarkable difference in terms of the topmost layers can be explained by the presence of shallow, air-filled contraction cracks, also mapped during the GPR surveys (Fig. 4D), and increasing thus greatly the measured specific resistivity values. As the longitudinal measurements

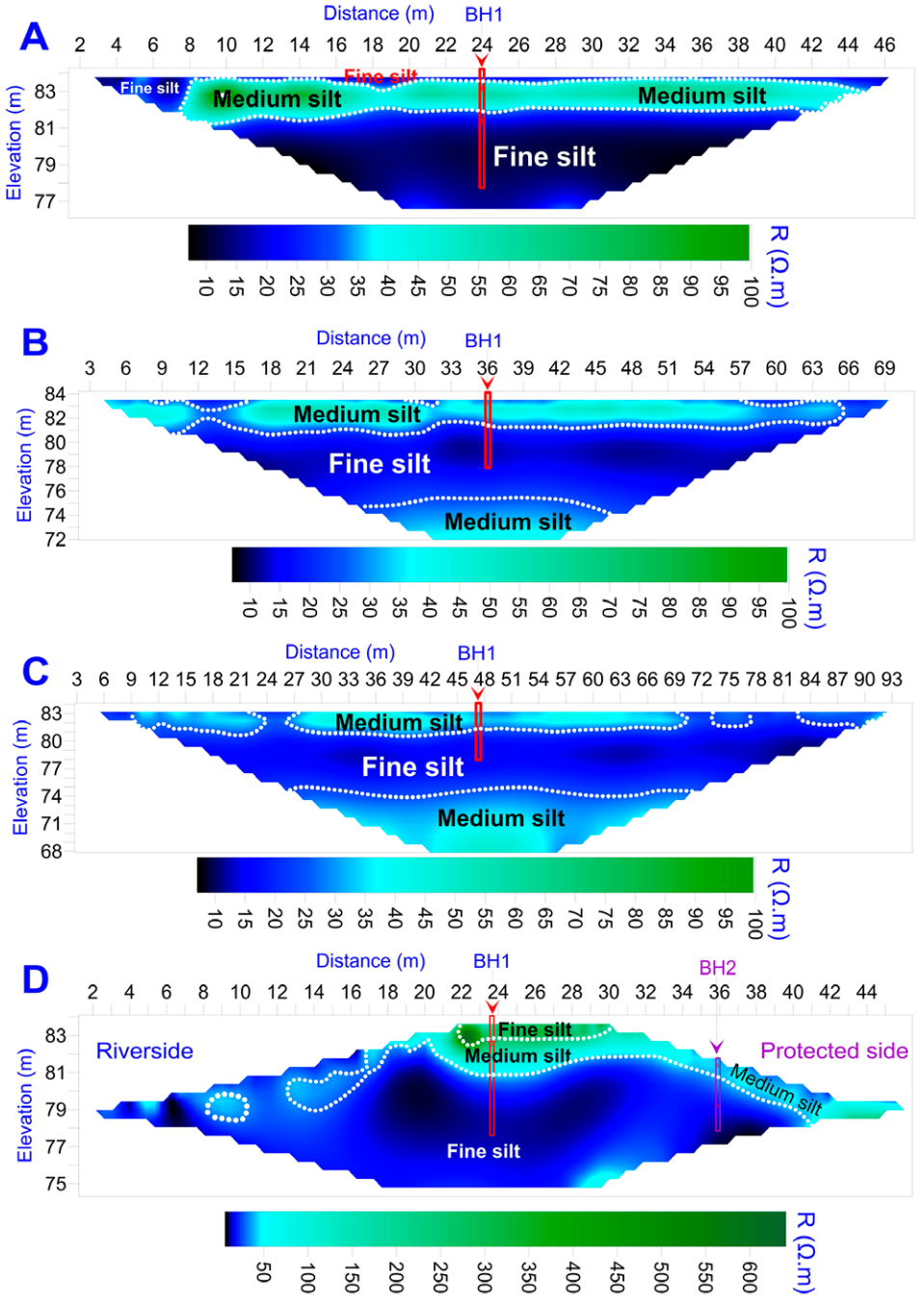

Figure 4. Interpretation of electrical resistivity tomography profiles measured longitudinally using A) 1.0 m, B) 1.5 m, and C) 2 m electrode spacing, and D) transversally using 1 m electrode spacing. The profiles had the same centre point at 13.00 lkm of the Tisza levee

were made on the edge of the levee crown, the effect of air-filled voids was insignificant in their case. Although the electrode spacing of the transverse profile was 1.0 m, it enabled the identification of the higher resistivity unit below the structure and the presence of higher resistivity lenses (30–50 Ωm) close to the riverside slope of the levee.

Sedimentological analysis

The first borehole (BH-1) exposed three units (Fig. 5A); a fine silty layer from the surface until a 1.0 m depth with a D_{50} value between 12 and 15 µm, a medium silty layer at depths between 1.0–2.8 m with a D_{50} value from 15 to 20 µm, and a fine silty layer again, below 2.8 m with a D_{50} value ranging from 10 to 15 µm (Fig. 5A). Especially in the lower unit, the grain-size curve reflects sudden changes at some points, but these are not that significant to move the D50 value into another grain size class. Consequently, we did not separate further sedimentary units at BH-1. The overall mean grain size values for the individual units were 14 µm, 16 µm and 13 µm, meaning that although there is some difference in averages, the levee body is generally composed of fine and medium silt.

The second borehole (BH-2), drilled on the protected slope of the levee, exposed two units (Fig. 5C). The first unit contained a very fine sand layer (0–20 cm) and a fine sand layer (20–40 cm) with mean grain sizes ranging from 93 to 155 µm. The second unit was built up of medium silty layers (40–100 cm; 260–320 cm, 360–400 cm) with a D50 value ranging from 16 to 19 µm and fine silty layers (100–260 cm, 320–360 cm) cm with a D_{50} value ranging from 10 to 15 µm (Fig. 5C). The mean grain size of units was 124 and 15 µm, respectively.

Concerning borehole BH-1 water content of samples exhibited a significant variation with depth (Fig. 5B). A relatively high 25% water content was measured from the topmost samples, which was caused by the rainy weather preceding the measurements and sampling. From 0.8 m, moisture decreased to 21% and remained stable till 1.6 m. A further decrease was experienced below, and an average value of 16% was obtained between 2 m and 4 m. At the bottom of the borehole, from 4.4 m, values reached up again to 25 % (Fig. 5B).

Samples of borehole BH-2, located on the protected side of the levee, exhibited lower water content values in general (Fig. 5D). Here, the topmost layers, mostly composed of fine sand, had low values, being just below 10 %; thus the effect of precipitation was not seen here as a matter of the low retention capacity of sand. In the rest of the profile, water content increased continuously, reaching a stable 20–25 % value from 2.4 m (Fig. 5D).

Factors influencing resistivity

Specific resistivity values, determined at the depths of the sediment samples, were plotted against water content and mean grain size (D_{50}) values, considered to be

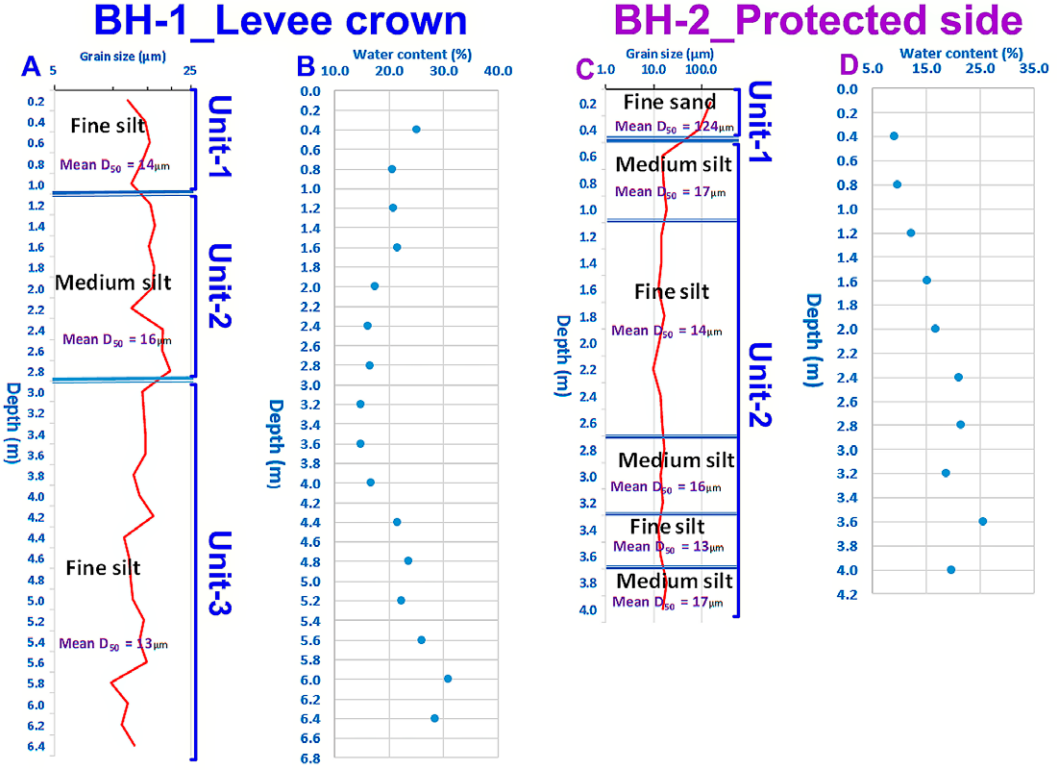

Figure 5. Vertical change of mean grain size (D_{50}) and water content in borehole BH-1 and BH-2

among the key parameters defining resistivity. No relationships could be identified in BH-1 when plotting all water content and D_{50} values. However, it was realised that if sedimentological units are handled separately, then clear trends can be recognised, though with a different slope (Fig. 6) and coefficient of determination. In the case of the upper part of the profile (from 0 to 320 cm), both water content and grain size had a well identifiable influence on the measured resistivity values. As expected, the previous exerted an inverse, while the latter a directly proportional effect on values (Fukue et al., 1999; Lamotte et al., 1994; Oludayo, 2021; Siddiqui & Osman, 2012; Cosenza et al., 2006; Sudha et al., 2009; Samouelian et al., 2005). At the same time, rather insignificant relationships were seen in the lower part of the profile, meaning resistivity stayed the same regardless of changes in water content and grain size (Fig. 6A). It must be emphasised that in this section, grain size values varied within a very narrow range (11–15 µm). The different behaviour of the two units might be explained by the degree of compaction during construction which also affects the porosity of the material. As the core of levees is compacted usually at a much higher degree (Inim et al., 2018; Zhu et al., 2007; Melo et al., 2021; Seladji et al., 2010), this necessarily leads to lower resistivity values, which are only slightly modified by the variation of water content.

In the case of borehole BH-2, relationships were analysed only for the lower, silty part of the profile, as the uppermost fine sand layer was represented only by one sample. In this borehole, no relationship could be identified between resistivity and grain size (Fig. 6B), possibly because fine and medium silty materials alternated frequently and grain size variation within layers was insignificant (Fig. 5C). On the other hand, water content showed a considerable increase downwards. Therefore, a strong relationship (R^2=0.907) was found with specific resistivity (Fig. 6A). This also means that thin layers with a slight change in grain size could not be separated using resistivity measurements at the present resolution.

Nevertheless, as water content showed much greater variability, and still, the effect of grain size could be recognised, we are convinced that it is possible to detect general compositional changes along the levee system of the Tisza River. As water content showed a considerable variation in both profiles (from 10 to 30

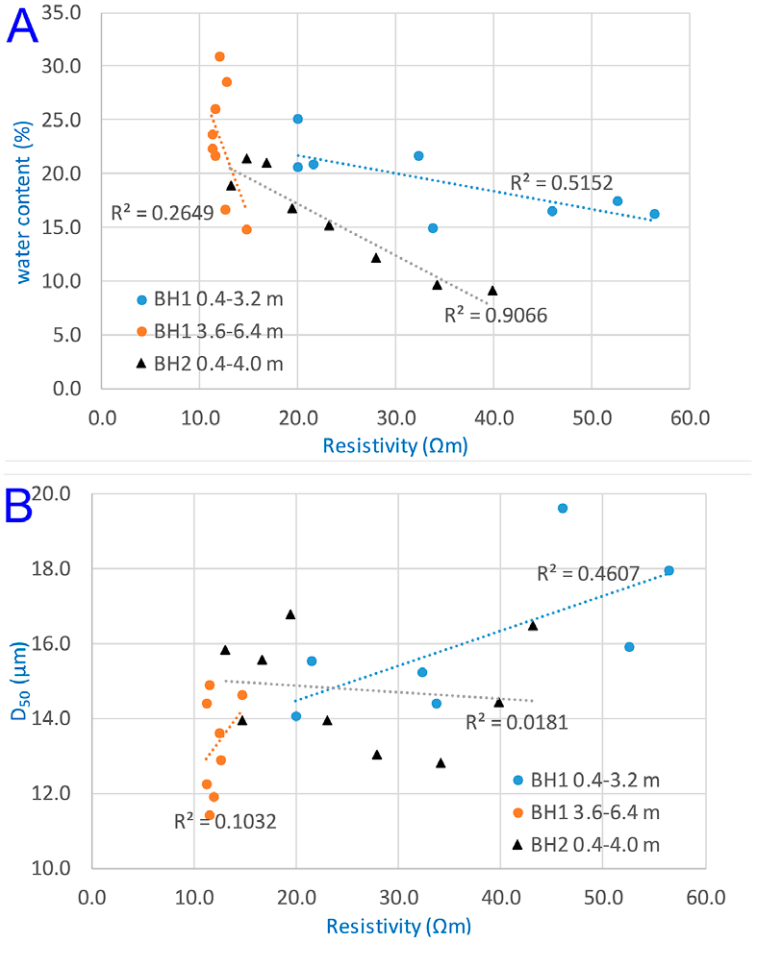

Figure 6. Relationship between A) specific resistivity and water content and B) specific resistivity and grain size in different structural units of the levee body

%), i.e. both dry and close to saturation materials were sampled, it is possible to give a range of resistivity values being representative of the primarily silty (10–20 μm) material of the levee at usual moisture conditions. In general, the experienced 10–60 Ωm specific resistivity corresponds well to the empirical values given for alluvial materials by Keller and Frischknecht, (1966) and Loke, (2004). However, it is lower than the values reported by Busato et al., (2016), who identified 50–100 Ωm for an earthen levee composed mainly of clayey sand and having low moisture content. Similarly, Himi et al., (2018) found that clayey layers in a dam structure had a specific resistivity below 100 Ωm. Different water contents can be responsible for the dissimilarities in these later cases.

Assessment of the structure and composition of the investigated levee section from the aspect of flood risk

Flood hazard on the protected side of the levee is greatly determined by the structure and composition of the earthwork itself. For the reliable evaluation of the investigated levee section, structure and composition were assessed by combining the results of the different methods applied since each technique has its advantages and disadvantages concerning penetration depth, resolution or acquisition time.

Based on the control data provided by the drillings, it was obvious that the interfaces between the main units can be detected clearly by both GPR and ERT (Fig. 7). However, the upper interface at a depth of ~1 m could only be partially identified by longitudinal ERT profiles even using a 1 m electrode spacing (Fig. 4A). On the other hand, this cover layer can be clearly seen on the transversal ERT profile (Fig. 4D). In the meantime, the second interface at ~3 m appears almost at the same place on both ERT and GPR profiles (Fig. 7C). The fact that there was no sharp variation in water content at this depth suggests that even small changes in composition (shift from medium to fine silt) can be detected using the combination of techniques.

Concerning the structure of the levee at the study site, each method has confirmed that there are three major units within the levee body: 1) a fine silt, clayey levee core, 2) a medium silt layer, made for increasing the height of the structure, and 3) a fine silt blanket on the top to inhibit seepage (Fig. 3, 4 and 5). Additional-

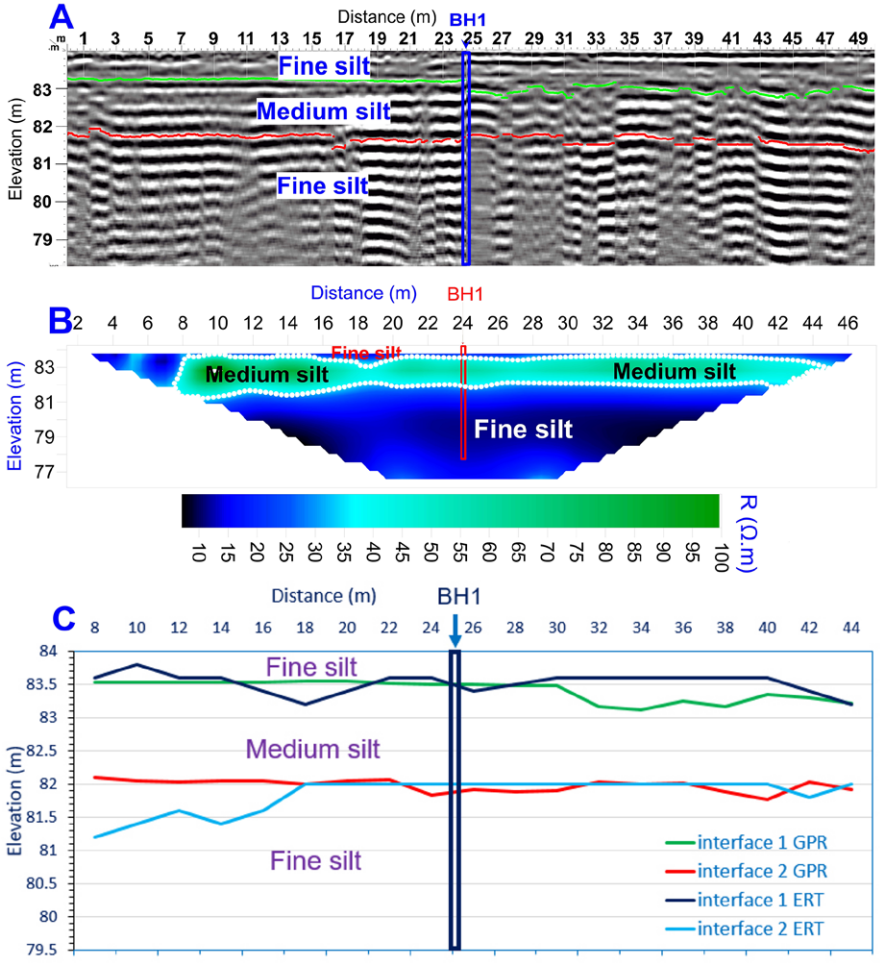

Figure 7. Combination of A) GPR and B) ERT results in the same profile to determine C) the depth of interfaces

ly, on the protected side, a thin (0.4 m) sand sheet was identified, but this could only be detected using borehole data. ERT could not resolve the sand cover because even at a 1 m electrode spacing, the vertical resolution remained around 0.5 m.

From the aspect of flood safety, the structure of the levee at the investigated profile is advantageous in the sense that the number of layers is limited, i.e. the structure is not as complex as reported elsewhere (Zorkóczy, 1987; Schweitzer, 2001; Szlávik, 2003), and therefore, the occurrence of contour seepage, appearing along structural interfaces, is less probable (Szűcs, et al., 2019). A clayey wedge, an important structural element in mitigating sub-levee seepage at the riverside foot of the levee (USCE, 2000, Szűcs et al., 2019), can also be recognised on the ERT profile (Fig. 4D). On the other hand, a discontinuity appears in the fine silt blanket at the riverside edge of the levee crown. Still, the interpretation is difficult because of the high gradient of resistivity change between the top of the levee and the levee body (Fig. 7). The only exception is a short, 600 m long unit, where a third interface at ~3.5 m can be observed, which first appears separately, but then replaces the previous one (Fig. 8). This unit requires further investigation to map the cause of differences, and assess their effect on flood safety.

The levee section under investigation is primarily composed of fine and medium silt. Except for a thin layer of sand, and clayey blocks in the core of the structure, there is no significant change in the composition of major structural units. In this sense, the structure is rather homogeneous and mostly built up of moderately aquitard silty materials, which can be one of the reasons for the frequently detected seepage during floods. However, it is important to underline that geotechnical parameters, such as porosity, density and filtration velocity, were not assessed in detail. Meanwhile, cracks identified by the GPR survey in the upper part of the levee can also significantly decrease the flood resistance of the structure.

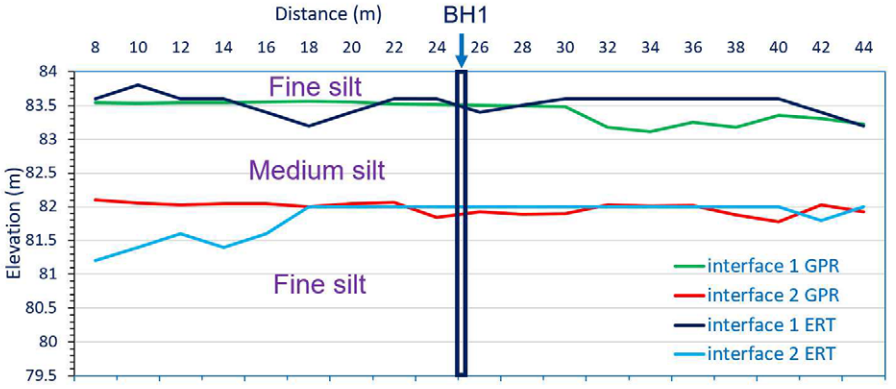

Figure 8. The longitudinal change of structural interfaces along the investigated levee section based on 200 MHz GPR data

levee and the levee body (Fig. 4D). This feature can be one reason for the observed piping during higher flood events.

On most of the levee investigated by GPR, the structure of the top layers does not change significantly, i.e. two interfaces at depths of ~1 m and ~2 m can be identified (Fig. 8). This also means that the structure recognised in the levee body at the ERT profiles can be extended to these sections as far as the GPR data refer to a very similar structure in the top 4 m of the levee body.

Though it is not closely related to the levee body itself, but based on the obtained ERT profiles made with a 1,5 and 2 m electrode spacing, a less aquitard unit, composed most probably of medium silt, is located beneath the structure, which can result in the development of sub-levee seepage during floods. Sub-levee seepage is a hazardous flood phenomenon, as it can lead to the development of sand boils on the levee's protected side, thus increasing flood risk (Nagy, 2000; Ojha et al., 2001; Tímár, 2020).

Conclusions

GPR, ERT and drilling results with different spatial resolutions and penetration depths were compared and combined to assess the structure and composition of a levee section exhibiting various unwanted flood phenomena.

From a methodological aspect, we found that at the usual dimensions and composition of the levees along the Lower Tisza River, GPR can be applied to investigate the upper 3-4 m of these structures. The use of low frequency 80 MHz GPR does not increase pen-

etration depth significantly. In contrast, higher frequency 200 MHz GPR is capable of detecting not only structural interfaces but various defects as well in the upper layers. Concerning ERT, at 1 m electrode spacing, it is possible to capture structural changes. Still, penetration depth covers only the levee body, and no information can be obtained from sub-levee conditions. This requires an increase in spacing. Although water content has a primary role in determining the obtained specific resistivity values, based on the present study, it is still possible to detect structural units composed of slightly different materials.

Considering the above, the optimum measurement strategy for the future is first to perform longitudinal surveys using GPR, by which major changes in levee structure can be detected, and sections for more time-consuming ERT measurements can be easily identified. By determining the specific resistivity range of fine and medium silt among various moisture conditions at the study site, it is possible later to separate aquitard (clay) and non-aquitard (sand) materials without drilling the levees of the Lower Tisza River.

The increased frequency of seepage and piping at the investigated site can mainly be explained by the primarily silty composition of the levee body. The number of structural units is low, which is advantageous in terms of contour seepage; however, the fine silt/clayey cover on the riverside slope of the structure might not be continuous; therefore, the identified medium silt layer in the upper half of the levee body can also contribute to increased seeping and piping during floods, to which contraction cracks in the topmost layer of the structure can also contribute. In the meantime, sub-levee conditions, i.e. a coarser sedimentary unit, are also precursors of seepage phenomena.

Acknowledgements

We acknowledge Sándor Kovács for his contribution to GPR data acquisition and Szabolcs Gáti for his assistance during ERT measurements. We also thank Dávid Filyó and Gergő Magyar for their immense help during drilling.

References

Abu-Hassanein, Z. S., Benson, C. H., & Blotz, L. R. (1996). Electrical resistivity of compacted clays. *Journal of geotechnical engineering*, 122(5), 397-406.

Antoine, R., Fauchard, C., Fargier, Y., & Durand, E. (2015). Detection of leakage areas in an earth embankment from GPR measurements and permeability logging. *International Journal of Geophysics*, 2015.

Bittelli, M., Salvatorelli, F., & Pisa, P. R. (2008). Correction of TDR-based soil water content measurements in conductive soils. Geoderma, 143(1-2), 133-142.

Busato, L., Boaga, J., Peruzzo, L., Himi, M., Cola, S., Bersan, S., & Cassiani, G. (2016). Combined geophysical surveys for the characterization of a reconstructed river embankment. *Engineering Geology*, 211, 74-84. https://doi.org/10.1016/j.enggeo.2016.06.023

Casagrande, A. (1937). *Seepage Through Dams*. Journal of the New England Water Works Association, republished in Contributions to Soil Mechanics 1925-1940, Boston Society of Civil Engineers, Boston, MA, pp. 295-336.

Chlaib, H. K., Mahdi, H., Al-Shukri, H., Su, M. M., Catakli, A., & Abd, N. (2014). Using ground penetrating radar in levee assessment to detect small scale animal burrows. *Journal of Applied Geophysics*, 103, 121-131.

Cleary, P. W., Prakash, M., Mead, S., Lemiale, V., Robinson, G. K., Ye, F., Ouyang, S., & Tang, X. (2015). A scenario-based risk framework for determining consequences of different failure modes of earth dams. *Natural Hazards*, 75(2), 1489-1530. https://doi.org/10.1007/ s11069-014-1379-x.

Constable, S. C., Parker, R. L., & Constable, C. G. (1987). Occam's inversion: A practical algorithm for generating smooth models from electromagnetic sounding data. *Geophysics*, 52(3), 289-300.

Cosenza, P., Marmet, E., Rejiba, F., Cui, Y. J., Tabbagh, A., & Charlery, Y. (2006). Correlations between geotechnical and electrical data: A case study at Garchy in France. *Journal of Applied Geophysics*, 60(3-4), 165-178.

deGroot-Hedlin, C., & Constable, S. (1990). Occam's inversion to generate smooth, two-dimensional models from magnetotelluric data. *Geophysics*, 55(12), 1613-1624. https:// doi.org/10.1190/1.1442813.

Di Prinzio, M., Bittelli, M., Castellarin, A., & Pisa, P. R. (2010). Application of GPR to the monitoring of river embankments. *Journal of Applied Geophysics*, 71(2-3), 53-61.

Desai, C.S. (1970). Seepage in Mississippi River Banks, Analysis of Transient Seepage Using a Viscous-

Flow Model and Numerical Methods, Miscellanous Paper S-70-3, Report 1. USACE Waterways Experiment Station, Vicksburg, MS.

Dezert, T., Fargier, Y., Lopes, S. P., & Cote, P. (2019). Geophysical and geotechnical methods for fluvial levee investigation: A review. *Engineering Geology*, 260, 105206.

Fukue, M., Minato, T., Horibe, H., & Taya, N. (1999). The micro-structures of clay given by resistivity measurements. *Engineering geology*, 54(1-2), 43-53.

Galli, L. (1976). Az árvízvédelmi földművek állékonyságának vizsgálata. Budapest: Országos Vízügyi Hivatal, available at: https://library.hungaricana.hu/hu/view/VizugyiKonyvek_078/?pg=57&layout=s (in Hungarian)

Goyal, V. C., Gupta, P. K., Seth, S. M., & Singh, V. N. (1996). Estimation of temporal changes in soil moisture using resistivity method. *Hydrological processes*, 10(9), 1147-1154.

GSSI (2018) RADAN 7 software, accessible at: https://www.geophysical.com/software.

Gupta, S. C., & Hanks, R. J. (1972). Influence of water content on electrical conductivity of the soil. *Soil Science Society of America Journal*, 36(6), 855-857.

Himi, M., Casado, I., Sendros, A., Lovera, R., Rivero, L., & Casas, A. (2018). Assessing preferential seepage and monitoring mortar injection through an earthen dam settled over a gypsiferous substrate using combined geophysical methods. *Engineering geology*, 246, 212-221. https://doi.org/10.1016/j.enggeo.2018.10.002.

Huang, W. C., Weng, M. C., & Chen, R. K. (2014). Levee failure mechanisms during the extreme rainfall event: a case study in Southern Taiwan. *Natural Hazards*, 70(2), 1287-1307. https://doi.org/10.1007/s11069-013-0874-9.

Inim, I. J., Tijani, M. N., & Affiah, U. E. (2018). Experimental assessment of electrical properties of lateritic soils as an alternative non-destructive method for compaction monitoring. *International Journal of Geotechnical Engineering*, 12(3), 252-257. DOI: 10.1080/19386362. 2016.1270792.

Ishida, T., & Makino, T. (1999). Effects of pH on dielectric relaxation of montmorillonite, allophane, and imogolite suspensions. Journal of Colloid and Interface Science, 212(1), 152-161.

Jodry, C., Lopes, S. P., Fargier, Y., Sanchez, M., & Côte, P. (2019). 2D-ERT monitoring of soil moisture seasonal behaviour in a river levee: A case study. *Journal of Applied Geophysics*, 167, 140-151.

Keller, G. V., & Frischknecht, F. C. (1966). *Electrical methods in geophysical prospecting.* Oxford: Pergamon Press Inc. pp. 517.

Kovács, D. (1979). Árvízvédelem, folyó-és tószabályozás, víziutak Magyarországon [Flood control, regulation of rivers and lakes and waterways in Hungary]. National Water Management Authority (OVH), Budapest.

Lamotte, M., Bruand, A., Dabas, M., Donfack, P., Gabalda, G., Hesse, A., Humbel, F-X. & Robain, H. (1994). Distribution d'un horizon à forte cohésion au sein d'une couverture de sol aride du Nord-Cameroun: apport d'une prospection électrique [Distribution of hardpan in soil cover of arid zones. Data from a geoelectrical survey in northern Cameroon]. *Comptes Rendus de l'Academie des Sciences Serie II,* 318, 961-968. Available from: https://www.researchgate.net/publication/222649758_Electrical_resistivity_survey_in_soil_science_A_review [accessed Jul 18 2022].

Lee, B., Oh, S., & Yi, M. J. (2020). Mapping of leakage paths in damaged embankment using modified resistivity array method. *Engineering Geology*, 266, 105469. https://doi.org/10.1016/j.enggeo.2019.105469

Li, Y., Craven, J., Schweig, E. S., & Obermeier, S. F. (1996). Sand boils induced by the 1993 Mississippi River flood: Could they one day be misinterpreted as earthquake-induced liquefaction?. *Geology*, 24(2), 171-174.

Loke, M.H. (2004). Tutorial: 2-D and 3-D Electrical Imaging Surveys, 2004 Revised Edition. Tutorial: 2-D and 3-D Electrical Imaging Surveys, (July), 136.

Loke, M. H., & Barker, R. D. (1996). Rapid least – squares inversion of apparent resistivity pseudosections by a quasi – Newton method1. *Geophysical prospecting*, 44(1), 131-152.

McCarter, W. J. (1984). The electrical resistivity characteristics of compacted clays. *Geotechnique*, 34(2), 263-267.

de Melo, L. B. B., Silva, B. M., Peixoto, D. S., Chiarini, T. P. A., de Oliveira, G. C., & Curi, N. (2021). Effect of compaction on the relationship between electrical resistivity and soil water content in Oxisol. *Soil and Tillage Research*, 208, 104876. https://doi.org/10.1016/j.still.2020.104876

Mezősi G. (2022). *Natural hazards and the mitigation of their impacts*. Switzerland: Springer International Publishing AG, pp. 260.

Michot, D., Dorigny, A., & Benderitter, Y. (2001). Mise en evidence par resistivité electrique des ecoulements préférentiels et de l'assèchement par le mais d'un calcisol de Beauce irrigué. *Comptes Rendus de l'Académie des Sciences-Series IIA-Earth and Planetary Science*, 332(1), 29-36. Available from: https://www.researchgate.net/publication/222649758_Electrical_resistivity_survey_in_soil_science_A_review [accessed Jul 18 2022].

Nagy, L. (2000). Geotechnical problems of dikes (Az árvízvédelmi gátak geotechnikai problémái). *Vízügyi Közlemények*, 82(1), 121–146. (in Hungarian)

Nagy, L. (2010). Az árvízvédelmi gátak hossza. Nemzetközi összehasonlítás. *Hidrológiai Közlöny*, 90(5), 65-67, (in Hungarian).

Ojha, C. S. P., Singh, V. P., & Adrian, D. D. (2001). Influence of porosity on piping models of levee failure. *Journal of geotechnical and geoenvironmental engineering*, 127(12), 1071-1074.

Oludayo, I. (2021). Effect of Grain Size Distribution on Field Resistivity Values of Unconsolidated Sediments. 7(1), 12–18.

OVF (2014). Árvízi kockázati térképezés és stratégiai kockázatkezelési terv készítése (Flood risk mapping and strategic risk management plan), project report of the National Water Directorate Hungary, accessible at: http://www.vizugy.hu/vizstrategia/documents/B91A47EC-E3B8-4D58-A15F-3E522958BEE8/Orszagos_elontes_1e_web.pdf

Perri, M. T., Boaga, J., Bersan, S., Cassiani, G., Cola, S., Deiana, R., Simonini, P., & Patti, S. (2014). River embankment characterization: the joint use of geophysical and geotechnical techniques. *Journal of Applied Geophysics*, 110, 5-22.

Pozdnyakova, A., & Pozdnyakova, L. (2002). Electrical fields and soil properties. Proceedings of 17th World Congress of Soil Science, Thailand, vol. 14-21, pp. 1558, August 2002.

Radzicki, K., Gołębiowski, T., Ćwiklik, M., & Stoliński, M. (2021). A new levee control system based on geotechnical and geophysical surveys including active thermal sensing: A case study from Poland. *Engineering Geology*, 293, 106316. https://doi.org/10.1016/j.enggeo.2021.106316

Rahimi, S., Wood, C. M., Coker, F., Moody, T., Bernhardt-Barry, M., & Kouchaki, B. M. (2018). The combined use of MASW and resistivity surveys for levee assessment: A case study of the Melvin Price Reach of the Wood River Levee. *Engineering Geology*, 241, 11-24.

Saarenketo, T. (1998). Electrical properties of water in clay and silty soils. *Journal of applied geophysics*, 40(1-3), 73-88.

Samouëlian, A., Cousin, I., Tabbagh, A., Bruand, A., & Richard, G. (2005). Electrical resistivity survey in soil science: a review. *Soil and Tillage research*, 83(2), 173-193.

Sandmeier geophysical software (2016). REFLEXW guide. Introduction to the processing of GPR-data within REFLEXW, 23p.

Sandmeier geophysical Software, 2016. Reflex 8.

Santamarina, J.C., Klein, K.A., & Fam, M.A. (2001). Soils and Waves: Particulate Materials Behavior, Characterisation and Process Monitoring. New York: John Wiley and Sons,

Schweitzer, F. (2001). A magyarországi folyószabályozások geomorfológiai vonatkozásai = Geomorphological aspects of Hungarian river regulation works. *Földrajzi értesitö*, 50(1-4), 63-72. (in Hungarian)

Seladji, S., Cosenza, P., Tabbagh, A., Ranger, J., & Richard, G. (2010). The effect of compaction on soil electrical resistivity: a laboratory investigation. *European journal of soil science*, 61(6), 1043-1055. https://doi.org/10.1111/j.1365-2389.2010.01309.x.

Sentenac, P., Benes, V., Budinsky, V., Keenan, H., & Baron, R. (2017). Post flooding damage assessment of earth dams and historical reservoirs using non-invasive geophysical techniques. *Journal of Applied Geophysics*, 146, 138-148.

Siddiqui, F. I., & Osman, S. B. A. S. (2012). Integrating geo-electrical and geotechnical data for soil characterization. *International Journal of Applied Physics and Mathematics*, 2(2), 104-106.

Sheishah, D., Kiss, T., Borza, T., Fiala, K., Kozák, P., Abdelsamei, E., Tóth, C., Grenerczy, G., Gergely Páll, D., & Sipos, G. (2022). Mapping subsurface defects and surface deformation along the artificial levee of the Lower Tisza River, Hungary. *Journal of Applied Geophysics* (under review)

Sudha, K., Israil, M., Mittal, S., & Rai, J. (2009). Soil characterization using electrical resistivity tomography and geotechnical investigations. *Journal of Applied Geophysics*, 67(1), 74-79.

Szlávik L. (2003). Az elmúlt másfél évszázad jelentősebb Tisza-völgyi árvizei és az árvízvédelem szakaszos fejlesztése. = Significant floods of the Tisza in the last one and a half century and the gradual improvement of flood protection. *Vízügyi Közlememények*, 4, 31-43. (in Hungarian)

Szűcs, P., Nagy, L., Ficsor, J., Kovács, S., Szlávik, L., Tóth, F., Keve, G., Lovas, A., Padányi, J., Balatonyi, L., Baross, K., Sziebert, J., Ficzere, A., Göncz, B., & Dobó, K. (2019). Árvízvédelmi ismeretek = Flood Protection, available at: http://hdl.handle.net/20.500.12944/13490 (in Hungarian)

Tímár, A. (2020). Árvízvédelmi töltések potenciális veszélyforrásai a Körösök vidékén= Potential Sources of Danger of Flood Protection Dams in the Körös River Area. *HADMÉRNÖK*, 15(1), 107-119.

Tresoldi, G., Arosio, D., Hojat, A., Longoni, L., Papini, M., & Zanzi, L. (2019). Long-term hydrogeophysical monitoring of the internal conditions of river levees. *Engineering Geology*, 259, 105139.

USACE – U.S. Army Corps of Engineers (2000). EM 1110-2-1913, Engineering and Design - Design and Construction of Levees. Department of the Army, USACE, Washington, DC.

Utsi, E.C. (2017). Ground Penetrating Radar Theory and Practice. In-Ground Penetrating Radar Theory and Applications. Butterworth-Heinemann publication, Elsevier, 209 p.

Yoon, G. L., & Park, J. B. (2001). Sensitivity of leachate and fine contents on electrical resistivity variations of sandy soils. *Journal of hazardous materials*, 84(2-3), 147-161.

Jiao-Jun, Z. H. U., Hong-Zhang, K. A. N. G., & Gonda, Y. (2007). Application of Wenner configuration to estimate soil water content in pine plantations on sandy land. *Pedosphere*, 17(6), 801-812. https://doi.org/10.1016/S1002-0160(07)60096-4.

Zorkóczy, Z. (1987). Árvízvédelem = Flood protection. Budapest: Országos Vízügyi Hivatal (in Hungarian).

ISSN 0354-8724 (hard copy) | ISSN 1820-7138 (online)

Evaluation of Off-site Effects of Wind-eroded Sediments Especially the Content of Pesticides

Katalin Csányi[A], Andrea Farsang[A*]

Received: May 27, 2022 | Revised: September 26, 2022 | Accepted: September 26, 2022
doi: 10.5937/gp26-38144

Abstract

Wind-eroded sediment, as an environmental transport pathway of toxic elements and pesticids, can result in environmental- and human exposure far beyond the agricultural areas where it has been applied. In our research we quantified the pesticide residues moving in the soil near Szeged (Hungary) on the original soil surface of agricultural areas with a portable wind tunnel. Before the experiments, a portion of the sample area was treated with chlorpyrifos and pendimethalin. A control area was also selected. In 2017-2019, a total of 42 wind event experiments were conducted by examining the topsoil samples. During the experiments, moving soil particles were trapped at various heights (5-10 cm, 20-25 cm and 50-55 cm) and the pesticide concentrates by GC-MS were measured. The enrichment ratios (ER) were calculated, and statistical analyzes were also carried out (SPSS). The measurements obtained that the pendimethalin ER is much higher in the rolled fraction (mean: 13.7) than chlorpyrifos (mean: 2.9). Our measurements showed that the enrichment of chlorpyrifos and pendimethalin can be detected in the rolling and suspended soil particles.

Keywords: wind erosion; chlorpyrifos; pendimethalin; wind tunnel experiment

Introduction

Due to the frequency of extreme weather events (extreme rainfall, drought) associated with climate change, furthermore intensive soil use, inadequate agricultural cultivation and agrotechniques, there has been an increase in soil deflation sensitivity. Wind erosion now poses a risk not only to sandy soils, but also to degraded, dusty, fertile, chernozem soils. Cultivation can significantly accelerate wind erosion (Stefanovits & Várallyay 1992; Farsang et al. 2011; 2013; Farsang & Barta 2004; Liu et al. 2007).

At medium wind speeds, significant dust emissions have been observed in different countries of Europe (Szatmári, 1997; Gossens, 2002; Bärring et al., 2003). According to a report by the United Nations Environment Program in 1991 (UNEP), more than 46% of the total degradation of arid areas is caused by wind erosion (Zheng, 2009). According to Eurostat (Internet 4, 2018), approximately 11.4% of the EU area is affected by medium to severe soil erosion (more than 5 tonnes per hectare per year). The total annual soil loss in the EU is estimated at 950 Mt (Internet 4, 2018). Korcz et al. (2009) found that 52% of the European Union's PM10 emissions come from agriculture.

The proportion of areas affected by wind erosion is also significant in Hungary. Much of the country is covered with sand and loam soils, which are heavily exposed to deflation. More than 60% of the lowland areas are utilized as arable land, which further increases the vulnerability (Farsang, 2016; Pásztor, 2018). The annual wind speed is 2-4 m/s in the country. The highest monthly wind speed averages are during early spring (March, April) when most of the croplands are uncovered. Maximum wind speeds above 10 m/s are also often measured in April (In-

[A] University of Szeged, Department of Geoinformatics, Physical- and Environmentalgeography, Hungary, Szeged, 6722 Egyetem u. 2-6; farsang@geo.u-szeged.hu
[*] Corresponding author: Andrea Farsang; e-mail: farsang@geo.u-szeged.hu

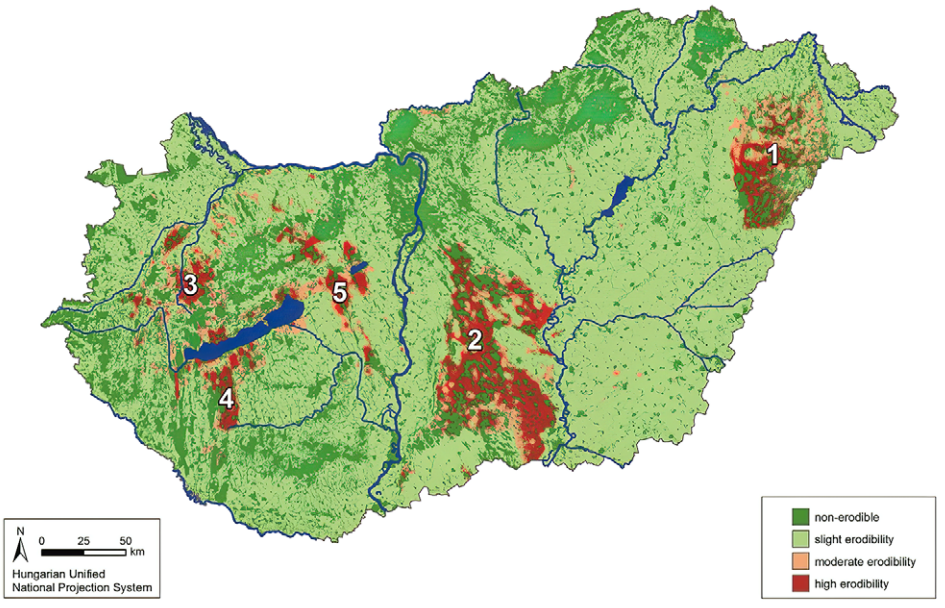

Figure 1. Wind erosion susceptibility map of the Hungarian soils. The five distinct areas: Nyírség (1), Danube–Tisza Interfluve (2), glacis in the foreground of the Transdanubian Mountains (3), Inner Somogy (4), Transdanubian loess region (5) (Pásztor et al. 2016)

ternet 2, 2016; Pásztor, 2018). According to the results of Pásztor et al. (2016), the total area affected by wind erosion in Hungary is about 10,000 km2, which is about 10% of the country's area. In their research, besides the physical diversity of soils, in addition to the wind speed of a given area, the surface cover was also used for classification (Pásztor et al., 2016; Pásztor, 2018) (Fig. 1). Bartus et al. (2019) investigated the risk of wind erosion in Csongrád County during their research. It was determined that 37.5% of the area of Csongrád County (our research area) is exposed to wind erosion every year.

The physical degradation of nutrient-rich topsoil is not the only problem. Agricultural soils account for a significant source of airborne particulate matter (PM10, PM2,5) because of wind erosion and tillage activities (Gill et al., 2006). Contaminants (heavy metals and other potentially toxic substances, for example, pesticide residues) can adhere to the surface of soil particles. So deflation can become a significant human health problem, especially for the inhabitants of settlements where arable land under intensive cultivation is dominant. The airborne particles released by the wind have a huge impact on human and animal health. Due to their size, they can easily reach the bronchial tube by inhalation, causing severe human diseases (asthma, heart and lung diseases, and also cancer) (Besancenot et al., 1997; Toy et al., 2002; Järup, 2003; Riksen, 2004; Bach, 2008; Sterk & Goossens, 2007; ; Kim et al., 2015; Internet 1). The finest particles (dust) can travel over large distances. Small particles can travel from 500 km to thousands of kilometres during moderate wind storms (Pye, 1987). The largest amounts of pesticides and heavy metals are usually adsorbed to the fine particles (Agassi et al., 1995; O'Hara et al., 2000). These contents can also be normally enriched in the fine (suspended) particles (Clymo et al., 2005). As a result, more and more studies are now being conducted on the off-site effects of wind erosion (Larney et al., 1999; Farsang et al., 2013; Bento et al., 2016; Csányi et al., 2019a, b).

Based on the results of previous canal research in this area (Szeged), it can be concluded that hummus enrichment in wind-driven sediment 1.1 (Farsang et al., 2013; Farsang et al., 2022). The humus displacement that can be registered during an erosive wide event is 5.5–6.9 g m^{-2}, the P displacement is 0.1–0.8 g m^{-2}, and the K displacement is 1.6–13.9 g m^{-2}. These values show an order of magnitude Sterk et al. (1996) with field-on-site measurement results.

Deflation processes can be well modelled with in-situ wind tunnels (Maurer et al., 2006; Farsang et al., 2022). This research study aims to evaluate the potential risks of agricultural dust using a portable wind tunnel. This study investigates the occurrence of chlorpyrifos and pendimethalin in wind-eroded sediment accrued from loess and sandy soil produced during wind erosion in wind tunnel experiments.

Materials and methods

Sample area

The study areas are located near Szeged. It's composed of Chernozem and Arenosol soils (Fig. 2). The in-situ wind tunnel studies were conducted in the summer of 2017-2019 (Fig. 3). The sample area was 20m×40m and 40×50m in 2017 and 2018 respectively. In 2019 we took ex-situ measurements, so we collected loam and sandy topsoil samples near Szeged.

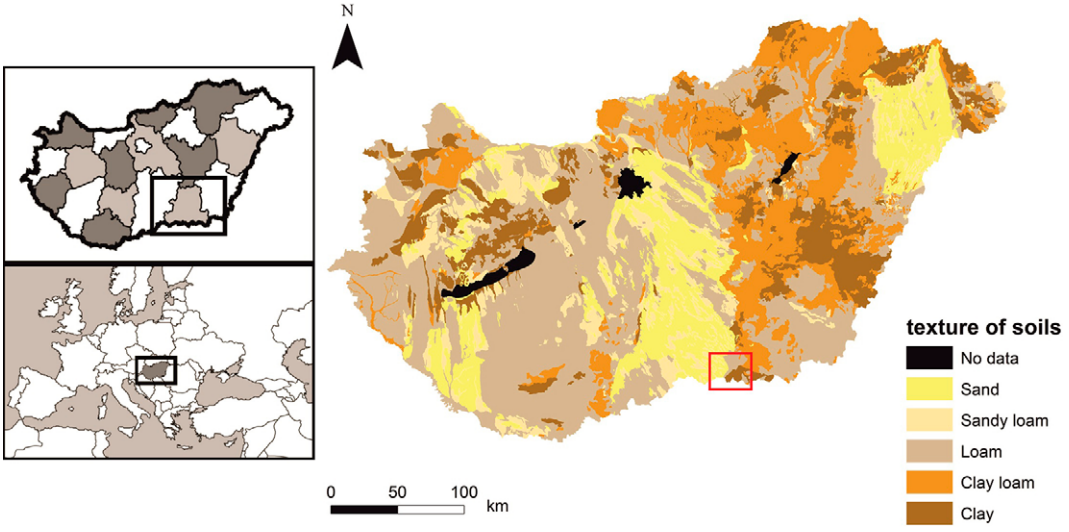

Figure 2. Location of the studied area and soil properties

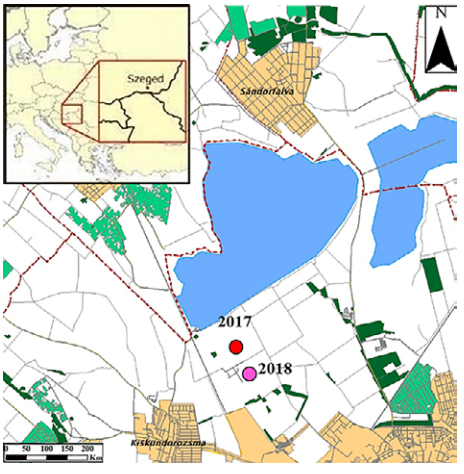

Figure 3. Sample points

Sampling and measurements

Measurement methods in 2017-2018

Two of the most commonly used pesticides in Hungary have been selected for the experiments (Internet 3., 2016). Before the experiment, a part of the sample area was treated with chlorpyrifos (2 l/ha) and pendimethalin (5 l/ha) (application rate is typically applied in agricultural fields). A control area was also selected. In the summer of 2017-2018, a total of 28 in-situ wind event tests were conducted. The undisturbed surface soil was measured in a portable and adjustable 12 m long field wind tunnel (Fig. 4) in-situ on the study plot. Each wind tunnel experiment was carried out with a duration of 10 minutes and approximately 13 ms-1 wind speed.

Wind velocity has been measured along horizontal and vertical profile lines during all experiments (Fig. 5) using a Lambrecht Jürgens 642 anemometer. The ground area blown within the wind tunnel covers 3.36 m². Samples were taken from the topsoil (0-5 cm) before and after the wind event at three different places in the wind tunnel. The rolling soil samples (sediments) were collected after each run at the end of the wind tunnel using a clean brush (Fig. 5).

Figure 4. The portable wind tunnel

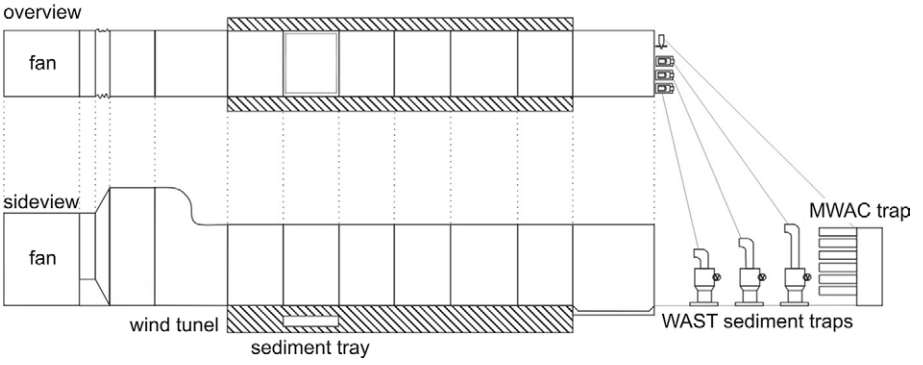

Figure 5. The location of the soil sample points, the WAST traps and the sediment traps at the end of the tunnel (Farsang et al. 2022)

Measurement methods in 2019

In the summer of 2019 14 ex-situ wind tunnel experiments were conducted (10 experiments on loam texture soil and 4 on sandy texture soil). We put on the ground a plastic sheet and an approximately 5 cm thin layer of the soil was spread on it. The soil was then sprayed with the prepared solution: pendimethalin solution was prepared by diluting Sharpen 330 EC herbicide that contains 330 g/l pendimethalin in water, chlorpyrifos solution was prepared by diluting Alligator™ insecticide that contains 480 g/l chlorpyrifos in water. The prepared soil was measured in a wind tunnel. Each deflation experiment were carried out with a duration of 10 minutes and approximately 12 ms-1 wind speed on the loam soil and 6 ms-1 on the sandy soil.

Samples were taken from the topsoil (0-5 cm) before and after the wind event at three different places in the wind tunnel. After each run, the rolling soil samples (sediments) were collected at the end of the wind tunnel using a clean brush and the suspended particles were collected by WAST (Wet Active Sediment Trap). This is a patented, horizontal, active, isokinetic, wet trap. Trap inlets are 5 10 cm, 20 25 cm, 50 55 cm high (Fig. 6). Distilled water was used for trapping. WAST samples were stored refrigerated in a borosilicate sample holder until laboratory measurement.

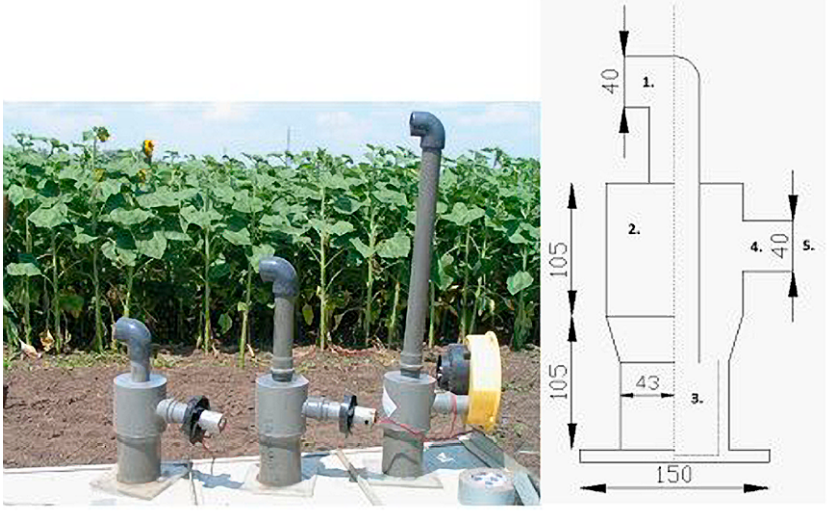

Figure 6. WAST trap and its components: 1. Inlet, 2. Trap, 3. Sampling jar, 4. Outlet, 5. Turbine extraction (values in mm) (Farsang et al. 2022)

Sample analysis

All laboratory analyses were carried out according to Hungarian standard procedures. After the appropriate preparation, the following parameters were determined: topsoil samples: (pH (H_2O)), $CaCO_3$ (%), Arany yarn test, OM %, total salt content (%), humidity (%); rolling soil samples and suspended fraction: chlorpyrifos, pendimethalin concentrations. Pesticide contents are determined by GC-MS-MS (EPA 8270D:2007 Rev.:4).

After that, the enrichment ratios (ER) of concentrations in the rolling samples were calculated (1). If the values of the enrichment factors are around 1 or less, the test component will not be enriched in the erosion-displaced sediment.

$$ER = \text{Element concentration}_{sediment}/\text{Element concentraion}_{soil} \quad (1)$$

Statistics

The statistical tests were carried out by SPSS software (IBM SPSS Statistics, Version 24). The Kolmogorov-Smirnov test was used to test the normality of all data. Spearman's coefficient was used for the non-parametric correlation analysis.

Results and Discussions

Soil properties

The topsoil sample properties are shown in Tables 1. The average humidity content was 1,44 %. The chernozem soils are characterized by a slightly alkaline pH (7.58-8.03), medium humus content (2.68-3.15%), a low to medium carbonate content (0.98-7.14 %) and a sandy loam-loam texture. No significant difference can be observed in the case of chernozem soils examined in 2017, 2018 and 2019, the observed differences do not affect the degree of wind erosion. The arenosol soil is characterized by a slightly alkaline pH (7.21), low carbonate content (1.26%) and sandy texture (Table 1.).

Chlorpyrifos and pendimethalin content in the wind-eroded sediment

Results of pesticide content in 2017

In 2017, we performed 13 wind tunnel experiments. Before the experimental run, part of the sampling area was treated with chlorpyrifos. Ten experimental runs were performed on the sprayed area and three on the control area.

The chlorpyrifos content (Fig. 8) of the treated topsoil varied between 0.004 and 009 mgkg-1. In the collected rolling soil fraction the concentration of chlorpyrifos varied between 0.014 and 0.096 $mgkg^{-1}$. The enrichment factors were calculated. These values

Table 1. Soil properties of the soil (Chernozem and sandy Arenolols) used in this study of 2017,2018 and 2019

N=28 (average)	pH (H_2O)	OM%	$CaCO_3$ (%)	Soil texture class	Total salt content (%)
Chernozem 2017	8,03	3,15	0,98	Sandy loam	0,03
Chernozem 2018	7,58	2,68	7,13	Loam	0,02
N=14 (average)					
Arenosol 2019	7,21	1,2	1,26	Sand	0,01
Chernozem 2019	7,69	3,1	7,14	Loam	0,04

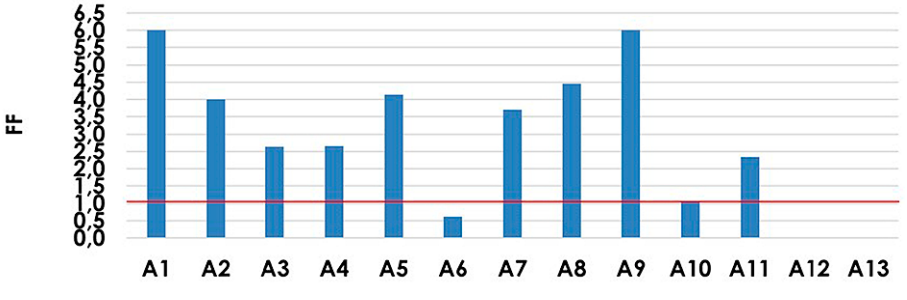

Figure 7. Chlorpyrifos enrichment ratios (ER) in the rolled sediment (A1-A11: Chlorpyrifos-treated area, A12-A13: control area)

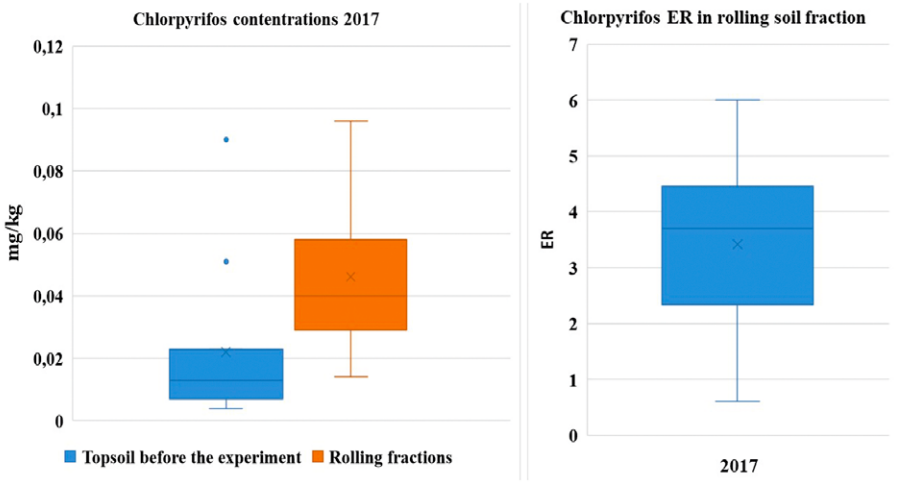

Figure 8. Results of concentration and enrichment ratio (ER) of chlorpyrifos in 2017

ranged from 0.61 to 6 (Fig. 7). No pesticide contamination and overgrowth were measured on the control plots (A12, A13). The average of the enrichment values of chlorpyrifos was 3.4 (Fig.8).

Results of pesticide content in 2018

In 2018, we performed 15 wind tunnel experiments. Before the experimental run, part of the sampling area was treated with chlorpyrifos and pendimethalin. Nine experimental runs were performed on the sprayed area and six on the control area.

The chlorpyrifos content (Fig. 9) of the treated topsoil varied between 0.01 and 0.1 mgkg^{-1}. In the collected rolling soil fraction the concentration of chlorpyrifos value ranged from 0.05 to 0.3 mgkg^{-1}. The enrichment factors were calculated. These values ranged from 0.6 to 7. The mean value of the enrichment was 2.9.

The pendimethalin concentration (Fig. 9) of the treated topsoil varied between 0.01 and 0.8 mgkg^{-1}. In the collected rolling soil fraction the concentration of pendimethalin varied between 0.07 and 2.1 mgkg^{-1}. The enrichment factors were calculated. These values ranged from 0.7 to 52,5. The average of the enrichment value of pendimethalin aswas 13.7

The results of the measurements showed that the ER of pendimethalin is much higher (ER:13,7) in the rolled fraction than ER (2,9) of chlorpyrifos.

Results of pesticide content in 2019

In the summer of 2019, we performed 14 ex-situ wind tunnel experiments on loam texture soil and 4 on sandy texture soil. Before the experimental run part of the collected soils was sprayed with chlorpyrifos and pendimethalin. Thirteen experimental runs were performed on the treated soils and one on the control soil sample.

The chlorpyrifos content of the treated loam texture soil varied between 2.03 and 23.03 mgkg^{-1}. In the collected rolling soil fraction the concentration of chlorpyrifos value ranged from 10.58 to 104.90 mgkg^{-1}. The enrichment factors were calculated. These values ranged from 0.88 to 20.85. The mean value of the enrichment factors was 4.98. The chlorpyrifos content of the treated sandy texture soil varied between 7.05 and 13.93 mgkg^{-1}. In the collected rolling soil fraction the concentration of chlorpyrifos value ranged from 15.01to 19.09 mgkg^{-1}. The values of enrichment factors ranged from 1.37 to 2.36. The mean value of the en-

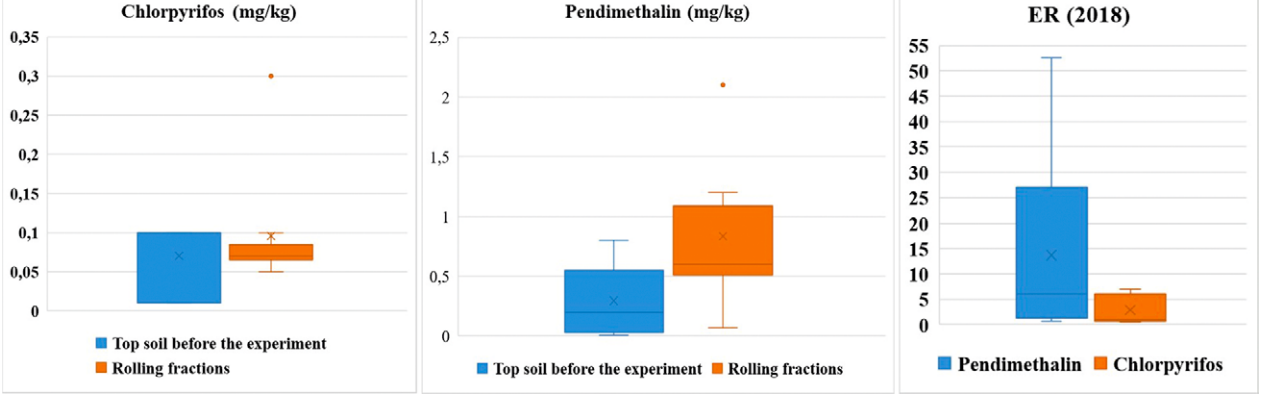

Figure 9. Results of concentration and enrichment of chlorpyrifos and pendimethalin in 2018

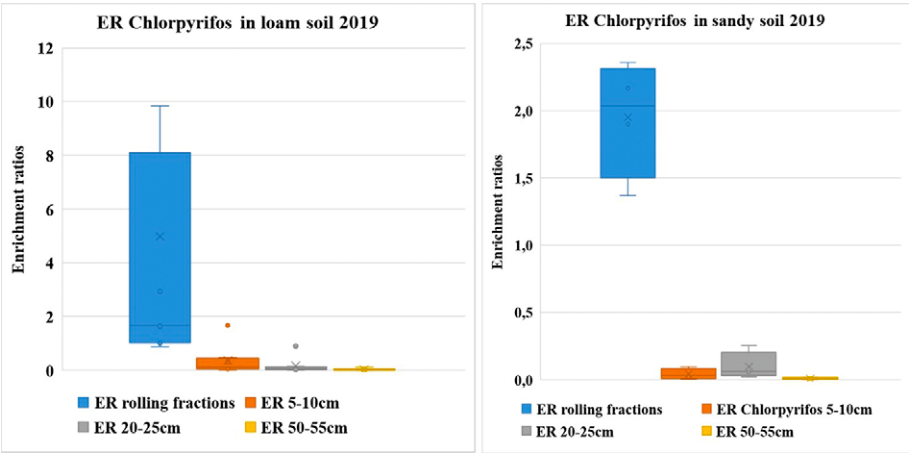

Figure 10. Enrichment of chlorpyrifos in texture of loam and sandy soil in 2019

richment factors was 1.95. In the case of chlorpyrifos-treated soil, the enrichment factor did not reach 1 in any of the suspended fractions (Fig. 10).

The pendimethalin concentration of the treated loam texture topsoil varied between 1.30 and 33.75 $mgkg^{-1}$. In the collected rolling soil fraction the concentration of pendimethalin varied between 13.60 and 358.60 $mgkg^{-1}$. In the rolling particles, the results of enrichment factors ranged from 1.51 to 42.74. The average of the enrichment values of pendimethalin was 9.01 in the samples of the rolling fractions. The average of the enrichment factor was greater than 1 at 5-10 cm too. In the case of sandy texture soil, the enrichment factor was as follows: in the rolling particles, the mean values were 2.05 (Fig. 11). The results of the measurements showed that the ER of pendimethalin is much higher in the rolled fraction than ER of chlorpyrifos.

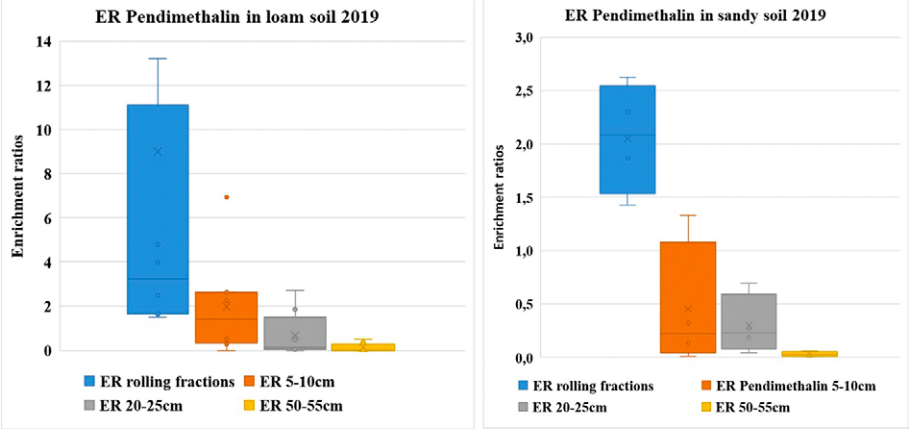

Figure 11. Enrichment of pendimethalin in the texture of loam and sandy soil in 2019

Discussion

Statistical studies were performed to explore the relationships between measured concentrations in soil and displaced sediment and enrichment factors. All statistical analyses were performed in SPSS 22. The Kolmogorov-Smirnov test was used to test the normality of all data. Because none of our data is normally distributed Spearman's correlation was computed to assess the relationship between pesticide contents. The statistical tests revealed a strong significant relationship between the pesticide's enrichment factors and the pesticide concentration of the topsoil and between pendimethalin ER chlorpyrifos ER as well ($p<0,01$) (Fig.12) (Table 2.).

Measurements in 2017 showed that the average enrichment values for chlorpyrifos were 3.4. The results of pesticide measurements in 2018 showed that pendimethalin ER was much higher in the rolled fraction (mean: 13.7) than in chlorpyrifos (mean: 2.9). Measurements in 2017, 2018 and 2019 showed that the tested pesticides were enriched in the rolled soil fraction in all measurements and in all tested plant protection products, which is due to the fact that the humus content (H%: 2.7-3.2)) ER: 1.1) is most enriched in this sediment fraction (Farsang et al., 2013; Farsang et al., 2021) and this organic colloid content is a very good binding surface for pesticides. Chernozem soils have a higher enrichment rate than sandy soils. In addition, a significant correlation can be found between the ER of chlorpyrifos and pendimethalin.

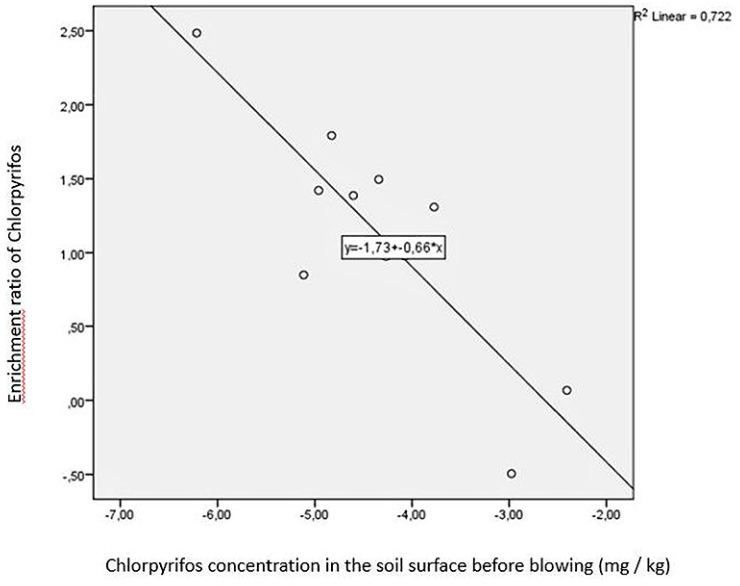

Figure 12. The connection between the Chlorpyrifos concentration in the soil surface before blowing and the ER of Chlorpyrifos

Table 2. Values of Spearmen's correlation coefficient

Spearman's rho	**Chlorpyrifos topsoil**	Correlation Coefficient	1,000					
		Sig. (2-tailed)						
		N	18					
	Pendimethalin topsoil	Correlation Coefficient	,951**	1,000				
		Sig. (2-tailed)	,000					
		N	18	18				
	ER Chlorpyrifos Rolling Part.	Correlation Coefficient	-,074	-,017	1,000			
		Sig. (2-tailed)	,771	,948				
		N	18	18	18			
	ER Pendimethalin Rolling Part.	Correlation Coefficient	-,219	-,177	,864**	1,000		
		Sig. (2-tailed)	,382	,483	,000			
		N	18	18	18	18		
	ER Chlorpyrifos 5-10 cm	Correlation Coefficient	-,867**	-,517	,817**	,783*	1,000	
		Sig. (2-tailed)	,002	,154	,007	,013		
		N	9	9	9	9	9	
	ER Pendimethalin 5-10 cm	Correlation Coefficient	-,850**	-,717*	,650	,683*	,917**	1,000
		Sig. (2-tailed)	,004	,030	,058	,042	,001	
		N	9	9	9	9	9	9

**. Correlation is significant at the 0.01 level (2-tailed).
*. Correlation is significant at the 0.05 level (2-tailed)

The results show that during each major wind erosion event the accumulation and spread of contaminants bound to the soil particles must be considered. Our results can be useful in quantifying agricultural pressures, tracking the spatial movement of materials moving by the wind (potential pollutants), and can be used in later landscape and settlement planning tasks (shelterbelts, etc.).

Conclusions

As a result of climate change, longer and longer dry periods are expected in the Hungarian Great Plain, which is favorable for wind erosion events. Therefore, it is very important to look at what the wind brings from the dry surface during such a wide-ranging event.

In this work, wind tunnel measurements were performed on Chernozem and Arenosol soils in the Southern Great Plain of Hungary. The present study aimed to investigate the pesticide contents of wind-eroded sediment. The measurements showed that the enrichment of chlorpyrifos and pendimethalin could be detected in the rolling particles. The analysed pes-

ticides were enriched in the rolling soil fraction. As shown by our study, airborne particulates can be contaminated with chlorpyrifos and pendimethalin too.

The above experiments show that there is adequate reason to take off-site airborne transport of pesticide-contaminated soil fractions seriously, especially during sufficiently long periods of drought. The results show that during each major wind erosion event the accumulation and spread of contaminants bound to the soil particles must be considered. Our results can be useful in quantifying agricultural pressures, tracking the spatial movement of materials moving by the wind (potential pollutants), and can be used in later landscape and settlement planning tasks (in the correct choice of tillage methods and tools, direction and quality, height, etc. of shelterbelts., etc.).

The increasing use of pesticides is a worldwide trend. The consequence of climate change is that in our region, more and more drought can be expected in the early spring and summer periods. Tillage carried out under inadequate moisture conditions (the soil is too dry) causes a deterioration of the soil structure, i.e. the soil becomes dusty. The consequence of this is that the risk of deflation also increases. For this reason, monitoring and estimating exposure to airborne pesticides will be very important in the near future.

Acknowledgements

We wish to thank Dr. Lajos Kadenczki and István Fekete for their kind assistance with the analytical work.
Funding information *The research was funded by the 'Thematic Network for the Sustainable Use of Resources – RING2017' project (program code: EFOP-3.6.2-16-201700010) and supported by the ÚNKP-19-3-I. New National Excellence Program of the Ministry for Innovation and Technology. Furthermore, the study was carried out with the support of OTKA 1K 116981, „In situ wind channel experimentation based on in situ wind channel experiments on different soil types, on-site and off-site effects".*

References

Agassi, M., Letey, J., Farmer, W.J., & Clark, P. (1995). Soil erosion contribution to pesticide transport by furrow irrigation. *Journal of Environmental Quality*, 24, 892-895

Bach, M. (2008). *Aolische Stofftransporte in Agrarlandschaftem*. Unbublished PhD Dissertation. Germany, Kiel: ChristianAlbrechts Universitat zu Kiel.

Bärring, L., Jönsson, P., Mattsson, J.O., & Åhman, R. (2003). Wind erosion on arable land in Scania, Sweden and the relation to the wind climate-a review. *Catena*, 52,173–190

Bartus, M., Barta, K., Szatmári, J., & Farsang, A. (2019). Csongrád megye talajainak szélcsatorna kísérletekre alapozott szélerózió veszélyeztetettség becslése. *Agrokémia és Talajtan*, 68(2), 225-242.

Bento, C.P.M., Goossens, D., Rezaei, M., Riksen, M., Mol, H.G.J., Ritsema, C.J., & Geissen, V. (2016). Glyphosate and AMPA distribution in wind-eroded sediment derived from loess soil. *Environmental Pollution*. https://doi.org/10.1016/j.envpol.2016.11.033

Besancenot, J. P., Boko, M., & Oke, P. C. (1997). Weather conditions and cerebrospinal meningitis in Benin (Gulf of Guinea, West Africa). *European journal of epidemiology*, 13(7), 807-815.

Clymo, A. S., Shin, J. Y., & Holmén, B. A. (2005). Herbicide sorption to fine particulate matter suspended downwind of agricultural operations: Field and laboratory investigations. *Environmental science & technology*, 39(2), 421-430.

Csányi, K., Barta, K., Szatmári, J., & Farsang, A. (2019a). A mezőgazdasági eredetű porok lehetséges környezeti hatásai, különös tekintettel a peszticidekre. In: Rákhely, G., Hodúr, C., Lemmer, B., Jákói, Z. (eds): *II. Sustainable Raw Materials International Project Week and Scientific Conference: Book of Abstracts,* University of Szeged, pp 74-74.

Csányi, K., Barta, K., Szatmári, J., & Farsang, A. (2019b). Potential environmental impacts of powders of agricultural origin, with particular regard to the *effects of pesticide, Southern Hungary. Geophysical Research Abstracts,* 21. https://meetingorganizer.copernicus.org/ EGU2019/EGU2019-16167.pdf

Farsang, A., Szatmári, J., Bartus, M., & Barta, K. (2022). Quantification of deflation-induced soil loss on chernozems: Field protocol and sediment trap development based on wind tunnel experiments, *Zeitschrift für Geomorphologie*, 63(4), 329-341.

Farsang, A., Barta, K., Szatmári, J., & Bartus, M. (2021). Szélerózió okozta talaj-, humusz- és tápanyag-áthalmozás különbségeinek feltárása különböző szerkezeti adottságú csernozjom talajokon terepi szélcsatorna kísérletek alapján. *Agrokémia és talajtan*, 70(2), 115-135. DOI: 10.1556/0088.2021.00096

Farsang, A., & Barta, K. (2004). A talajerózió hatása a feltalaj makro- és mikroelem tartalmára. *Talajvédelem (Journal of Soil protection),* 268-276.

Farsang, A., Duttmann, R., Bartus, M., Szatmári, J., Barta, K. & Bozsó, G. (2013). Estimation of Soil Material Transportation by Wind Based on in Situ Wind Tunnel Experiments. *Journal of Environmental Geography,* 6(3-4),13–20.

Farsang, A., Szatmári, J., Négyesi, G., Bartus, M., & Barta, K. (2011). Estimation of nutrient movement caused by wind erosion on chernozem soils in wind tunnel experiments. *Agrokémia és Talajtan*, 60(1), 87-102. https://doi.org/10.1556/Agrokem.60.2011.1.7

Funk, R., Deumlich, D., Voelker, L. & Steidl, J. (2004). GIS application to estimate the wind erosion risk in the Federal State of Brandenburg. In: Goossens D, Riksen M (Eds.), *Wind Erosion and Dust Dynamics: Observations, Simulations, Modelling.* ESW Publications, Wageningen, pp. 139–150.

Gill, T. E., Zobeck, T. M., & Stout, J. E. (2006). Technologies for laboratory generation of dust from geological materials. Journal of hazardous materials, 132(1), 1-13.

Goossens, D., Offer, Z., & London, G. (2000). Wind tunnel and field calibration of five aeolian sand traps. *Geomorphology*, 35(3-4), 233-252.

Gossens, D. (2002). On-site and off-site effects of wind erosion. In: Warren A (ed) *Wind erosion on agricultural land in Europe,* Office for Official Publications of the European Communities, EUR 20370, pp 29-38.

Järup, L. (2003). Hazards of heavy metal contamination. *British medical bulletin*, 68(1), 167-182.

Kim, K. H., Kabir, E., & Kabir, S. (2015). A review on the human health impact of airborne particulate matter. *Environment international,* 74, 136-143.

Korcz, M., Fudała, J., & Kliś, C. (2009). Estimation of wind blown dust emissions in Europe and its vicinity. *Atmospheric Environment*, 43(7), 1410-1420. https://doi.org/10.1016/j.atmosenv.2008.05.027

Larney, F.J., Cessna, A.J., & Bullock, M.S. (1999). Herbicide Transport on Wind-Eroded Sediment. Journal of Environmental Quality, 28(5), 1412-1421.

Liu, L.Y., Li, X.Y., Shi, P.J., Gao, S.Y., Wang, J.H., Ta, W.Q., Song, Y., Liu, M.X., Wang, Z. & Xiao, B.L. (2006). Wind erodibility of major soils in the farming-pastoral ecotone of China. *Journal of Arid Environments*, 68(4), 611-623. https://doi.org/10.1016/j.jaridenv.2006.08.011

Maurer, T., Herrmann, L., Gaiser, T., Mounkaila, M., & Stahr, K. (2006). A mobile wind tunnel for wind erosion field measurements. *Journal of Arid Environments* 66, 267–271 https://doi.org/10.1016/j.jaridenv.2005.11.002

O'Hara, S. L., Wiggs, G. F., Mamedov, B., Davidson, G., & Hubbard, R. B. (2000). Exposure to airborne dust contaminated with pesticide in the Aral Sea region. *The Lancet*, 355(9204), 627-628.

Pásztor, L. (2018). *Célspecifikus térbeli predikciók kidolgozása feladatorientált, térképi alapú talajinformációk előállítására.* Unpaplished DSc Dissertation. Budapest: Eötvös Lóránd University.

Pásztor, L., Négyesi, G., Laborczi, A., Kovács, T., László, E., & Bihari, Z. (2016). Integrated spatial assessment of wind erosion risk in Hungary. *Natural Hazards and Earth System Sciences*, 16(11), 2421-2432. https://doi.org/10.5194/nhess-16-2421-2016

Pye, K. (1987). *Aeolian Dust and Dust Deposits.* London, UK: Academic Press.

Riksen, M. (2004). Off-site effects of wind erosion on agricultural land in NW Europe. In: Goossens D, Riksen M (eds), *Wind erosion and dust dynamics: observations, simulations, modelling ESW Publications,* Wageningen University: Department of Environmental Sciences, Erosion and Soil and Water Conservation Group, pp. 103–122.

Stefanovits, P., & Várallyay, Gy. (1992). State and management of soil erosion in Hungary. In: *Proceedings of the soil erosion and remediation workshop*, US–Central and Eastern European Agro-Environmental Program, Budapest, pp. 79–95.

Sterk, G. & Goossens, D. (2007) On-site and off-site impacts of wind erosion in Europe: an overview. In: Jakubikova A, Uhlirova K. (eds), *Proceedings of the International conference on Off-site impacts of soil erosion and sediment transport,* Prague,1–3 October 2007, pp. 103–113.

Sterk, G., Herrmann, L., & Bationo, A. (1996). Wind-blown nutrient transport and soil productivity changes in southwest Niger. *Land degradation & development,* 7(4), 325-335.

Szatmári, J. (1997). Evaluation of wind erosion risk on the SE part of Hungary. *Acta Geographica Szegediensis*, 36, 121-135.

Toy, T.J., Foster, G.R., & Renard, K.G. (2002). *Soil erosion: Processes, Prediction, Measurement, and Control.* New York: John Wiley and Sons, pp. 338

Zheng, X. (2009). *Mechanics of wind-blown sand movements.* Berlin Heidelberg: Springer-Verlag, pp. 309

Online sources

Internet 1: WHO (2013) Health effects of particulate matter. Policy implications for countries in eastern Europe, Caucasus and Central Asia. http://www.euro.who.int/__data/assets/pdf_file/0006/189051/Health-effects-of-particulate-matter-final-Eng.pdf

Internet 2: MET (2016): www.met.hu/eghajlat/magyarorszag_eghajlata/altalanos_eghajlati___jellemzes/szel

Internet 3: KSH (2016): (https://www.ksh.hu/docs/hun/xftp/stattukor/novenyvedoszer.pdf

Internet 4: Eurostat (2018): Agri-environmental indicator-soil erosion. Statistics explained. https://ec.europa.eu/eurostat/statistics-explained/index.php?title=_grienvironmental_indicator-_soil_erosion&oldid=415938_

ISSN 0354-8724 (hard copy) | ISSN 1820-7138 (online)

Active Geomorphic Hazards in the Sâmbăta Valley, Făgăraș Mountains (Romania): a Tree-ring Based Approach

Patrick Chiroiu[A], Alexandru Onaca[A*], Andrei Matica[A], Iosif-Otniel Lopătiță[A], Oana Berzescu[A,B]

Received: April 28, 2022 | Revised: June 24, 2022 | Accepted: July 01, 2022
doi: 10.5937/gp26-37614

Abstract

The present study addresses, for the first time, the problem of spatio-temporal reconstruction of geomorphic processes using tree-rings in the Sâmbăta Valley (Romanian Carpathians). The dendrogeomorphic analysis was conducted in two different sites, one affected by snow avalanches and the other by rockfall. A total number of 130 *Picea Abies* were sampled in the two sites. The results yield 13 major snow avalanches between 1950 and 2020 and a return period of 3.3 years. The winters with the highest activity index were 1988, 1997 and 2012. The rockfall reconstruction highlights several years of intense activity: 1952, 1955, 2003 and 2012. Thus, the results of the present study provide evidence of active geomorphic processes in the studied area, indicating that tourists are highly exposed to geomorphic hazards, as both sites interfere with popular hiking trails. (Because Sâmbăta Valley is one of the most intensely frequented by tourists in the Făgăraș Mountains, it is a need for warning signs to be installed on the exposed trails.

Keywords: snow avalanches; rockfall; natural hazards; dendrogeomorphology; Romania

Introduction

In mountainous regions all over the world, slope processes such as snow avalanches, debris flows and rockfall can pose a serious threat to human lives and activities (Bollati et al., 2018). A better understanding of geomorphic processes, in terms of past occurrences, is an important task for the assessment of natural hazards and the associated risks, in areas where information on past process behavior is sparse or missing. The Romanian Carpathians have long been a mountainous region repeatedly affected by geomorphological hazards (Bălteanu, 1997). Several active geomorphological processes have frequently caused damage to tourism infrastructure, human activities and human fatalities (Micu et al., 2017). Due to the rapid development of the tourism infrastructure in the Carpathians in the XXth century, geomorphological processes like landslides, debris flows, rockfall, snow avalanches and river flooding can have a significant impact on touristic activities. Although these natural processes have the potential to negatively affect humans, infrastructure and activities and the environment (Gratton et al., 2015), a comprehensive understanding of their behavior is still poor in the Romanian Carpathians (Voiculescu & Ardelean, 2012). It is, therefore, a high demand to improve knowledge of the spatio-temporal occurrence of past events because this might lead to

[A] West University of Timișoara, Department of Geography, Romania; V. Pârvan, no. 4, Timișoara, 300223, Timiș, Romania; patrick.chiroiu@e-uvt.ro; alexandru.onaca@e-uvt.ro; andrei.matica00@e-uvt.ro; iosif.lopatita00@e-uvt.ro; oana.berzescu@e-uvt.ro
[B] Institute for Advanced Environmental Research, West University of Timișoara; V. Pârvan, no. 4, Timișoara, 300223, Timiș, Romania
[*] Corresponding author: Alexandru Onaca; e-mail: alexandru.onaca@e-uvt.ro

hazard prevention and mitigation at a regional and local scale (Copien et al., 2008).

Little information exists regarding the frequency, magnitude, and timing of these mountain-slope hazards due to the lack of archive data on past occurrences in the Romanian Carpathians (Voiculescu et al., 2016). Nevertheless, the occurrence and characteristics of past geomorphic processes on forested slopes can be deciphered using a tree-ring based approach. This method proved to be one of the most accurate and reliable dating approaches, providing annual and, in some cases, intra-annual resolution on geomorphic activity over the past centuries (Stoffel et al., 2006b). Moreover, dendrochronology allows the differentiation between geomorphic processes, mainly based on the position of growth disturbances within the annual tree ring (Stoffel et al., 2005). In various mountainous regions all over the world, studies have been carried out to reconstruct debris flows (Bollschweiler et al., 2007, Tichavsky et al., 2017), rockfall (Perret et al., 2004, Mainieri et al., 2019), snow avalanches (Corona et al., 2010, Favillier et al., 2017) and flash floods (Casteller et al., 2015).

Previous studies in the Romanian Carpathians revealed that the aforementioned geomorphic processes could sometimes reach catastrophic levels in the Făgăraș Mountains (Voiculescu & Ardelean, 2012), where many touristic hiking routes are exposed to rockfall, debris flows or snow avalanches. On the northern slope of the Făgăraș Mountains, Sâmbăta Valley is one of the most exposed and intensely frequented by tourists due to its high accessibility and spectacular relief. Despite that snow avalanches and rockfall frequently impact the trekking and the climbing routes in the Sâmbăta Valley, no previous study assessed the reconstruction of spatio-temporal patterns of these processes. Therefore, the aims of the present study are (i) to reconstruct major events on a forested snow avalanche path using dendrochronology and (ii) to analyze rockfall activity on a forested slope, based both on a tree-ring approach and visual scar counting.

Study area

The Sâmbăta Valley (45°37'N, 24°47'E) is located on the northern slope of the Făgăraș Mountains, the highest mountain range in Romania (Figure 2). Stretching around 11 km from south to north, between the main ridge and the Sâmbăta de Sus Tourist Complex, situated at the foot of the Făgăraș Mountains, Sâmbătă is a typical Carpathian north-facing glacial valley. Geology is dominated by schists, gneisses and crystalline limestones lithology belonging to the Supragetic nappe. The elevation ranges between 670 m and 2470 m (Gălășescu Peak). During the most extended glacial advance (22 ka BP), a valley glacier 4.5 km long reached down to 1150 m within this valley. During the Lateglacial, several readvances were documented in the Southern Carpathians (Ruszkiczay-Rüdiger et al., 2016). The Pleistocene glaciers sculpted the landscape and created glacial cirques and valleys. The dominant present-day processes are snow avalanches, rockfall, debris flows, gully erosion and solifluction.

The predominant air mass circulation in this region is from west to east. The mean annual precipitation at the nearby Bâlea Lake weather station (2038 m, 45°36'17"N, 24°37'01"E, period 1979-2020) is 1365 mm. The highest rainfalls are in the warm seasons (e.g., May-August), when heavy rainstorms are most frequent, whereas snowfall is characteristic between November and April. Above 2000 m, the ground is covered by snow for around 200-250 days/year. The mean annual air temperature at the Bâlea Lake weather station is 0.8 °C but increases to 4.6 °C at 1406 m (at Păltiniș weather station). A general overview of the annual meteorological patterns is depicted in Figure 1.

The treeline stands around 1800, but the hillslopes are predominantly non-forested above 1500 m due to intense geomorphic and pastoral activity. Only below

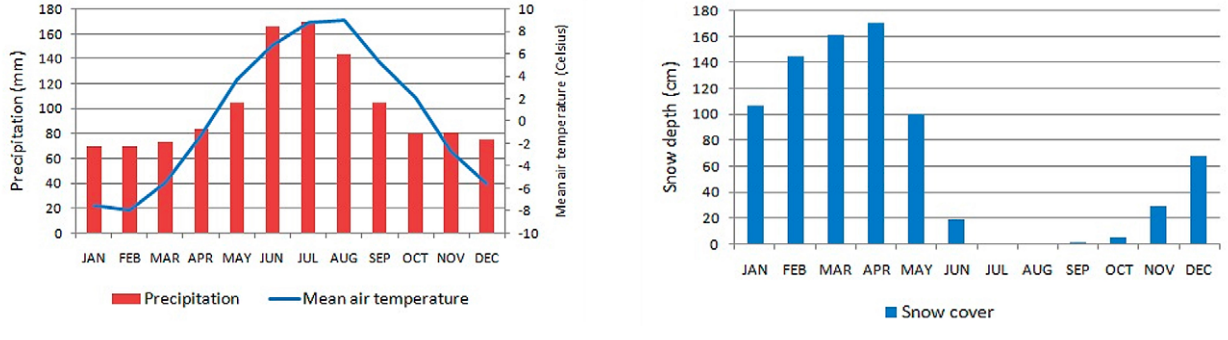

Figure 1. Temperature, precipitation and snow cover at Bâlea Lake Weather Station (1979-2020)

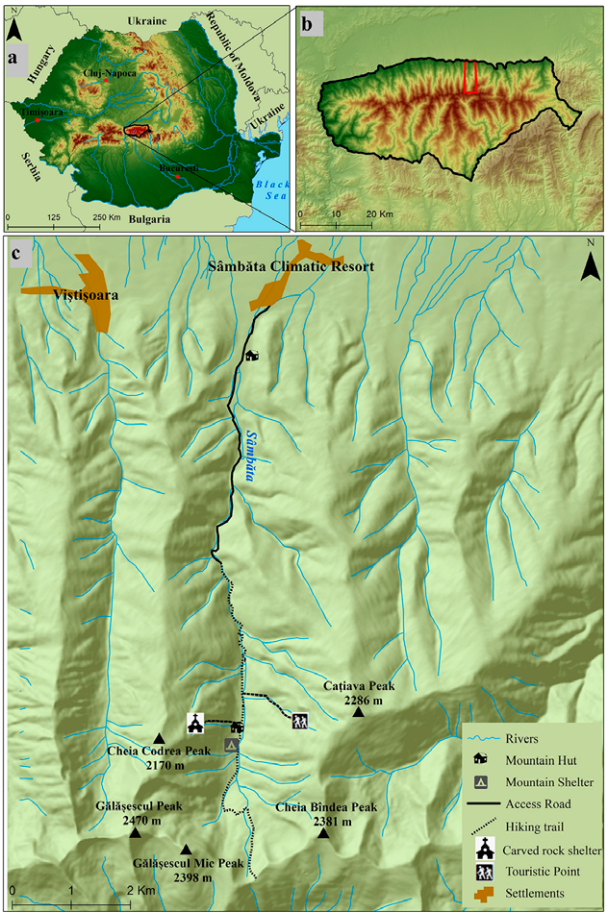

Figure 2. Location of the a. Făgăraș Mountains in Romania; b. The Sâmbăta Valley within the Făgăraș Mountains; and c. Map of Sâmbăta Valley

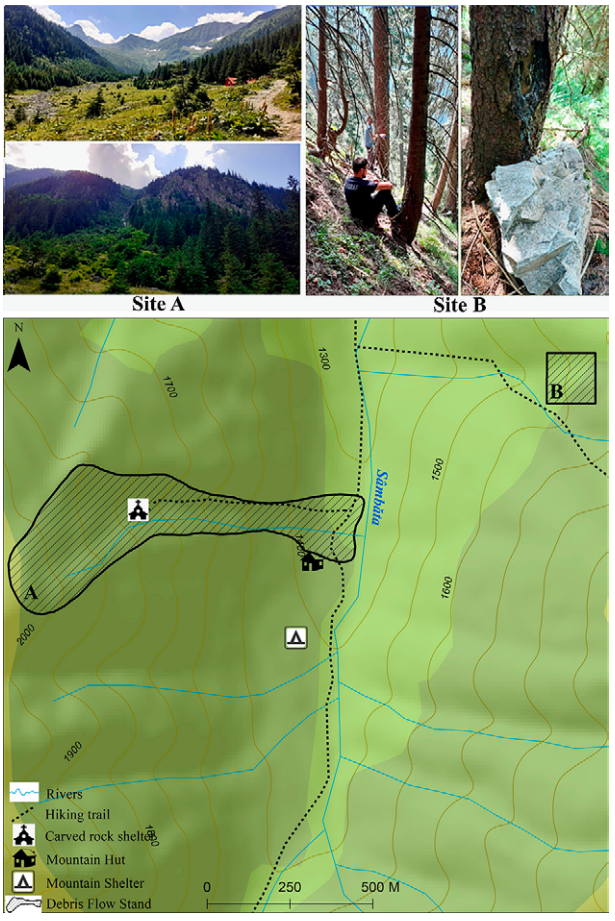

Figure 3. Location of the two analyzed sites in the Sâmbăta Valley (site A - snow avalanches, site B - rockfall)

1500 m, a dense *Picea abies* forest covers the hillslopes. Above the treeline, alpine and subalpine herbs and shrubs carpet the hillslopes. Reduced surfaces within this valley are covered with unconsolidated scree deposits or correspond to highly inclined, intensely fractured bedrock. These nearly vertical and highly sensitive to weathering outcrops constitute the primary sediment sources for rockfall and debris-flow events and the material scoured from the channels during heavy rainfalls.

The trails in the Sâmbăta Valley are one of the most popular in the Făgăraș Mountains and, due to the breathtaking landscape, attract high numbers of visitors, especially during the summer. At 1350 m, the Valea Sâmbetei chalet is located on a sizable depositional fan created by the Codrea torrent on the western slope of the valley. The chalet was a hunting house at the beginning of the last century, but in the 1930s it became a tourist lodge. From the chalet, a steep trail ascends to 1600 m to a carved rock shelter where one of the most beloved theologians in the Romanian Orthodoxy settled his praying site around the middle of the XXth century. Pilgrims from all over Romania visit this sacred place, although the trail is highly exposed to snow avalanches, rockfall and debris flow. On the eastern slope of the valley, another trail starts in the vicinity of the Valea Sâmbetei. It ascends to Piatra Caprei Peak, this path being highly endangered by rockfall as well.

The dendrogeomorphological approach was conducted on two different sites (Figure 3). The first site is the avalanche path following the Codrea creek in the vicinity of the Sâmbăta Valley chalet. Between the confluence of this creek with Sâmbăta valley and the source area, the path spans a vertical range of about 800 m. The upper basin hillslopes have a high gradient, with a mean slope angle of 39°. Between the apex of the fan and the confluence with the Sâmbăta Valley, the mean inclination of the slope decreases to 33°. The majority of the trees growing on the torrential cone show morphological evidence of former snow avalanche activity. The second site is located at the foot of a rockfall producing wall known as Piatra Caprei, around 1700 m. Most of the trees at the base of this rock wall show clear signs of disturbances (mainly impact scars) as a result of intense rockfall activity. Trekking trails cross both sites, but there is no sign warning of snow avalanche/rockfall danger.

Material and methods

Terrain analysis and geomorphic mapping

Initial examination of satellite imagery, aerial photographs and topographic maps of the study area were followed by a geomorphic survey undertaken in the field. Finally, a digital elevation model for the Sâmbăta Valley, including the two investigated sites, was constructed from digitized elevation contours of the 1:25000 topographic maps using ArcGIS. The contour lines were interpolated into a raster grid surface using Topo to Raster tool. The forest cover and the delineation of the two sites were assessed based on aerial photographs and satellite imagery.

Sampling design

The present analysis is based on two sampling campaigns that took place in 2014 (60 trees at site A) and 2021 (20 trees at site A and 50 trees at site B.) Hence, to reconstruct the occurrence of geomorphic processes in the study area, a total number of 130 *Picea abies* trees have been sampled using Pressler increment borers (ø 5.15 mm, max. length 40 cm). Selected trees generally exhibit clear evidence of geomorphic disturbance (Stoffel and Bollschweiler, 2009), such as impact scars, broken trunks, tilted and bent stems, flagged branches, uprooting and apex loss. For site A, sampling was carried out along the lateral limits of the avalanche path (see Figure 11), generally along the transportation zone and, where available, inside the path and in the run-out zone. At site B, more severely damaged trees and individuals with a higher number of visible impact scars were selected for the present analysis.

Sampling procedures were adapted to the type and location of visible anomalies in tree morphology, as suggested by Stoffel and Bollschweiler (2009), considering that growth reactions are usually better developed in the proximity of the impact (Stoffel and Corona, 2014). Between two and five increment cores were extracted per tree, with an increasing number of samples for trees with multiple visible scars. Finally, additional information was collected for each tree: exact position (using a differential GPS Trimble GeoExplorer XH6000), stem diameter at sampling height, type and description of growth anomaly, number and height of scars, specific terrain features and surrounding vegetation.

Sample analysis

All collected samples were air-dried, mounted and finely sanded (with grit from 100 to 800) following standard dendrochronological procedures described by Bräker (2002). Using marker years from a local reference chronology (Chiroiu et al., 2015), samples were visually crossdated, and for each tree-ring the exact year of formation was assessed. Tree-rings were then measured using a LINTAB-5 positioning table, connected to a Leica stereo-microscope and TSAP-Win Professional 4.64 software (Rinn, 2013).

The reconstruction of past occurrences of geomorphic processes requires the identification and precise dating of growth disturbances (referred hereafter as GD). In the present study, the following GD were used (Stoffel and Bollschweiler, 2009): (i) onset of compression wood, (ii) first year with abrupt growth suppression and (iii) abrupt growth release, (iv) onset of callus tissue formation, and (v) first year with tangential rows of traumatic resin ducts - referred hereafter as TRD - (Stoffel, 2008). According to Stoffel et al. (2006b), TRD and callus tissue found just at the beginning of the growth ring (i.e. early earlywood) were associated to snow avalanches (for site A), while TRD and callus tissue found later within the annual ring (middle and late earlywood and latewood) were considered being inflicted by other processes (rockfall and debris flows). TRD were only considered the result of geomorphic events if they formed compact, continuous and tangential rows.

Subsequently, we assessed the intensity of each identified GD (weak, intermediate and strong) and based on the classification system proposed by Stoffel and Corona (2014), we defined five intensity classes. The methodological steps adressed in the present study, from sample collection to results is depicted in Figure 4.

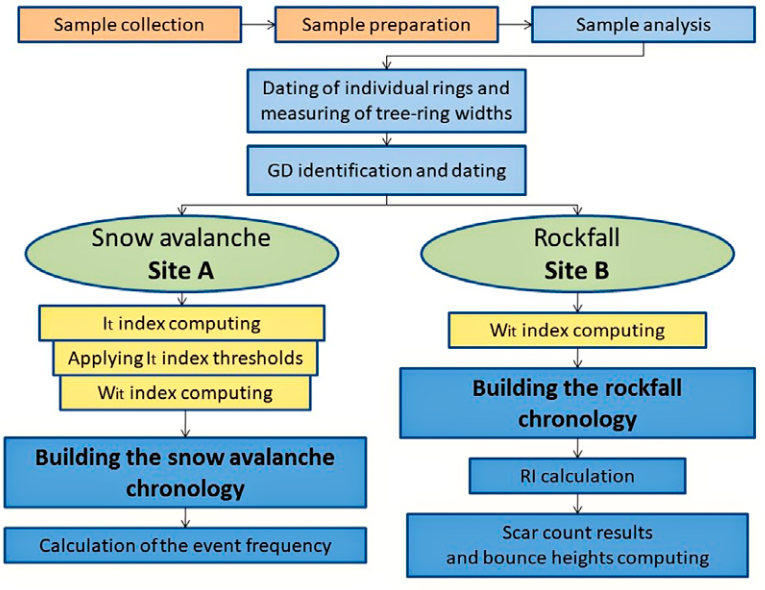

Figure 4. Methodological steps used for each of the investigates sites

Snow avalanche reconstruction and frequency

The snow avalanche reconstruction for site A is based on the total number of GDs and the semi-quantitative Shroder I_t index (Shroder, 1980). The I_t index is defined as the ratio between trees showing growth responses and all sampled trees being alive in that year, following the formula:

$$I_t = \frac{\sum_{i=1}^{n} Rt}{\sum_{i=1}^{n} At} \cdot 100$$

- where Rt = responding trees in year t; and At = sampled trees alive in year t.

Snow avalanche event years were assessed by applying sample depth adapted thresholds for GD and It, as suggested by Stoffel et al. (2013). In the present study, we used the following thresholds for avalanche filtering: GD≥3 and I_t≥15 (no. of available trees ≤20), GD≥5 and I_t≥10 (no. of available trees between 21 and 50) and GD≥7 and I_t≥7 (more than 50 trees available).

The strength of the dendrogeomorphic signal is evaluated using the semi-quantitative intensity weighted index (W_{it}) proposed by Kogelnig-Mayer et al. (2011) and based on the five intensity classes mentioned above:

$$W_{it} = \left[\left(\sum_{i=1}^{n} GDt5 \cdot 5 \right) + \left(\sum_{i=1}^{n} GDt4 \cdot 4 \right) + \left(\sum_{i=1}^{n} GDt3 \cdot 3 \right) + \right.$$
$$\left. + \left(\sum_{i=1}^{n} GDt2 \cdot 2 \right) + \left(\sum_{i=1}^{n} GDt1 \cdot 1 \right) \right] \cdot \frac{\sum_{i=1}^{n} Rt}{\sum_{i=1}^{n} At}$$

- where $GDtn$ = GD assigned to the Intensity n Class (n=1 to 5); Rt = responding trees in year t; At = trees alive in year t.

Snow avalanche frequency is expressed as a return period and is calculated as a ratio between the length of the chronology and the number of reconstructed events (Casteller et al., 2011). Considering that the sample depth increases as we advance towards the present, tree-ring based avalanche reconstructions yield a better resolution for more recent periods. However, the limited number of trees available for older periods will influence the quality of the reconstructed frequency (Corona et al., 2010). Therefore, in this paper we calculate the return period for two different time intervals: 1950-2020 (70 years) and 1980-2020 (40 years). We expect that the results for the 40 years will best reflect the present frequency for major snow avalanche events in the study area.

Rockfall analysis

The occurrence of rockfall at site B was analyzed by GD dating and counting of visible scars on the sampled trees (Trappman & Stoffel, 2013, Mainieri et al., 2019). In addition, to evaluate the bouncing heights of downslope moving rock fragments, the average height of visible scars was noted (Schneuwly et al., 2008).

The GD based rockfall reconstruction accounts for the total number of responses per year to detect years or periods with more intense process activity. To assess the strength of the dendrogeomorphic signal, we calculated the W_{it} index for each year. The recurrence interval (RI) was calculated for each tree, representing the average number of years passing between two GDs on a single tree (Stoffel et al., 2005). The RI is

Table 1. Reccurence interval classes

RI classes	Class 1	Class 2	Class 3	Class 4	Class 5	Class 6
Number of years between 2 events	No GD	RI<10	10<RI<20	20<RI<30	30<RI<40	RI>50

calculated as a ratio between the tree's age and the number of events detected. To visualize differences of rockfall intensity along the slope, trees were assigned to different RI classes (Table 1).

Following bark and cambial injury, a tree will react by forming callus tissue which will gradually overgrow and heal the wound. The process requires several years, mainly depending on the scar size, the age and health of a tree. Thus, recent as well as older scars remain visible on the stem. In the scar count approach, we followed recommendations by Trappmann and Stoffel (2013). Unusually long, vertical scars and scars found on the downslope part of the tree were excluded from the count.

Results

Tree ages and growth disturbances

The trees analyzed in the present study reveal a mean number of 64 annual rings, with a minimum of 11 and a maximum of 289 years. Due to the sampling height and because, in most cases, the tree's pith was not reached, the age values are relative and do not reflect the absolute ages of sampled trees. Nevertheless, there is a clear difference in tree ages between the forest stands growing at the two sites. At site A, the average age of the stand is 35 years, with the oldest individual counting 86 tree rings, while at site B, trees are much older, with a mean number of 110 annual tree-rings and most of the trees exceeding 100 years.

The samples analyzed in this study allowed the identification of 711 GDs related to snow avalanches and rockfall. The different types of responses are shown in Figure 5. A number of 280 GDs were associated with snow avalanche disturbance, whilst 431 GDs were most probably inflicted by rockfall and debris flows.

Because avalanches mainly tilt trees in their downslope movement, compression wood was the most frequent response found at site A (39.5%). On the other hand, rockfall impacts damage tree stems, inducing wounds, thus promptly activating anatomical reactions in the form of callus tissue and TRD. Accordingly, at site B, almost half of the GD was in the form of TRD.

Snow avalanche reconstruction and frequency

Based on the number of GD and the semi-quantitative I_t index, we were able to reconstruct a total number of 13 major snow avalanche events at site A, the reconstructed chronology covering the period 1950 – 2021. As shown in Figure 6, the years with major events reconstructed are the following: 1976, 1988, 1992, 1995, 1996, 1997, 2005, 2006, 2007, 2008, 2012, 2016 and 2019. In addition, event years 1992 and 1995 with GD values falling close beneath the GD threshold were included in the chronology due to the spatial cluster-

Investigated site	Total number of GD	Reaction wood		Growth supression		Growth release		TRD		Callus tissue	
		No.	%	No.	%	No.	%	No.	%	No.	%
Site A	339	134	39.5	79	23.3	3	0.9	109	32.2	14	4.1
Site B	372	86	23.1	55	14.8	14	3.8	184	49.5	33	8.9

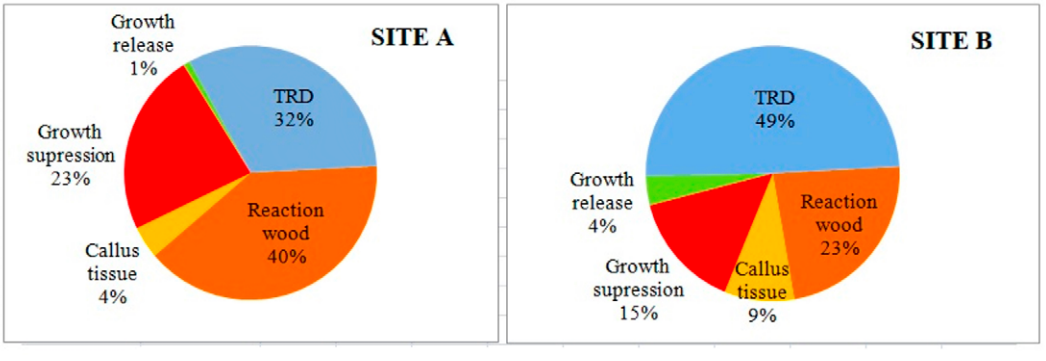

Figure 5. Distribution of GD types at the two investigated sites

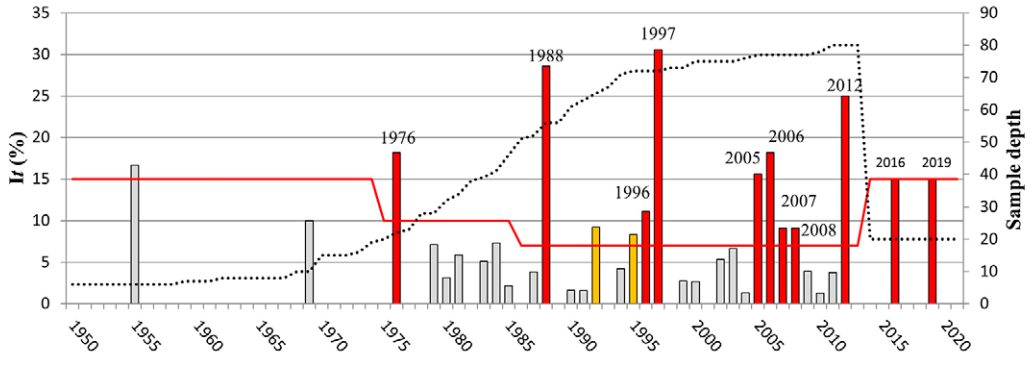

Figure 6. Histograms showing the snow avalanche chronology for site A based on the I_t index (bars – I_t values; red line – I_t threshold; dotted line – sample depth)

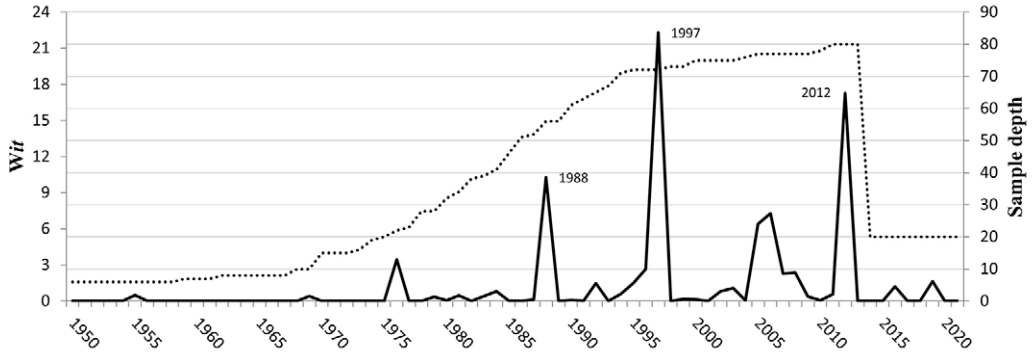

Figure 7. Histogram showing the dendrochronological signal strength for site A based on the reaction intensity (W_{it} index)

ing of strong reactions (Schneuwly-Bollschweiler et al., 2012).

The dendrochronological signal strength based on the semi-quantitative Wit index (Figure 7) is consistent with the reconstructed event chronology. Moreover, it highlights the years 1988, 1997 and 2012 as characterized by strong and long-lasting reactions, pointing to the magnitude of the events. On the other hand, moderate values of the W_{it} index (1.5 – 3) were obtained for event years 1992, 1993, 2007, 2008, 2016 and 2019.

The frequency of major events, expressed as an average return period, is 5.3 years for the whole extent of the chronology (1950-2021) and 3.3 years for the interval 1980-2021. We can also observe clustering of events in two periods (1995-1997 and 2005-2008), with avalanches occurring every year.

Rockfall analysis

The identification and dating of rockfall induced growth disturbances allowed the reconstruction of 224 events. The century-long reconstructed chronology (Figure 8) spans from 1900 to 2020 and points to several years of intense rockfall activity (GD>5): 1952, 1955, 2003, 2007, 2010, 2012 and 2019. Eight trees exhibited GDs in 1944, all in the form of weak to moderate reaction wood. This finding rather suggests the influence of another disturbing factor, such as intense

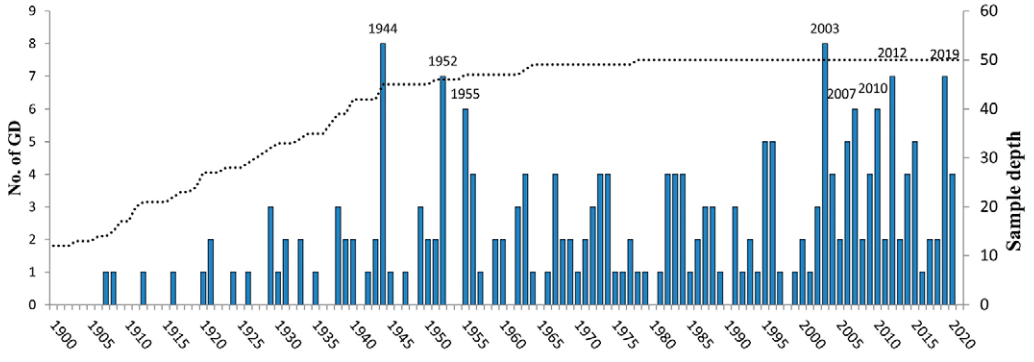

Figure 8. Histogram showing the total number of growth disturbances per year at site B

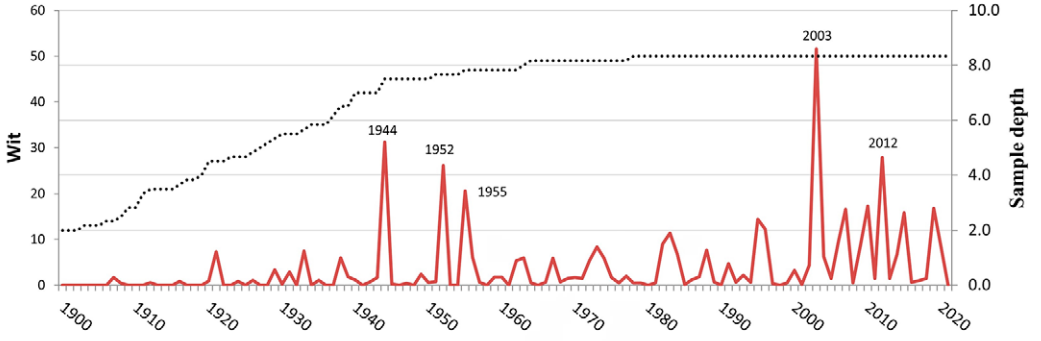

Figure 9. Histogram showing the semi-quantitative W_{it} index at site B

creep activity. We thereby exclude the year from the final rockfall reconstruction.

The chronology also indicates periods with a higher number of responses, such as 1972-1974, 1982-1984 and 1995-1996, with an increased dendrochronological signal as well (see Figure 9). The last 20 years of the chronology concentrate 35% of the identified GD, with virtually every year recording an event. Due to decreasing sample depth, the first 50 years of the chronology (1900-1950) showed a lower number of detected events (19%). The W_{it} index highlights the years 1952, 1955, 2003 and 2012 with a strong dendrochronological signal.

The recurrence interval calculated for each tree resulted in an average period of 27.4 years between two impacts on the same tree. In this regard, the RI varies between 6.4 and 105 years, while nine of the selected trees showed no GD in the tree-ring sequence. The spatial distribution of trees associated with different recurrence interval classes is depicted in Figure 10A, showing a decreasing of the RI as we move downslope and further away from the rockfall source area.

The visual counting of impact scars allowed us to identify a total number of 140 scars. Five of the 50 analyzed trees did not present any observable evidence of past rockfall impact, while the mean value of visible scars per tree for the rest of the 45 trees is 3.1. Results for each tree are illustrated in Figure 10B. The heights of the visible scars vary between 13 cm and 257 cm, with an average value of 67.8 cm. Around half of the scars (49.3%) are located between 20 and 60 cm, while another 23,5% lie between 60 and 100 cm. We only found two scars higher than 200 cm on the selected trees.

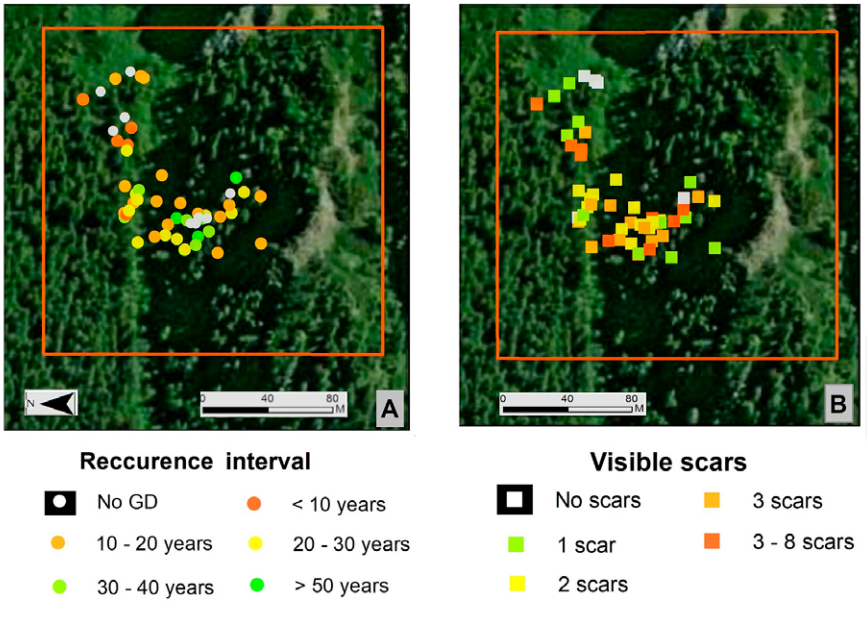

Figure 10. Recurrence interval classes for each tree - dendrogeomorphic approach (A) and visible scars counting approach (B)

Discussion

Snow avalanche reconstruction

The robustness of the snow avalanche chronology decreases in time, being biased by sample depth. Even if the I_t index is specially designed to lower the influence of sample size, the chronology clearly shows a rise in event frequency as the sample size increases. Because 75% of the analyzed trees at site A reached sampling height after 1975, a sample size of only 20 trees hinders efficient event detection in the first 25-year segment of the chronology. Another specific limitation of the dendrochronological approach states that major events tend to blur responses in the upcoming years (Stoffel & Bollschweiler, 2009). This could be the case for the 1976, 1988 and 1997 events, as each of them were followed by „avalanche-free" periods of 8 up to 12 years. In this sense, the 2005-2008 interval, with yearly reconstructed events, could point to the lower magnitude of the snow avalanches. Therefore, the avalanche frequency calculated for site A should be regarded as a minimum frequency. Most probably, snow flows and minor avalanches occur every winter, and the present reconstruction only highlights the major events.

During the last decade, several tree-ring-based snow avalanche reconstructions (Table 2) have been undertaken in the Southern Carpathians (Voiculescu & Onaca, 2012; 2014; Meseșan et al., 2014; 2017; 2018; Pop et al., 2015; 2017a; 2017b; Chiroiu et al. 2015; 2015; Voiculescu et al., 2016; Todea et al., 2020). Some of the event years reconstructed in the present paper were also found in other mountain ranges, such as the 1997 avalanche (in Parâng, Șureanu, and Piatra Craiului Mountains) and the 2005 avalanche (Parâng, Șureanu and Făgăraș Mountains). This suggests a common meteo-climatic trigger which could also be connected to the general athmospheric circulation.

Rockfall analysis

At site B, rockfall is the only geomorphological process causing growth disturbances in trees, except creep movements which mainly induce GDs in the form of reaction wood. Even if cambial damage (trunk wounds) can be inflicted by animal browsing and falling of nearby trees, we argue that the rockfall chronology is relevant for site B, at least for the peak years. Still, the actual rockfall rate is blurred by several factors: forest density, sample depth, stem diameter, hidden scars and the fact that a falling fragment generally injures more than one individual in its trajectory (Stoffel & Perret, 2006a; Stoffel et al., 2006b). While the RI is generally decreasing downslope (Figure 8A), we can also identify protected areas which show clusters of trees with no GD detected.

The scar counting approach does not yield sufficient information in our study, as the correlation between the number of visible scars and the number of reconstructed events is very low (r = 0.06). This result is mainly influenced by the bark thickness and the specific healing mechanisms of *Picea abies*, which seal the wounds faster than other tree species (Trappman & Stoffel, 2013).

Documented major events in the Sâmbăta Valley

One of the main reasons for including site A in the present analysis was the clear evidence of debris-flow

Table 2. Southern Carpathians tree-ring based snow avalanche reconstructions (avalanche years identified in the present study as well are marked with red)

Authors and year	Mountain range	No. of avalanche paths	Sampled trees	Major avalanche years
Voiculescu and Onaca, 2012	Bucegi Mts	1	62	1998, 2003
Voiculescu and Onaca, 2014	Bucegi Mts	2	114	1967, 1969, **1976**, 1981, 1985, **1988**, 1998, 2003
Meseșan et al., 2014	Parâng Mts.	1	22	1935, 1987, 1989, 1991, 1995, **1997**, 1999, 2003, 2004, **2005, 2008**, 2010, **2012**
Pop et al., 2015	Parâng Mts.	1	57	1915, 1937, 1942, 1956, 1966, 1983, 1986, **1997**, 1999, 2001, **2005, 2008**
Chiroiu et al., 2016	Făgăraș Mts.	1	33	**2005**
Pop et al., 2017a	Șureanu Mts.	1	54	1947, 1965, 1971, 1975, 1986, **1997**, 2000, **2005, 2007**, 2010
Pop et al., 2017b	Piatra Craiului Mts.	2	235	1985, 1987, 1991, 1995, **1997**, 1999, 2000, 2003, **2005, 2007**, 2009, 2011
Meseșan et al., 2017	Parâng Mts.	2	115	1998, **2005**
Meseșan et al., 2018	Parâng Mts.	3	235	1915, 1935, 1937, 1938, 1942, 1944, 1950, 1956, 1959, 1970, 1974, **1976**, 1980, 1982, 1983, 1986, 1987, **1988**, 1991, 1995, **1996, 1997**, 1998, 1999, 2000, 2001, 2003, **2005, 2006, 2008**, 2010, **2012**
Todea et al., 2020	Parâng Mts.	1	57	1994, **1997**, 1999, **2005, 2007, 2008**, 2010, **2012**, 2014, 2016, 2018

occurrence and the recorded major event which took place in 1968 (Cioacă, 1970). The process was triggered in the night between the 21st-22nd of August, after a period of heavy rainfall which had maximum values on the 20th and 21st of August. Even if the GD analysis points to some processes occurring in spring and summer (which have been excluded from the avalanche reconstruction), unfortunately, none of the selected trees showed evidence of the 1968 debris-flow event. The only print observed is found in the forest stand's age structure, colonizing site A (Figure 11). Cioacă (1970) notes that the debris flow had an unusual trajectory being deviated to the right. Age analysis shows that all of the sampled trees in the southern part of the debris fan germinated in the early ,70s or later. Destructive events can remove entire parts of forest stands, thus erasing tree-ring evidence of past processes. Regarding the results of our analysis, we argue that this could be the case for the 1968 event. Another major debris-flow event in the Sâmbăta valley occurred in August 2007 and affected the forest road, the tourist trail, a few cars and damaged electricity poles (Petre et al., 2012).

In 1996 a snow avalanche affected the Mountain Rescue cabin located 160 m to the south of Valea Sâmbetei chalet (Petre et al., 2012). Moreover, in February 2012, another snow avalanche affected the kitchen of the Valea Sâmbetei chalet.

Following heavy rainfall in April 2021, a giant snow avalanche occurred in the Pârâul Vârtejelor creek, which is a small tributary of Sâmbăta valley on the eastern slope. The major event has broken hundreds of trees and transported most of them into the Sâmbăta channel (Figure 12). The deposited tree trunks entirely covered a valley sector of around 200 meters at the confluence with Pârâul Vârtejelor. In mid-July 2021, a snow deposit with a thickness of 1-3 m, almost entirely covered by dead trees, was

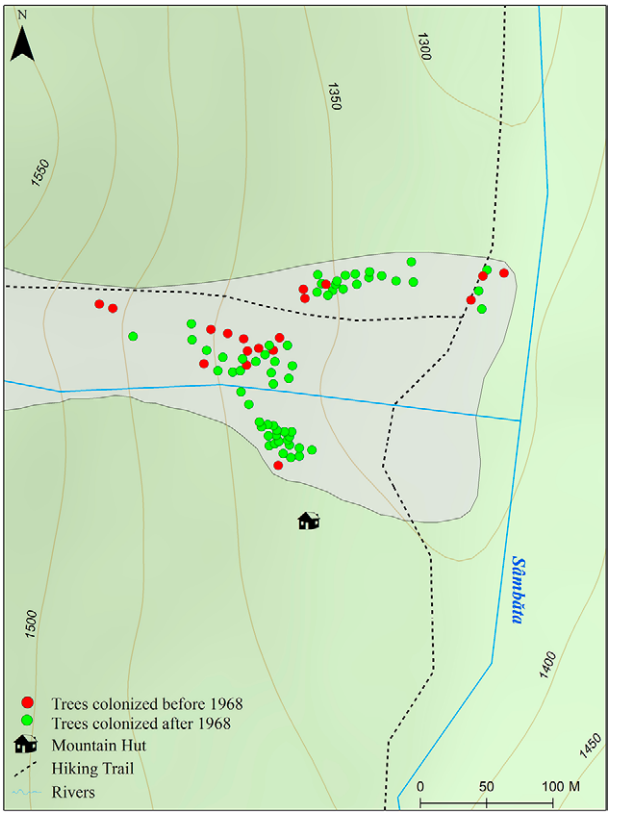

Figure 11. Succession analysis (trees established before the debris flow event in 1968 - RED, trees established after 1968 - GREEN)

Figure 12. Effects of the major 2021 snow avalanche event on the eastern slope of the Sâmbăta Valley: clear signs of avalanche destruction along the newly created path (a) and the several meters thick wood and debris deposit located in the run-out zone at the confluence with the Sâmbăta Valley (b)

still present in the Sâmbăta Valley at 1150 m. The avalanche also destroyed the forest road on the eastern side of the Sâmbăta Valley. In the same year, in March, the snow depth reached 2 m at 1400 m, and the Valea Sâmbetei chalet was closed for tourists due to closed trails and high risks of avalanches (https://www.monitorfg.ro/2021/03/23/cabana-valea-sambetei-acoperita-de-zapada/).

Conclusions

In the present paper, we reconstructed the activity of snow avalanches and rockfall at two sites located in the Sâmbăta Valley (Romanian Carpathians) using dendrogeomorphology. Regarding the snow avalanche reconstruction, the young age of the majority of the trees limits the timespan to 70 years. The results highlight 13 major avalanche events which occurred on the studied path in the period 1950-2020, with the highest dendrogeomorphic signal obtained for 1988, 1997 and 2012. The minimum return period of major events is 3.3 years, but most probably, weak to moderate avalanches can occur every year. This is a common limitation of the dendrogeomorphic method, due to the fact that tree-rings exhibit anatomical responses only if the respective tree is impacted by the avalanche. Therefore, it should be noted that the reconstructed frequency is valid only for major events. The rockfall reconstruction at site B highlights years with more intense process activity: 1952, 1955, 2003 and 2012. As falling rocks can leave trees unharmed in their downslope trajectory, some events are impossible to reconstruct by the tree-ring approach. On the other hand, downslope moving fragments can impact more than one tree, therefore altering the event reconstruction. Eventually, in the same respect, old and hidden scars are hard or impossible to identify and date.

Nevertheless, our study demonstrates that geomorphic hazards in the Sâmbăta Valley, a top-rated touristic destination for hikers and off-piste skiers, are remarkably active. The most recent event occurred in April 2021 on the valley's eastern slope. This giant snow avalanche created a new avalanche path by severely affecting the forest cover, indicating that if specific conditions and triggers are met, destructive and life-threatening events can also occur in areas with no signs of past disturbances. Regarding tourist exposure to geomorphic hazards, the main trail, which runs along the valley up to the Fereastra Mare saddle, is repeatedly crossed by avalanche couloirs and debris flow cones. Also, secondary trails, which climb the eastern slope (Piatra Caprei trail) and western slope (Arsenie Boca shelter), have sectors located beneath steep unconsolidated rock walls. Finally, tourists visiting the Sâmbăta Valley should be more effectively informed about the geomorphic hazards they are exposed to by installing warning signs for rockfall, snow avalanches and debris flows.

In future studies on geomorphic hazards related to snow avalanches, debris flows and rockfall, it is of utmost importance to identify and understand the complex topo-climatic factors responsible for triggering catastrophic events.

Aknowledgements

The research leading to these results has received funding from the NO Grants 2014-2021, under Project contract no. 30/2020.

References

Bălteanu, D. (1997). Geomorphological hazards of Romania. In: *Geomorphological hazards of Europe*, Embleton, C., Embleton-Hamann, C. (eds.). Amsterdam: Elsevier, 409-427.

Bollati, I., Crosa Lenz, B., Golzio, A., & Masseroli, A. (2018). Tree rings as ecological indicator of geomorphic activity in geoheritage studies. *Ecological indicators*, 93, 899-916. 10.1016/j.ecolind.2018.05.053

Bollschweiler, M., Stoffel, M., Ehmisch, M., & Monbaron, M. (2007). Reconstructing spatio-temporal patterns of debris-flow activity using dendrogeomorphological methods. *Geomorphology*, 87, 337–351, 10.1016/j.geomorph.2006.10.002.

Bräker, O.U. (2002). Measuring and data processing in tree-ring research - a methodological introduction. *Dendrochronologia*, 20, 203–216, 10.1078/1125-7865-00017.

Casteller, A., Villalba, R., Araneo, D., & Stöckli, V. (2011). Reconstructing temporal patterns of snow avalanches at Lago del Desierto, southern Patagonian Andes. *Cold Regions Science and Technology*, 67, 68-78. 10.1016/j.coldregions.2011.02.001.

Casteller, A., Stoffel, M., Crespo, S., Villalba, R., Corona, C., & Bianchi, E. (2015). Dendrogeomorphic reconstruction of flash-floods in the Patagonian Andes. *Geomorphology*, 228, 116-123, 10.1016/j.geomorph.2014.08.022.

Chiroiu, P., Stoffel, M., Onaca, A., & Urdea, P. (2015). Testing dendrogeomorphic approaches and thresholds to reconstruct snow avalanche activity in the Făgăraș Mountains (Romanian Carpathians). *Quaternary Geochronology*, 27, 1–10, 10.1016/j.quageo.2014.11.001.

Chiroiu, P., Ardelean, A.C., Onaca, A., Voiculescu, M., & Ardelean, F. (2016). Assessing the anthropogenic impact on geomorphic processes using tree-rings: a case study in the Făgăraș Mountains (Southern Carpathians), *Carpathian Journal of Earth and Environmental Sciences*, 11(1), 27-36.

Cioacă, A. (1970). Un torent de grohotișuri în Munții Făgăraș [A torrent of talus in the Făgăraș Mountains]. *Terra*, 5, 39-43.

Copien, C., Frank, C., & Becht, M. (2008). Natural hazards in the Bavarian Alps: a historical approach to risk assessment. *Natural Hazards*, 45, 173-181. 10.1007/s11069-007-9166-6.

Corona, C., Rovera, G., Lopez Saez, J., Stoffel, M., & Perfettini, P. (2010). Spatio-temporal reconstruction of snow avalanche activity using tree rings: Pierres Jean Jeanne avalanche talus, Massif de l'Oisans, France. *Catena*, 83, 107-118. 10.1016/j.catena.2010.08.004.

Favillier, A., Guillet, S., Morel, P., Corona, C., Lopez Saez, J., Eckert, N., Ballesteros Cánovas, J.A., Peiry, J-L., & Stoffel, M. (2017). Disentangling the impacts of exogenous disturbances on forest stands to assess multi-centennial tree-ring reconstructions of avalanche activity in the upper Goms Valley (Canton de Valais, Switzerland). *Quaternary Geochronology*, 42, 89-104. 10.1016/j.quageo.2017.09.001.

Kogelnig-Mayer, B., Stoffel, M., Schneuwly-Bollschweiler, M., Hübl, J., & Rudolf-Miklau, F. (2011). Possibilities and limitations of dendrogeomorphic time-series reconstructions on sites influenced by debris flows and frequent snow avalanche activity. *Arctic, Antarctic, and Alpine Research*, 43, 649–658. 10.1657/1938-4246-43.4.649.

Mainieri, R., Lopez Saez, J., Corona, C., Stoffel, M., Bourrier, F., & Eckert, N. (2019). Assessment of the recurrence intervals of rockfall through dendrogeomorphology and counting scar approach: A comparative study in a mixed forest stand from the Vercors massif (French Alps). *Geomorphology*, 340. 10.1016/j.geomorph.2019.05.005.

Meseșan, F., Pop, O.T., & Gavrilă, I. (2014). Snow avalanche activity in Parâng Ski Area revealed by tree rings. *Studia UBB Geographia LIX* 2, 47-56.

Meseșan, F., Pop, O.T., & Gavrilă, I. (2017). Calculating snow-avalanche return period from tree-ring data. *Natural Hazards*. 10.1007/s11069-018-3457

Meseșan, F., Man, T.C., Pop, O.T., & Gavrilă, I.G. (2018). Reconstructing snow-avalanche extent using remote sensing and dendrogeomorphology in Parâng Mountains. *Cold Regions Science and Technology*, 157, 97-109. 10.1016/j.coldregions.2018.10.002

Micu, M., Jurchescu, M., Șandric, I., Mărgărint, M.C., Chițu, Z., Micu, D., Ciurean, R., Ilinca, V., & Vasile, M. (2017). *Mass movements*. In: *Landform Dynamics and Evolution in Romania*, Rădoane, M., Vespremeanu-Stroe, A. (eds.). Switzerland: Springer, 765-821.

Perret, S., Dolf, F., & Kienholz, H. (2004). Rockfall into forests: analysis and simulation of rockfall trajectories – considerations with respect to mountainous forests in Switzerland. *Landslides*, 1, 123–130. 10.1007/s10346-004-0014-4.

Petre, A.C., Nedelea, A., Comănescu, L., & Munteanu, A. (2012). Terrain susceptibility to geomorphological processes and their impact on tourism infrastructure in the Sâmbăta valley (Făgăraș Mountains). *Procedia Environmental Sciences*, 14, 257-266. 10.1016/j.proenv.2012.03.025.

Pop, O.T., Gavrilă, I.G., Roșian, G., Meseșan, F., Decaulne, A., Holobâcă, I.H., & Anghel, T. (2015). A century-long snow avalanche chronology reconstructed from tree-rings in Parâng Mountains (Southern Carpathians, Romania). *Quaternary International*, 415, 230–240. 10.1016/j.quaint.2015.11.058

Pop, O.T., Meseșan F., Gavrilă I.G., & Timofte C. (2017a). Tree-ring-based reconstruction of snow avalanche frequency in Șureanu Mountains (Southern Carpathians, Romania). *Proceedings of the Romanian Geomorphology Symposium, 33rd edition,* Iași, Mihai Niculiță, Mihai Ciprian Mărgărint (eds.), Editura Universității Al. I. Cuza, Iași, 89-91.

Pop O.T., Munteanu A., Meseșan F., Gavrilă I.G., Timofte C., & Holobâcă, I.H. (2017b). Tree–ring–based reconstruction of high–magnitude snow avalanches in Piatra Craiului Mountains (Southern Carpathians, Romania). *Geografiska Annaler Series A – Physical Geography,* 100 (2), 99–115. 10.1080/04353676.2017.1405715

Pop, O.T., Munteanu, A., Meseșan, F., Gavrilă, I.G., Timofte, C., & Holobâcă, I.H. (2018). Tree-ring-based reconstruction of high-magnitude snow avalanches in Piatra Craiului Mountains (Southern Carpathians, Romania). *Geografiska Annaler*, 100(2), 99–115.

Rinn, F. (2013). *TSAP-Win Time Series Analysis and Presentation for Dendrochronology and Related Applications - User Reference*. Heidelberg: Rinntech, pp. 91.

Ruszkiczay-Rüdiger, Z., Kern, Z., Urdea, P., Braucher, R., Madarász, B., & Schimmelpfennig, I. (2016). Revised deglaciation history of the Pietrele–Stânișoara glacial complex, Retezat Mts, Southern Carpathians, Romania. *Quaternary International*, 415, 216–229. 10.1016/j.quaint.2015.10.085.

Schneuwly, D.M., Stoffel, M., & Bollschweiler, M. (2008). Formation and spread of callus tissue and tangential rows of resin ducts in Larix decidua and Picea abies following rockfall impacts. *Tree Physiology*, 29, 281–289, 10.1093/treephys/tpn026.

Schneuwly-Bollschweiler, M., & Schneuwly, D.M. (2012). How fast do European conifers overgrow wounds inflicted by rockfall?. *Tree Physiology*, 32, 968-975. 10.1093/treephys/tps059.

Shroder, JR. J.F. (1980). Dendrogeomorphology: review and new techniques of tree-ring dating. *Progress in Physical Geography,* 4(1), 161-188. 10.1177/030913338000400202.

Stoffel, M., Lievre, I., Monbaron, M., & Perret, S. (2005). Seasonal timing of rockfall activity on a forested slope at Täschgufer (Valais, Swiss Alps) – a dendrochronological approach. *Zeitschrift für Geomorphologie*, 49, 89–106.

Stoffel, M., & Perret, S. (2006a). Reconstructing past rockfall activity with tree rings: some methodological considerations. *Dendrochronologia*, 24, 1–15. 10.1016/j.dendro.2006.04.001.

Stoffel, M., Bollschweiler, M., & Hassler, G.R. (2006b). Diferentiating events on a cone influenced by debris-flows and snow avalanche activity – a dendrogeomorphological approach. *Earth Surface Processes and Landforms*, 31(11), 1424-1437, 10.1002/esp.1363.

Stoffel, M. (2008). Dating past geomorphic processes with tangential rows of traumatic resin ducts. *Dendrochronologia*, 26(1), 53-60, 10.1016/j.dendro.2007.06.002.

Stoffel, M., & Bollschweiler, M. (2009). What tree rings can tell about earth-surface processes. Teaching the principles of dendrogeomorphology. *Geography Compass*, 3, 1013-1037, 10.1111/j.1749-8198.2009.00223.x.

Stoffel, M., Butler, D.R., & Corona, C. (2013). Mass-movements and tree-rings: A guide to dendrogeomorphic field sampling and dating. *Geomorphology*, 200, 106-120, 10.1016/j.geomorph.2012.12.017.

Stoffel, M., & Corona, C. (2014). Dendroecological dating of (hydro-)geomorphic disturbances in trees. *Tree-Ring Research*, 70, 3–20, 10.3959/1536-1098-70.1.3.

Tichavsky, R., Šilhán, K., & Tolasz, R. (2017). Tree ring-based chronology of hydro-geomorphic processes as a fundament for identification of hydro-meteorological triggers in the Hrubý Jeseník Mountains (Central Europe). *Science of the Total Environment*, 579, 10.1016/j.scitotenv.2016.12.073

Todea, C., Pop, O., & Germain, D. (2020). Snow–avalanche history reconstructed with tree rings in Parâng Mountains (Southern Carpathians, Romania). *Revista de Geomorfologie*, 22, 73-85, 0.21094/rg.2020.099

Trappmann, D., & Stoffel, M. (2013). Counting scars on tree stems to assess rockfall hazards: A low effort approach, but how reliable?. *Geomorphology*, 180–181, 180–186, 10.1016/j.geomorph.2012.10.009.

Voiculescu, M., & Ardelean, F. (2012). Snow avalanche disturbance of high mountain environment. Case study – the Doamnei glacial valley, the Făgăraș Massif – Southern Carpathians. *Romanian Carpathians*, 7, 95-108.

Voiculescu, M., & Onaca, A. (2012). Snow avalanche assessment in the Sinaia ski area (Bucegi Mountains, Southern Carpathians) using the dendrogeomorphology method, *Area*, 45(1), 109–122.

Voiculescu, M., & Onaca, A. (2014). Spatio-temporal reconstruction of snow avalanche activity using dendrogeomorphological approach in Bucegi Mountains Romanian Carpathians, *Cold Regions Science and Technology*, 104–105, 63–75.

Voiculescu, M., Onaca, A., & Chiroiu, P. (2016). Dendrogeomorphic reconstruction of past snow avalanche events in Bâlea glacial valley-Făgăraș massif (Southern Carpathians), Romanian Carpathians. *Quaternary International*, 415, 286-302, 10.1016/j.quaint.2015.11.115.

Internet 1: Monitorul https://www.monitorfg.ro/2021/03/23/cabana-valea-sambetei-acoperita-de-zapada/ (05.04.2022).

ISSN 0354-8724 (hard copy) | ISSN 1820-7138 (online)

Human-nature Relationship and Public Perception of Environmental Hazards along the Maros/Mureş River (Hungary and Romania)

György Sipos[A*], Viktória Blanka-Végi[A], Florina Ardelean[B], Alexandru Onaca[B], Zsuzsanna Ladányi[A], Attila Rácz[C], Petru Urdea[B]

Received: August 15, 2022 | Revised: September 28, 2022 | Accepted: September 30, 2022
doi: 10.5937/gp26-39657

Abstract

Public participation is increasingly important in flood and environmental management planning. Accordingly, understanding the attitude of local society to natural values and their relations with the environment is highly important to realize successful development projects. This study aimed to analyze the human-nature relationship, the public perceptions of environmental hazards and people's engagement with water management related and human interventions at Maros/Mureş River through a public survey. The survey was carried out in 11 Romanian and Hungarian settlements using the random walking method to interview the local public. The results show that people are a little pessimistic concerning the state of the river, and there are misbeliefs about the general problems affecting its present environmental status. Meanwhile, the perception of flood hazard is governed by the fading memory of the last high-risk flood event in 1970. The engagement of residents is mostly affected by socio-demographic parameters. However, the regularity they visit the river is also very important. Consequently, informing people on apparent environmental issues and processes can greatly help the socially inclusive implementation of water management measures along the river.

Keywords: Maros/Mureş River; public survey; human-nature relationship; human interventions; river and floodplain management

Introduction

River and floodplain ecosystems are under the pressure of several factors. The most important of these are intensifying rate of human interventions and climate change (Tockner & Stanford, 2002), which can frequently lead to changes in water regime (Kiss et al., 2019), deterioration of water quality (Muyere & Moyce, 2017), degradation of floodplain ecosystems (Entwistle et al., 2019) and morphological changes (Kiss & Blanka, 2012; Amissah et al., 2018). Besides obvious natural hazards, rivers and related ecosystems are also important in providing a diverse set of services for society, such as recreation, food, health, agriculture, and transportation (Hale et al., 2019; Jähnig et al., 2022). Therefore, river-related resources and the effective functioning of the natural environment have high importance to the local population (Wang et al., 2016, Oyedotun

[A] University of Szeged, Department of Geoinformatics, Physical and Environmental Geography, 6722 Szeged, Egyetem u. 2-6, Hungary, gysipos@geo.u-szeged.hu, blankav@geo.u-szeged.hu, ladanyi@geo.u-szeged.hu
[B] University of West Timisoara, Department of Geography, Str. Pestalozzi 16A, Timisoara, 300115, România, florina.ardelean@e-uvt.ro, alexandru.onaca@e-uvt.ro, petru.urdea@e-uvt.ro
[C] University of Szeged, Department of Sociology, 6722 Szeged, Petőfi sgt. 30-34, Hungary, atiracz@socio.u-szeged.hu
[*] Corresponding author: György Sipos; e-mail: gysipos@geo.u-szeged.hu

& Ally, 2021). Water management lately recognized that all these challenges and requirements should be managed in their complexity; thus, a new concept: Integrated Flood and Environmental Risk Management (FERM), has been developed, recognizing the close connection between managing flood risk and managing risks to the physical environment and the biological ecosystems (Osti, 2018). This concept also emphasizes the necessity of stakeholder inclusion, including community participation.

Consequently, the inclusion of local stakeholders and the public in the planning process of flood and environmental management plans and interventions is a key question, as the inputs from locals can minimize the risk of inadvertent negative consequences, and at the same time, local knowledge and interests can make positive contributions to projects (Osti, 2018). Public participation in the planning process of flood and environmental management of rivers is also encouraged by the EU Water Framework Directive (EU WFD 2000), which is advised to allow people to influence the outcome of plans and working processes. Public involvement should involve awareness raising of flood and environmental hazards and risks and address also the need to increase the public's understanding of the problems and the need for solutions (Hophmayer-Tokich, 2005).

To realize an efficient public inclusion, it is important to understand the human–nature relationship, i.e. to reveal the many ways humans are linked with the natural environment (Seymour, 2016) and the environmental factors influencing the perceptions of the river-floodplain ecosystem (Cockerill, 2015; Flotemersch & Aho, 2021). For analyzing the human-nature relationship and the public's perceptions of environmental values and hazards, qualitative or quantitative social surveys, e.g. questionnaires, can be an effective method and help to comprehensively analyze the perceptions and attitudes of the target population (White et al., 2005).

Rivers, such as the Maros/Mures, and their floodplains are important natural resources in the Carpathian Basin, providing several benefits for the ecosystem and society. The Maros/Mures River is the most significant water resource for irrigation and industrial activity in the Hungary-Romania cross-border region. Besides, it feeds a thriving riparian ecosystem and has a unique geomorphological character. Several factors endanger the availability and quality of its resources. Among these, human interventions and climate change have to be emphasized.

The primary objective of this study was to revealthe relationship of local people to the river and its floodplain ecosystem and their perception of environmental hazards and human interventions in order to identify public preferences and people's engagement with water management issues. Additionally, we also aimed to understand the role of socio-demographic, residential and life-style related parameters behind the environmental awareness of local communities.

Study area

The study was carried out in the south-eastern part of the Carpathian Basin along the lowland section of the Maros/Mureş River, belonging to both Romania and Hungary. The area of the river's catchment is approximately 30 000 km², and situated mostly in Romania (92%). Its total length is 769 km, while its so-called lowland section from Lipova to Szeged is 175 km, out of which 125 km is situated in Romania, 22 km is part of the border between Romania and Hungary, and 28 km is situated in Hungary (Laczay, 1975) (Fig. 1).

The variability of the water stage is high even in the lowland section. Two major floods may develop annually on the river. The first is due to snowmelt in early spring, and the second is caused by early summer rainfall, usually in June (Boga & Novaky, 1986). The greatest flood on record occurred in 1970 and caused severe problems along the entire river. After 1970 significant floods occurred in 1974, 1975, 1981, 1998, 2000 and 2006. Following the April-June floods, the rest of the year is characterized by low stages. During the past 20 years, the length and intensity of low stages increased, partly due to climate change and increasing reservoir capacity on the tributaries in the upland catchment (Konecsny & Bálint, 2009).

Along the Hungarian section, the floodplain is dominated by forests, but in the surroundings of the settlements, croplands and more or less cultivated gardens can also be found. At the same time, the Romanian floodplain is dominated by grasslands, although floodplain forests also occur in smaller or larger patches (Oroszi, 2009). The most important human impacts at present are reservoir construction since the 1980s' on the upland reaches and gravel and sand extraction on the lowland sections (Konecsnyi & Balint, 2009). Gravel and sand have been quarried from the river for a long time; however, extraction volume has increased significantly in the past decades, especially in Romania. The activity is the most intensive on the Pauliş-Mandruloc section, where the banks and the channel have practically quarried away.

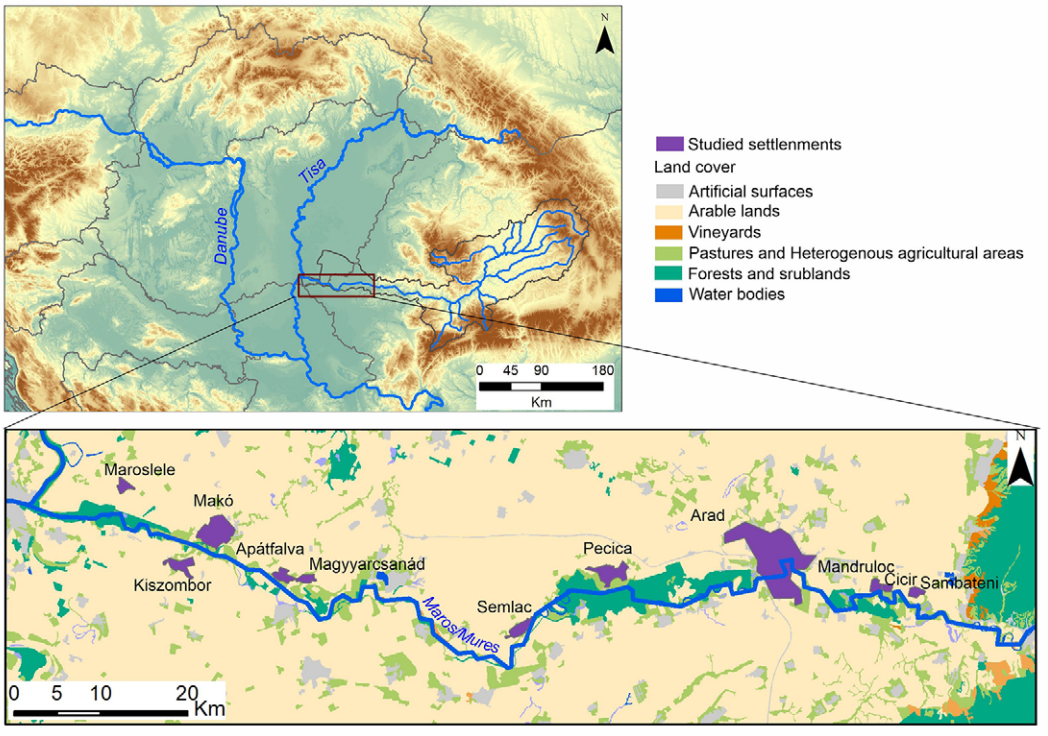

Figure 1. Location of the studied settlements along the Maros/Mures River

Data and methods

The perception and opinion of people on the Maros/Mureş River and its environment were investigated by a public survey. The survey was carried out on six Romanian settlements: Arad (county seat and largest town in the region, population over 160 000), Pecica (a smaller town, population about 13 000) and four villages with a population below 5 000 (Sâmbâteni, Cicir, Mandruloc and Semlac) (RPL, 2011); and on 5 Hungarian settlements: Makó (the largest settlement on the Hungarian section, population about 23 000), and on four villages with population below 5000 (Magyarcsanád, Apátfalva, Kiszombor and Maroslele) (KSH 2018) (Fig. 1).

The overall methodology of the research was both qualitative and quantitative. As Letenyei (2004) emphasizes, the two approaches can and should be combined in social research, as certain issues can only be evaluated based on expert-oriented interviews, while the overall representativity can only be reached by alienating ourselves from the respondents and using statistical methods (Bryman, 2001).

During social surveys, reliability and validity are key issues. Reliability can be increased by ensuring the representativity of the sampling (Babbie, 2003; Neuman, 2006; Firebaugh, 2008), while validity highly depends on good question formulation and that responders understand the questions and provide meaningful answers (Letenyei & Racz, 2011). In the case of the present research, representativity and reliability were increased by questioning a large sample (0.2 % of the population at Arad, 1 % at Mako and 1-2 % at other settlements) and by designating separate interview zones at each settlement either to cover the entire settlement or to represent each of the urban geographical districts. The survey was made using the random walking method, meaning that the interviewers were allowed to ask anybody within a previously set zone. The delineation of interview zones also prevented the repeated questioning of respondents. The number of required questionnaires at a given settlement was determined based on the settlement's weight concerning the region's total population. In all, 1062 surveys were finally completed. The validity of the surveys was based on preliminary interviews performed in three settlements along the studied section of the river to test the questions of the survey and on the local experience of experts studying the geographical and environmental problems along the river for a long time. The dataset of the questionnaires was processed and analysed in SPSS software.

The questionnaire was mostly composed of closed-ended nominal, ordinal and multi-optional questions. Warm-up questions were related to the major challenges of the settlement and the values

worth of protection. In the second set of questions, respondents were asked about general environmental issues and problems related to the Maros/Mureş River. Subsequently, locals' relationship to the river was explored, i.e. how frequent and what for they visit it. Finally, their preference for future management of problems and developments was investigated. The interview was closed by entering some of the respondent's social parameters (age, gender, education, occupation).

Results

Human-nature relationship

The perception of the local population on the natural values was surveyed to reveal their preferences and opinion about the state of the environment and the factors influencing public perceptions. Furthermore, the engagement of the people with the river-floodplain ecosystem was assessed by their interactions with the river and the usage of the recreational and provisioning ecosystem services.

Perceptions of natural values along the Maros/Mureş

The opinion of the local population about the natural values was assessed by asking respondents to rank the importance of different natural values in their environment. The Maros/Mureş River was ranked to be the 2nd and 3rd most important natural value in Hungarian and Romanian settlements, respectively (Fig. 2). The first place was taken by forests in Romania and by clean air in Hungary. It is noteworthy that in the case of Arad, the importance of forests (40%) outscored clean air (27%), which we expected to be in the first place. The Maros/Mureş was ranked to 1st place mostly by respondents with a university degree, i.e. 32% of them mentioned it as the most important natural value in or around their settlement. In comparison, these values were 25% and 19% for people of secondary and primary educational background, respectively. Those who visit the Maros/Mureş regularly (73% of respondents) were more concerned about the river (27%) and forests (34%) than those who did not. The latter group voted mostly for clean air (46%).

As the condition of the riverside greatly determines the local use of the river, the opinion of the respondents about the state of the river's environment was surveyed by asking their opinion on how well the riverside is managed at their settlement and whether their community respects the river and its natural values or not. The evaluation of the people's opinion about the management of the riverside was made on a 4-point rating scale. In this respect, a significant difference was found between the two countries: Romanian and Hungarian settlements scored on average 2.17 and 2.90, respectively (Fig. 3a). In Romania, the worst results were received at Cicir (average score: 1.33) and Mandruloc (1.66). In these two villages, none of the respondents thought the riverside was well managed, which is understandable as the river is most affected by gravel and sand quarrying at these settlements. The situation in Arad (2.28) and Pecica (2.15) seems to be better; here, more than 30% thought the riverside was rather well managed or well managed. This suggests that great-scale quarrying and the destruction of natural values are striking for locals too. On the Hungarian side, the state of the riverside was evaluated significantly better. The best value was measured at Makó (3.05); here, more than 70% of respondents rated the riverside rather well managed or well managed, which is definitely due to the recreational developments (adventure park) made recently on the riverside. In Hungary, the lowest value was measured on the anyway unregulated and unmanaged border section of the river.

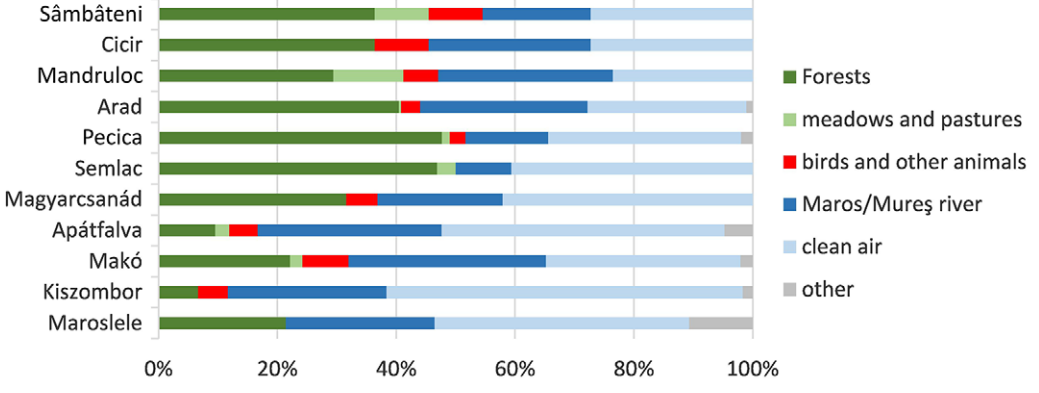

Figure 2. The relative importance of natural values for respondents at the surveyed settlements

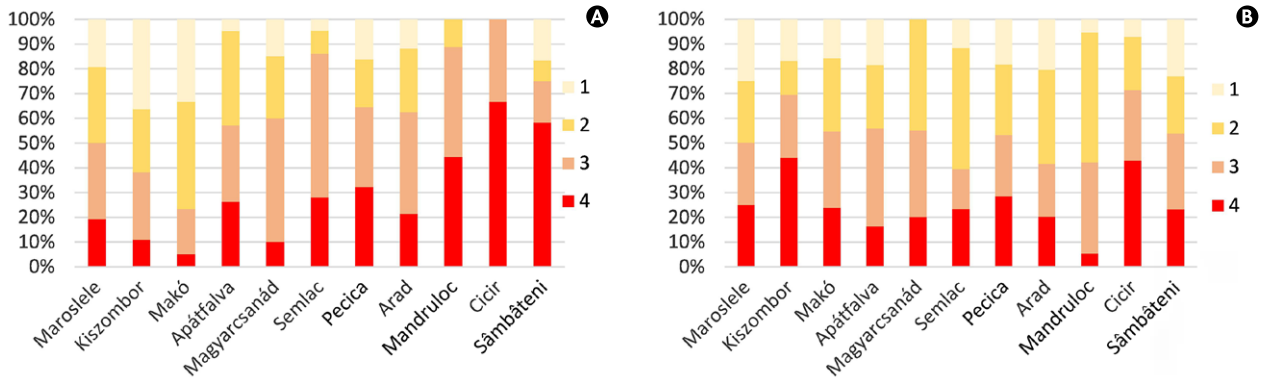

Figure 3. a) The evaluation of the state of the riverside (4 - well managed, 3 - rather well managed, 2 - rather unmanaged, 1 - unmanaged). b) Public opinion about whether the local community respects the river and its natural values or not (4 –respect, 3 – yes rather than no, 2 - no rather than yes, 1 – not respect)

It was also surveyed whether the local community respects the river and its natural values or not. The evaluation was also made on a 4-point rating scale. Only slight differences were found between the two countries, as average values were 2.49 and 2.69 in Romania and Hungary, respectively. Therefore, on a community level, people feel that the river is slightly more valued in Hungary than in Romania. In terms of settlement types, we did not find significant variability. It is positive that even at the settlement where the lowest ranking was measured, 40% of the respondents thought that their community respected the river and its natural values (Fig. 3b).

Interaction of the people with the floodplain ecosystem

The interaction of the local people with the river/floodplain ecosystem was surveyed by exploring the respondent's habits of visiting the river and the type of recreational and provisioning benefits they use.

73% of the respondents claimed that they visit the river regularly. There is a slight but not very significant difference between genders in this respect, as 78% of men and 68% of women answered yes to this question. Differences can also be observed between different age groups. The proportion of people who visit the river is decreasing with age. Under the age of 50, 80% visited the river, while it was 68% over 50 and only 55% over 65. A much more significant dependence was found in terms of the educational level of respondents. Only 49% of people with primary education visit the river regularly, while at those with secondary and tertiary levels this value grows to 75% and 89%, respectively. This observation can be explained by various factors, e.g. differences in the overall mobility, economic situation and age of the respondents. Visiting the river seems to have a clear relationship with the physical distance and the accessibility of the riverside from the settlement. The most important finding is that more than two-thirds of local people are related in some ways to the river; thus, their needs and expectations must be considered when planning river management and development measures. (Fig. 4)

Those who visit the river regularly mostly go for walking at the riverside, fishing, and bathing in the river, regardless of location, age, gender, and educational level (Fig. 5). In Romania, 88%, in Hungary, 79% of respondents who visit the river go there with the purpose to take a walk. The difference is not significant and is caused mainly by the results of Arad (93%). Around one-fourth of the people visiting the Maros/Mureș do fishing and angling. The third most

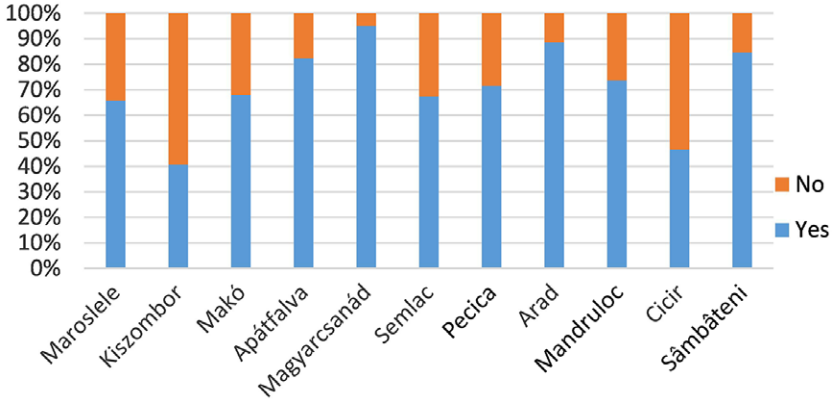

Figure 4. The proportion of those who visit the river regularly

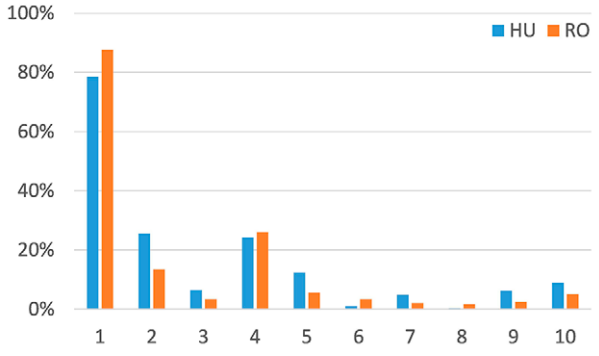

Figure 5. The distribution of activities made at the Maros/Mureş (1: walking on the riverside, 2: bathing, 3: water sports, 4: fishing and angling, 5: cultivating land, 6: grazing animals, 7: collecting firewood, 8: washing cars, I: taking away sand, J: other)

popular activity was bathing. In this respect, Hungarian results were significantly higher. Similar differences were found in the case of water sports, probably due to the availability of more facilities along the Hungarian section. In the case of agricultural activities, cultivation of land is generally more popular in Hungary; however, in Romania, it shows high spatial variability. Both crop growing and animal grazing are widely performed activities in the smaller villages upstream of Arad; there, 30-60% marked cultivation of lands and 20-33% marked animal grazing as major activities.

Environmental hazards

The perception of the local population on environmental problems and hazards and some adaptation and development measures were also surveyed. To an open-ended question about the last environmental problem the responder had met, 25% of the respondents reported something in relation to the river. The settlements where river-related answers were the most frequent were Arad (33%), Mandruloc (60%) and Apatfalva (47%). Responders at Mandruloc emphasized the destruction of the river bank by sand extraction, while at Apátfalva, people were mostly concerned about pollution and the state of forests along the river.

The respondents were also asked to select three environmental hazards from a list of seven which affect the Maros/Mureş the most. On both sides of the border, solid-waste disposal was considered the most important issue (Fig. 6). This is understandable, as plastic bottles drifting on the river and heaps of garbage on the floodplain are well visible and understandable problems for everybody. The second and third places were taken by industrial and sewage water contamination. Although water quality has improved considerably through the years, the Maros/Mureş has still got a quite bad reputation among locals in this respect. Sewage water was highlighted by the greatest number of respondents in Arad (71%) and Pecica (69%), while industrial pollution was mostly emphasized in Arad (50%) and Apatfalva (50%). Interestingly, Romanian respondents (except at Arad) were significantly less worried about industrial pollution than Hungarians. However, in preliminary interviews, Hungarians said water quality problems are mostly related to the Romanian industry.

Tree logging seems to be a significant problem on both sides of the border; however, Hungarians assume it is a slightly greater problem, which is interesting if we consider that Romanian respondents were much more concerned about the state of forests in an earlier question. A possible reason can be that at settlements, such as Cicir, hardly any forests have remained by now. According to Romanian respondents, gravel and sand quarrying proved to be the fourth most important environmental problem affecting the river. Unsurprisingly, residents of Cicir (93%) and Sambateni (92%) were very concerned, though one-third of respondents at Arad also emphasized this issue. Climate change was considered a less important hazard. Interestingly, going downstream, people were increasingly concerned about this issue.

The environmental state of the river is considered to be changing by 59% of respondents (67% of Hungarians and 54% of Romanians). In terms of the direction of change (positive or negative), Romanian respondents are more pessimistic. The distribution of answers was affected by settlement type; urban residents felt positive changes a little more frequently than people living in villages. The difference might be that people living in Arad, Makó or Pecica can experience more infrastructural developments next to the river.

Respondents were also asked what information circulated on the river in their community. Most of the answers were related to increasing pollution and

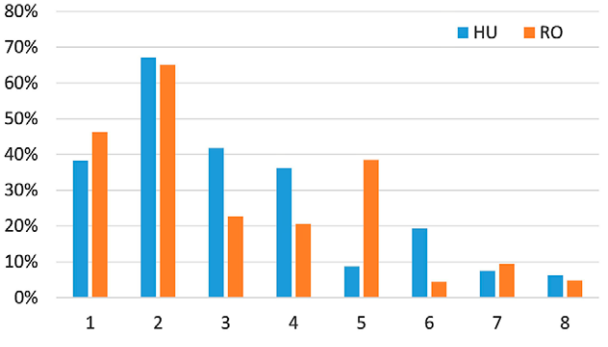

Figure 6. The relevance of various environmental problems along the Maros/Mureş according to the respondents (1. municipal wastewater effluents, 2. solid-waste disposal, 3. industrial pollution, 4. logging, 5. sand and gravel quarrying, 6. climate change, 7. artificial structures on the floodplain, 8. other)

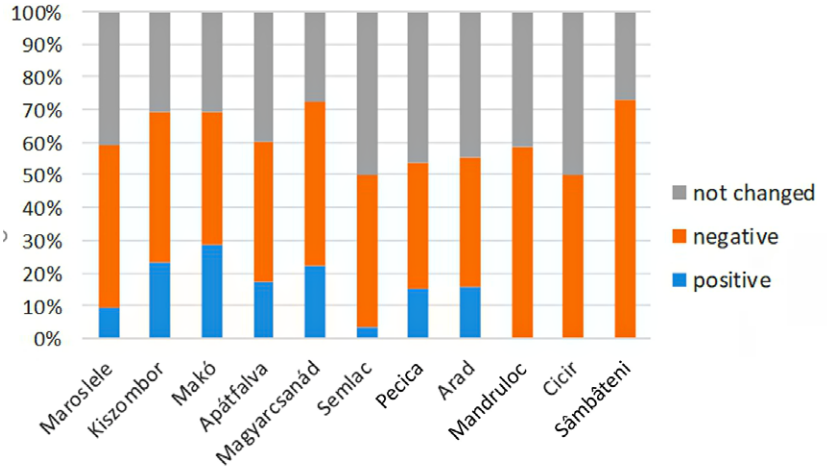

Figure 7. Public perception of changes in the environmental state of the river

decreasing water levels as the most widely known and believed changes. Positive answers mostly referred to riverside developments in Makó and Arad (Fig. 7).

As a consequence of the hydrological character of the river, flooding is a significant natural hazard. However, only 52% and 32% of respondents are anxious about the floods of the Maros/Mureș in Hungary and Romania, respectively (Fig. 8). This result is especially interesting in the case of Hungarian settlements, which are more endangered (most of the Romanian settlements surveyed are situated on terraces, above the flood level of the river). The proportion of respondents who are afraid of floods is increasing by age: below the age of 30 only 39%, between 30 and 50 already 49%, between 50 and 70 54%, and over the age of 70 as much as 70 % has fears about flooding. Concerning the answers to flood hazard remarkable differences were found in terms of genders. Based on the results, men perceived much lower flood hazard than women, especially in Romania (23% vs 44%) but in Hungary (43% vs 55%) as well.

Management and development measures

The acceptance of human interventions was not influenced by respondents' gender, age or educational level; however, there were some remarkable differences between the two countries. On average, 17% of respondents said that no intervention should be allowed on the river, but in this respect, the Hungarian value (22%) was significantly higher than the Romanian (12%) (Fig. 9).

Not surprisingly, flood protection was the most supported type of possible action (60%), and it was equally accepted on both sides of the border. Nevertheless, we expected higher values in this case. A possible explanation for lower support can also be related to the generally moderate fear of flooding (Fig. 8). The

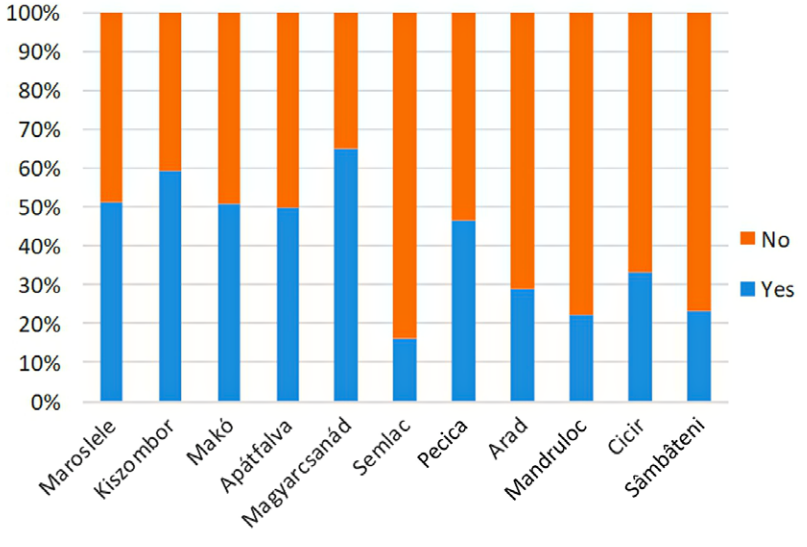

Figure 8. Public perception of flood hazard at the surveyed settlements. The proportion of respondents being afraid or not of floods

greatest difference between countries was observed in tourism-related actions. It is striking that Hungarian respondents (26%) seemed to be much less supportive in this respect than Romanians (51%).

The respondents less favoured hard interventions. However, Romanian residents were significantly more supportive, as 25% said that actions related to improving river navigation (dredging, construction of stone structures) are acceptable. In contrast, in the case of Hungarian residents, this value was only 15%. Finally, on average, only 11% of the respondents said that industrial interventions such as quarrying should be allowed in the future. In this respect, the values measured in the two countries were less different.

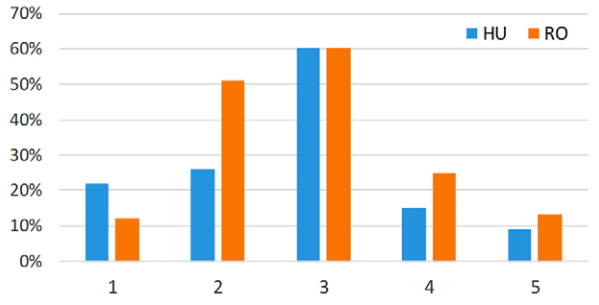

Figure 9. The acceptance of different human interventions according to the respondents (1: no interventions, 2: interventions for tourism, 3: interventions for flood protection, 4: interventions for transportation, 5: interventions for the industry)

Discussion

Public perception in river and floodplain management is important to improve and protect the quality of river-floodplain ecosystems and to mitigate environmental hazards since the public acceptance of any actions improves the success and sustainability of measures (de Groot, 2012; Souza et al., 2021).

Regarding the present survey, the perception of natural values and environmental hazards, as well as their relationship to the river, is greatly affected by socio-demographic variables, especially by the educational level of the respondents. Those who have a higher level degree are more engaged with the problems related to the river. This finding is in line with the observations of some other researchers (e.g. Ioana-Toroimac, 2020; Gomez-Cunya, 2022). On the other hand, Schaich (2009) concluded that lifestyle-related variables are more important in perceiving river ecosystems than socio-demographic variables. This approach can also be adapted to our results if we consider the tendency of increased engagement by those who regularly visit the river. Nevertheless, the two groups largely overlap in the case of the study area, i.e. those who are well educated and those who regularly visit the river. This dichotomy emphasizes the plurality of perceptions, which must be considered during the preparation of management plans (D'Souza et al., 2021)

The public opinion regarding the well-management of the riparian area is determined mostly by the type and intensity of human interventions made at the riverside of the Maros/Mureş. The recreational and aesthetic developments improve the perception compared to the less manicured riverside. Infrastructural developments characterize mostly urban settlements; therefore, people in villages are less satisfied with the condition of the river. Similar tendencies were reported by Suren (2009) and Khew et al. (2014), who found that excessive plant growth in riparian areas reflects the lack of management for the public. However, other studies emphasized that the public prefers wild, more natural riparian zones and floodplains (de Groot, 2012; Saha et al., 2020). The discrepancy emerges mainly because of the difference in target groups surveyed, i.e. people generally prefer lush vegetation at the riverside, but those visiting and using the river regularly may have a different perception and prefer a more intensively managed environment. Of course, over-exploited sections, such as those affected by sand extraction, adversely affect locals' perception.

It is positive that about half of the surveyed people thought that their community respect the river and its natural values. It is noteworthy, however, that among people who do not visit the Maros/Mureş the average rating on the local community's respect for the river and its natural values was higher than those who have a more direct relationship with the river, which suggests that the latter group is more pessimistic or more sensitive concerning the state of the river and its environment. An important finding of our study was that almost three quarters of local people (73%) have a direct relationship with the river. They mostly visit the river for recreational purposes, but agricultural activities are also important. This means that the needs and expectations of the local public have to be considered during river management; thus, improving public engagement in planning river management measures is crucial.

The studied section of the Maros/Mureş river faces several environmental problems and hazards. The most visible and, therefore, the most frequently mentioned is solid waste disposal. Among environmental problems, industrial and sewage water contamination of the riv-

er was also frequently mentioned by the respondents, which means that although water quality has improved since the 1990s, the bad reputation of the river in this respect remained. People emphasized gravel and sand quarrying only in the settlements mostly affected by great-scale sediment extraction. On both sides of the border, people see rather negative changes in the state of the river. Based on local opinions, the deterioration of the environment is a very significant issue in Romania, while Hungarians reported fewer problems. In all, we can see that locals are usually aware of the problems related to the Maros/Mureş. However, they are mostly concerned about things affecting their close environment and apparent at their settlements, and they are unaware of overall processes along the river.

In terms of river management, it is also an important issue that a relatively low proportion of respondents are concerned about flood hazard, which suggests that the 1970 flood is fading from the collective memory of local societies. This hypothesis is also supported by the fact that the older the respondents were, the higher risk they perceived, meaning that the lack of direct experience leads to decreasing awareness among younger generations. Several other authors made similar findings in various contexts (e.g. Burningham, 2008; Pagneux et al., 2011; Comănescu & Nedelea, 2016), thus, decreasing flood risk perception with time passing since the last event is a general problem and has to be considered during strategic planning. Besides, similarly to the findings of David (1971) and House (1996), males were less worried about floods than females because of their greater risk acceptance (Marshall, 2004)

Nevertheless, the most accepted interventions on the river are related to flood protection, while people are against the industrial utilization of the Maros/Mureş. Developments related to tourism were supported less than expected in Hungary, assuming that Hungarians are either pessimistic about the developments or are unaware of the river's touristic potential. On the other hand, Romanian residents probably see an important opportunity in developments or think any soft tourism interventions would help improve the river's deteriorated environment.

Conclusion

In all, the people living along the lowland section of the Maros/Mureş are a little pessimistic concerning the present and the future of the river. We assume, however, that there are certain misbeliefs on a community level concerning the general problems affecting the river. Nevertheless, it is positive that most people have a direct relationship with the river by visiting the riverside, and half of the surveyed people thought that their community respect the river and its natural values.

The results indicate that the preferences and motivations of local people are very complex and influenced by several socio-demographic and environmental factors. Thus, further analyses would be beneficial in the topic to better understand public perceptions and preferences of the river-floodplain ecosystem and human interventions and to reveal existing knowledge gaps and misbeliefs. Consequently, we think that informing people on apparent processes, finding the ways of inclusive planning processes, and improving the cooperation willingness of the local population would be very important. This way, they would accept future management decisions and activities more easily. As there is a considerable demand for the recreational use of the river, supporting riverside developments would be highly desirable. We assume that in this way, the relationship of local people to the river would be more direct, and the necessary improvement of environmental conditions, especially in Romania, would attract more people to the Maros/Mureş in the future.

References

Amissah, G.J., Kiss, T., & Fiala, K. (2018). Morphological Evolution of the Lower Tisza River (Hungary) in the 20th Century in Response to Human Interventions. *Water*, 10(7), 884 doi:10.3390/w10070884

Babbie, E. (2010). *The practice of social research*. Belmont

Boga, L., & Novaky, B. (eds.) (1986). *Magyarorszag vizeinek mőszaki-hidrologiai jellemzese. A felszini vizkeszlet mutatoi: Maros*. Budapest: Vizgazdalkodasi Intezet

Bryman, A. (2001). *Methods of Sociological Research*. Oxford University Press. p. 540.

Burningham, K., Fielding, J., & Thrush, D. (2008). 'It'll never happen to me': understanding public awareness of local flood risk. *Disasters*, 32(2), 216-238.

Cockerill, K. (2016). Environmental reviews and case studies: public perception of a high-quality river: mixed messages. *Environmental Practice,* 18(1), 44-52. doi: 10.1017/S14660466150 0 040X

Comănescu, L., & Nedelea, A. (2016). Floods and public perception on their effect. Case Study: Tecuci Plain (Romania), year 2013. *Procedia Environmental Sciences,* 32, 190-199.

David, E.L. (1971). Public perception of water quality. *Water Resources,* 7, 453–457.

Entwistle, N.S., Heritage, G.L., Schofield, L.A., & Williamson, R.J. (2019). Recent changes to floodplain character and functionality in England. Recent changes to floodplain character and functionality in England. *Catena*, 174, 490-498. DOI: 10.1016/j.catena.2018.11.018

EU WFD (2000). Directive 2000/60/EC of the European Parliament and of the Council establishing a framework for the Community action in the field of water policy

Firebaugh, G. (2008). *Seven Rules for Social Research.* Princeton University Press, p.272.

Flotemersch, J., & Aho, K. (2021). Factors influencing perceptions of aquatic ecosystems. *Ambio*, 50, 425–435. DOI: 10.1007/s13280-020-01358-0

Gomez-Cunya, L. A., Tilt, J., Tullos, D., & Babbar-Sebens, M. (2022). Perceived risk and preferences of response and recovery actions of individuals living in a floodplain community. *International Journal of Disaster Risk Reduction,* 67, 102645.

De Groot, M. (2012). Exploring the relationship between public environmental ethics and river flood policies in western Europe. *Journal of Environmental Management,* 93(1), 1-9.

Hale, R. L., Cook, E. M., & Beltrán, B. J. (2019). Cultural ecosystem services provided by rivers across diverse social-ecological landscapes: A social media analysis. *Ecological Indicators*, 107, 105580.

Hophmayer Tokich, S. (2005). *Public participation under the EU water framework directive - processes and possible outcomes.* https://ris.utwente.nl/ws/portalfiles/portal/17709578/public_participation.pdf

House, M. (1990). Public perception and water quality management. *Water Science and Technology,* 34, 25–32. doi: 10.1016/S0273-1223(96)00850-5.

Howarth, W. (2009). Aspirations and realities under the water framework directive: proceduralisation, participation and practicalities. *Journal of Environmental Law,* 21(3) 391-417. https://doi.org/10.1093/jel/eqp019

Ioana-Toroimac, G., Zaharia, L., Neculau, G., Constantin, D. M., & Stan, F. I. (2020). Translating a river's ecological quality in ecosystem services: An example of public perception in Romania. *Ecohydrology & Hydrobiology,* 20(1), 31-37.

Jähnig, S. C., Carolli, M., Dehnhardt, A., Jardine, T., Podschun, S., Pusch, M. Scholcz, M., Tharme, R.E, Wantzen, K.M., & Langhans, S. (2022). Ecosystem Services of River Systems–Irreplaceable, Undervalued, and at Risk. In: *Encyclopedia of Inland Waters,* 2nd edition. Tockner, K. & Mehner, T. (eds.). Elsevier.

Khew, J.Y.T., Yokohari, M, & Tanaka, T. (2014). Public perceptions of nature and landscape preference in Singapore. *Human Ecology*, 42, 979–988. DOI: 10.1007/s10745-014-9709-x

Kiss, T., & Blanka, V. (2012). River channel response to climate- and human-induced hydrological changes: Case study on the meandering Hernád River, Hungary. *Geomorphology*, 175-176, 115-125. DOI: 10.1016/j.geomorph.2012.07.003

Kiss, T., Fiala, K., Sipos, Gy., & Szatmári G. (2019). Long-term hydrological changes after various river regulation measures: are we responsible for flow extremes? *Hydrology Research*, 50(2), 417-430. DOI: 10.2166/nh.2019.095

Konecsny K., & Balint G. (2009). Low water related hydrological hazards along the lower Mureș/Maros river. *Riscuri şi catastrofe*, 872022071584-5273

KSH (2018). Magyarország közigazgatási helynévkönyve, 2018. január 1., Budapest: Központi Statisztikai Hivatal, pp. 48.

Laczay, I. (1975). A Maros vizgyűjtője es vizrendszere. In *Vizrajzi Atlasz Sorozat 19 Maros*. Budapest: VITUKI; 4–7.

Letenyei, L. (2004). *Telepuleskutatas. A telepulesi es tersegi tervezes tarsadalomtudomanyos alapozasa.* Budapest: L'Harmattan Kiado, 147–185.

Letenyei, L., & Racz A. (2011). Mintavetel terepmunka kozben. In: *Roma kutatasok, 2010. Elethelyzetek a tarsadalom peremen.* Kurucz, E. (ed). Budapest: Nemzeti Csalades Szocialpolitikai Intezet, pp.45–75.

Marshall, B.K. (2004). Gender, race, and perceived environmental risk: The "white male" effect in Cancer Alley, LA. *Sociological Spectrum*, 24, 453–478. doi: 10.1080/02732170490459485.

Mujere, N., & Moyce, W. (2017). Climate Change Impacts on Surface Water Quality. In: Ganpat, W., & Isaac, W. (eds.). *Environmental Sustainability and Climate Change Adaptation Strategies.* IGI Global, 322-340.

Neuman, W. L. (2006). *Social Research Methods: Qualitative and Quantitative Approaches.* Edinburgh: Pearson Education Limited, p. 458.

Oroszi V. (2009). *Hullámtér-fejlődés vizsgálata a Maros magyarországi szakaszán.* PhD Dissertation. Szeged: University of Szeged.

Osti, R.P. (2018). *Integrating Flood and Environmental Risk Management: Principles and Practices.* ADB East Asia Working Paper Series, Asian Development Bank. p. 51. DOI: 10.22617/WPS189607-2

Oyedotun, T.D.T., & Nasrudeen Ally, N. (2021). Environmental issues and challenges confronting surface waters in South America: A review. *Environmental Challenges*, 3, 100049. DOI: 10.1016/j.envc.2021.100049

Pagneux, E., Gísladóttir, G., & Jónsdóttir, S. (2011). Public perception of flood hazard and flood risk in Iceland: a case study in a watershed prone to ice-jam floods. *Natural hazards*, 58(1), 269-287.

RPL (2011). *Populația stabilă pe județe, municipii, orașe și localități componenete la RPL_2011*. In: Recensământul Populației Și Locuințelor 2011, Romania. (in Romanian). Available at: https://www.recensamantromania.ro/rpl-2011/rezultate-2011/

Saha, D., Das, D., Dasgupta, R., & Patel, P. P. (2020). Application of ecological and aesthetic parameters for riparian quality assessment of a small tropical river in eastern India. *Ecological Indicators*, 117, 106627.

Schaich, H. (2009). Local residents' perceptions of floodplain restoration measures in Luxembourg's Syr Valley. *Landscape and Urban Planning*, 93(1), 20-30.

Seymour, V. (2016). The human–nature relationship and its impact on health: A critical review. *Frontiers in public health*, 260. doi: 10.3389/fpubh.2016.00260

D'Souza, M., Johnson, M. F., & Ives, C. D. (2021). Values influence public perceptions of flood management schemes. *Journal of Environmental Management*, 291, 112636.

Suren, A.M. (2009). Using Macrophytes in Urban Stream Rehabilitation: A Cautionary Tale. *Restoration Ecology*, 17(6), 873–883.

Tockner, K., & Stanford, J. A. (2002). Riverine flood plains: present state and future trends. *Environmental conservation*, 29(3), 308-330.

Wang, P., Chen, B., Yuan, R., Li, C., & Li, Y. (2016). Characteristics of aquatic bacterial community and the influencing factors in an urban river. *Science of the Total Environment*, 569-570, 382–389. doi: 10.1016/j.scitotenv.2016.06.130 .

White, P.C.L., Vaughan Jennings, N., Renwick,A. R., & Barker, N. H. L. (2005). Questionnaires in ecology: a review of past use and recommendations for best practice. *Journal of Applied Ecology*, 42(3), 421-430. DOI: 10.1111/j.1365-2664.2005.01032.x

ISSN 0354-8724 (hard copy) | ISSN 1820-7138 (online)

Three Centuries of Dynamics in the Lowland Section, induced by Human Impact – a Sociogeomorphic Approach

Fabian Timofte[A*], Petru Urdea[A,B]

Received: April 29, 2022 | Revised: June 10, 2022 | Accepted: July 01, 2022
doi: 10.5937/gp26-37632

Abstract

This study aims to analyze one of the most dynamic sections in the lower part of the Mureș River, Lipova-Arad sector. The geological and tectonic context influenced the shifts of the watercourse at both a regional scale and a local one. The channelization works have shortened the length of the channel by 1/3 of it. The flood events in the 70s and the mining activity have also influenced the evolution of the river in last decades. Accelerating the geomorphological processes, mostly after the great floods, have narrowed the channel by 35%, and have reduced the total islands surface by almost 80%. In this context, the Mureș River try to reach the dynamic equilibrium state had before the human interventions. Under the anthropic pressure the geomorphological processes have been accelerated and the landscape left behind in Lipova-Arad section, along the Mureș River suffered important changes.

Keywords: meanders; historical changes; channel migration; GIS; sociogeomorphology; Mureș River; Romania

Introduction

The people used the methods for watercourses regulation from ancient times, in order to control both the discharge and water level for settlements supply. At the same time, the minor riverbeds are anthropic affected for the propose of flood protection, easier navigation, irrigation and hydroelectricity or for a better water management (Church, 2015).

The regulation of alluvial channels changes the balance between the discharge and the sediment budget, so considerable changes in the geometry of the cross sections and the planform parameters of course may occur (Petts, 1984). These changes are the response of the river for recovery the dynamic equilibrium state (Andrews, 1986; Carling, 1988). The velocities and direction of the river downstream are changing and the flow is governed by the relative frequency of sediments from tributaries unaffected by regulation (Petts, 1984).

Even if the channelization process based on good intentions, the engineers could not predict the impact on the channel morphology and the intensity of geomorphological processes. The cross section analysis is missing for recent period because of a lack infrastructure. On this line, we focused on the assessment of planform parameters of the minor riverbed. Channel pattern is the view of the river reach from above (satellite, plane, drone etc.). There are three main patterns of the minor riverbed: meandering, braiding and relatively straight channels (Leopold & Wolman, 1957). Rust (1978) refines the classification with anastomosing type and Miall (1977) introduces the wandering channel type.

[A] West University of Timișoara, Department of Geography, Romania, V. Pârvan, no. 4, Timișoara, 300223, Timiș, Romania; fabian.timofte@e-uvt.ro; petru.urdea@e-uvt.ro
[B] Institute for Advanced Environmental Research, West University of Timișoara, V. Pârvan, no. 4, Timișoara, 300223, Timiș, Romania
[*] Corresponding author: Fabian Timofte, e-mail: fabian.timofte@e-uvt.ro

The Mureș River is one of the biggest fluvial link between Transylvanian and Pannonian basin. For millennia, this path was used to carry natural resources to Tisa River (as an intermediate stop), and then further to central Europe and Balkan Peninsula (Kovach, 1980).

The flow direction of the Mureș River frequently changed during the Quaternary and this fact is reflected in its symmetrically arranged alluvial fan, and in the huge number of paleomeanders from the Pleistocene-Holocene period (Mike, 1991). Swamps and extensive wetlands have surrounded the meandering sectors, and the river have flooded large areas every year. The floods sometimes lasted for months, until the lateral depositional structures facilitated the evacuation of excess water (Sipos et al., 2012). The geotechnical works emerged as a strategy for fixing this problem, in order to facilitate an optimum navigation.

The scientific purpose of this study was born as a need for quantifying at a local scale the changing rates of the Mureș River channel in his depositional area. Compared to other previous studies (Timofte et al., 2016; Timofte, 2019), the temporal analysis scale was doubled and the spatial scale have been reduced, focusing on the most dynamic sector in Mureș lowland section - Lipova-Arad sector. The main findings of the previous papers regarding the analysis of some morphometric parameters for the Romanian part of alluvial fan.

Study area

The catchment of the Mureș River is 29.767 km² (Ujvari, 1972), of which 28.310 km² in Romania - 11.7% of the country's surface (A.B.A.M., 2015) - which represents 94% of the surface of the entire basin. The highest point of the basin is 2509 m above sea level, Peleaga Peak in Retezat Mountains, and the lowest point is 82 m a.s.l., located on the confluence point with Tisa River in the area of Szeged city (Sipos et al., 2012). As much as the river basin surface and its multiannual average discharge, 186 m³/s, (A.B.A.M., 2015), the Mures river is on second position in Romania, after Siret with 36083 km² and 222 m3/s (Diaconu & Zăvoianu, 1983).

The lowland section of the river is located from the apex (to the west of Lipova) to Szeged, in the southwestern part of Panonian Basin. The total length of the watercourse is around 175 km. In this area Mureș river built-up a huge alluvial fan (Kiss et al., 2104). The average slope for Lipova-Nădlac sector is 0.28 m/km.

Study area covers the eastern part of the deposition area (Fig.1), between Lipova city (123 m, 46° 05' N, 21° 41' E) and Arad city (105 m, 46° 09' N, 21° 20' E). The entire segment is a part of Arad County. A simple visual analysis of the cartographic representations shows off that this part is one of the most dynamic portion from the entire lowland section. The floodplain outline is obvious, especially on the left side, where the contact with the high plain of Vinga is made by a terrace level. On the right side, the contact with tabular plain of Arad is quite smooth (Posea, 1997).

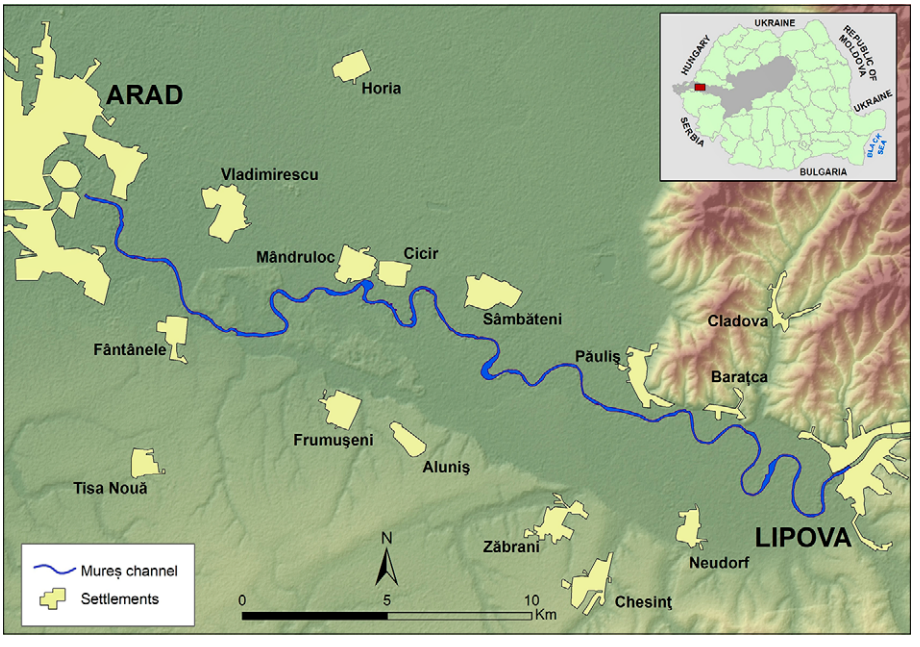

Figure 1. Location of the study area

Geological and geomorphological framework

The Quaternary evolution of the lower Mureş area is connected to the tectonic and geomorphological dynamic of this contact area between Carpathian orogen and Pannonian Basin, a large back-arc basin formed in Middle Miocene on a structural basement of the Carpathian type (Polonic, 1985). In the lower Mureş area are recognize the presence of a complex faults systems, at the level of the Pannonic basement, being individualized horsts and grabens, disposed from East to West, Caransebeş Graben, Buziaş-Battonya Horst, Sînnicolau Mare-Szeged Graben, fragmented by transverse faults, Jimbolia–Lipova fault and Sînnicolau Mare-Arad fault, all covered by Neogene sedimentary deposits (Visarion & Săndulescu, 1979). In detail, the Sînnicolau Mare-Szeged Graben is presented as two half-grabens, Szeged half- graben and Makó half-graben, in fact with the asymmetric tectonic trough character (Balázs et al., 2017). The continuous neotectonic subsidence, with varying speed, remained active in the Quaternary time, which explains the thickness of 600-700 m of the Quaternary deposits in Szeged area (Timár & Rácz, 2002).

The entire evolution of the lower Mureş sector from Midle Pleistocen to the Holocen is connected to the organization of the drainage system in the south central Tisa valley, coupled with Tisa graben evolution and with subsidence rates, flow direction, discharges and load dynamics in the Tisa-Criş-Mureş fluvial system (Kiss et al., 2015). In addition, the channel river spatial evolution was connected to the formation of an extensive alluvial fan, with a radial length of 80-100 km and 9000 km2 area, with a high density of paleochannels, in a tectonic active area. The successive courses of paleo-Mureş were driven by the local erosional base represented by the floodplain area of Criş and Tisa rivers in variable conditions of slope. The water discharges – between 2600-2700 m^3/s, 9,6 ± 1.3 ka and 680 m^3/s, 1.6 ka -, and loads, with effect on the behavior of the river, with the predominance of anastomosing, meandering or braiding, marked in the appearance of sectors with distinct paleochannel pattern (Kiss et al., 2014). The active tectonic area Mako-Szeged played a decisive role in fixing the course on the E-W axis, with the confluence point in the Szeged area at 1.6 ka (Kiss et al., 2014).

For entire area the contemporary tectonic activities are characterize by a high contrast between negative and positive vertical movements and opposite of horizontal velocity, which maintains the seismicity of the area, with polikinetic earthquakes with a magnitude of over 5 (Oros et al., 2018). For the extremely lower Mureş section, in the confluence Tisa-Mureş area the recent subsidence movements has values of 3 - 4.1 mm/y (Cornea et al., 1979; Joó, 1992), which plays an important role in maintaining a certain status for the local erosional base.

Geotechnical works and sociogeomorhpology

Our analysis of the Mureş evolution in the last three centuries highlights the fact that, in the last two centuries human intervention has been, for certain sectors, essential for adjusting the drainage in the flooding regime and, last but not least, for alluvial plain morphology reconfiguration, for the channel migration zone. This situation imposed a kind of approach compatible with the specific of sociogeomorphology, after which the geomorphic landscapes is seen as the result of interactions between physical and human processes (Ashmore, 2015). Both physical and human processes are critical for explaining how rivers have evolved and how they might adjust in the future. So, we find that in the case of the lower Mures, from a sociogeomorphological perspective, the human and physical processes, as well as interactions between these processes, drive and/or inhibit river adjustment (Mould et al., 2018), specific for a socio-natural system with human and physical components.

The human interventions on the main channel through regulation works were done in order to control the transport and to protect the settlements. We could not find out yet the information about the moment in time when each meander was regulated, but a situation plan highlights the fact that the meander from Arad was incised after 1815 according to Johann Mihalik's plan (Sipos et al., 2012). For all that, we suppose the channelization locally started in the end of 18th century, not before 1776[1], because the map from that year shows an unaltered channel. An extra argument is the map from 1792 that shows three fresh paleomeanders near Lipova and Mândruloc[2]. A number of six bigger meanders were incised before the second part of 19th century (Fig. 2), the information is available on the second topographic survey of Habsburg Empire map (1860-1865). After few decades, the meander incision process has been resumed in the end of 19th century, but with a less intensity (Kiss et al., 2011).

A vision of this kind, which, from another point of view, has a relevance for the history of riverbeds and alluvial plain mapping, we find in a situation plan at a scale of 1: 7.200, made by the Austrian engineer, Fried Braun in 1793 for a sector of Mureş (Fig. 3), downstream of Lipova. A detailed mapping marks

[1] https://maps.hungaricana.hu/en/MOLTerkeptar/1707/?list=eyJxdWVyeSI6ICJtYXJvc2NoIn0
[2] https://maps.hungaricana.hu/en/MOLTerkeptar/29235/?list=eyJxdWVyeSI6ICJtYXJvc2NoIn0

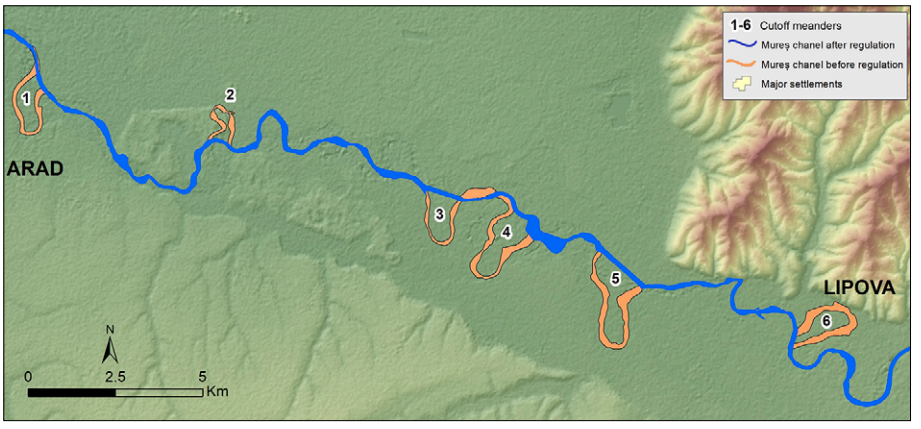

Figure 2. Meanders incised before the second part of the 19th century

the banks of the minor riverbed with their change in the floods of 1790 - indicated in a separate note -, by a dotted line the thalweg, as well as the rapids of the riverbed "*Treppelweeg*". Alluvial point bars, islands, river tributaries, abandoned meanders „*alte Todt Marosch*", and the accumulation of ice floes with the formation of an ice jam are also mapped, explaining the specific situation, even 4 weeks of each winter. In correlation with the economic component - agricultural terrains and industrial use (sand quarries, tiling, etc.) -, and the cadastral classification, represented by characteristic colors, the correction of the meander loop with a more accentuated dynamics is marked „*Neuer durchschitt*". For geomorphological mapping, this way of cartographic approach is a remarkable one for that period, the genetic-thematic cartography of the relief being sketched only towards the end of the 19th century (Passarge, 1912).

The floods from 70s

This is the generic name used to describe the events that affected the carpathian rivers in 1970 and 1975. For most of them, the discharged reached the historical maximum. The flood wave of Mureș River exceeded 2300 m³/s at Arad hydrological station (Fig. 4) and covered the whole floodplain.

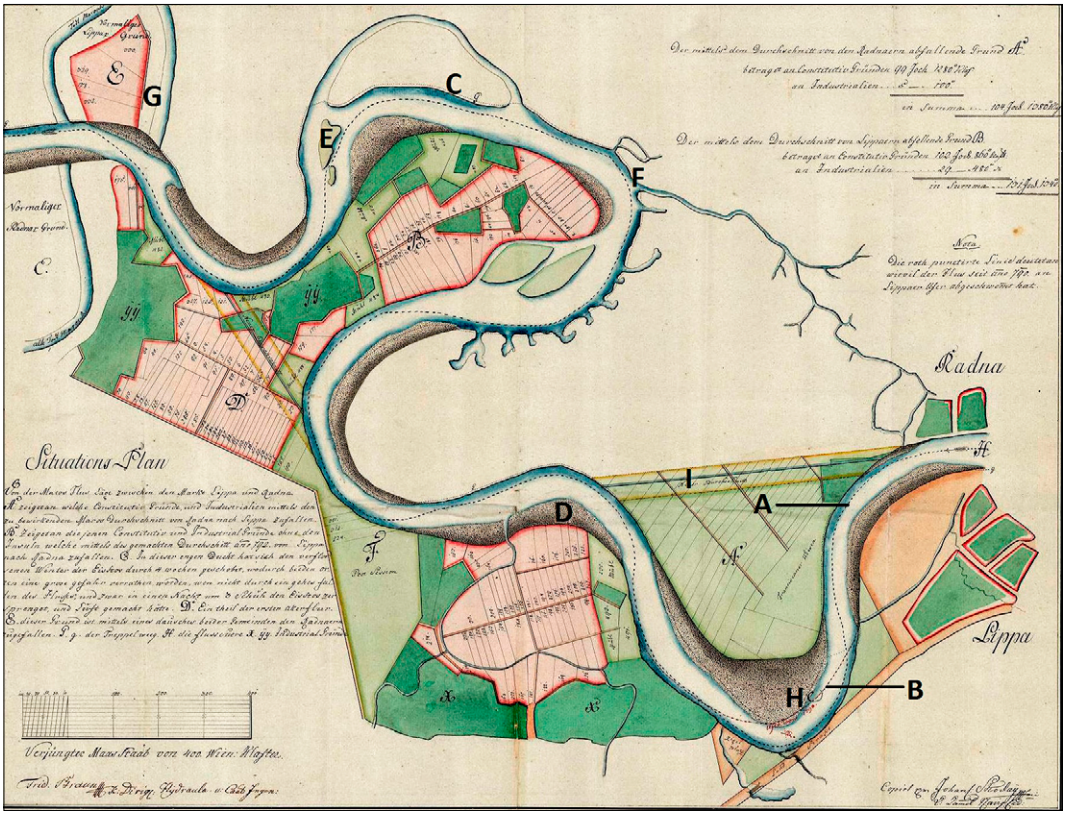

Figure 3. Situation plan of the Mureș River near Lipova city. A – thalweg; B – thalweg during floods; C – rapids; D –point bars; E – central bars; F – river tributary; G- abandoned meander; H – ice floes; I – meander correction. (Data source - https://maps.hungaricana.hu/en/MOLTerkeptar/5333/)

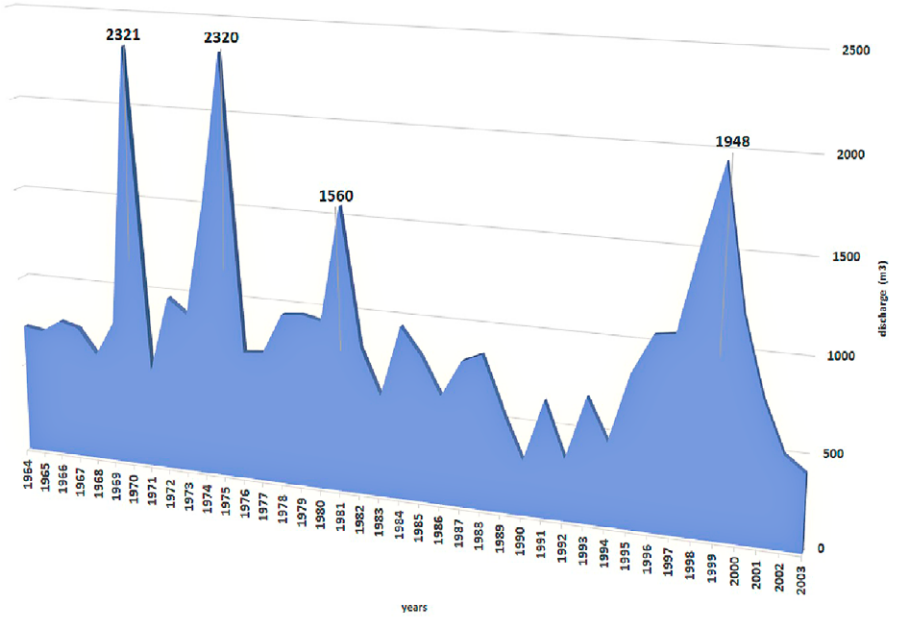

Figure 4. The maximum discharge at Arad hydrological station between 1964 and 2003 (after Zaharie, 2010)

An important consequence of the floods from 70s was related with the geomorphological impact in changing the configuration of the riverbed. For settlements protection the national authority built-up flood embankment: 4.7 km on the left bank in Lipova and 9.86 km on the right bank near Sâmbăteni (Timofte et al., 2016).

Data and methods

In the first instance, we have extracted the primary data for transforming analysis from different cartographic representations (Fig. 5). The first one is the Map of Lippa (Lipova) district that cover the entire section with only one sheet. This map is a base map for a well-known representation called Mercy map. This one portrays the Mureș channel before any geotechnical works. The next three maps are part of Habsburg and Austro-Hungarian military survey missions. Detailed situation plans for some parts of the watercourse supplement the basis maps. Because of coarse scale and cartometric reasons, for the first two sources only the length and sinuosity parameters have been analyzed.

For some representations, the acquisition and drawing period took more than 1 year, only for convention we decided to assign only one year for each cartographic source. The Romanian military and topographic surveys cover the 20th century especially the middle decades, highlighting the impact of the great floods that affected the Mureș drainage basin.

The orthophotos for the present day century are the best resource for evaluating the Mureș channel because of its higher accuracy. In contrast to the maps, orthophotos are untainted data sources; the researcher is free to interpret in his own way the shapes of the landforms and the limits between them.

There are many ways to investigate fluvial landforms, from the in situ methods to the remote ones. The geomorphologists seek all the information that could explain the origin and the evolution of the forms created by flowing waters. We applied a digital analysis in order to characterize the Mureș channel and its surroundings for the last three centuries.

Against the background of development of digital platforms, the geomorphology adopted (as the majority of research domains) the resources provided by computational analysis. The software and the tools are special created to fulfill the scientific needs. Also for fluvial geomorphology have been adapted software solutions which integrate the data for a proper analysis.

Specific for meandering rivers is the sinuosity index (the ratio between the total length of the centerline and the straight line that link the heads of the centerline). According to this index, there are three channel types: straight with $Si < 1.05$, sinuous with $Si < 1.5$ and meandering with $Si > 1.5$ (Rinaldi et al., 2016). The length of the channels always correlates with the sinuosity index. The increasing or decreasing in length depends on the analysis scale. It is proven fact that human interventions in meanders correction diminishes the lengthiness of the rivers, but these are not the only causes of length degradation. Largely, the natural processes are also important in channel evolution. It is true that an-

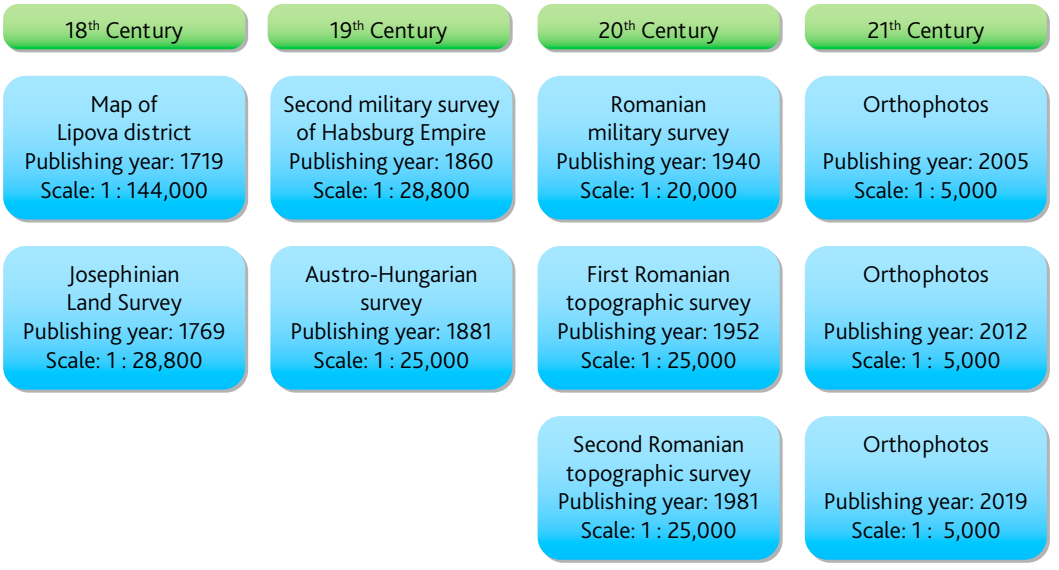

Figure 5. Cartographic data sources grouped by century

thropic pressure is increasing the intensity of water erosion, but sometimes meander chute cutoffs is influenced by a higher variation in discharge.

The most powerful instrument for digital analysis in the fluvial geomorphology is GIS analysis, included both in proprietary and open source software (Kondolf & Piégay, 2016). Using the ArcGIS software and some especially developed tools, we examined the information from the cartographic sources.

The first part of the analysis was to draw the channel and to extract the islands polygons from all the data sources. After that, we availed the Polygon to centerline tool to generate the centerline based on Thiessen polygons (Dilts, 2015). It was the basis for the almost all the investigation we made upon the minor riverbed. Channel migration toolbox was a good support for calculating the migration rate and particularly the width at a given distance (Legg et al., 2014).

For assessing the islands parameters, we calculated the surface and the elongation index using the Minimum Bounding Geometry tool from ArcGIS with the smallest convex polygon enclosing the input feature.

Results

Watching the Mureș River behavior during the built-up of his alluvial fan, we can say that he changed a lot his own pattern, especially because of climate conditions and through load inputs (Sipos et al., 2012).

The most obvious fact is the Mureș channel in the analyzed sector had a different aspect. The maps from 18th century displayed a much-braided riverbed[3] (even if this one looks very artistic). For sure, the presence of many branches in Păuliș-Vladimirescu (Glogovăț) sector (Fig. 6), which crossed the riparian forest on both sides, imposed a custom channel type, very close to the anastomsing.

Overall, the analyzed section can be assigned to meandering channel class (Fig. 7), the only exceptions being the first examined year and the moment after the end of meanders incision process.

Figure 6. The map of Mureș River in 1805 (https://maps.hungaricana.hu/en/MOLTerkeptar/11020/view/?bbox=13858%2C-3920%2C14989%2C-3459); Păuliș-Vladimirescu sector in the frame

[3] https://maps.hungaricana.hu/en/HTITerkeptar/2154/view/?bbox=5773%2C-3473%2C11154%2C-1274

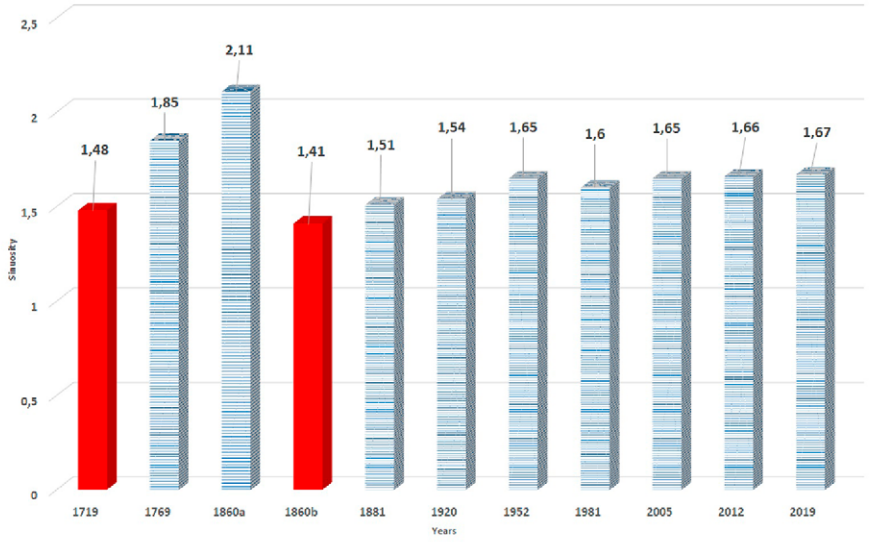

Figure 7. Sinuosity index evolution: 1860a-before incision; 1860b-after incision

Even if the general tendencies of this index are for increasing, some events in the history of evolution can drop down the values of sinuosity. A lower value for the end of the 20th century is associated with the floods that affected the Mureș River catchment.

Length variation

The main events that affect the length of Mureș River in Lipova-Arad sector are connected with the channelization in the end of the 18th century and in the first part of the 19th, the total length dropped down with almost 20 km. The graph below (Fig. 8) shows the difference in length for a base value of 41419 meters in 1719. For each period, we calculated the fluctuation in relation to previous stage.

The great floods from the 1970 and 1975 changed the configuration for some meanders, especially the meander near Sâmbăteni. The total length dropped after that hazard by almost 1.5 km. Due to intensification of geomorphological processes, river tendency is to increase his channel length, mostly in the meandering areas, in the last two periods the increasing rate is more than 150 m.

Channel migration

A specific fluvial activity is related with channel migration. The lateral erosion is related with specific avulsion processes. Based on centerlines from 4 periods we have calculated the total and average migration (Table 1). The first column of the table depicts the surface of the polygons created by the watercourse on the both sides. For the first two periods, the shifted surface is around 300 ha (which means almost 10 ha/year and 13 ha/year), and the values for the last two in-

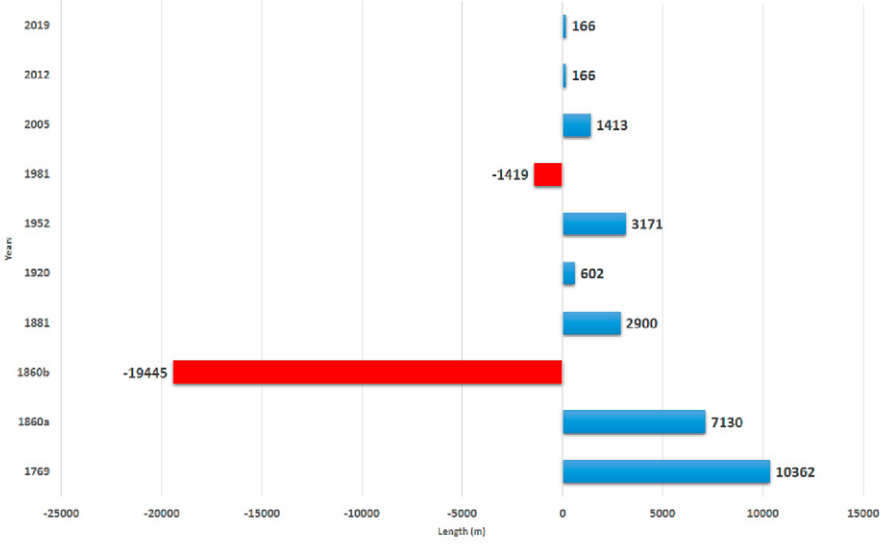

Figure 8. The differences in length for each consecutive analyzed period: 1860a-before incision; 1860b-after incision

tervals is ± 60 ha (around 10 ha/year and 7 ha/year). A less anthropic pressure gives the difference for the last period, for in the last few years mining activity has a lower impact on the channel. The second column of the table is the ratio between the migration area and the length of the centerline in order to correct the values based on channel length.

Table 1. Channel migration results

Analyzed period	Migration shape area (ha)	Length average migration (m)
1952-1981	286.06	62
1981-2005	308.55	66,87
2005-2012	68.56	14,86
2012-2019	54.04	11,71

Width variation

The channel width is in close contact with the transport and deposition activity of the rivers, especially with load amount. Perpendicular lines to the centerlines with 100 m distance was drawn in order to quantify the width of the Mureș course in Lipova-Arad sector. There are important differences especially for the maximum width in each period (Fig. 9), because of development of the mid-channel bars and islands. After the floods from 70s, the characteristics of the channel have changed and width as well. The watercourse width mean values are quite close (around 100 m) except the period of 80s, when the rate is close to 150 m. The minimum values are located in the upper part (between Lipova and Păuliș), where the slope is a little bit higher than in the rest of the analyzed surface.

Mid channel bars

The image of the river in the lower part reflects all the processes from the entire catchment. Islands and channel bars formation is conditioned by the discharge and load. The numerical evolution of these forms is closely related with the general conditions for channel development. The number of depositional landforms in the watercourse doubled from 1920 to 1981 (Table 2) due to great floods events: 1924, 1927, 1932, 1940, 1942, 1970, and 1975 (Timofte, 2019). The mining activity and the sand and gravel extraction directly from the channel determined an accelerated linear and lateral erosion, which led to a regression of mid-channel bars and islands as well.

Obvious differences can be distinguished when the surface of islands is examined. A double num-

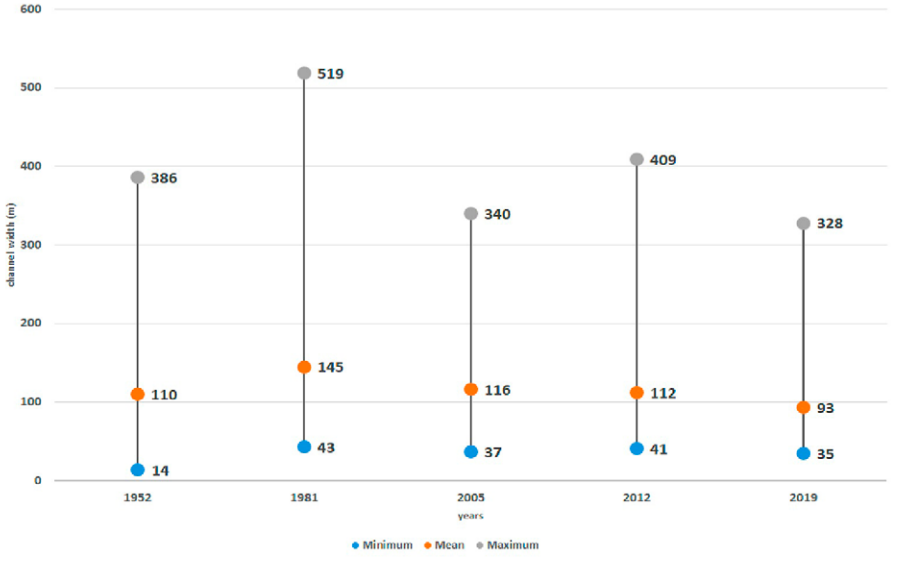

Figure 9. The width channel variation between 1952 and 2019

Table 2. The number and surface of mid-channel bars in the last century

Analyzed year	Number of mid-channel bar	Total surface (m²)	Max. surface (m²)	Mean surface (m²)	Min. surface (m²)
1920	11	607837	176319	55257	4373
1952	13	536150	135554	41242	6828
1981	24	805626	184284	33567	251
2005	18	233246	72459	12958	430
2013	17	208888	70509	12287	278
2019	13	164147	77592	12626	669

ber of forms does not mean a double surface of them. In the first part of 20th century, the islands and mid-channel bars had large surfaces (especially the small ones) while in the last 50-70 years the surface decreased, because some islands were attached to the banks.

Discussion

The lowland Mureș (which overlaps the alluvial fan) can be analyzed at different scales with multiple evaluation possibilities. The first scale is the entire section of the river, the second could be only the Romanian (or Hungarian) territory crossed by the river, the third scale is represented by the sections with accentuated dynamics and the fourth is the scale for morphological sectors imposed by the configuration of the river channel.

The Mureș channel in the study area can be divided in 3 morphological sectors according to planform configuration (Timofte et al., 2016). The first sector, Lipova-Păuliș, 16.6 km length, has three meanders, the second, Păuliș-Fântânele, 22.1 km length, has seven meanders and the last one is Fântânele-Arad sector with 7.7 km has two meanders. Likewise, the slope values are quite different for each morphological sector: 0.39 m/km for the first, 0.47 m/km for the second and 0.41 m/km for the third (Timofte et al., 2016). Dividing the section into morphological sectors is important for quantifying the local shiftings.

The second meander from the Păuliș-Fântânele section is the most interesting meander in terms of evolution (the central bend in the Fig 10). The first flow path followed by the river (before incision) was the south direction. With a straight channel, the flow direction changed to the north, until the floods from 70s, when the huge discharge favored the meander chute cutoffs. From that moment, the old path to the south was reactivated. The meander shape was extracted for the earliest periods not only from cartographic sources, but from the prints on the ortophotos. Total amplitude of the meander was 3015 meters in the last three centuries.

Pauliș-Fântânele seems to be the most dynamic sector in the entire study area. This fact is due to the intensive mining activity. In the last decades at least 15 sand and gravel pits was located in this area, mostly the alluvium being extracted directly from the channel (Timofte et al., 2016). In this way is very hard for the river to reach the state of dynamic equilibrium. In that manner the variation in length will be unexpected, even if the river tendency is to permanently increasing its length.

The water velocity modifies the riverbed parameters. In-channel deposits are a good indicator for the changes that occur in flow regime. The area and the form of the mid channel bars/islands are not so dependent on each other (Fig. 11), because the most developed forms are not the most elongated. For the maximum and minimum surface and elongation, the value of regression coefficient is around 0.12. Local conditions like the presence of water currents in the channel is important for the genesis and evolution of these bars/islands. That fact will affect the width of the channel.

The flow regime depends on climatic conditions that will influence the geomorphological processes in the future. According to Sipos et al., 2014, some climatic predictions for the Mureș catchment area show that the temperature will increase in the spring season that means a suddenly melting of snow. The precipitation amount will also increase in the next 30 years and the discharge will be directly influenced. The flood risk will increase, that will accentuate the erosion processes.

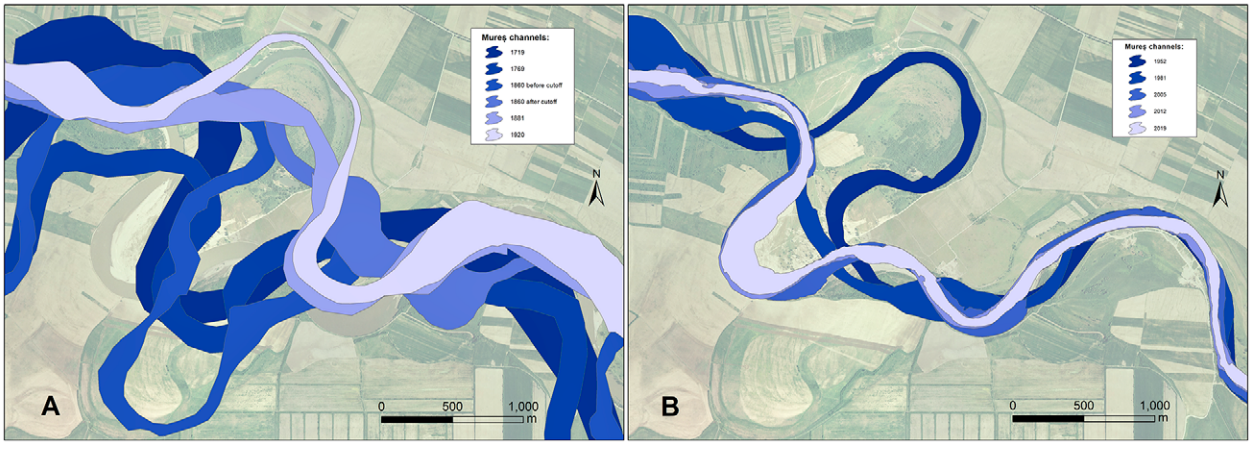

Figure 10. The meander near Sâmbăteni in two periods: 1719-1920 (A) and 1952-2019 (B)

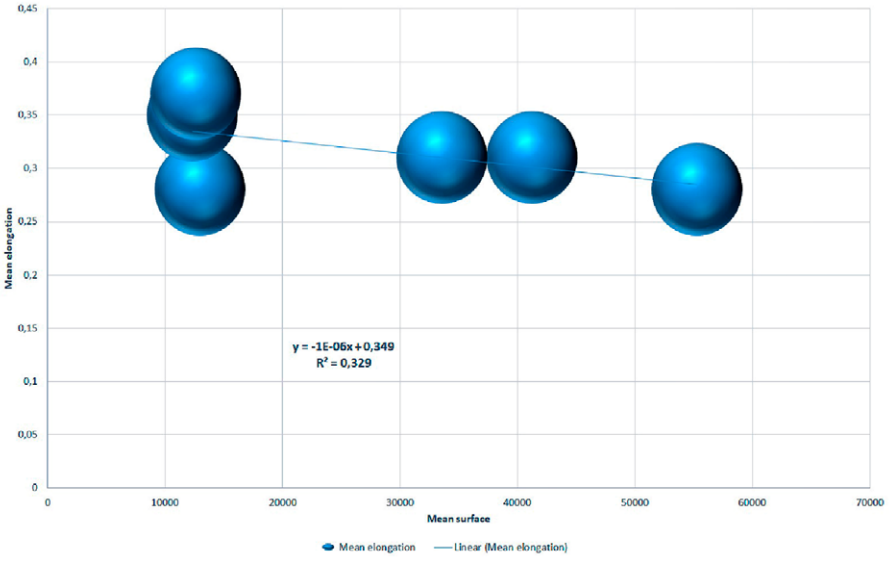

Figure 11. The regression between the mean surfaces of the mid channel bars/islands and mean elongation index

Conclusions

Connected to the manner of sociogeomorphology approach, the scale parameter is very important in landforms analysis. We chose to focus on e regional scale for the first sector of Mureș lowland section (Lipova-Arad) and the obtained results are quite different. Taking into account the specificity of the contemporary tectono-geological and general geomorphological landscape evolution, in relation to the other previous studies, we increased the temporal scale and reduced the spatial one.

Analyzing some channel parameters of Mureș River in a sector of lowland section, we can say without any hesitation that the Mureș River evolved in accordance with anthropic pressure (regulations, mining activity). The geotechnical works modified the planform parameters of the channel: the length have shortened by ⅓ whilst the slope increased, accelerating the erosion. However, the length parameter, with only one exception, has been calibrated by a continuously increasing. Through a constantly anthropic pressure imposed by the mining activity, the width has been altered, from 145 m in 1981 to 93 m in 2019. The channel bars surface changes are aligned with the changes of width parameter, from 80.5 ha in 1981 to 16.4 ha in 2019. Also the number of these microforms decreased from 1981 due to a new channel configuration.

The channel pattern changed during the analyzed period, from a braided and anastomosing in the 18th century to a relatively straight (for some sectors) in the 19th century (only after regulation works) and a meandering in the 20th and 21th centuries. Based on sinuosity index, we can say that Mureș River is still seeking the equilibrium estate had before the anthropic interventions.

References

Bălteanu, D. (1997). Geomorphological hazards of Romania. In: *Geomorphological hazards of Europe*. Embleton, C., Embleton-Hamann, C. (eds.). Amsterdam: Elsevier, 409-427.

A.B.A.M. (2015). Planul de management al riscului la inundații, Administrația Bazinală de Apă Mureș, Târgu Mureș, 202 p.

Andrews, E., D. (1986). Downstream effects of Flaming Gorge Reservoir on the Green River, Colorado and Utah. *Geological Society of America Bulletin*, 97, 1012–1023.

Ashmore, P. (2015). Towards a sociogeomorphology of rivers, *Geomorphology*, 251, 149-156, 10.1016/j.geomorph.2015.02.020.

Balázs, A., Granjeon, D., Matenco, L., Sztanó, O., & Cloetingh, S. (2017). Tectonic and climatic controls on asymmetric half-graben sedimentation: Inferences from 3-D numerical modeling. *Tectonics*, 36, 2123–2141, 10.1002/2017TC004647.

Carling, P., A. (1988), Channel change and sediment transport in regulated U.K. Rivers. *Regulated Riv-*

ers: Research and Management, 2, 369–387, 10.1002/rrr.3450020313.

Cornea, I., Drăgoescu, I., Popescu, M., & Visarion, M. (1979). Harta mișcărilor crustale verticale recente pe teritoriul RS România. *Studii și cercetări de Geologie, Geofizică, Geografie*, 17(1), 3-30.

Church, M. (2015). *The regulation of Peace River: A case study for river management*. Chichester: John Wiley & Sons Ltd., 278 p.

Diaconu, C., & Zăvoianu, I. (1983). Scurgerea apei. In: *Geografia României, I -Geografia fizică.* București, Academiei, pp. 310-329.

Dilts, T.E. (2015). *Polygon to Centerline Tool for ArcGIS*. University of Nevada Reno. Available at: http://www.arcgis.com/home/item.html?id=bc642731870740aabf48134f90aa6165

Joó, I. (1992). Recent vertical surface movements in the Carpathian Basin, *Tectonophysics*, 202, 129-134.

Kiss, T., Oroszi, V., G., Sipos, G., Fiala, K., & Benyhe, B. (2011). Accelerated overbank accumulation after nineteenth century river regulation works: A case study on the Maros River, Hungary. *Geomorphology*, 135, 191-202. 10.1016/j.geomorph.2011.08.017.

Kiss, T., Sümeghy, B., & Sipos, Gy. (2014). Late Quaternary paleodrainage reconstruction of the Maros River alluvial fan, *Geomorphology*, 209, 49-60. 10.1016/j.geomorph.2013.07.028.

Kiss, Hernesz, P., Sümeghy, B., Györgyövics, K., & Sipos, G. (2015). The evolution of the Great Hungarian Plain fluvial system- Fluvial processes in a subsiding area from the beginning of the Weichselian, *Quaternary International*, 388(3), 142–155, 10.1016/j.quaint.2014.05.050.

Kondolf, G.M., & Piégay, H. (eds.) (2016). *Tools in Fluvial Geomorphology*. Chichester, UK: John Wiley & Sons, 560 pp.

Kovacsh, G. (1980). Date cu privire la transportul sării pe Mureș în secolele X-XIII-lea, *Ziridava*, 12, 193-200.

Legg, N.T., Heimburg, C., Collins, B.D., & Olson, P.L. (2014). *The Channel Migration Toolbox: ArcGIS Tools for Measuring Stream Channel Migration*. Department of Ecology State of Washington, no. 14-06-032, 14 p.

Leopold, L., B., Wolman, M., G., 1957, River channel patterns: braided, meandering and straight, *Geological Survey Professional Paper.*

Miall, A.D. (1977), A review of the braided river depositional environment. *Earth-Science Reviews*, 13, 1-62.

Mike, K. (1991). *Magyarország ősrajza és felszíni vizeinek története*. Budapest: Aqua Kiadó, p. 361–577.

Mould, S., Fryirs, K., & Howitt, R. (2018). Sociogeomorphic river recovery: integrating human and physical processes in rehabilitation, Proceedings of the 9th *Australian Stream Management Conference,* 12–15 August 2018, Hobart, Tasmania, 8 p.

Oros, E., Popa, M., & Diaconescu, M. (2018). The Seismogenic sources from the West and South-West of Romania. In. *Seismic hazard and risk assessment,* Vacareanu, R., & Ionescu, C. (eds.). Springer International Publishing AG, 53-69.

Petts, G., E. (1984). *Impounded rivers: Perspectives for ecological management.* Chichester, UK: John Wiley & Sons, 326 p.

Polonic, G. (1985). Neotectonic activity at the eastern border of the Pannonian Depression and its seismic implications. *Tectonophysics*, 117, 109-115.

Posea, G. (1997). *Câmpia de Vest a României (Câmpia Banato-Crișană).* București: Fundația „România de Mâine", 429 p.

Rinaldi, M., Bussettini, M., Surian, N., Comiti, F., & Gurnell, A. M. (2016). Guidebook for the evaluation of stream morphological conditions by the Morphological Quality Index (MQI). Version 2. Istituto Superiore per la Protezione e la Ricerca Ambientale.

Rust B.R. (1978). A classification of alluvial channel systems. *Fluvial Sedimentology — Memoir*, 5, 187-198.

Sipos, G., Ardelean, C., Ardelean, F., Ardelean, M., Blanka,V., Katona, O., Kiss, T., Kovács, F., Boudewijn van L., Mezősi, G., Onaca, A., Právetz, T., Rakonczai J., Rácz, A., Sümeghy, B., Timofte, F., Tobak, Z., Tóth, O. & Urdea, P. (2012). *Past, Present, Future of the Maros / Mureș River.* UVT Timișoara. 212 p.

Sipos, G., Blanka, V., Mezősi, G., Kiss, T., & Leeuwen, B., V. (2014). Effect of climate change on the hydrological character of River Maros, Hungary-Romania. *Journal of Environmental Geography,* 7, 49–56. 10.2478/jengeo-2014-0006.

Timár, G., & Rácz, T. (2002). The effects of neotectonic and hydrological processes on the flood hazard of the Tisza region (E. Hungary). *EGU Stephan Mueller Special Publication,* 3, 267–275.

Timofte, F., Onaca, A., Urdea P., & Právetz, T. (2016). The evolution of Mureș channel in the lowland section between Lipova and Nădlac (in the last 150 years), assessed by GIS analysis. *Carpathian Journal of Earth and Environmental Science,* 11(2), 319 - 330.

Timofte, F. (2019). Evoluția văii Mureșului și a rețelei de așezări în sectorul Lipova-Cenad (unpublished Phd dissertation). Timișoara: University of Timișoara, 231 p.

Visarion, M., & Săndulescu, M. (1979). Structura subasmentului Depresiunii Panonice în România (sectorul central și sudic), *Stud. Cerc. Geol., Geofiz., Geogr., Geofizică,* 17, 2, 191–201.

Zaharie, M. (2010). *Contribuții la monitorizarea scurgerii debitelor lichide ale râului Mureș în zona Arad.* Timișoara: Politehnică, 122 p.